Performance analysis of NACA0017 based Vertical Axis Wind Turbines: With and without augmentation devices

Thesis submitted by
SATYAJIT DAS KARMAKAR

Doctor of Philosophy (Engineering)

Department of Mechanical Engineering
Faculty Council of Engineering & Technology
Jadavpur University
Kolkata, India

2025

JADAVPUR UNIVERSITY
FACULTY OF ENGINEERING AND TECHNOLOGY

INDEX NO. **270/20/E**

1. **Title of the Thesis**: Performance analysis of NACA0017 based Vertical Axis Wind Turbines: With and without augmentation devices

2. **Name, Designation and Institution of the Supervisor:**

Dr. Himadri Chattopadhyay
Professor,
Department of Mechanical Engineering
Jadavpur University,
Kolkata –700032, India

3. **List of Publications:**

   (a) **International Journals**

   - ✓ Das Karmakar, S., & Chattopadhyay, H. (2022). A review of augmentation methods to enhance the performance of vertical axis wind turbine. Sustainable Energy Technologies and Assessments, 53, 102469.
   - ✓ Das Karmakar, S., Rahman, S. M., & Chattopadhyay, H. (2023). Numerical investigations on the performance of Darrieus vertical axis wind turbine with NACA0017 blade profile. Progress in Computational Fluid Dynamics, an International Journal, 23(5), 292-302.
   - ✓ Das Karmakar, S., & Chattopadhyay, H. (2025). Numerical Investigation of Duct Augmented Vertical Axis Wind Turbine With Cambered Airfoils. Journal of Fluids Engineering, 147(5).
   - ✓ Das Karmakar, S., & Chattopadhyay, H. (2025). A comprehensive look into the sustainability of wind power. Renewable and Sustainable Energy Reviews, 217, 115694.

4. **List of Patents:** Nil

5. **List of Presentations in National/International Conferences and Workshops:**

   (a) Das karmakar, S., Chattopadhyay, A., Rahman, S. M., Chattopadhyay, H. "Renewable Energy Sources for Power Generation: Recent Trend in India", Proceeding of International Conference on Energy and Sustainable Development (ICESD 2020), February 15, Jadavpur University, Kolkata, India. ISBN 978-93-83660-56-8.

(b) Das karmakar, S., Rahman, S. M., Chattopadhyay, H. “Performance analysis of vertical axis wind turbine using NACA0017 airfoil section”, Proceedings of the 48th National Conference on Fluid Mechanics and Fluid Power (FMFP 2021), December 27-29, 2021, BITS Pilani, Pilani Campus, RJ, India. ISSN 2195-4356.

(c) Das karmakar, S., Chattopadhyay, H. ”Numerical study of ducted vertical axis wind turbine with NACA0017 airfoil”, Proceedings of the 9th International and 49th National Conference on Fluid Mechanics and Fluid Power (FMFP2022), December 14-16, 2022, IIT Roorkee, Roorkee, India.

(d) Das karmakar, S., Rahman, S. M., Chattopadhyay, H. ”A 3D CFD study on the performance of straight-bladed darrieus vertical axis wind turbine with NACA0017 airfoils”, Proceedings of the 9th National Conference on Wind Engineering (NCWE 2023), March 03-04, 2023, BITS Pilani, Hyderabad, India.

JADAVPUR UNIVERSITY
FACULTY OF ENGINEERING AND TECHNOLOGY

STATEMENT OF ORIGINALITY

I, **Shri Satyajit Das Karmakar** registered on 10^{th} **August, 2020**, do hereby declare that this thesis entitled **"Performance analysis of NACA0017 based Vertical Axis Wind Turbines: With and without augmentation devices"** contains literature survey and original research work done by the undersigned candidate as part of Doctoral studies.

All information in this thesis have been obtained and presented in accordance with existing academic rules and ethical conduct. I declare that, as required by these rules and conduct, I have fully cited and referred all materials and results that are not original to this work.

I also declare that I have checked this thesis as per the "Policy on Anti Plagiarism, Jadavpur University, 2019", and the level of similarity as checked by iThenticate software is 4 %.

Signature of the Candidate : Satyajit Das Karmakar

Date : 24/07/2025

Certified by Supervisors :
(Signature with date, seal)

24.7.25

Dr. Himadri Chattopadhyay
Professor
Dept. of Mechanical Engg.
JADAVPUR UNIVERSITY
Kolkata-700 032, India

(Prof. Himadri Chattopadhyay)

JADAVPUR UNIVERSITY
FACULTY OF ENGINEERING AND TECHNOLOGY

CERTIFICATE FROM THE SUPERVISOR

This is to certify that the thesis entitled **"Performance analysis of NACA0017 based Vertical Axis Wind Turbines: With and without augmentation devices"** submitted by **Shri Satyajit Das Karmakar**, who got his name registered on 10^{th} **August, 2020** for the award of **Ph.D. (Engg.)** degree of Jadavpur University is absolutely based upon his own work under the supervision of **Prof. Himadri Chattopadhyay** and that neither his thesis nor any part of the thesis has been submitted for any degree/diploma or any other academic award anywhere before.

24.7.25

Dr. Himadri Chattopadhyay
Professor
Dept. of Mechanical Engg.
JADAVPUR UNIVERSITY
Kolkata-700 032, India

(**Dr. Himadri Chattopadhyay**)
Professor,
Department of Mechanical Engineering
Jadavpur University,
Kolkata –700032, India

Signature of the Supervisor
and date with Official seal

……

Dedicated

to

My Family

……

कर्मण्येवाधिकारस्ते मा फलेषु कदाचन ।
मा कर्मफलहेतुर्भूर्मा ते सङ्गोऽस्त्वकर्मणि॥

— **Bhagavad Gita**, Chapter 2, Verse 47

You have a right to perform your prescribed duties,
but you are not entitled to the fruits of your actions.
Never consider yourself to be the cause of the results of your activities,
nor be attached to inaction.

* * * * * * * * *

The Road Not Taken

Two roads diverged in a yellow wood,
And sorry I could not travel both
And be one traveler, long I stood
And looked down one as far as I could
To where it bent in the undergrowth;

Then took the other, as just as fair,
And having perhaps the better claim,
Because it was grassy and wanted wear;
Though as for that the passing there
Had worn them really about the same,

And both that morning equally lay
In leaves no step had trodden black.
Oh, I kept the first for another day!
Yet knowing how way leads on to way,
I doubted if I should ever come back.

I shall be telling this with a sigh
Somewhere ages and ages hence:
Two roads diverged in a wood, and I—
I took the one less traveled by,
And that has made all the difference.

--- **Robert Frost**

* * * * * * * * *

Acknowledgements

Research has been defined as the systematized effort to gain new knowledge. This journey to new insights becomes easier when one receives proper direction and encouragement. During my journey of Ph.D. work, there were many ups and downs. I would like to express my sincere gratitude to those people who helped me to overcome all the hurdles throughout my PhD period. First and foremost, I would like to gratefully acknowledge my PhD supervisor, Prof. Himadri Chattopadhyay for his invaluable guidance, thorough encouragement and total involvement in my endeavour through every step to complete my research work. It is not an exaggeration to say that my curiosity and eagerness in research was evoked by Prof. Himadri Chattopadhyay. The importance of supervision is well-known to anyone who conducts research. In this context, I would thank my supervisor for his unconditional support to take new challenges in achieving the target at the right time.

It is my pleasure to express my heartiest gratitude to my parents (Shri Arup Das Karmakar and Smt. Swapna Das Karmakar) and my elder sisters for standing by me always and keeping faith in me. I want to thank them for their continuous support and motivation.

Signature: Satyajit Das Karmakar

24/07/2025

(Satyajit Das Karmakar)

Abstract

Vertical Axis Wind Turbines (VAWTs) offer several advantages over their horizontal counterparts (HAWTs), particularly in urban environments and turbulent wind conditions, due to their portability, omnidirectional wind acceptance, and compact design. While VAWTs exhibit relatively lower efficiency in low-turbulence, steady wind environments, they tend to outperform HAWTs under highly turbulent and directionally varying conditions. However, widespread adoption of VAWTs is hindered by their inherent limitations, including poor self-starting capabilities, intermittent positive torque generation, and lower energy conversion efficiency. To address these challenges and improve energy extraction, the present research explores augmentation techniques aimed at optimizing the aerodynamic performance of VAWTs. These methods include innovative modifications to inlet flow paths, blade geometry optimization, and advanced structural enhancements such as ducting and cowling systems, all intended to reduce negative torque and enhance wind inflow velocity.

Among the key parameters influencing VAWT performance, the selection of a suitable blade profile plays a pivotal role. This study reports a detailed two-dimensional transient CFD simulation of a Darrieus type lift based turbine using the NACA0017 airfoil which has chosen due to its promising starting torque characteristics. The Unsteady Reynolds-Averaged Navier–Stokes (URANS) equations were solved with SST $k-\omega$ turbulence modeling to assess turbine behavior across varying inlet wind speeds. The performance of NACA0017 was compared with the widely studied NACA0015 profile, with specific focus on instantaneous net torque coefficients across a range of tip speed ratios (TSRs). Results indicate that NACA0017 delivers comparable power coefficients, reaching values of 0.21, 0.23, and 0.25 at inlet wind velocities of 3 m/s, 4 m/s, and 5 m/s respectively, thereby validating its viability for enhanced turbine design.

To further improve the performance of VAWTs, the concept of duct augmentation was explored. This technique leverages a strategically designed duct to accelerate the incoming airflow and reduce wake effects, resulting in greater energy capture. A two-dimensional numerical investigation was carried out on a ducted VAWT with NACA0017 blades and compared against its bare blade counterpart. The analysis encompassed key performance indicators such as coefficient of power (C_P), torque ripple factor, wake velocity deficit, turbulent intensity, and vorticity distribution. The results reveal a significant enhancement in turbine efficiency with duct augmentation: the C_P increases nearly fivefold (ranging from 0.5 to 0.7) at a TSR of 3.5 for inlet velocities between 3 and 4 m/s. Additionally, the torque ripple was found to be minimized at this

TSR, indicating a smoother and more stable torque output under ducted conditions.

Extending the analysis into three dimensions, a comprehensive CFD simulation was conducted for a VAWT equipped with NACA0017 blades and augmented with flat plate deflector. The URANS SST $k-\omega$ model was used to resolve turbulent flow characteristics. At both 4 m/s and 5 m/s, the deflector-equipped turbine achieved higher power coefficients, peaking at 0.28 and 0.29, respectively compared to the bare rotor. Flow visualization using the Q-criterion indicated more organized vortex structures and reduced aerodynamic losses with the deflector, especially at the optimal TSR of 2.5.

Beyond the technical enhancements, this work also addresses the broader question of sustainability in wind energy systems. Despite their promise as a clean energy source, VAWTs and wind power in general, must be evaluated holistically in terms of economic viability, environmental impact, and societal acceptance. A literature based sustainability assessment was performed, highlighting key performance indicators such as greenhouse gas emissions, water usage, and ecosystem impact. While wind energy offers considerable advantages over conventional fossil based systems, challenges remain in areas such as waste management, biodiversity disruption, and community integration. The study emphasizes the need for a balanced and comprehensive approach to evaluating the long-term sustainability of wind energy technologies.

In conclusion, this thesis presents a multifaceted investigation into the aerodynamic optimization and sustainability evaluation of VAWTs. Through computational modeling, augmentation strategies, and holistic impact assessments, the research contributes to the development of more efficient and environmentally responsible wind energy systems suitable for modern decentralized power generation.

Contents

List of Figures

List of Tables

List of Abbreviations

A

AHP	**A**nalytical **H**ierarchy **P**rocess
ANP	**A**nalytical **N**etwork **P**rocess
ARA	**A**dditive **R**atio **A**ssessment

B

BIWT	**B**uilding **I**ntegrated **W**ind **T**urbine
BWT	**B**ladeless **W**ind **T**urbine

C

CAGR	**C**ompound **A**nnual **G**rowth **R**ate
CAWT	**C**ross **A**xis **W**ind **T**urbine
CCS	**C**arbon **C**apture and **S**equestration
CFD	**C**omputational **F**luid **D**ynamics
CFL	**C**ourant-**F**riedrichs-**L**ewy number
CFRP	**C**arbon **F**ibre-**R**einforced **P**lastics

F

FEM	**F**inite **E**lement **M**ethod
FRP	**F**ibre-**R**einforced **P**lastics
FVM	**F**inite **V**olume **M**ethod

G

GBT	**G**uide **B**ox **T**unnel
GFRP	**G**lass **F**ibre-**R**einforced **P**lastics
GHG	**G**reenhouse **G**as

H

HAWT	**H**orizontal **A**xis **W**ind **T**urbine

I

IEA	**I**nternational **E**nvironmental **A**gency

L

LCA	**L**ife **C**ycle **A**ssessment
LCCA	**L**ife **C**ycle **C**ost **A**nalysis
LCI	**L**ife **C**ycle **I**nventory
LCOE	**L**evelized **C**ost of **E**lectricity

M

MAUT	**M**ulti **A**ttribute **U**tility **T**heory
MCDM	**M**ulti-**C**riteria **D**ecision **M**aking
MODM	**M**ulti **O**bjective **D**ecision **M**aking

N

NACA	**N**ational **A**dvisory **C**ommittee for **A**eronautics
NIMBY	**N**ot **I**n **M**y **B**ack**Y**ard
NOTS	**N**umber of **T**ime **S**tep

O

ODGV	**O**mni **D**irectional **G**uide **V**ane

P

PAGV	**P**ower **A**ugmentation **G**uide **V**ane

Q

QORCD	**Q**uadratic **O**rthogonal **R**ibrations **C**ombination **D**esign

R

RANS	**R**eynolds-**A**veraged **N**avier-**S**tokes

S

SDG	**S**ustainable **D**evelopment **G**oals

SST	**S**hear **S**tress **T**ransport
T	
TSR	**T**ip **S**peed **R**atio
TSS	**T**ime **S**tep **S**ize
U	
URANS	**U**nsteady **R**eynolds-**A**veraged **N**avier-**S**tokes
V	
VAWT	**V**ertical **A**xis **W**ind **T**urbine
VIV	**V**ortex**I**nduced**V**ibrations
VSA	**V**ortical **S**tator **A**ssembly
W	
WAG-RH	**W**ind **A**ccelerating and **G**uiding **R**otor **H**ouse
WECT	**W**ind **E**nergy **C**onversion **T**echnology
WGD	**W**ind **G**athering **D**evice

List of Symbols

A list of all the symbols, their representative quantities and units has been provided below so as to familiarize the readers with the frequently used symbols within this thesis.

Scalar Symbols (English Alphabets)

A	Rotor cross-sectional area	m^2
a_1	SST model constant (typically 0.31)	
c	Chord of the blade	m
C_P	Power coefficient	
C_T	Torque coefficient	
D	Diameter of rotor	m
D_ω	Cross-diffusion term in SST k–ω model	
F_2	Blending function in SST model	
G_ω	Generation term for ω	
G_k	Generation term for k	
H	Height of rotor	m
k	Turbulent kinetic energy	m^2/s^2
N	Revolutions per minute	
n	Number of blades	
P	Power	W
p	Pressure	Pa
P_k	Production of turbulent kinetic energy	$kg/(m{\cdot}s^3)$
R	Radius of rotor	m
Re	Reynolds Number	
S	Shear strain	s^{-1}

S_ω	Source term for ω	
S_k	Source term for k	
T	Torque	N·m
t	Time	s
u_τ	Friction velocity	m/s
u_i	Mean velocity component in the i-th direction	m/s
v	Free stream air velocity	m/s
x_i	Spatial coordinate in i-direction	m
y	Distance from wall to center of first mesh cell	m
y^+	Non-dimensional wall distance	
Y_ω	Dissipation term for ω	
Y_k	Dissipation term for k	

Scalar Symbols (Greek Alphabets)

ε	Turbulence dissipation rate	m^2/s^3
γ	Torque ripple factor	
Γ_k	Effective diffusivity of k	
Γ_ω	Effective diffusivity of ω	
λ	Tip Speed Ratio (TSR)	
μ	Dynamic viscosity	Pa·s
μ_t	Turbulent (eddy) viscosity	Pa·s
Ω	vorticity	s^{-1}
ω	Rotor rotational speed	rad/s
ω (turbulence)	Turbulent specific dissipation rate	s^{-1}
ρ	Density of air	kg/m^3
σ	Rotor solidity	
τ'_{ij}	Reynolds stress tensor	Pa
τ_w	Wall shear stress	Pa

CHAPTER 1

Introduction

1.1 Background and motivation

The global energy demand has increased significantly due to the rapidly growing world population over the past few decades. The growing interest in wind energy arises from a convergence of critical global issues that demand a transition from conventional fossil fuel-based systems to more sustainable energy alternatives. One of the primary drivers is the depletion of fossil fuel reserves, which threatens long-term energy security and exposes nations to geopolitical risks. With the increasing scarcity of oil, coal, and natural gas, the prices of fossil fuels have been rising steadily, making traditional energy sources economically less viable for both developing and developed economies.

Additionally, the combustion of fossil fuels releases vast amounts of greenhouse gases (GHGs) such as carbon dioxide (CO_2), methane (CH_4), and nitrous oxide (N_2O), which are the principal contributors to global warming and climate change. This has triggered international concern over rising temperatures, melting glaciers, erratic weather patterns, and an increase in the frequency of extreme climate events.

Another serious consequence of fossil fuel dependency is environmental pollution, including air and water contamination, acid rain, and land degradation—all of which adversely impact human health and ecosystems. At the same time, the global energy demand continues to rise exponentially, driven by rapid industrialization, urbanization, and population growth, particularly in emerging economies.

In this context, rural electrification presents another critical challenge. Many remote and underdeveloped regions still lack access to reliable electricity. Wind energy offers a promising solution, as it enables decentralized power generation that can cater to off-grid communities without relying on costly and extensive transmission infrastructure.

Thus, there is a need for non-conventional energy sources to maintain environmental sustainability and preserve the natural world. Different renewable energy resources such as solar, wind, hydro, and biomass are becoming important due to these factors. The

share of renewable energy to the global energy consumption was 11.2% and electric power generation was 29% in 2020 (Murdock et al., 2021).

Among various renewable and sustainable energy alternatives, wind energy stands out as the fastest-growing source. Its appeal lies in the fact that it is clean, non-polluting, free from carbon emissions, and abundantly available across many geographical regions. wind energy has been used for centuries for providing power to water pumps and grain grinding machines due to its abundant availability and cost-effectiveness (Ackermann & Söder, 2000; Yannopoulos et al., 2015). Nowadays, wind energy is being used as a primary form of energy for the generation of electrical power and is the fastest growing renewable source of energy that has a minimal negative impact on the environment (Rahman & Chattopadhyay, 2023). The global cumulative installed wind capacity has increased significantly since the year 2000 and reached 743 GW in 2020 (Murdock et al., 2021). Furthermore, technological advances and economies of scale have made wind energy an increasingly cost-competitive option in both grid-connected and standalone energy systems.

Wind energy is harnessed by converting the kinetic energy present in atmospheric air movement into mechanical or electrical energy. This conversion is achieved through the use of wind turbines that operate on fundamental aerodynamic principles involving the creation of either drag force, lift force, or a combination of both.

Drag force is the resistance encountered by a surface in the direction of the airflow. Turbines utilizing drag-based mechanisms rely on the pressure differential created by the movement of wind, which directly pushes the blades. Traditional windmills and Savonius-type vertical axis wind turbines (VAWTs) often use this principle. Lift force, on the other hand, acts perpendicular to the direction of airflow. It is generated due to the difference in air velocity across the surfaces of an airfoil (blade), as described by Bernoulli's principle. Modern horizontal axis wind turbines (HAWTs) primarily utilize lift-based aerodynamic forces for higher efficiency and rotational speed. Lift and drag forces on an airfoil is shown in Figure 1.1.

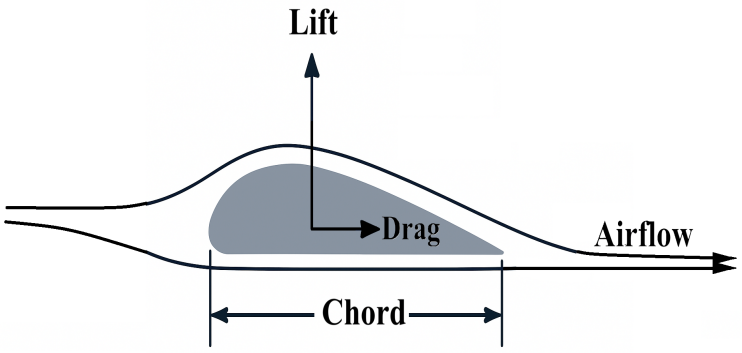

Figure 1.1: Lift and drag forces on an airfoil relative to chord and airflow direction

Historically, wind energy has been used for centuries, particularly for mechanical applications such as pumping water and grinding grain. These early uses demonstrated wind's value as a sustainable and decentralized energy source long before the advent of electricity.

The wind energy conversion technology (WECT) is applied to harness the maximum possible energy from the wind. It has three stages: energy resource assessment, hardware development and manufacturing and finally installation. In the first stage, the wind power potential is evaluated for several parts of the world. The second and third stages are comprised of the design, manufacturing and installation of an efficient wind turbine system.

Wind Resource Assessment: This is the foundational stage where the wind profile of a specific site is measured and analyzed. Parameters such as average wind speed, wind direction, turbulence intensity, and seasonal variations are recorded using anemometers, wind vanes, and remote sensing tools (e.g., LIDAR). This data helps determine the site's suitability and the expected energy yield. For example, Rahman and Chattopadhyay assessed the wind power potential of the Eastern and North-eastern parts of India by introducing a new technique to calculate the parameters involved in wind assessment (Rahman & Chattopadhyay, 2020).

Hardware Development: Based on the site characteristics, an appropriate wind turbine is selected or developed. This includes choosing the rotor diameter, number of blades, hub height, and turbine type (HAWT or VAWT). Engineers also consider system components such as generators, control units, pitch mechanisms, and safety systems.

Installation and Commissioning: Once the equipment is selected, the wind turbine is erected at the site. This stage involves the construction of foundations, mounting of the turbine tower and nacelle, installation of blades, electrical connections, and synchronization with the power grid or storage systems. Post-installation, the system is tested and commissioned for operational readiness.

The kinetic energy from the wind is extracted by the wind turbine and subsequently, converted into electrical power. Rated power, efficiency, power and torque coefficients are the few power characteristics of a wind turbine. The term power coefficient (C_P) is expressed as the ratio of the mechanical output power output of the turbine to the power of the free-stream wind power flowing through the turbine cross-section. In 1919, Albert Betz, a German physicist, proved that a wind turbine can achieve a maximum coefficient of power of 0.59 (16/27), also known as the Betz coefficient (Betz, 1966). There are basically two types of wind turbine systems. namely horizontal axis wind turbine (HAWT) and vertical axis wind turbine (VAWT). HAWT is widely used in wind energy conversion technology as it has high power efficiency compared to VAWT despite the requirement of a complex yaw mechanism (Mohammed et al., 2019). HAWTs also require high wind velocity and huge empty space to prevent aerodynamic interferences

(W.-H. Chen et al., 2017). Wind flow is highly turbulent in nature and also inconsistent in urban areas, so VAWTs are more effective in urban areas as they have simple structures less noisy and occupy very small space for operation (Bhutta et al., 2012; Toja-Silva et al., 2013). However, self-starting problems and low efficiency are the main disadvantages of the VAWTs (Bhutta et al., 2012; Eriksson et al., 2008; Toja-Silva et al., 2013).

Horizontal Axis Wind Turbines (HAWT) are designed with twisted and tapered blades to ensure optimum aerodynamic performance. However, their arrangement in wind farms requires careful spacing to minimize the effects of wake interference from adjacent turbines. Specifically, in crosswind configurations, turbines must be spaced 3 to 5 rotor diameters apart, while in downwind setups, the spacing increases to 6 to 10 diameters to prevent significant performance loss. As a result, HAWT farms generally exhibit a lower power density, typically ranging between 2 to 3 watts per square meter. The power density, in this context, refers to the power extracted divided by the total land area occupied by the turbines.

In contrast, Vertical Axis Wind Turbines (VAWT) offer several distinct advantages. They feature a single moving part—the rotor—and do not require a yaw mechanism, making them mechanically simpler. The blades are usually of uniform cross-section and untwisted, which simplifies manufacturing and reduces costs, making VAWTs more cost-effective than HAWTs. Additionally, their design allows for a higher power density by minimizing the spacing between turbines in an array, with potential power densities reaching up to 30 watts per square meter. VAWTs are well-suited for installation in low- to medium-wind-speed regions and are particularly effective in urban environments, including integration into high-rise buildings. Their omni-directionality eliminates the need for yaw control, and their quiet operation, aesthetic appeal, and better performance in turbulent wind conditions make them ideal for decentralized wind energy generation.

1.2 Classification of VAWTs

Based on the rotor blade design VAWTs are mainly classified into two groups one is drag-type and another is lift type VAWTs (Sagharichi et al., 2018; Tong, 2010). Figure 1.2 shows the classification of wind turbines based on their rotational axis. Drag type VAWTs have concave cup-shaped blades and the turbine rotates because of the pushing force of the wind. Drag type VAWT includes Savonius rotor and Sistan rotor. The Savonius turbine, developed by the Danish engineer Sigurd Savonius in 1931, operates based on drag principles. It consists of two or more concave blades where the wind striking one surface generates motion while the other surface provides resistance. This configuration offers advantages such as a simple construction, high structural strength, and high starting torque, even under weak wind conditions. However, its efficiency is

relatively low, typically in the range of 19% to 23%, and the operating tip speed ratios generally do not exceed unity. Savonius drag type VAWT produces high torque but low rotational speed which generates comparably less electrical power than the lift type (Akwa et al., 2012; Jin et al., 2015; Roy & Saha, 2013). Savonius turbines are best suited for applications that require high torque at low speeds, such as water pumping.

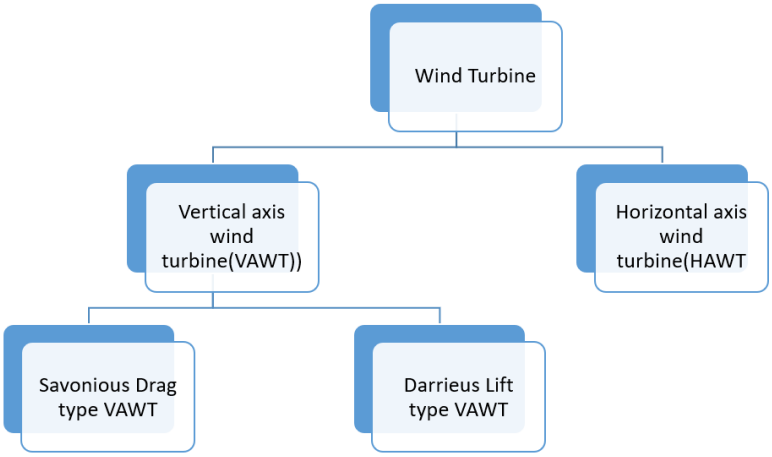

Figure 1.2: Classification of wind turbines

H-rotor and Darrieus rotor fall into the category of the lift-type VAWTs which have airfoil shaped blades. The turbine starts rotating as the aerodynamic lift forces are created when the wind flow interacts with the blades. The Darrieus turbine, is a lift-driven VAWT model patented by the French aeronautical engineer George Jean Marie Darrieus in 1931. It comes in several design variants, mainly differing in blade shape. The first commercial version appeared in 1975. Darrieus turbines are known for their simple construction and relatively high efficiency, with a theoretical maximum approaching 59%, and for achieving high tip speed ratios. A unique characteristic of this design is that the rotor generates a number of force peaks during each revolution equal to the number of blades. Nevertheless, a significant drawback is the inherent lack of self-starting torque (Jin et al., 2015), necessitating auxiliary mechanisms for initial rotation. A combination of both lift type and drag type VAWT or a hybrid model was able to solve this problem (Riegler, 2003). Example of VAWT and HAWT is shown in Figure 1.3.

The rotor blades of VAWTs do not always provide positive torque during operation unlike HAWTs (Zeiner-Gundersen, 2014). The overall performance of the VAWTs decrease due to the negative torque created in the counter direction. Many innovative designs have been implemented to improve the performance of VAWTs, and this includes different configurations and blade profiles. The flow augmentation system is able to increase the coefficient of power (C_P), hence improving the output power of different types of VAWTs.

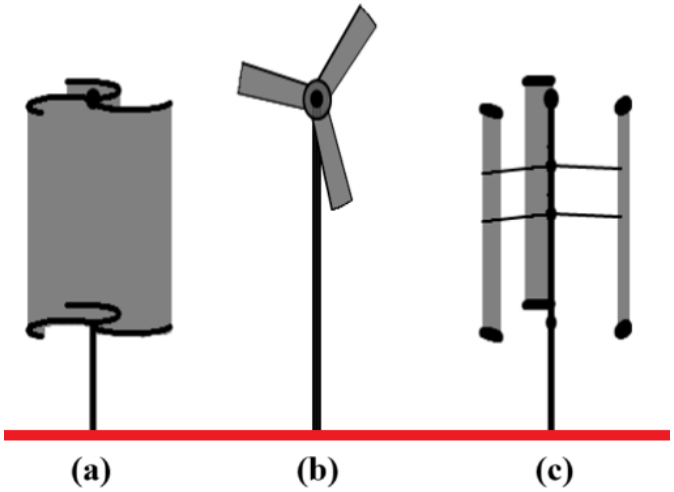

Figure 1.3: (a) Savonius drag VAWT (b) HAWT (c) Darrieus lift VAWT

1.3 Parameters affecting VAWT performance

There are several parameters which affect the performance of VAWT such as the number of blades, blade shape, pitch angle, wind speed, tip speed ratio (TSR) and rotor solidity. We must consider an important parameter known as the rotor solidity (σ) while specifying the rotor design and it can be expressed as

$$\sigma = \frac{nc}{2R} \tag{1.1}$$

Where n, c and R are the number of blades, chord length of the blade and radius of the rotor respectively. The toque coefficient (C_T) and power coefficient (C_P) are used to evaluate the performance of wind turbines. C_T and C_P are denoted by

$$C_T = \frac{2T}{\rho A R v^2} \tag{1.2}$$

$$C_P = \frac{P}{\rho H R v^3} \tag{1.3}$$

where P is the power calculated as $P = TN/60$, N is the number of revolutions per minute (rpm), T is the torque in N·m, ρ is the density of air, v is the free stream velocity, and A is the cross-sectional area of the rotor.
C_P and C_T are related through the tip speed ratio (TSR) of the airfoils as:

$$C_P = C_T \times TSR \tag{1.4}$$

where

$$TSR = \frac{\omega R}{v} \tag{1.5}$$

Here, ω is the angular velocity in rad/s, R is the rotor radius, and v is the free stream velocity.

As already mentioned, VAWT provided relatively low power and hence modifications of the rotor and augmentation of the stator part have been considered by researchers for improving the energy efficiency. A review of performance enhancement on VAWT was conducted by Wong et al., 2017. As a rapidly growing field of research, the latest state-of-art in this area is already due. This review paper tries to summarize various flow augmentation techniques that can be used to increase the power generated by the wind turbine. The paper is organized in the following manner: the next section introduces various augmentation devices. Subsequently, following the structure of the prior review (Wong et al., 2017) augmentation by modification of inlet flow from a particular direction and omni-direction is discussed. Several innovative designs tried by researchers and blade modifications are considered next and finally building integrated augmentation for VAWT is discussed. This paper will also serve as an information hub by mentioning the most relevant work for each augmentation method.

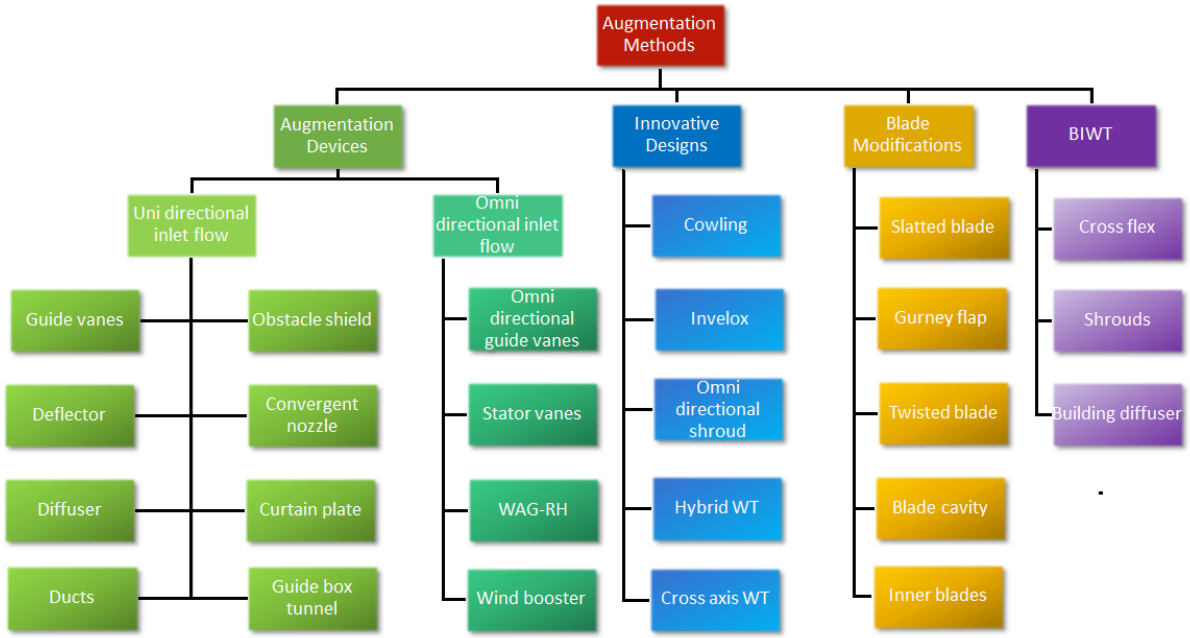

Figure 1.4: Classification of various augmentation methods

Classification of various augmentation methods has been presented in Figure 1.4 which enumerates all the methods. It may be noted that augmentation can be achieved by installing devices or modifying designs.

1.4 Overall objective of the present work

The Objective of the present work are as:

- Examine the current state of wind energy conversion technology and summarize the aspects of sustainability of wind power.
- Analyze the aerodynamic performance of the NACA0017 blade profile for Darrieus-type VAWTs and compare it with existing profiles (such as NACA0015) under different wind speeds and tip speed ratios (TSR).
- To numerically simulate and evaluate the effectiveness of duct enhancement in VAWT performance equipped with NACA0017, focusing on improvements in power coefficient (C_P), torque characteristics, and flow dynamics.
- Investigate the performance of the NACA0017 airfoil for Darrieus-type VAWT augmented with a deflector using a 3-D numerical simulation.

1.5 Organization of thesis

Chapter 1, Introduction provides a comprehensive background on wind energy and its increasing significance in contemporary energy systems. It highlights the comparative advantages and limitations of Vertical Axis Wind Turbines (VAWTs) versus Horizontal Axis Wind Turbines (HAWTs), particularly emphasizing VAWTs' suitability for urban and turbulent environments despite their lower efficiency under ideal conditions. The motivation for this research stems from the need to improve the performance of VAWTs through augmentation techniques. The chapter concludes by outlining the specific objectives and scope of the present study.

The second chapter, Literature Review offers a detailed review of previous studies focused on VAWT performance enhancement and various augmentation strategies. It delves into the significance of blade profile selection and summarizes key findings from research involving blade design modifications. Additionally, it discusses advancements in duct augmentation along with other augmentation techniques and evaluates their impact on turbine output.

The third chapter addresses the sustainability aspects of wind energy technology, focusing on its economic viability, environmental impact, and social implications. It compares the sustainability metrics of wind energy with those of conventional fossil fuel-based power generation. Challenges such as waste management, biodiversity concerns, and health and social impacts are discussed. The chapter aims to provide a holistic understanding of the broader implications of deploying wind energy systems, particularly improved VAWTs, in diverse settings.

Chapter 4 investigates the aerodynamic performance of the NACA0017 blade profile and compares it with the widely used NACA0015 profile. The analysis focuses on variations in torque and power coefficients under different operating conditions. It further

examines how changes in blade geometry influence the overall efficiency of the wind turbine, providing insights into optimal blade design for enhanced energy extraction.

Chapter 5 explores the integration of a duct system into the VAWT configuration to improve aerodynamic performance. The design and simulation of the duct are described in detail. A comparative analysis is conducted between the performance of bare and ducted VAWTs, evaluating enhancements in power coefficient, reduction in torque ripple, and the effect of varying TSR values. The influence of wind speed on the effectiveness of duct augmentation is also examined.

Chapter 6, three-dimensional CFD simulations, where a deflector-augmented VAWT with NACA0017 profile was evaluated. The 3D simulations confirmed an increased C_P range of 0.20–0.25 and validated the structural and aerodynamic advantages of NACA0017 in high TSR regimes. A comparative analysis is conducted between the performance of bare and deflector augmented VAWTs, evaluating enhancements in power coefficient and Q-criterion values.

The final chapter summarizes the key findings derived from the numerical simulations and augmentation analyses. It discusses the implications of the results for future VAWT design, especially in urban and turbulent wind environments. The chapter concludes with recommendations for future research, highlighting potential directions for further improving turbine efficiency and developing comprehensive methods for sustainability evaluation in wind energy systems.

This PhD thesis aims to bridge that gap by conducting a thorough investigation into various flow augmentation techniques and design innovations for enhancing the performance of VAWTs. The study will evaluate device configurations, aerodynamic interactions, urban integration, and experimental outcomes, thereby contributing to the development of more efficient, compact, and viable urban wind energy systems.

CHAPTER 2

Literature Review

2.1 Introduction

The power generated by a wind turbine is dependent on the wind speed and varies with the cube of incoming wind speed. Thus, the performance of a wind turbine system improves with even slight increase in the incoming wind speed. For open flow, the maximum efficiency of a wind turbine is approximately 59%, as set by the Beltz limit (Betz, 1966). However, the maximum efficiency can go beyond this limit with the help of augmentation devices which concentrate the wind flow and increase the mass flow (Jamieson, 2011). Flow augmentation has been recognized as a vital approach to improve the performance of VAWTs. Augmentation can be achieved through devices such as ducts, guide vanes, deflectors, and stators which serve to redirect, concentrate, or accelerate incoming wind.

As already noted, VAWTs have demonstrated relatively lower power output, prompting researchers to explore rotor modifications and stator augmentation strategies in pursuit of enhanced energy efficiency. Several researchers, including Wong et al., 2017, have carried out performance reviews highlighting these enhancement techniques. The present literature review attempts to consolidate the current state of research: wherein the focus is directed toward various flow augmentation mechanisms that influence power generation. A segment of the work introduces diverse augmentation devices employed in VAWT systems, followed by a categorization that aligns with prior literature (Wong et al., 2017), wherein modification of the inlet flow—both unidirectional and omnidirectional—has been analyzed. Further, efforts involving novel blade designs and structural innovations are discussed; additionally, building-integrated augmentation techniques for urban VAWT deployment are also examined. This work, thus, aims to serve as a knowledge base by collating and presenting key contributions relevant to each identified augmentation approach.

2.2 Augmentation devices for VAWTs

2.2.1 Unidirectional flow

Numerous simulations and experiments have been conducted on the performance of the VAWTs with augmentation devices by various researchers. Most of the augmented devices have stator parts placed at the upwind side of the turbine. Stator parts can have different shapes e.g. straight plate or curved plate. These plates act as a shield which reduces the negative torque created on the VAWT and guide the wind flow to the channel for a better angle of attack. They also increase the wind velocity by concentrating more wind flow towards the turbine.

2.2.1.1 Darrieus lift type VAWT

Augmentation by Guide vanes

The effects of the guide vane row on the performance of a straight-bladed lift type VAWT were studied by Takao et al., 2009. They have introduced three arc plates on the guide vane row which can be rotated around the rotor as shown in Figure 2.1. Guide vanes positioned on the upstream side act as a yaw mechanism. With the guide vane, the maximum C_P of the turbine is increased by 1.8 times, though the performance degraded during low TSR as the inlet angle changed drastically due to guide vanes. Effects of guide vane geometry, the number of guide vanes and the distance of the guide vanes from the rotor were also investigated. Optimum results were found when the distance of the guide vanes lies within the range of 125 mm and 150 mm.

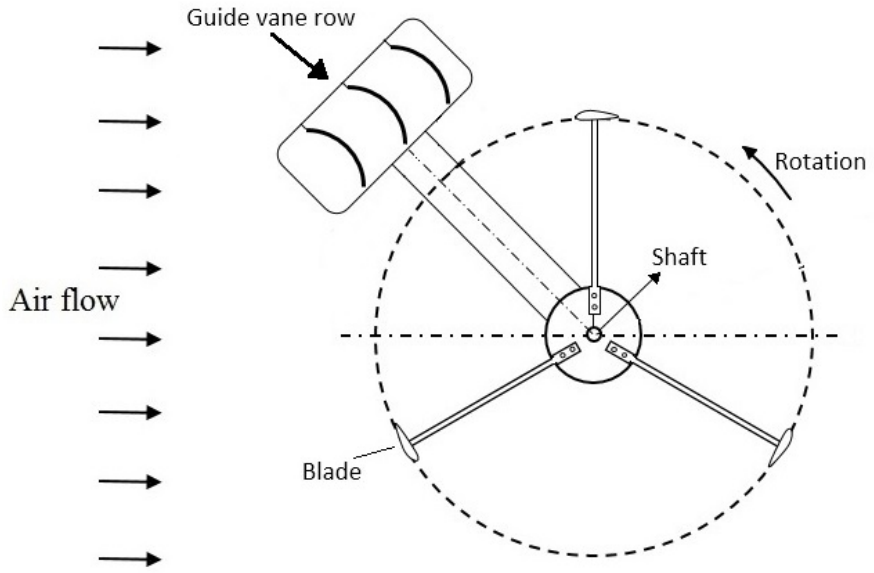

Figure 2.1: VAWT with guide vane row and tail vane

Augmentation by deflector of different shapes

Many researchers incorporated a simple plate diffuser with VAWT to improve aerodynamic performance. The effect of performance parameters like length, position and inclination angles of upstream flat plate deflector on the power coefficient has been investigated by Wong, Chong, Poh, et al., 2018. Wind velocity accelerated by 25% in the near-wake region by the deflector which has been found in their experimental studies. Numerical results predicted an improvement of 33% in power coefficient as compared to conventions VAWT (Wong, Chong, Sukiman, et al., 2018).

Two lift type counter-rotating VAWTs with straight plate deflector mounted on the upstream side were studied by Kim and Gharib, 2013, 2014. The position of upstream deflector is shown in Figure 2.2. The deflector increased the local wind velocity in the immediate vicinity of VAWT by tailoring inlet wind flow and thus increased the output power. However, performance degraded when the deflector was placed very near to the turbine due to wake formation. There was an increase in peak power coefficient by three folds when the ratio of the deflector width and the rotor diameter was 0.33. The study applied only to some special models of wind turbines having a low coefficient of power and high solidity in a low Reynolds number flow regime.

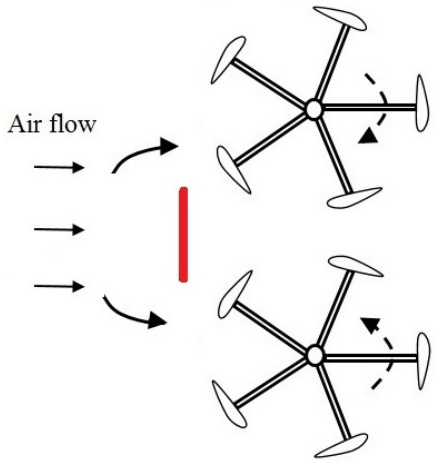

Figure 2.2: Top view and side view of upstream deflector

Jin et al., 2018 also performed experiment on two counter-rotating straight-bladed vertical-axis wind turbines with an upstream deflector as shown in Figure 2.3 and investigated the performance parameters by varying the height of the deflector, deflector width and the distance of the deflector to VAWTs. The aerodynamic performances improve significantly by placing the turbine outside the near wake region. SST turbulence model predicted closer results to the experiments and the numerical results deferred from experimental results by 10.3%. The maximum power coefficient increased up to 0.45 under optimum height, width and distance of deflector from turbine.

A curved plate deflector installed at the upstream side of the three-bladed Darrieus turbine was investigated both numerically and experimentally by Stout et al., 2017 as

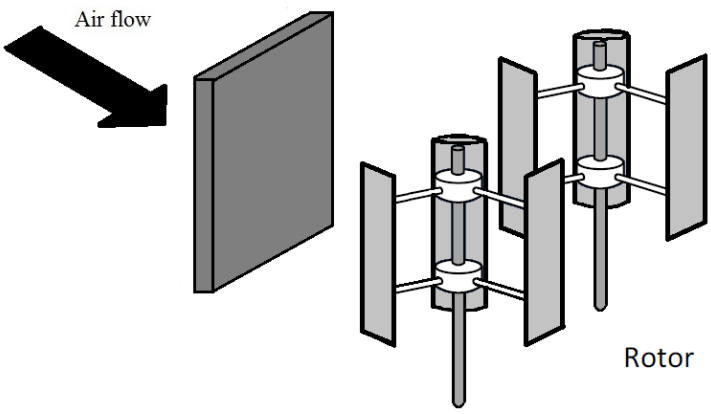

Figure 2.3: Upstream deflector with two counter-rotating VAWT

depicted in Figure 2.4. The deflector primarily reduces the negative torque by redirecting the wind stream from returning blade. Results predicted the maximum power coefficient of 0.208 and 0.213 when the width angle of the deflector was 45° and 36° respectively.

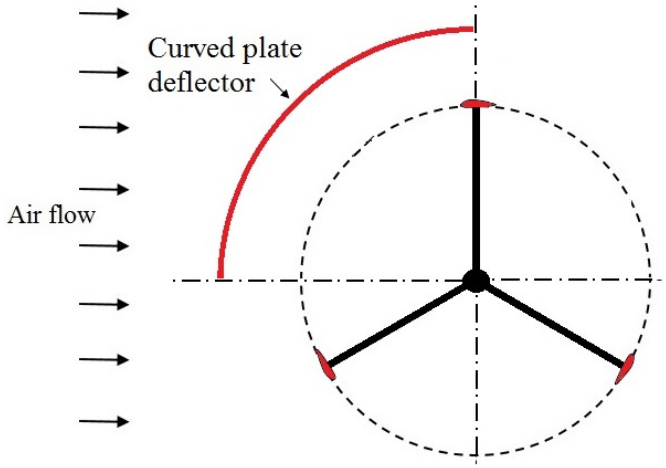

Figure 2.4: Position of curved plate deflector

Zhao et al., 2021 introduced a rhombus shape deflector on the upstream side of twin VAWT to investigate the flow mechanism. The schematic diagram of the rhombus shape deflector incorporated with twin VAWT is shown in Figure 2.5. Results revealed that the wind velocity increased at blades and also a better angle of attack was achieved in the presence of a deflector. A maximum torque coefficient of 0.28 was achieved as compared with the bare turbine. However, the performance of the twin-turbine was dependent on the wind directions.

Augmentation by diffuser of different shapes

Hashem and Mohamed, 2018 computationally investigated a new wind capturing structure named 'wind-lens' consisting of a shroud, diffuser and flanges. Wind lens technology increases the wind flow rate approaching towards VAWT by reducing the

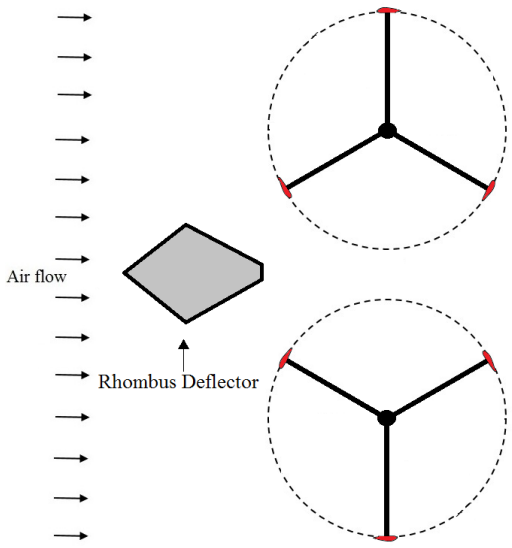

Figure 2.5: Twin VAWT with rhombus deflector

flow separation in the diffuser. Also, a low-pressure region is created at the exit of the diffuser due to vortex formation by the wind lens structure. Three types of wind lens structures namely flat-panel, curved surface and cycloidal surface diffuser were examined which is shown in Figure 2.6. The analysis predicted that the cycloidal surface diffuser is more effective than the other two. Maximum C_P was found to be 1.37 for cycloidal surface diffuser.

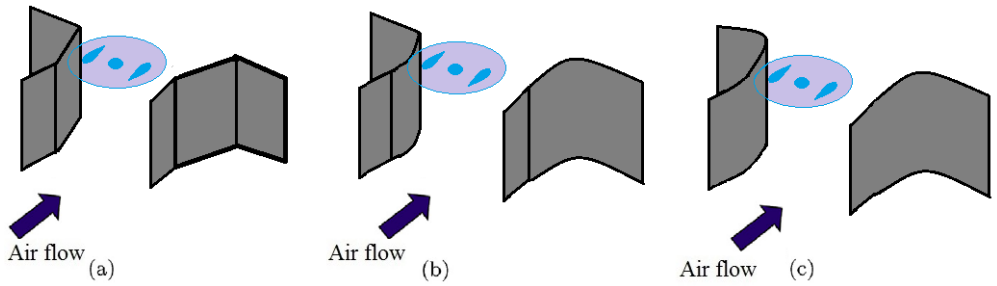

Figure 2.6: Wind lens structure a) flat panel b) curved surface c) cycloidal surface diffuser

Kuang et al., 2022 introduced a 'wind-capture-accelerating' device as an external diffuser system to enhance the power of VAWT. Figure corresponding to wind capturing device is shown in Figure 2.7. This device consists of a rear flange, diffuser and an anterior ejector. The flange and ejector stabilize the flow field and increases the pressure difference, thus improving the diffuser capability. Aerodynamic performances were studied by three-dimensional numerical analysis and results showed that the diffuser with a curved inner surface performed better than the flat one and the power coefficient was found to be 0.25 at 1.5 TSR when the diffusion angle was 20°.

Augmentation by Duct

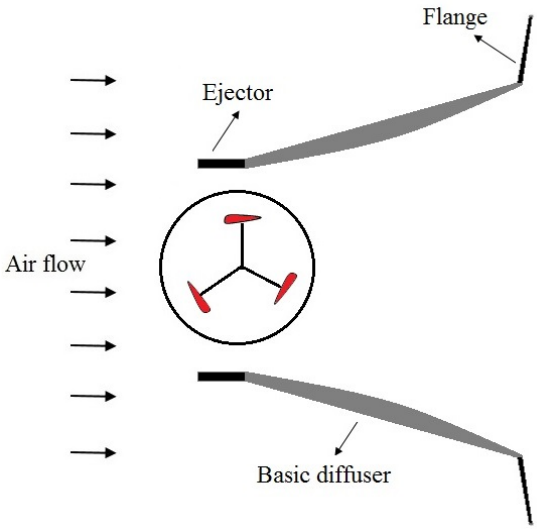

Figure 2.7: Top view of an external diffuser with ejector and flange

De Santoli et al., 2014 studied a VAWT integrated with a duct as shown in Figure 2.8 using FVM formulation. When the wind entered the narrower section of the convergent duct, the speed increased due to the venturi effect. Thus, the power generated by the VAWT also increased with the cube of wind velocity. Experimental results showed that more power was generated at the same wind speed with the integration of the duct. The power increased by 125%. However, this design has some disadvantages due to large duct size and relatively high cost.

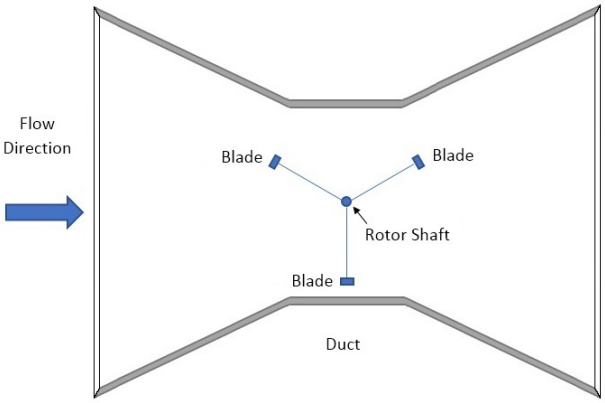

Figure 2.8: Top view of VAWT with integrated duct

2.2.1.2 Savonius drag type VAWT

Pioneering studies (Dewan et al., 2021; M. H. Mohamed et al., 2010, 2011; Roy & Saha, 2013) on inlet modification of drag type wind turbine was conducted by introducing an obstacle shield in the Savonius wind turbine. In their work on the three-bladed and two-bladed Savonius turbine, a shield was used as an obstacle at the front of return-

ing blade as shown in Figure 2.9. The obstacle plate improves the self-starting ability of the turbine irrespective of all positions. The coefficient of power was found to be 0.25 and 0.21 for two-bladed and three-bladed Savonius rotors respectively. Both the power coefficient and static torque have increased with the introduction of an obstacle in the form of a plate.

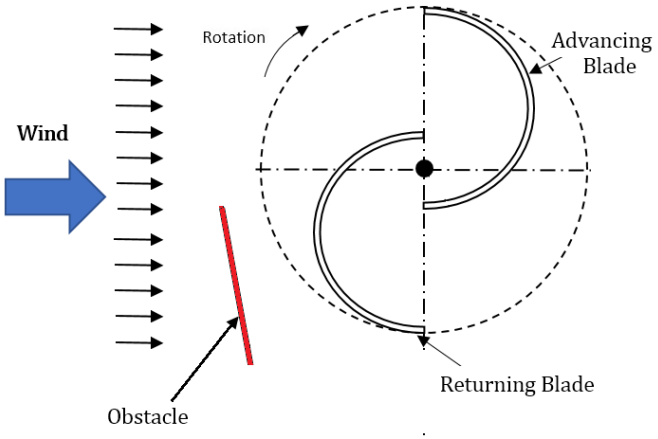

Figure 2.9: Savonius turbine using an obstacle plate

Shikha et al., 2003 introduced a Savonius wind turbine with a convergent nozzle suitable for low wind speed regions. The nozzle concentrator is made up of two converging plates which allow wind to enter only from a single direction as shown in Figure 2.10. Results revealed that the wind turbine performed better when the number of blades of the rotor increased up to six as positive torque was created at blades by the converging wind. However, the efficiency of the Savonius rotor decreases with a further increase in the number of blades as distortion and interference occur while wind flows through the confined space between the blades. Results showed that the wind speed was increased by 3.7 times when the optimal nozzle length was 55 cm with the inlet to outlet ratio of 0.15.

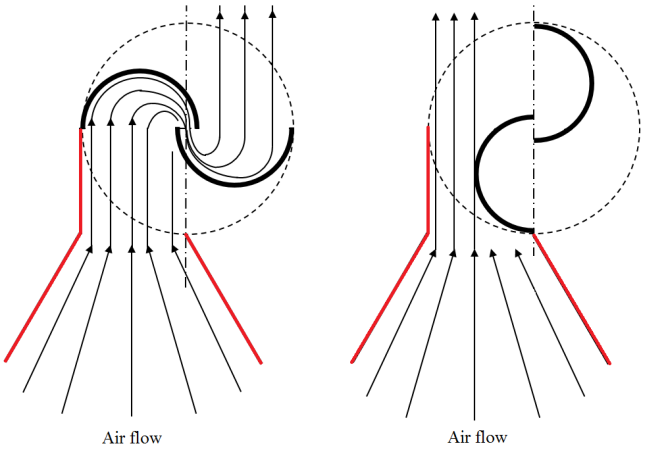

Figure 2.10: Two-bladed rotor with concentrating nozzle

Mohammadi et al., 2018 studied subsonic convergent nozzle as shown in Figure 2.11. The nozzle maximised the air intake to the concave side of the advancing blade and prevented the wind to impinge on the convex side of returning blade. Different shapes of nozzle with the same inlet and outlet area such as simply shaped nozzle, simply shaped nozzle with tail, curved nozzle and curve nozzle with tail were investigated. Results predicted that there was an improvement in the maximum power coefficient from 0.13 to 0.39. However, by utilizing the nozzle, the operation of VAWT becomes dependent on the wind direction.

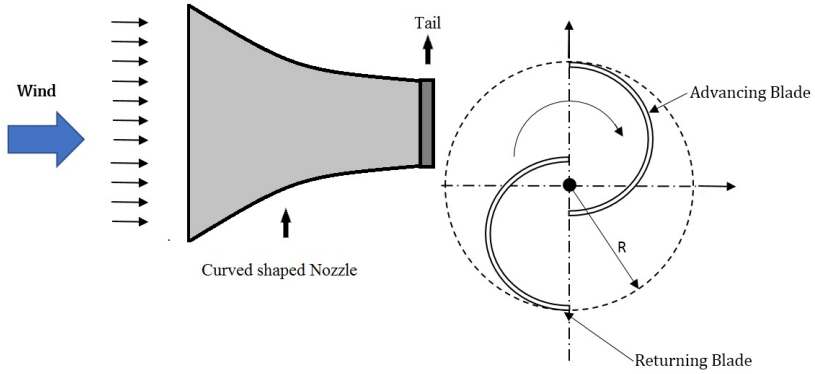

Figure 2.11: Curved shape nozzle with tail

A Savonius wind turbine with a curtain plate was introduced by Altan and Atilgan, 2008, 2010 as depicted in Figure 2.12. The entry portion of the turbine becomes narrower with the introduction of a curtain plate which increases the wind speed on the upstream side. The longer the curtain plate, the more is the wind collected by the turbine. The convex surface of the blade does not experience any negative torque due to this curtain plate. The effect of parameters such as angle and length of the curtain plate were investigated. The study showed that curtain plate with angles of $\alpha = 45°$ and $\beta = 15°$ provide an optimum result where α and β are the angle of curtain plate 1 and 2 respectively. Using this technique, there was an increase of 38.5% in maximum power.

Irabu and Roy, 2007 introduced a Savonius rotor with a guide box tunnel (GBT). The guide-box tunnel consists of a movable front wall at the inlet and a diverging movable wall at the outlet as shown in Figure 2.13. For the closing and opening of the movable wall, a manual or automatic operation system was required. GBT enhances the performance of the rotor in the low wind velocity regions. Experimental results found that the maximum power coefficient for the two and three-bladed rotor were 1.23 and 1.5 times higher than bare turbine respectively. The maximum output power for the two-bladed rotor is about 1.08 times higher compared to the three-bladed rotor.

Shaughnessy and Probert, 1992 conducted experiments on a Savonius drag type wind turbine employed with a V-shaped deflector plate at the upstream side as presented in Figure 2.14. The distance of the deflector from the turbine and the angle of the V-

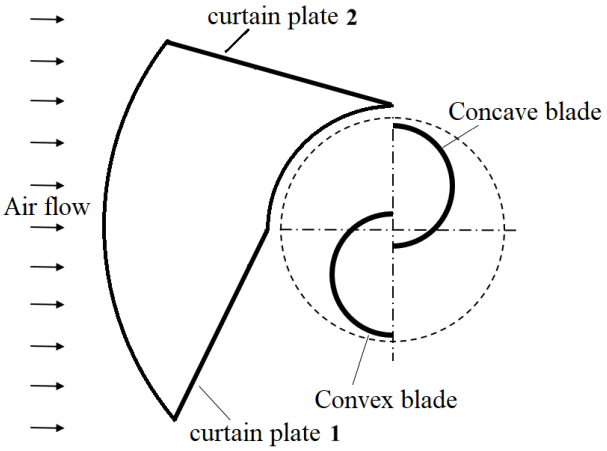

Figure 2.12: Curtain plate arrangement

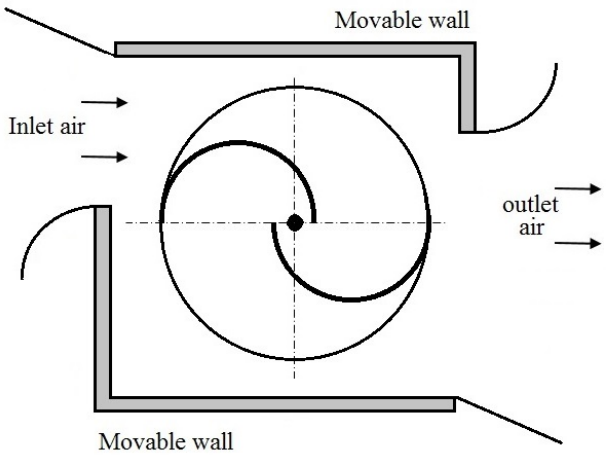

Figure 2.13: Savonius wind turbine with guide-box tunnel

shaped deflector are two important factors in augmentation. The deflector was able to enhance optimal power output by approximately 20%. Maximum C_P was achieved when the deflector was inclined at an angle of $37°$.

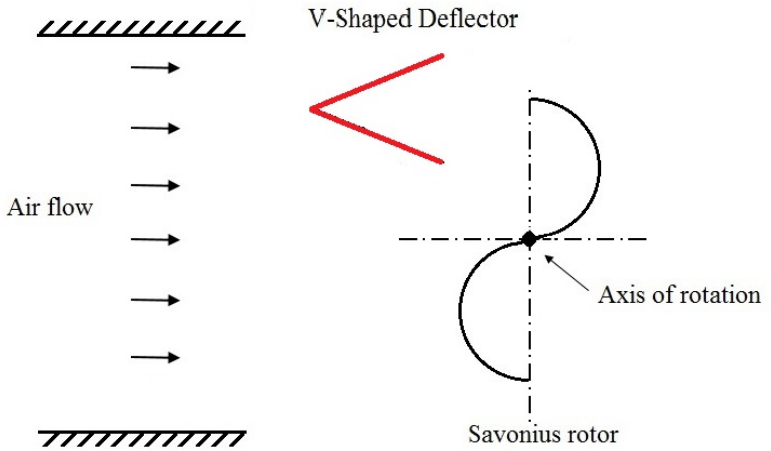

Figure 2.14: Deflector plate of V-shaped

Nimvari et al., 2020 proposed a new concept to improve the power coefficient of VAWT by using a porous deflector to eliminate the negative effects of the wake region caused by a solid deflector. The schematic diagram of the Savonius rotor incorporated with a porous deflector on the upstream side is shown in Figure 2.15. The effect of different geometrical parameters like deflector porosity, height, angle and distance from the rotor was studied numerically. Results revealed that the wake region created behind the deflector breakdowns into smaller vortices, when the wind flows through the porous deflector and lesser fluctuations were observed in the flow field. The maximum power coefficient was enhanced by 10% at a TSR of unity for optimum configuration. The self-starting ability of the turbine was also improved as the static torque coefficient was increased by 2 times between $0°$ to $30°$ angular position.

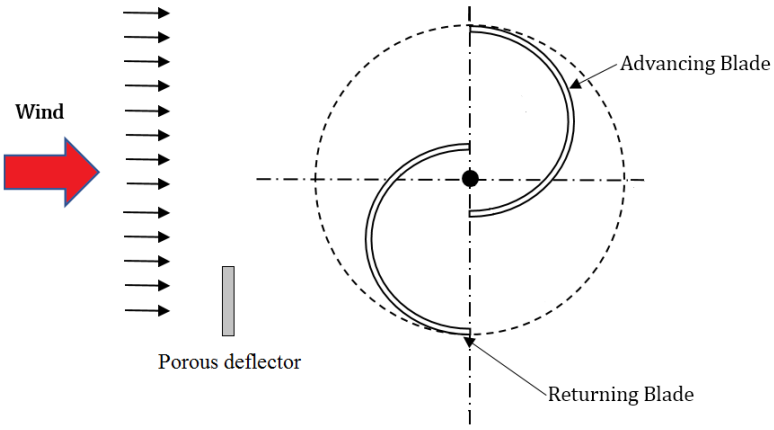

Figure 2.15: Savonius VAWT with porous deflector

El-Askary et al., 2015 introduced a new concept for directing the wind to the VAWT by providing three different designs of guide plates as illustrated in Figure 2.16. This deflector guide system consists of two deflector plates where the first plate guides the wind flow towards the concave side of the advancing blade. Another plate reduces the negative torque by restricting the wind to impinge on the convex side of returning blade and increases the positive torque by directing the wind to the concave side of the same returning blade. It was observed that the curved shaped guide system performed better than the other two designs. The maximum power coefficient was found to be 0.52 at a TSR of 1.1. However, the generation of a wide wake region and the formation of vortex shedding around the guide plate system are the main drawbacks.

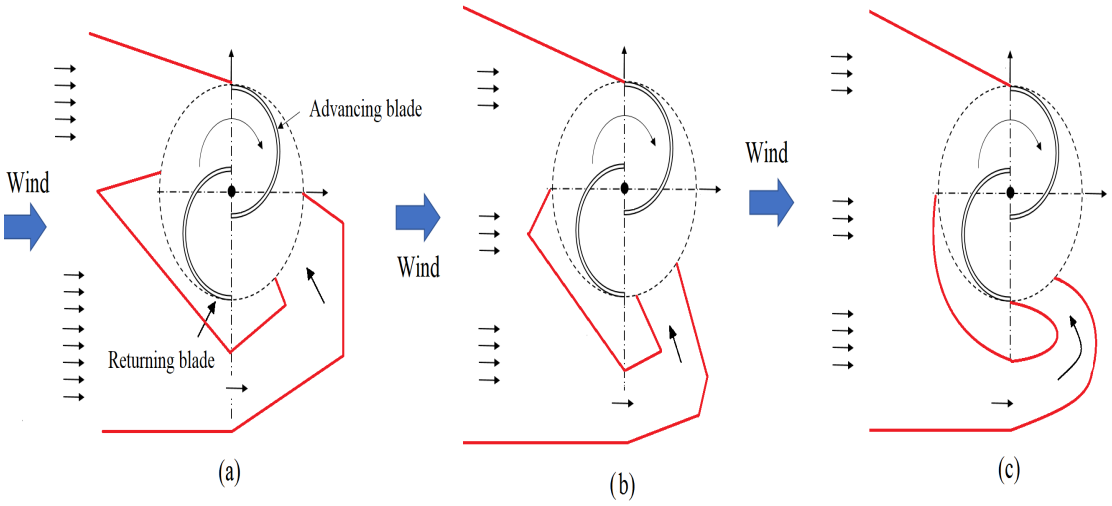

Figure 2.16: (a) and (b) straight deflectors of two different designs and (c) curved deflector

A Sistan wind turbine with power augmentation guide vane (PAGV) (W. T. Chong et al., 2012, 2013) is shown in Figure 2.17. Numerical simulations, as well as experiments, were carried out on PAGV with different shapes and sizes of guide vanes. The incoming wind velocity increased due to the venturi effect created by the multiple guide vanes which also guide the air to enter into the rotor blades at a maximum angle of attack. Experiments revealed that there is an improvement of 73.2% in angular speed of the rotor at 3 m/s wind speed with PAGV. Also, the self-start ability of the turbine improved. The larger size and robust design are the few limitations of this device.

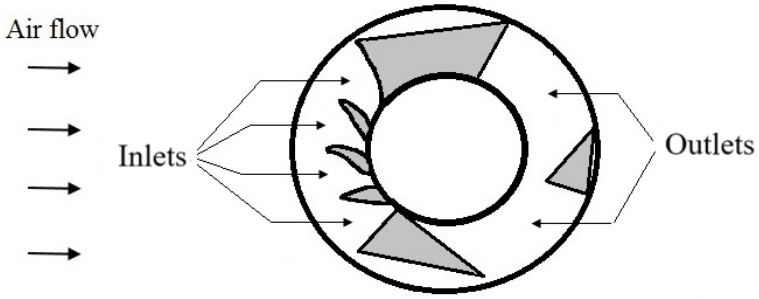

Figure 2.17: Cross-section of power augmented guide vane

Table 2.1: Summary of augmentation devices for unidirectional drag type VAWT

No.	References	Design	Rotor type	Method of investigation	Enhance-ment in C_P	Figure No.	Remarks
1	Takao et al., 2009	Guide vane row	3 straight bladed H rotor	Experimental	1.8 times	Figure 2.1	Increase positive torque
2	Kim and Gharib, 2013, 2014	Straight blade upstream deflector	5 straight bladed H rotor	Experimental	3 times	Figure 2.2	Increase positive torque
3	Jin et al., 2018	Straight blade upstream deflector	3 straight bladed H rotor	Experiment; RANS simulation; SST turbulence model	36.36%	Figure 2.3	Reduces negative torque
4	Stout et al., 2017	Curved plate deflector	3 straight bladed H rotor	Experiment and RANS simulation with RNG turbulence model	1.266%	Figure 2.4	Reduces negative torque
5	Zhao et al., 2021	Rhombus deflector	3 straight bladed H rotor	2.5D simulation (STAR CCM+) with Spalart-Allmaras model	23%	Figure 2.5	Increases wind velocity and improves the angle of attack

Continued on next page

Table 2.1 – continued from previous page

No.	References	Design	Rotor type	Method of investigation	Enhance-ment in C_P	Figure No.	Remarks
6	Hashem and Mohamed, 2018	Diffuser (wind lens)	2 straight bladed H rotor	2D simulation with realizable turbulence model	3.9 times	Figure 2.6	Increases wind velocity by reducing flow separation
7	Kuang et al., 2022	External diffuser (wind capture device)	3 straight bladed H rotor	3D CFD with IDDES	51.73%	Figure 2.7	Accelerates wind and improves power coefficient
8	De Santoli et al., 2014	Duct	3 straight bladed H rotor	Experiment and CFD simulation	125%	Figure 2.8	Concentrates wind flow
9	M. H. Mohamed et al., 2010, 2011	Straight plate	2 and 3 bladed Savonius rotor	OPAL software with turbulence closure model; validated with experimental data (Hayashi et al., 2005)	27% for both	Figure 2.9	Creates obstacle for the returning blade
10	Shikha et al., 2003	Convergent nozzle	5 straight bladed H rotor	Experimental	3.7 times	Figure 2.10	Concentrates airflow

Continued on next page

Table 2.1 – continued from previous page

No.	References	Design	Rotor type	Method of investigation	Enhance-ment in C_P	Figure No.	Remarks
11	Mohammadi et al., 2018	Subsonic convergent nozzle	2 bladed Savonius rotor	CFD simulation with SST turbulence model	3 times	Figure 2.11	Concentrates airflow
12	Altan and Atilgan, 2008, 2010	Curtain plate	3 straight bladed H rotor	Experiment and CFD simulation with RNG turbulence model	38.5%	Figure 2.12	Concentrates airflow and reduces negative torque
13	Irabu and Roy, 2007	Guide-box tunnel	2 and 3 bladed Savonius rotor	Experiment	1.23 times (2 bladed), 1.5 times (3 bladed)	Figure 2.13	Reduces negative torque by concentrating airflow
14	Shaughnessy and Probert, 1992	V-shaped deflector	2 bladed Savonius rotor	Experiment	20%	Figure 2.14	Guides wind stream

Continued on next page

Table 2.1 – continued from previous page

No.	References	Design	Rotor type	Method of investigation	Enhance-ment in C_P	Figure No.	Remarks
15	Nimvari et al., 2020	Porous deflector	2 bladed Savonius rotor	CFD simulation validated with experimental data Sheldahl et al., 1978	10%	Figure 2.15	Reduces wake behind deflector and improves self-starting ability
16	El-Askary et al., 2015	Guide plate	2 bladed Savonius rotor	CFD simulation validated with Fujisawa and Gotoh, 1992	1.6 times	Figure 2.16	Increases positive torque and reduces negative torque
17	W. T. Chong et al., 2012, 2013	PAGV	Sistan turbine	Experiment and CFD simulation validated with Oler et al., 1983	5.8 times	Figure 2.17	Positive torque increases by deflecting airflow

The summary of augmented devices for unidirectional VAWT is shown in Table 2.1. It may be noted that most of the experiments have been performed with deflectors of different shapes as an augmentation device to reduce negative torque on the blades for Darrieus lift type VAWT. Augmentation up to 125% was achieved when a duct was introduced at the inlet although such modifications call for a strong support structure. In case of Savonius drag type VAWTs, convergent nozzle and different shaped guide plates were used as an augmentation device for most of the experiments. However, PAGV integrated VAWT system provided optimum results and enhanced power output by 5.8 times.

2.2.2 Omni directional flow

One of the limitations of the single-direction wind flow VAWT is that, there must be a yaw mechanism for augmentation systems. In the case of omni directional wind flow VAWT, the augmented devices can capture wind from any direction and there is no requirement for a yaw mechanism.

2.2.2.1 Darrieus lift type VAWT

A lift type VAWT with an H rotor surrounded by omni directional guide vanes (ODVG) was suggested by W. Chong et al., 2013. These omni directional guide vanes usually have two wall ducts, located at the upper side and lower side as shown in Figure 2.18. As the guide vanes direct the wind to VAWT blade at an optimum angle of attack, the wind speed increases and the self-start behaviour also improves. Negative torque and fluctuation in speed due to turbulence were reduced by using these omni directional guide vanes. While the system works efficiently in a turbulent regime, the drawback is the high initial setup cost. A wind tunnel experiment was performed with an H-type VAWT having a five-bladed rotor. Results showed that the torque coefficient increased by 58% at a TSR of 2.5 and 39% at a TSR of 5.1. The rotational speed of the turbine was increased by 182% and there was an improvement in output power by 3.48 times when compared with VAWT without guide vanes.

Minor modifications to the ODGV were performed by Wong et al., 2014 as shown in Figure 2.18(c) by dividing the vanes into two parts with a 10° angle bent. Results found that the modified guide vanes further enhance the airflow velocity in the second half of the cycle. There was an increase of 31.65% in power coefficient compared with original ODGV and 147.1% when compared with a single VAWT.

An omnidirectional stator mounted around an H-rotor VAWT was introduced by Nobile et al., 2014 where the stator part has two conical surfaces as depicted in Figure 2.19. The back pressure is reduced inside the stator part as conical surfaces cause turbulent mixing. NACA0018 airfoil shapes were used for the straight blade to cap-

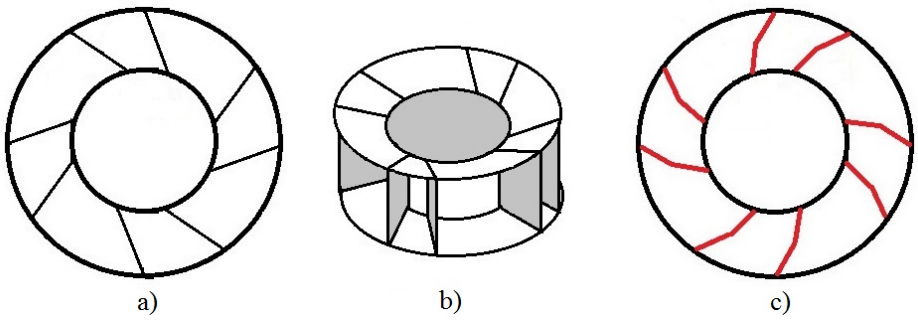

Figure 2.18: (a) Top view of original ODGV (b) isometric view of ODGV (c) a special designed of ODGV

ture the wind. The converging and diverging surfaces on upstream and downstream sides accelerated and decelerated the flow respectively. The shading regions generated by the stator blade reduced the drag forces at the downstream side. So, higher positive torque was generated in the downstream region. Three different pitch angles of the blade, $+30°, 0°$, and $-30°$, were studied for the performance analysis of the rotor. CFD results suggested that there was an increase of 30–35% in average CP and CT at TSR of 2.75 when compared with VAWT having no stator vanes. The optimum performance was found at $0°$ pitch angle.

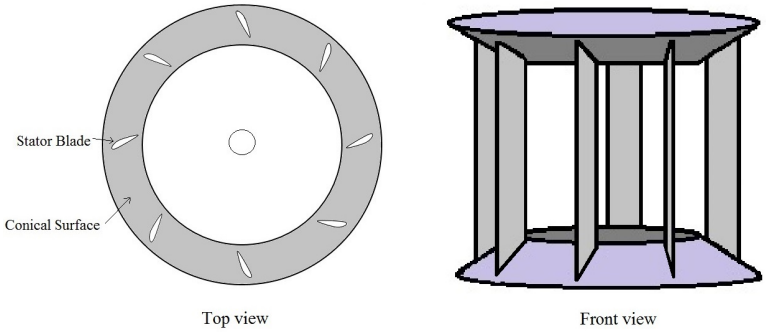

Figure 2.19: Novel stator design of augmented VAWT

Y. Li et al., 2018 proposed a new wind gathering device (WGD) incorporated with VAWT to improve the performance as illustrated in Figure 2.20 (a). Instead of surrounding the rotor, this truncated-cone-shaped WGD was installed at upper and lower sides of the H-rotor to gather more wind at increased velocity. Wind tunnel test and numerical investigations were performed to study the structural parameters including height of the WGD, cone angle and the distance from the rotor with the help of the quadratic orthogonal rotation combination design (QORCD) method. Results showed the improvement in both static torque and power coefficients when cone angle was at 45° and cone height was less than 60% of rotor height. An improvement of 25% in torque coefficient was achieved when compared with bare VAWT.

Further research was carried out on WGD by changing the shape to a curved-outline

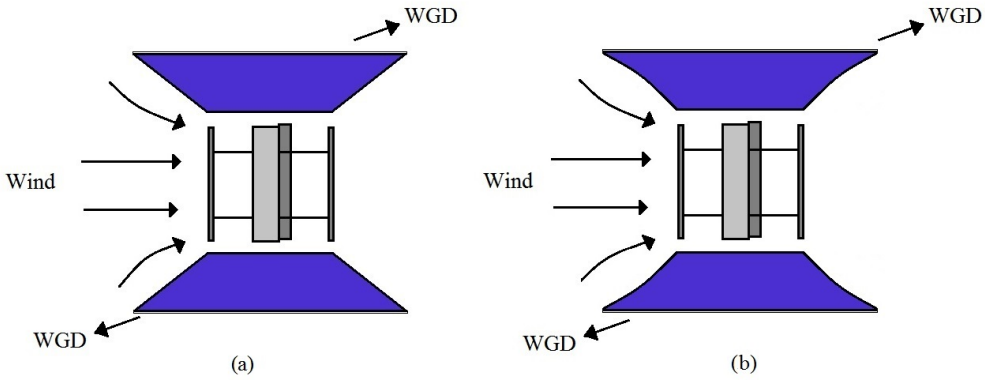

Figure 2.20: (a) Truncated-cone-shaped WGD and (b) curved-outlined-shaped WGD

to reduce the size of the WGD (Y. Li et al., 2020) as shown in Figure 2.20(b). The curved-outline shape is formed by a B-spline curve of cubic fourth order. Results showed that the maximum power coefficient was enhanced by 13.3%, especially at low wind speed and the maximum starting moment increased by 14.8% at 16° inlet and 4° outlet angle.

2.2.2.2 Savonius drag type VAWT

Burlando et al., 2015 presented a new flow augmentation technique of drag type VAWT with airfoil-shaped stator vanes. A numerical wind tunnel technique was used to investigate the flow around the multi-stage VAWT. The position of stator vanes around the three-bladed rotor is fixed with respect to the inlet at a phase difference of 120°. The wind flow converges when passing through the space provided between the stator blades and thus avoiding the speed-up effect in a multi-stage rotor. Experimental and numerical results showed that the wind speed increases up to 10% at the entrance between stator vanes.

Experimental and simulation work were performed on Zephyr type omni-directional drag type VAWT by Pope, Dincer, and Naterer, 2010; Pope, Rodrigues, et al., 2010. Figure 2.21 illustrates Zephyr VAWT having stator vanes with reverse winglets or tabs mainly used in urban areas. This design performs well at low TSR due to its higher solidity ratio although the peak performance is lower during strong wind blows. The stator vane with no tabs model shows a better power coefficient than the tabular stator vane. The tabular designed stator vane has a maximum power coefficient of 0.098 at 0.43 TSR whereas the no tab model predicted a peak power coefficient of 0.12 at 0.48 TSR.

A vortical stator assembly (VSA) was introduced by T.-Y. Chen and Chen, 2015 to improve the power coefficient of a drag type VAWT rotor with six numbers of half-tube blades. The VSA has two loop plates at the top and bottom and six numbers of guide vanes are installed in between two loop plates as shown in Figure 2.22. A strong vortical

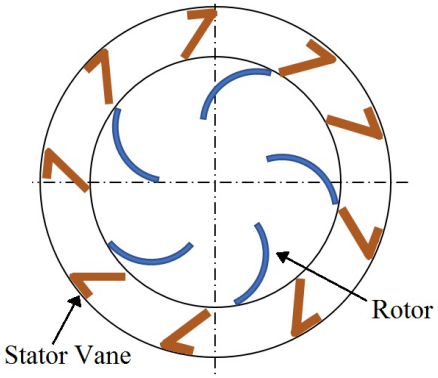

Figure 2.21: Top view of Zephyr type VAWT

flow is generated as air comes from all directions entering tangentially in the VSA due to the arrangements of guide vanes and thus increasing the wind speed and reducing the negative torque on the returning blade. To assess the performance of VSA, a wind tunnel model-based experiment was conducted by varying the number and length of guide vanes and outer VSA diameter. The results predicted that a VSA with 6 numbers of guide vanes has the peak performance where the diameter of VSA was about 1.82 times the rotor diameter. At 6 m/s, VSA was able to enhance the rotational speed, maximum power output and torque by 318%, 910% and 200% respectively.

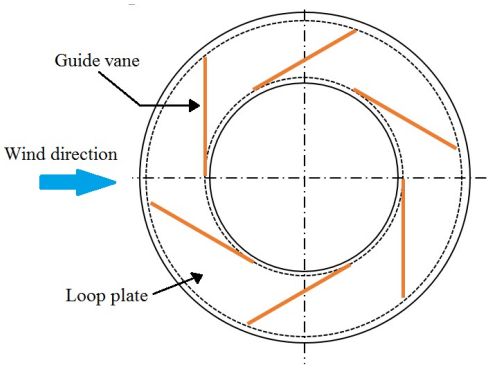

Figure 2.22: A six guide vane VSA

A new technology called rotor house surrounding Savonius VAWT was proposed by Manganhar et al., 2016. The wind accelerating and guiding rotor house (WAG-RH) consists of four vertical walls, which are separated by equal distance and tilted by $45°$ with the axis, as shown in Figure 2.23. These four walls are supported by hollow round plates at the top and bottom. Tilted walls reduce negative torque by directing the wind stream to returning blades and the wind velocity increased in the rotor space due to the venturi effect created by WAG-RH. Experimental work was performed by Manganhar et al., 2019 which showed that the WAG-RH was able to increase the power coefficient up to 0.218 from 0.125. As the rotor is enclosed in the rotor house, it provides safety for birds and also improves visual aesthetics.

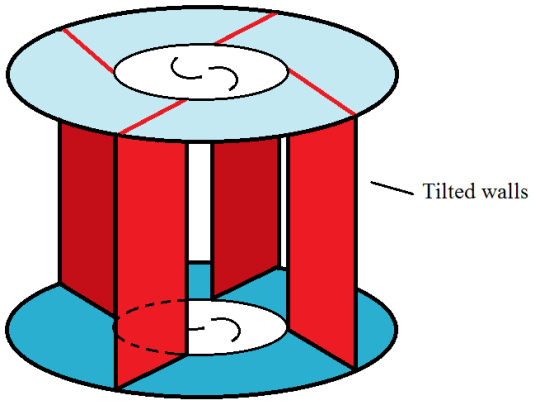

Figure 2.23: Savonius rotor surrounded by WAG-RH

Kalluvila and Sreejith, 2018 suggested some modifications to the rotor and introduced a guiding blades system around the drag type Savonius turbine for low wind speed regions with high turbulence. This system is comprised of eight guide blades with two different angular arrangements. Four blades are inclined at $6.7°$ with a radial line and the remaining four make a $45°$ angle with the radial line as presented in Figure 2.24. Wind tunnel experiments and CFD simulations were carried out to investigate the performance of VAWT. Results revealed that the maximum power coefficient reached a value of 0.28 at a TSR of 0.85 with these guide blade arrangements. The turbine performs efficiently in low wind speed regions and shows better self-start ability due to increased torque.

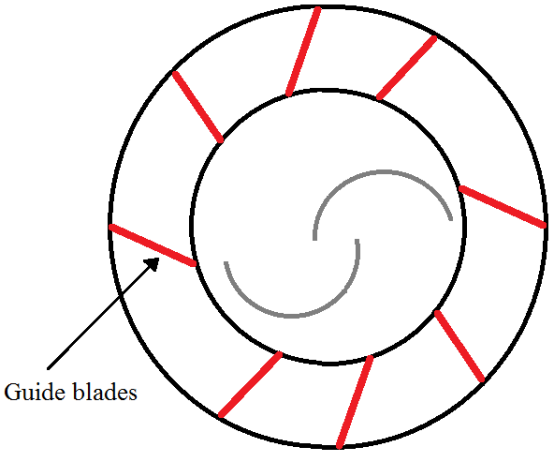

Figure 2.24: Savonius rotor with guide blades design

Tian et al., 2019 introduced a 20 bladed 'Banki' turbine with a passive-pitch shield (PPS) which could capture the wind from any direction by adjusting its pitch angle passively. Figure 2.25 illustrates the passive pitch shields consisting of two plates, installed on the upstream side and a downstream side. The upstream plate is placed perpendicular to the wind flow direction to reduce negative torque generated during the upwind

half-cycle by preventing the wind flow. The downstream plate is placed parallel to the wind flow direction and its function is to change the angle of PPS according to the wind flow direction. An improvement of 46.32% in power coefficient was noticed from the results for the A-type shield and the arc type shield was least effective.

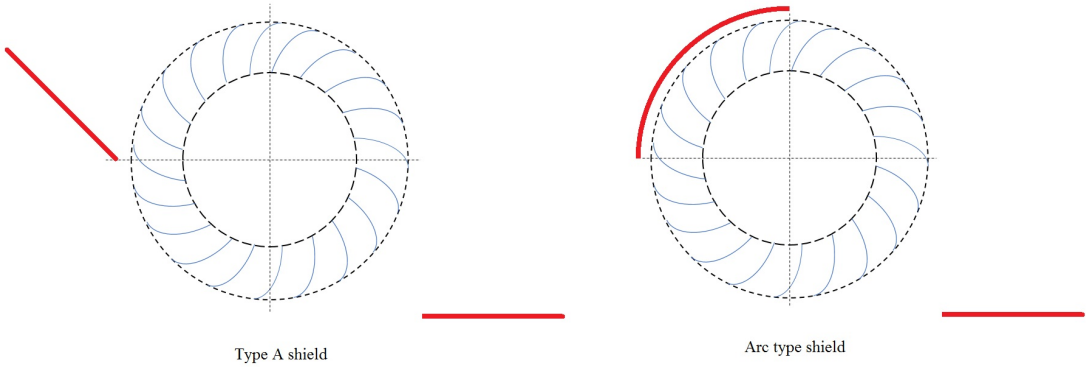

Figure 2.25: Two different passive pitch shield design

The summary of augmentation methods for omnidirectional VAWT is tabulated in Table 2.2 which shows that ODGV and stator vanes performed better as augmentation devices in all operating conditions by concentrating the airflow to increase the positive torque. VSA was able to increase the maximum power output by 910%.

Table 2.2: Summary of studies on augmentation devices for omnidirectional VAWT

No.	References	Design	Rotor type	Method of investigation	Enhance-ment in C_P	Figure No.	Remark
1	W. Chong et al., 2013	ODGV	5 straight bladed H rotor	RANS SST turbulence model and experiment	3.48 times	Figure 2.16 a) and b)	Reduce negative torque by concentrating the airflow
2	Wong et al., 2014	ODGV	Single straight bladed H rotor	CFD simulation with SST turbulence model	147%	Figure 2.18c)	Reduce negative torque by concentrating the airflow
3	Nobile et al., 2014	Stator	3 straight bladed H rotor	CFD simulation with SST turbulence model validated with experiment of Ali et al., 2012	30–35%	Figure 2.19	Concentrating the airflow
4	Y. Li et al., 2018, 2020	Wind gathering device	4 straight bladed H rotor	CFD simulation with SST turbulence model	35%	Figure 2.9	Concentrating the airflow and reducing negative torque

Continued on next page

Table 2.2 – Continued from previous page

No.	References	Design	Rotor type	Method of investigation	Enhance-ment in C_P	Figure No.	Remark
5	Burlando et al., 2015	Stator (Airfoil shape)	3 bladed Savonius rotor	Experiment and OpenFOAM simulation with RNG turbulence model	10%	–	Deflect and concentrate the airflow
6	Pope, Dincer, and Naterer, 2010; Pope, Rodrigues, et al., 2010	Zephyr stator vanes	5 bladed Savonius rotor	Experiment and CFD simulation with RNG turbulence model	22%	Figure 2.21	Deflect wind flow and reduce turbulence flow
7	T.-Y. Chen and Chen, 2015	Vortical stator assembly	6 half tube blade rotor	CFD simulation with SST turbulence model validated by experimental data of Sheldahl et al., 1978	910%	Figure 2.22	Concentrating the airflow and reducing negative torque

Continued on next page

Table 2.2 – Continued from previous page

No.	References	Design	Rotor type	Method of investigation	Enhance-ment in C_P	Figure No.	Remark
8	Manganhar et al., 2016	WAG-RH	4 bladed Savonius rotor	CFD simulation (SST turbulence model) and experiments	1.7 times	Figure 2.23	Concentrating the airflow
9	Kalluvila and Sreejith, 2018	Guiding blades	2 bladed Savonius rotor	Experiment and 2D CFD simulation (turbulence model)	–	Figure2.24	Concentrating the airflow
10	Tian et al., 2019	Shield	20 bladed Banki turbine	CFD simulation (SST turbulence model)	46.32%	Figure 2.25	Deflect wind flow and reduce negative torque

2.3 Innovative designs for augmentation of VAWTs

In this section, some novel power augmentation devices are discussed such as cowling, INVELOX, shrouds shaped turbine, hybrid model and cross axis wind turbine (CAWT) that are different in designs from typical wind turbines. The wind that enters into the augmentation system may be from a horizontal direction, a particular direction or all directions and exits in a perpendicular direction downwardly or upwardly.

2.3.1 Cowling devices

A new concept of cowling device incorporated with VAWT that produces higher efficiency in a wider range of wind speeds was proposed by Alam and Golde, 2013; Ali et al., 2012. Wind Energy Technology Pty Ltd. Australia developed this new cowling device comprised of an inner vent tube around the turbine, an induction chimney and an outer tail section as shown in Figure 2.26. When the cowling device is aligned with the incoming wind, the outer tail section guides the wind to flow evenly over both sides of the cowling. A pressure difference is created on both sides of the turbine when the cowling is not aligned with the incoming wind. This mechanism leads to smooth performance of yaw mechanism. The inner vent tube guides the flow to recirculate inside the VAWT and the chimney allows the airflow to exit from the cowling. It also induces a swirling effect due to the pressure difference created at the vent tube which increases the driving force of the turbine. CFD simulation, as well as a wind tunnel experiment, was conducted which showed the rotational speed of the turbine covered by cowling has increased by 3 times as compared to that of the bare rotor.

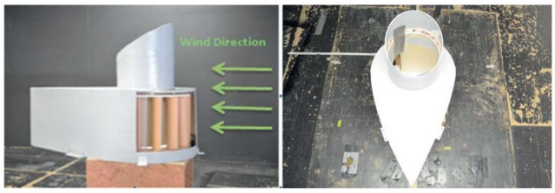

Figure 2.26: Wind turbine with cowling device (Ali et al., 2012)

Loganathan et al., 2015 performed a similar study on a cowling device that was employed in a cyclonic VAWT as depicted in Figure 2.27. The cowling device has many shells of cylindrical shapes that surround the turbine with small gaps. As the wind enter the turbine, it forces the concave blades to rotate and exit upwardly from the outlet. The wind cannot interact with the returning convex blades as the half portion of the outer shell is remain in a closed position always and the inner shell prevents the wind to discharge through the rear blades rather it guides the wind to the top outlet. The main feature of this device is that it is able to reduce the negative torque by guiding the

wind direction coming from the rear blades and exhausting to the atmosphere and thus increasing the efficiency. For experiments, 8 and 16 numbers of blades for the cyclonic turbine were tried. It was found that the turbine with lower numbers of blades showed better performance and the cowling device was able to increase the rotational speed of the rotor by 40% for 8 bladed wind turbine and by 26% for 16 bladed wind turbines.

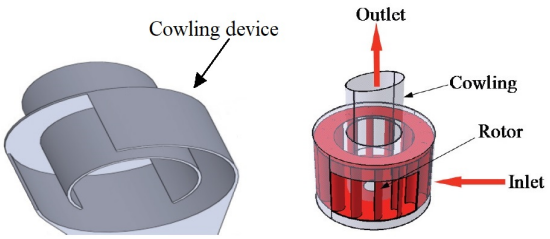

Figure 2.27: Cowling device on cyclonic VAWT (Loganathan et al., 2015)

Y. X. Yao et al., 2013 presented a new type of VAWT with tower cowling where a Savonius drag type wind rotor is mounted in the cylindrical space available at the centre of the tower. The tower has eight baffle plates surrounding the wind turbine which is shown in Figure 2.28. These adjustable baffle plates help to generate positive torque by forcing the wind on the inner part of the blades. Subsequently, it reduces the negative torque by preventing the wind to force on the outer parts of the blade. This cowling increases the incoming wind speed of the VAWT which produces higher torque and also improves self-start behaviour. The tower has been provided with an extended roof on each floor for easy maintenance of wind turbine and thus which increases the fatigue life and lowering the maintenance cost. Numerical simulations have been performed on both wind turbines with tower cowling and without tower cowling which indicated a 2.4 times enhancement in power coefficient for tower cowling design. RNG k-ε model has been used for turbulence closure using Fluent software. Results show a high static pressure difference created at the blades of the turbine with tower cowling that provides a large pushing force on the blades. The optimum performance is obtained when the diameter of the tower cowling set at 800 mm and 8 numbers of arc-shaped baffles tilted at 15° angles. The wind rotor is configured with two blades, each having 210 mm chord length and 10° blade obliquities providing the maximum power coefficient of 0.48 at a TSR value of unity.

2.3.2 INVELOX design

Allaei and Andreopoulos, 2014; Allaei et al., 2015 suggested a new technology to harness wind energy called INVELOX (increased velocity) which acts as a wind delivery system with increased velocity to the wind turbine as shown in Figure 2.29. In this technology, the wind is captured omni- directionally by a funnel and forced to pass

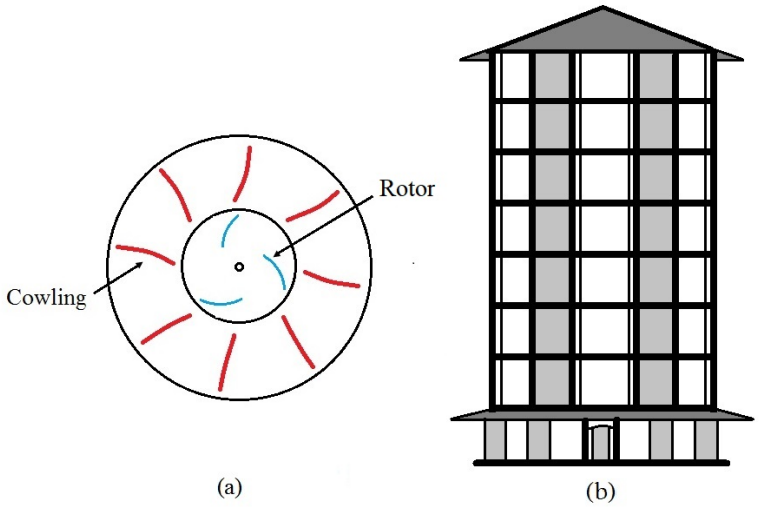

Figure 2.28: (a) Cross-sectional top view of cowling and (b) Tower cowling

through a tapering passage that automatically increases the wind flow. It has 5 primary components, i) intake part, ii) wind accelerating section, iii) Venturi section for boosting wind speed, iv) turbine and energy converting devices and v) diffuser part. The design offers three distinct advantages over conventional wind turbines. First, its omni directional wind capturing capability eliminates the need for yaw control. Second, its venturi section enhanced the velocity of wind passing through the turbine. Lastly, it eliminates the tower mounted turbines that are complex, large and inefficient. The turbine generator system is placed at grounded horizontal section of INVELOX which reduces the installation and maintenance cost while providing solutions to issues like radar interference, environmental impact and optical flickering. The separate locations of wind capturing shroud and turbine generator system allow designers to increase the intake size according to speed requirements by maintaining the same turbine size. CFD simulation and field demo tests were conducted in Chaska, Minnesota to investigate the flow filed inside INVELOX. Finite element-based discretization based COMSOL and FVM discretization based ANSYS software were used for numerical calculations and these results were compared with field demo test data. A Realizable turbulence model was used for closure. Results showed that the INVELOX system was able to produce 80 - 560% more electrical power when compared with traditional wind turbines. The total average energy production was estimated to increase by nearly 314%. However, a strong support structure is needed due to its large size. Modifications of INVELOX design by using the nozzle diffuser section and by introducing a novel curtain design were studied by researchers (Anbarsooz et al., 2019; S. R. Hosseini & Ganji, 2020; Nardecchia et al., 2021; Patel, 2018; Sotoudeh et al., 2019).

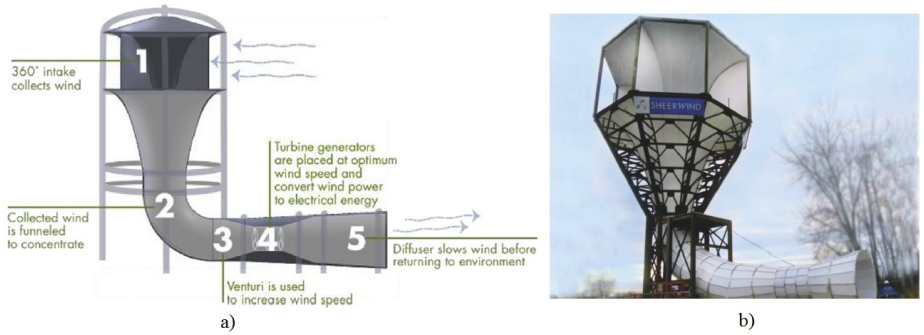

Figure 2.29: a) INVELOX with 5 components b) Demo of fielded INVELOX (Allaei & Andreopoulos, 2014; Allaei et al., 2015)

2.3.3 Omni directional shroud

Zhang et al., 2013 conducted CFD modelling as well as wind tunnel tests on a shroud shaped wind turbine as represented in Figure 2.30. The hemispherical shroud and turbine blades were the two main components of the whole structure. The shroud has five chambers of diffuser shape that can collect wind from omni-direction with increased velocity and guided it to the upward direction where the turbine is placed. The turbine working on impulse principles had twisted shaped blades which was used to improve the self-start ability under variable wind environments and the shroud structure provided protection for the turbine. A three-dimensional numerical investigation was performed by Star CCM+ software with turbulent model and the results were validated by experiments. Results showed that the outlet velocity increased by 1.3 times of inlet velocity and wind energy increased by 2.5 times. This novel design is capable of working under different wind conditions, especially in urban areas with low wind speeds. However, the turbine experienced a non-uniform flow distribution around blades and variable aerodynamic loads were acting on blades as the wind passed through one or two sections of the shroud system at a given instant.

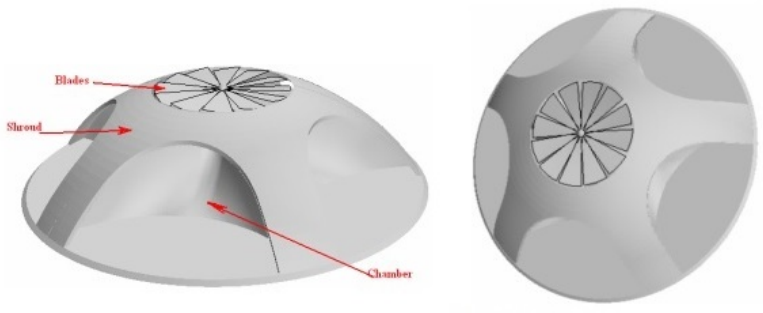

Figure 2.30: Novel wind turbine with shroud structure (Zhang et al., 2013)

Ying et al., 2015 further studied the non-uniformity of flow behaviour in shrouds by numerical analysis and validated it with a wind tunnel test. An impulse turbine was used for the investigation which had a stator part consisting of guide vanes. Thin plate

guide vanes had an arc-shaped geometry in front which became straight at the rear. This geometrical feature increases the approaching wind velocity and directed it to turbine blades with a better angle of attack. The wind turbine model was shielded by a cover with a 20-40% opening to investigate the non-uniform flow behaviour. Numerical simulations were carried out to study the effect of the number of blades on C_P by Star CCM+ finite volume-based software incorporated with the Realizable turbulence model. The optimum power coefficient was achieved with the impulse turbine having 20 blades. Experimental results revealed that the self-start ability of the turbine was improved significantly even under a low wind velocity of 1.6 m/s. Maximum CP was found in the range of 0.06-0.12 under 20-40% non-uniform flow passing area, which was 29-65% less as compared to uniform flow.

2.3.4 Hybrid wind turbine

Bhuyan and Biswas, 2014 proposed a hybrid system that comprised both lift type H-rotor and Savonius drag rotor to overcome the self-starting issue. The Savonius rotor was incorporated with the Darrieus turbine to enhance its self-starting ability and it acted as a starter for the whole hybrid system. Experiments were conducted for different Re numbers and different overlap ratios. Results showed that the device is able to self-start for all angular positions as the positive torque value increases and it performed way better than other lift types VAWTs. The maximum power coefficient was found to be 0.34 at a TSR of 2.29 for a 0.15 overlap ratio.

Numerical analysis has been performed by A. Hosseini and Goudarzi, 2019 on a new hybrid model where a Bach-type Savonius rotor was incorporated with a Darrieus turbine. This hybrid design is having two tiers and one 3-bladed Darrieus turbine with four numbers of 2-bladed Bach type Savonius turbine installed in each tier as depicted in Figure 2.31. URANS equations were solved by ANSYS fluent and SST model was adopted for turbulence modelling. Results predicted that a maximum power coefficient of 41.4% was obtained at a TSR value of 2.5 and the system was highly efficient in a wide range of operating conditions.

2.3.5 Cross axis wind turbine

A novel cross axis wind turbine (CAWT) was proposed by W.-T. Chong, Muzammil, et al., 2017; W.-T. Chong, Wong, et al., 2017 to overcome the limitations of both HAWT and VAWT. The CAWT consists of three vertical blades connected with six horizontal blades by connectors as presented in Figure 2.32. CAWT can capture the wind from both omni-direction and the bottom of the turbine through the horizontal and vertical blades. Vertical airflow from the bottom side is caused by the elevation of buildings or guide vanes or omnidirectional shrouds. Horizontal blades generate a lift force

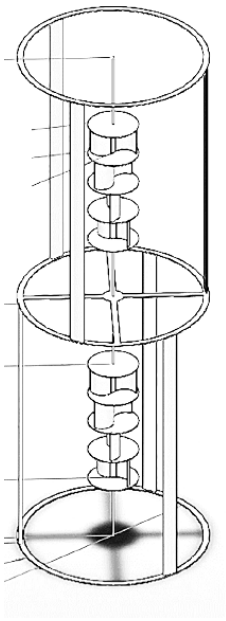

Figure 2.31: Bach type Savonius turbine with H-rotor in a hybrid model (A. Hosseini & Goudarzi, 2019)

while interacting with vertical wind flow resulting in an improved self-start ability. An experimental test was conducted on roof-top CAWT and results showed that the maximum rotational speed achieved by CAWT was 166% higher as compared to VAWT. Numerical analysis was carried out on CAWT incorporated with a guide vane shroud at the bottom of the turbine. The shroud was made up of a series of deflectors that collect the wind from all directions and delivered it to CAWT in an upward direction. CFD simulation was performed to investigate only the flow behaviour by selecting the SST turbulence model. Analysis showed that guide vanes deflected the horizontal wind to vertically upward direction and deflected wind interact with the CAWT.

2.4 Blade modification for achieving augmentation

Several studies have been performed to improve the overall performance of VAWT by modifying the geometrical configuration of turbine blades without requiring any extra augmentation components(Al-Ghriybah et al., 2019, 2021; Bianchini et al., 2019; J. Chen et al., 2015; Das Karmakar et al., 2023; Hara et al., 2014; Ismail & Vijayaraghavan, 2015; O. S. Mohamed et al., 2020; Reupke & Probert, 1991; Roshan et al., 2021; Saad et al., 2021). Figure 2.33 shows the Different blade modification techniques that are able to provide better self-start ability. Airfoil modification techniques include slatted blade with flaps, slotted airfoil, gurney flap with dimple, single cavity airfoil, rotor with inner blades, double-bladed rotor and twisted blade rotor.

Reupke and Probert, 1991 introduced a Savonius rotor with slatted blades and the

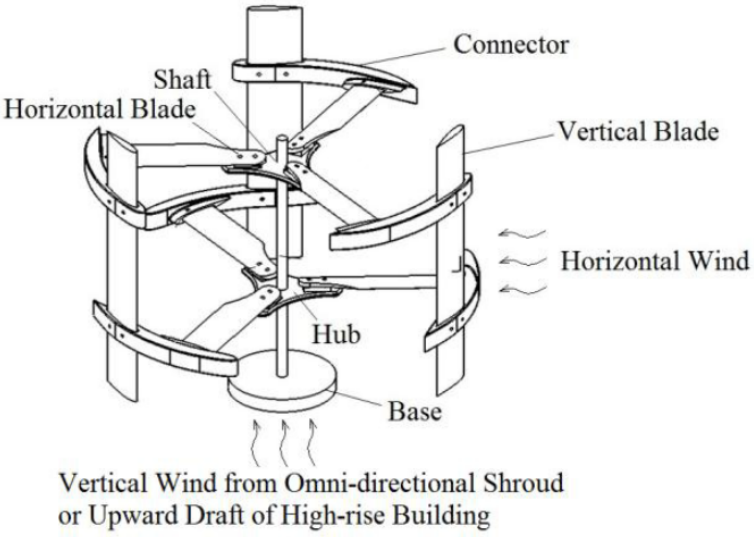

Figure 2.32: Structure of CAWT (W.-T. Chong, Muzammil, et al., 2017; W.-T. Chong, Wong, et al., 2017)

curve blades having an array of hinged flaps mounted on it. The negative torque reduces significantly on the returning blade when the flaps open due to pressure differences developed on the two sides of the blade. At very low TSR, higher torque is generated by the slatted Savonius VAWT as compared to that of the traditional VAWT. Although, the self-starting capability improves with the introduction of slatted blade, the peak power coefficient decreases from 0.18 to 0.05. A turbine with slotted airfoil blades was introduced by O. S. Mohamed et al., 2020. Due to the pressure difference between the upper and lower side of the blade, a slot helps to generate a jet flow which eliminates the flow separations at a medium angle of attack. Maximum CP was found to be 0.3 at a TSR value of 2. Ismail and Vijayaraghavan, 2015 suggested a modification to the blade design which has an inward semi-circular dimple and a Gurney flap at the trailing edge of the NACA-0015 airfoil. It maximises the torque coefficient rather than increasing the lift coefficient. The average tangential force was increased by up to 40%. A new design of the Darrieus turbine having vertically straight blades with an opening near the trailing edge was proposed by J. Chen et al., 2015. The new arrangement enhanced the self-starting ability of the Darrieus turbine but the overall CP was decreased. Roshan et al., 2021 investigate the effect of blade cavities on the performance of VAWT. Maximum CP was enhanced by 18% at a TSR of 3.5 when a single cavity was provided on the upper surface near the trailing edge of the blade.

Al-Ghriybah et al., 2019, 2021 studied the influence of two inner blades on the overall performance of Savonius VAWT. Different blade angles were investigated and numerical results showed that the maximum power coefficient of 0.19 was obtained at a TSR of 0.5 with a 120° blade angle when the inner blade was installed parallelly with the rotor tip. Hara et al., 2014 introduced a double-bladed VAWT where the inner and outer

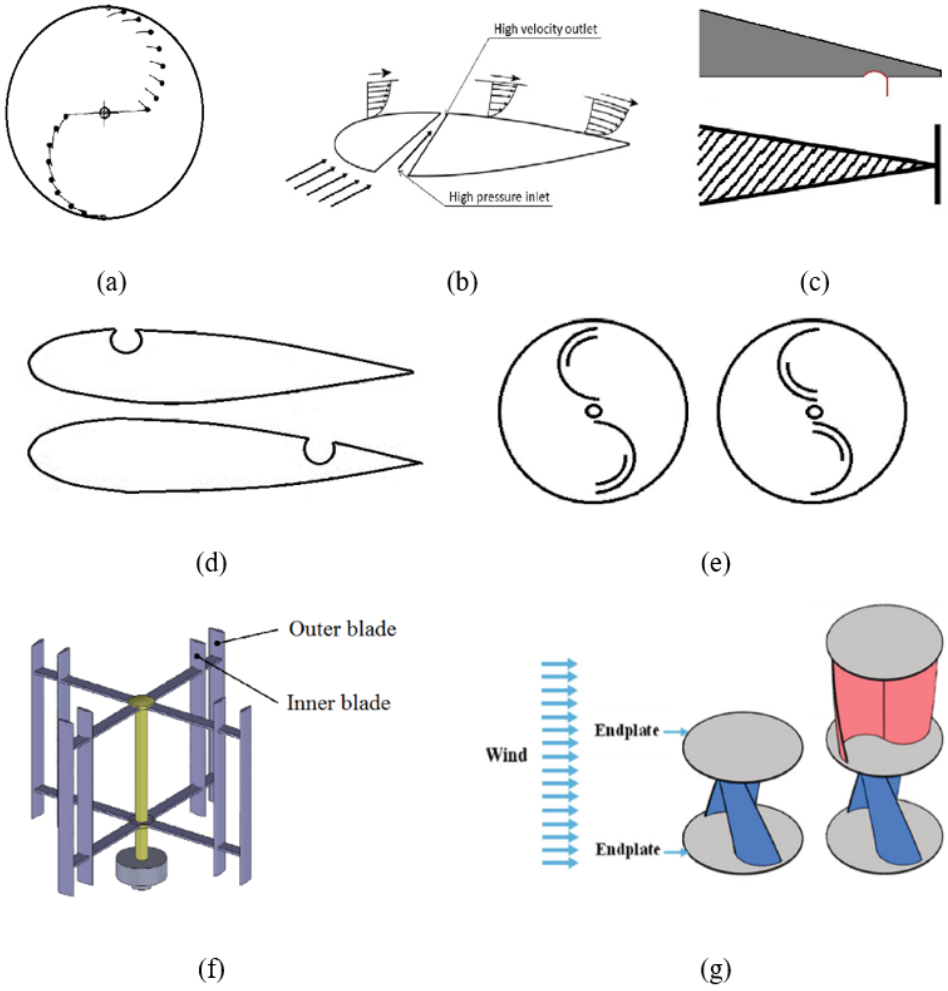

Figure 2.33: Different turbine blade modification techniques (a) slatted rotor with 16 flaps (Reupke & Probert, 1991) (b) slotted airfoil (O. S. Mohamed et al., 2020) (c) gurney flap with dimple (Bianchini et al., 2019; Ismail & Vijayaraghavan, 2015) (d) single cavity airfoil (Roshan et al., 2021) (e) Savonius rotor with inner blades (Al-Ghriybah et al., 2019, 2021) (f) double-bladed VAWT (Hara et al., 2014) (g) single and two-stage rotor with twisted blades (Saad et al., 2021)

blade is connected to the rotor arm. This blade modification improves self-start ability and delivered large starting torque than a single blade rotor. A twisted blade multi-stage Savonius rotor was developed by Saad et al., 2021. The twisted blade design is able to improve self-start capability and is suitable for very low wind speed regions. The new configuration led to a maximum C_P of 0.253 and 0.261 for two-stage and four-stage rotor respectively.

2.5 Building integrated augmentation system

When wind turbines are installed within buildings in urban areas, such systems are known as building integrated wind turbines. They can independently supply the generated power directly to the buildings reducing transmission power losses (Balduzzi et al., 2012). In 1930, Hermann Honnef, a German engineer first introduced the design concept of BIWT, to achieve power generation in the urban region (Heymann, 1998). There are mainly two categories of building integrated wind turbines (BIWTs) depending on the number of turbines and the position and their application. For the first category, one or two large-sized wind turbines are installed at the top of the high-rise buildings or positioned in between adjacent passages of two buildings or placed at a specially designed hole within a building. For the second category, several small wind turbines can be installed at the corner or a ridge of a building (W. T. Chong et al., 2016; Dayan, 2006; X. H. Wang et al., 2017). The efficiency of a turbine can be increased by harnessing the building aerodynamics as a concentrator to enhance the wind speed approaching towards turbine (Aguilo et al., 2004). Another way is to increase the efficiency by utilising the pressure differences between the buildings. When the wind is passing through high rise buildings in urban areas, the pressure difference is created on the windward and leeward faces of the buildings. The mean wind flow around a tall building is shown in Figure 2.34.

Wake and vortices create a positive pressure zone on the upwind side and negative pressure on the downwind side. This pressure difference increases the speed of the wind at the corner or edge of the buildings which are the best positions to install wind turbines (Dannecker & Grant, 2002; Grant et al., 2008). Buildings may be designed with some unique passages that connect low and high-pressure regions where the wind turbines can be easily mounted (Ayhan & Sağlam, 2012). Bahrain World Trade Centre is a very good example of BIWT. However, Visual aesthetics, flow augmentation, modularity, performance in turbulent conditions and ease of installation are the few desirable characteristics of BIWTs (Sharpe & Proven, 2010). Several researchers have presented augmentation devices specially designed to integrate with buildings for electricity generation.

Sharpe and Proven, 2010 proposed a Darrieus turbine with an innovative design

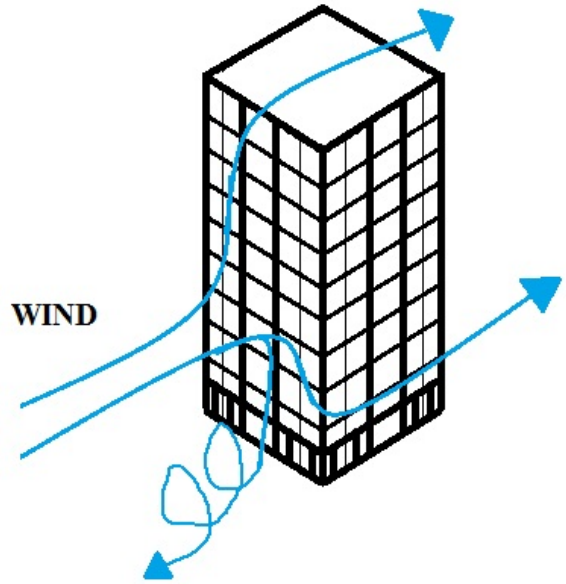

Figure 2.34: Wind flow around a tall building

called Crossflex having a flexible blade system. A cowling system integrated with Crossflex improves the flow augmentation by concentrating the wind flow. The design also beautifies the overall architecture of the building. In order to capture the wind of high concentration, the Crossflex system was placed at the ridge of the high rise building as shown in Figure 2.35 (a). It does not require a yawing mechanism. However, vibration on the building, load distribution and need of fixing arrangements are a few drawbacks of this system.

A new design BIWT have been introduced by Park et al., 2015 where wind turbines are mounted on the unutilized area of building skin combined with guide vanes. Figure 2.35 (b) shows the schematic diagram of BIWT combined with guide vanes that are installed in the empty region of the building skin. Incoming wind converges and accelerates due to the adjustable guide vanes and hence improves the overall performance of this system as the coefficient of power is proportional to the cube of incoming wind speed. Wind passing through the turbine flows out easily through an empty region formed between the building skin and the series of guide vanes. That empty region creates a pressure difference between adjacent guide vanes. To get an optimal design, a series of numerical simulations have been performed on the guide vanes, the shape of the rotor blades and the number of the blades by using the standard $\kappa - \omega$ model.

Their analysis showed that a smaller diameter rotor cannot generate adequate torque and the larger diameter rotor performed very poorly due to the narrow space at the back of the guide vanes. Results found that a wind turbine which has an eight-bladed rotor with a diameter of 30 cm provides the optimum performance. Two-step experiments were conducted for the performance evaluation of the guide vanes and the rotor on the

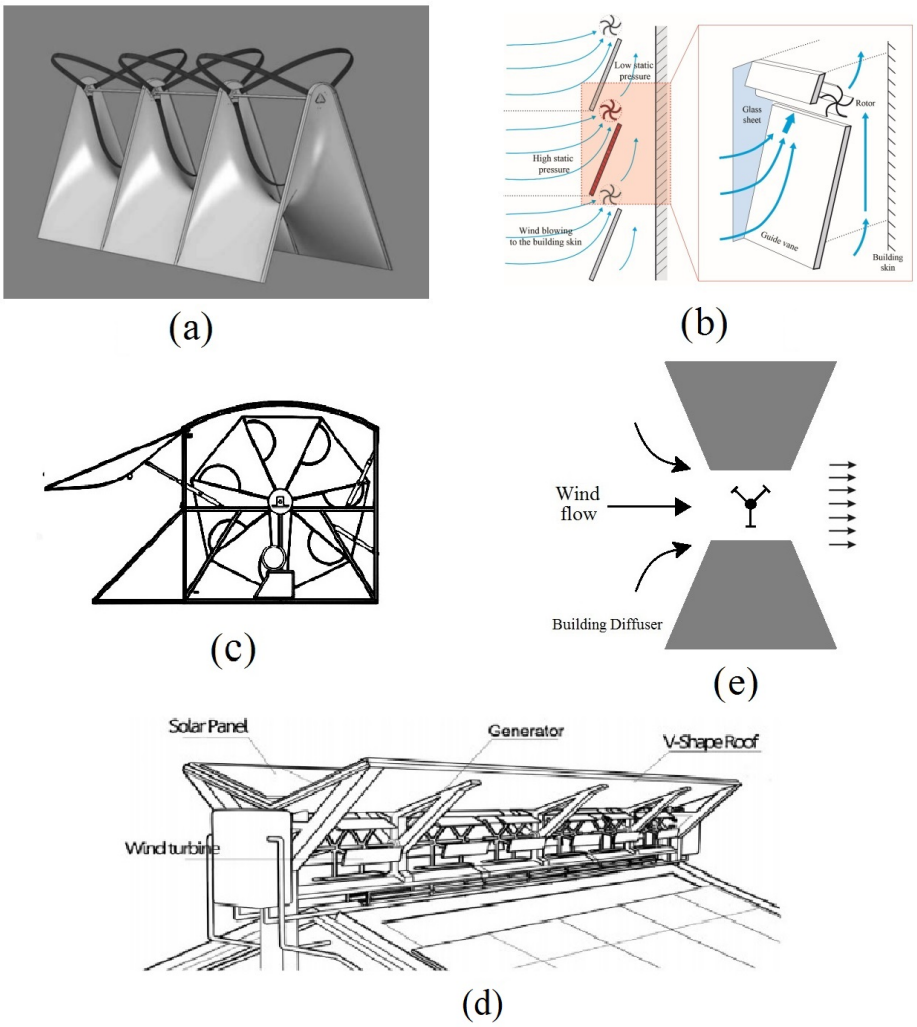

Figure 2.35: Different building integrated augmentation systems: a) Design of a Cross-flex turbine(Sharpe & Proven, 2010), b) BIWT combined with guide vanes c) Diffuser shaped shroud d) Vertical axis wind turbines below the V-shape roof (W. T. Chong et al., 2016) e) Top view of Trapezium BA-VAWT

optimum design. It was found that the power coefficient, C_P of the rotor was 0.381.

Krishnan and Paraschivoiu, 2016 proposed a wind turbine system integrated with a diffuser shaped shroud installed on the building roof to optimize a prototype VAWT developed by Groupe LML company, Canada. Realizable $\kappa - \varepsilon$ model was chosen and their outcomes were compared with the experimental data of Hayashi et al., 2005. The original diffuser shroud system is shown in Figure 2.35 (c). There was an increase in wind flow over the building due to the presence of the diffuser shroud system improving the wind turbine performance. A Savonius type rotor with a cylindrical shaped turbine was used in the system. The system has a ramp and a door at the frontal side of the turbine which functioned like a converging duct. The backward side of the turbine has two doors for the discharge of wind. The new improved design was able to increase the power coefficient from 0.135 to 0.34 which is about 2.5 times the initial coefficient of power.

A new hybrid wind-solar system for buildings was proposed by W. T. Chong et al., 2016 where VAWTs are installed in between the upper V-shaped solar panel roof and lower gable roof. The system has total six numbers of VAWTs as shown in Figure 2.35(d). The rotational axes of VAWTs are parallel to the roof ridge. The speed of the wind entering to VAWTs increases due to the venturi effect created by the upper and lower roofs which are functioned like a concentrator and diffuser. It also improves the self-starting behaviour of the VAWT. They performed a 2D numerical simulation as well as an experiment on this setup. The augmented factor for average wind speed was calculated as 1.44 from numerical simulation and 1.36 from experiment results. The energy generated by the system is approximately 773.16 kWh/year. This system is also equipped with water harvesting and ventilation vents as additional features. However, wind direction plays a major role in the performance of these VAWTs.

D. Li et al., 2021 introduced a new building augmented VAWT design where a VAWT was installed in between two buildings taking advantage of the wind gathering effect of the building diffuser. RANS based SST turbulence model was incorporated to study the effect of different shape parameters of diffusers on VAWT performance. The eight different types of building diffusers' sections were investigated including square, circle, isosceles triangle, trapezium, diamond, kidney and expansion-contraction air-foil. It was found that the building diffuser of trapezium-shaped shown in Figure 2.35 (e) performed better in terms of wind collecting and it provided a maximum power coef-ficient of 1.56 at a TSR of 4.62. However, at higher TSR, fluctuations of average torque coefficient were noticed due to the vortex formation at the wake region.

Table 2.3: Summary of TSR range, TSR for maximum C_P, maximum value of C_P and corresponding Indicated Power output of all augmentation devices.
A blank (–) indicates insufficient information.

No.	Type	Augmentation methods	TSR range	TSR for max C_P	Maximum C_P	Indicated Power (W)
1	**Unidirectional inlet flow**	Guide vane row (Takao et al., 2009)	0 to 3	2.1	0.205	27
2		Straight deflector (Kim & Gharib, 2013, 2014)	0 to 1.6	1.3	0.101	4
3		Straight deflector (Jin et al., 2018)	0.5 to 3.5	2.7	0.45	300
4		Curved deflector (Stout et al., 2017)	0.5 to 3	1.625	0.213	10
5		Rhombus deflector (Zhao et al., 2021)	1 to 3	2.4	0.275	14
6		Diffuser (wind lens) (Hashem & Mohamed, 2018)	2 to 8	5.5	1.366	630
7		External diffuser (Kuang et al., 2022)	0.5 to 3	1.5	0.3564	72
8		Duct (De Santoli et al., 2014)	–	–	–	3700
9		Straight plate (M. H. Mohamed et al., 2010, 2011)	0.2 to 1.4	0.8	0.25	–
10		Convergent nozzle (Mohammadi et al., 2018)	0 to 1.4	0.45	0.39	4
11		Curtain plate (Altan & Atilgan, 2008, 2010)	0 to 1	0.4	0.385	8.5

Continued on next page

Continued from previous page

No.	Type	Augmentation methods	TSR range	TSR for max C_P	Maximum C_P	Indicated Power (W)
12		Guide-box tunnel (Irabu & Roy, 2007)	0 to 1.3	0.7	0.26	0.5
13		Porous deflector (Nimvari et al., 2020)	0.5 to 1.4	1	0.27	–
14		Guide plate (El-Askary et al., 2015)	0 to 2.5	1.1	0.52	22
15	**Omnidirectional inlet flow**	ODGV (W. Chong et al., 2013)	2.5 to 5.1	5.1	0.4195	0.4352
16		ODGV (Wong et al., 2014)	2.5 to 5.1	5.1	0.3398	–
17		Stator (Nobile et al., 2014)	0 to 7	2.5	0.8	–
18		Wind gathering device (Y. Li et al., 2018, 2020)	0 to 2	1.6	0.23	22
19		Zephyr stator vanes (Pope, Dincer, & Naterer, 2010; Pope, Rodrigues, et al., 2010)	–	0.48	0.12	201
20		Guiding blades (Kalluvila & Sreejith, 2018)	0 to 1.3	0.85	0.28	–
21		Shield (Tian et al., 2019)	0.1 to 0.8	0.4	0.2802	–
22		Tower cowling (Y. X. Yao et al., 2013)	–	1	0.48	–

Continued on next page

Continued from previous page

No.	Type	Augmentation methods	TSR range	TSR for max C_P	Maximum C_P	Indicated Power (W)
23		Shroud (Ying et al., 2015)	0 to 1	0.7	0.18	–
24	**Innovative designs**	Hybrid (Bhuyan & Biswas, 2014)	1 to 5	2.3	0.34	–
25		Hybrid Bach type (A. Hosseini & Goudarzi, 2019)	1 to 5	2.5	0.414	–
26		Cross axis wind turbine (W.-T. Chong, Muzammil, et al., 2017; W.-T. Chong, Wong, et al., 2017)	0 to 1.4	0.8	0.0785	–
27	**Blade Modifications**	Slatted blade (Reupke & Probert, 1991)	–	–	0.024	–
28		Slotted airfoil (O. S. Mohamed et al., 2020)	–	2	0.3	–
29		Opening near trailing edge (J. Chen et al., 2015)	–	2.5	0.415	–
30		Blade cavities (Roshan et al., 2021)	–	3.5	0.27	–
31		Inner blades (Al-Ghriybah et al., 2019, 2021)	–	0.5	0.1885	–
32		Twisted blade (Saad et al., 2021)	–	0.8	0.261	–
33		Crossflex (Sharpe & Proven, 2010)	–	–	–	6000

Continued on next page

Continued from previous page

No.	Type	Augmentation methods	TSR range	TSR for max C_P	Maximum C_P	Indicated Power (W)
34	**BIWT**	BIWT with guide vane (Park et al., 2015)	–	–	–	1000
35		Diffuser shaped shroud (Krishnan & Paraschivoiu, 2016)	–	0.38	0.34	–
36		Building diffuser (D. Li et al., 2021)	–	4.62	1.56	–

Table 2.3 summarises the performance parameters and output for different augmentation devices. VAWTs generally operate in a relatively low power range as they are suitable for low wind speed applications. Literature does not provide the areas of wind turbine application and indicated power. Hence an estimate is carried out to calculate the indicated power for each augmentation device from the existing data available in the literature. Power output is calculated as

$$P = C_P \frac{1}{2} \rho A v^3 \tag{2.1}$$

2.6 Summary and concluding remarks

Producing a higher efficiency from a small wind turbine with a simple design has always been a challenge for researchers and engineers. This chapter attempts to summarize the current state-of-art on augmentation devices for VAWTs. While VAWTs have potential for contribution to the energy-pie, they have some limitations in self-starting ability, initial torque and coefficient of power. Thus, various flow augmentation mechanisms are important for achieving improved performance. It was found that the self-start ability and C_P of VAWT are increased significantly with the incorporation of augmentation devices. The following observations summarize the current status in the concerned area.

i. According to the flow direction, the augmentation devices are categorized into two groups, single directional inlet flow and omnidirectional inlet flow. Augmented devices are mainly installed on the upwind side for single directional flow. In the case of omnidirectional flow, devices are installed surrounding the wind turbine and capture the wind from all directions. For single directional types, there is a need for a yawing mechanism to capture the wind from different directions.

ii. The augmentation techniques are significantly enhancing the performance in terms of power coefficient values and self-start ability. Augmentation devices like deflector, guide vanes, converging duct, diffuser, and stator are incorporated with the VAWTs to create a venturi effect at the inlet. This results in higher positive torque and improves the self-start ability of VAWTs.

iii. Augmented devices for lift type VAWTs generate a greater lift force on the airfoil-shaped blade by directing the wind flow at an improved angle of attack and also minimize the negative torque during the second half of the revolution.

iv. In drag type VAWTs, augmented devices are used as deflectors to direct the wind towards the concave or advancing blade of the Savonius rotor, resulting in greater

positive torque and also preventing the wind flow to the convex or returning blade that reduces the negative torque acting in the counter direction.

v. Other innovative designs like INVELOX, Cowling, shroud, hybrid VAWT, and CAWT basically focus on increasing the wind speed by concentrating the wind and thus improving the VAWT's performance.

vi. Various blade modification methods provide better self-start ability and improve overall CP without installing any extra equipment.

vii. Building integrated augmented devices can be very effective if they are installed at the edge of a building as the high-pressure difference at the corners of the building increases the inlet wind flow to the turbine.

viii. The omnidirectional wind capture capability and better performance in turbulent regions make the building-integrated VAWTs more suitable for rooftop applications. However, large size, wider wake effect, inferior visual impressions, the requirement of strong structural support, and high setup cost are the few downward sides of VAWTs.

ix. The most promising augmentation devices include the duct, convergent nozzle, guiding vane, ODGV, PAGV, and vortical stator assembly, with data showing a maximum level of augmentation greater than 100%. However, the use of deflector and airfoils modification can be cost-effective but their overall augmentation gain is very less. There is a lot of future scope on these augmentation devices to improve their power coefficient as they are required no extra equipment.

x. The state-of-art survey highlights the fact that most of the studies on the area are based on numerical simulations and hence there is a need for conducting more experiments toward finding out optimal augmentation devices.

xi. With the need of more energy against the rising global pollution, augmentation techniques for the power generation shall be subject of interest for many decades in future.

CHAPTER 3

Sustainability of Wind Power

3.1 Introduction

Environmental challenges are intensifying and getting worse every day largely propelled by the combined effects of increased greenhouse gas emissions and global warming. These contribute significantly to the degradation of environment. At the same time, the demand for energy has undergone a significant upsurge in recent decades, primarily due to the rapid expansion of the world population. Therefore, the call for renewable energy sources becomes imperative to maintain environmental sustainability and meet the escalating demand for energy. Since wind energy does not rely on fossil fuels and uses an abundant natural resource, it stands out as a clean and renewable energy source which lowers pollution and greenhouse gas emissions. Its sustained popularity is rooted in both its widespread availability and its cost-effectiveness (Ackermann & Söder, 2000; Das Karmakar & Chattopadhyay, 2022; Yannopoulos et al., 2015). The development of new wind farms all over the world has contributed significantly to the renewable energy pie in recent years. Figure 3.1 illustrates the yearly progression of global wind energy installation capacity. The compound annual growth rate (CAGR) of installed wind power capacity is about 11% in the period 2015-2022. As the wind turbines convert kinetic energy of wind to electrical power using the wind energy conversion technology (WECT) without releasing any emissions or pollution during the process, it has been hailed as a superior form of green energy (Rahman & Chattopadhyay, 2020, 2023). However, it is crucial to acknowledge that it still contributes to greenhouse gas emissions. Beyond its functioning period, wind turbine technology has negative impact on the environment during its manufacturing and disposal phases. Sometimes, where wind energy is used with other conventional sources, greater usage of wind energy reduces the load on conventional thermal units, that result in higher fuel consumption owing to off-design (Stanek et al., 2018; Turconi et al., 2014). It is thus necessary to analyse the environmental consequences of wind energy over its life span and asses the sustainability.

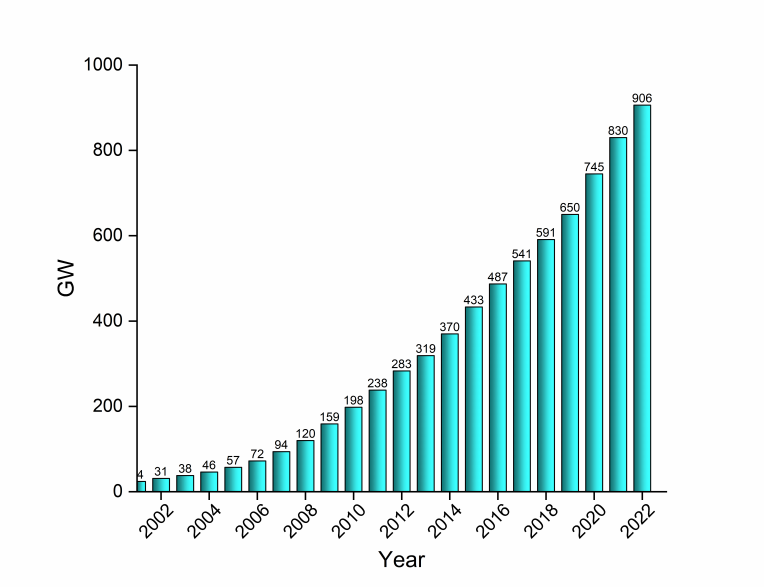

Figure 3.1: Development of global wind energy installation capacity (Council, 2023)

Sustainability or sustainable development, as originally articulated by the Brundtland Commission in 1989, entails meeting present-day requirements "without jeopardizing the capacity of future generations to fulfil their own" (Brundtland, 1987). In simpler terms, it means promoting economic growth without harming the environment or contributing to social inequalities (Sikdar, 2004). A three-petal flower conveys the essence of sustainability as shown in Figure 3.2. Thus a sustainable technology must be sound in terms of environmental social and economic concerns (Abraham, 2006). To achieve sustainability, one must stay within ecological bounds and gradually improve the material and social conditions for the environment and human health (Sikdar, 2003b).

In the context of the contemporary global situation, the concept of sustainable development goals (SDG) was bought by United Nations in 2015 with the aim of safeguarding the planet from and ensuring universal peace and prosperity by the year 2030 ("United Nations, 2015. Sustainable Development Goals (SDGs)", 2015). As of 2023 version, there are seventeen SDGs and wind turbine technology is directly linked to several sustainable development goals. Possibly most important among them are "affordable and clean energy (goal 7)", "industry, innovation and infrastructure (goal 9)", "sustainable cities and communities (goal 11)", "responsible consumption and production (goal 12)", "climate action (goal 13)". These goals will play a pivotal role in fostering comprehensive and sustainable global future, addressing energy needs, infrastructure, urbanization, and climate change. Assessment of sustainability is thus a global concern and suitable indicators are needed to be developed in the area (Sikdar, 2003a, 2009).

Studies have been carried out to assess the effects of wind turbines on the environment since long. Welch and Venkateswaran, 2009 hailed wind energy for 'dual sus-

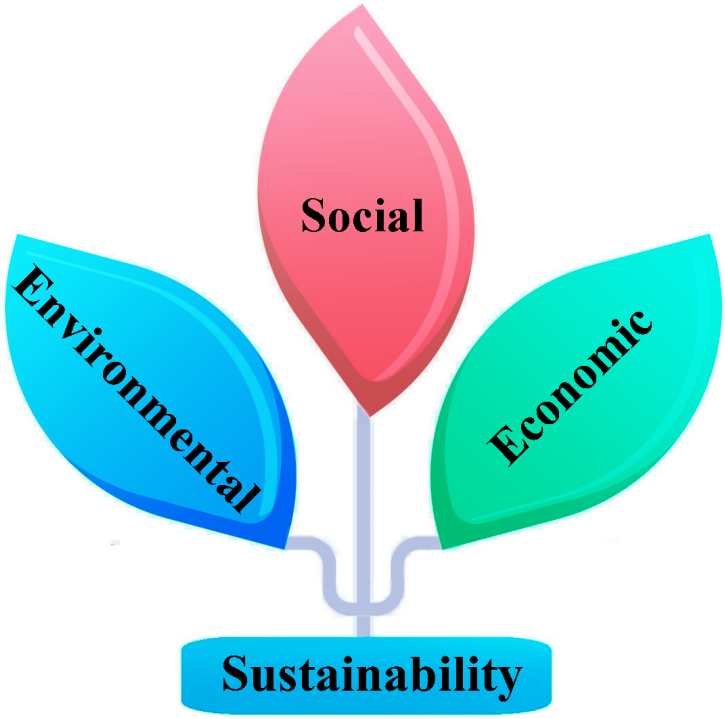

Figure 3.2: Three petals of sustainability

tainability' emphasizing the economic and environmental aspects. Leung and Yang, 2012 evaluated the negative effects of wind turbines on animals and birds and on environments in terms of noise and visual impacts. The impact of wind turbines on noise pollution, on the death of bird and bats, greenhouse gas emissions, and erosion of land surfaces was studied by S. Wang and Wang, 2015. Life cycle analyses of wind energy systems on the aspects of methodology, energy usage, energy production, performance, utilization of natural resources, and recycling was performed by Davidsson et al., 2012. Arvesen and Hertwich, 2012 categorised their study on the basis of turbine size and lifetime, regional coverage, and offshore versus onshore turbines.

The primary aim of this work is to examine the sustainability aspects of wind energy, considering various impact categories such as environmental concerns, social and human health issues, economic viability, waste management and technological advancement of the wind turbine system based on available literature. An extensive study, the survey of literature showed that aspects of sustainability are not thoroughly summarized in previously published works. One of the important works worth mentioning is that of Adeyeye et al., 2020, which tries to address the issue of sustainability by summarizing environmental and economic aspects of wind turbines, albeit leaving the societal aspects untouched.

Three major databases: Scopus, ScienceDirect, and Web of Science were thoroughly searched to find studies published since 1980. These three databases cover almost all the significant journals, conference proceedings, published reports and theses. It has

also been ascertained that no significant work has been published in the concerned field prior to this period. The search focused on specific keywords related to sustainability, wind energy, environmental impact, noise pollution, visual impact, NIMBY (not in my backyard) and recycling. In addition to using these keywords, the reference lists and citations of the identified studies were examined to uncover additional relevant research. The selected studies were then carefully screened and organized based on their core ideas and findings. The steps involved in this research process are illustrated in Figure 3.3.

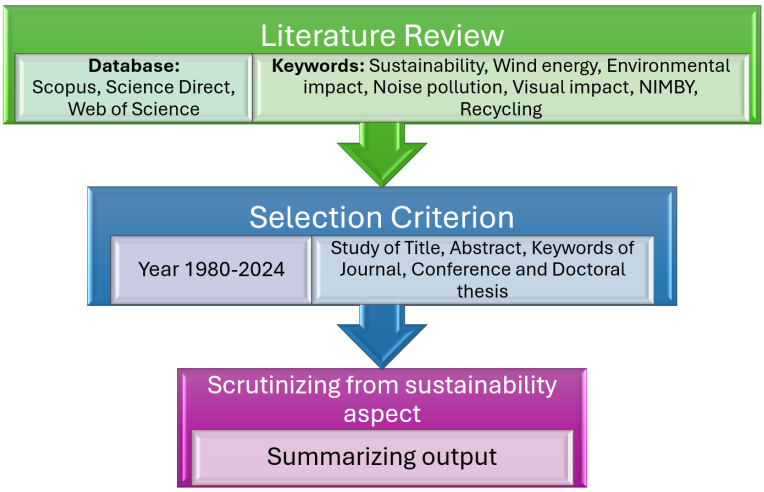

Figure 3.3: The methodology for state-of-art survey

3.2 Environmental concerns

According to a World Health Organization report, 24% of mortality are attributable to environmental factors (Adeyeye et al., 2020) . People must be able to live in clean environment with access to fresh water and air to breathe. For future generations to be able to live in healthy surroundings, efforts must be given to reverse the long-term effects of exponential industrial expansion and energy consumption. Businesses must commit to environmentally sustainable practises in order to support the growth of flourishing communities. Protecting global ecosystems and natural resources is vital to maintain health and welfare both now and in the future (W. H. Organization, 2023).

Environmental concerns of wind turbine are depicted in Figure 3.4. The concerned issues are dust and dirt movements, soil erosion and disposal of hazardous materials. The change in wind pattern due to the presence of wind turbines lead to environment issue by affecting flora and fauna. Noise is another factor affecting socio-environmental sustainability.

Moving dirt from one area to another is a part of the wind erosion process and may cause serious environmental harm. Dust has an impact, on the environment by blocking waterways introducing impurities harming plants and animals and promoting the growth

of blue green algae. Moreover wind erosion reduces productivity by depleting the rich top layer of soil (Chang et al., 2018). Presence of wind farms with too many wind turbines can significantly diminish the kinetic energy of neighbouring winds, which can even have consequences approximating the greenhouse effect. The turbulence produced by the turbines can cause the high winds to alter course near to the ground, which can subsequently encourage localised moisture loss. Studies found that the vertical temperature distribution, surface humidity, and latent heat fluxes can all be adversely affected by the wake turbulence of the rotor.

Environmental dangers connected to manufacturing include acidification, eutrophication, and ecotoxicity. The manufacturing process is responsible for more than 80% of abiotic depletion (Alsaleh & Sattler, 2019). The most hazardous material to use in production is copper, which accounts for 35% of the weight of the generator. Due to its non-biodegradability, copper builds up in both plants and animals, where it can interfere with metabolism and restrict plant growth. Due to these factors, it is difficult to dispose of turbines (Moreno-Camacho et al., 2019).

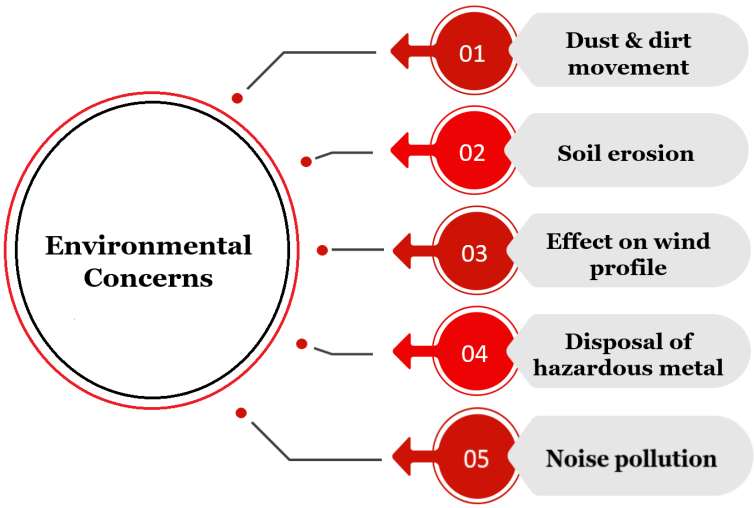

Figure 3.4: Environmental concerns of wind power

The use of wind energy increased at the highest rates between 2011 and 2021 in Brazil, China, Sweden, UK, France, Canada, while it decreased at the lowest rates in, Spain, India and Germany as presented in Table 3.1.

In the search of sustainable energy solutions, it is imperative to conduct thorough comparisons of wind energy performance against both conventional and renewable electricity generation systems, with a particular focus on greenhouse gas (GHG) emissions. The direct greenhouse gas emissions from operational phases can be computed using Life Cycle Assessment (LCA). Such assessments provide invaluable insights into the environmental impact and efficacy of different energy sources. Table 3.2 shows an estimate of the GHG emissions from different energy sources in terms of carbon dioxide (CO_2) emitted per kilowatt-hour (kWh) of electricity generated. The GHG emissions

Table 3.1: Wind energy capacity for various countries (BP, 2022; Sadorsky, 2021)

Country	**Wind Capacity (GW) in 2011**	**Wind Capacity (GW) in 2021**	**CAGR (2011–2021)**
China	46.4	329.0	21.6%
India	16.2	40.1	4.9%
Australia	2.1	9.0	15.5%
France	6.8	18.7	10.7%
Germany	28.7	63.8	8.3%
Spain	21.5	27.5	2.5%
Sweden	2.8	12.1	15.9%
UK	6.6	27.1	15.2%
Brazil	1.4	21.2	31.0%
Canada	5.3	14.3	10.5%
USA	45.7	132.7	11.3%

from fossil fuels range from 900-1200 g CO_2 e/kWh of electricity produced. Globally, the average emissions amount to approximately 600 g CO_2 e/kWh of electricity produced. The emissions from wind energy range in between 10-50 g CO_2 e/kWh whereas nuclear energy produces approximately 10-15 g CO_2 e/kWh.

Table 3.2: GHG emissions for different electricity generation plant (Ardente et al., 2008; Tremeac & Meunier, 2009)

Source	**GHG Emissions [g CO_2e/kWh]**
Fossil fuel	900–1200
Natural gas	400–500
Solar energy	50–100
Wind energy	10–50
Hydroelectric plants	15–40
Nuclear energy	10–15
Typical average (all sources)	600

Adopting wind power is unquestionably a viable way to reduce greenhouse gas emissions when it is replacing the use of fossil fuels. However, it's important to recognize the ongoing environmental effects related to its infrastructure. The LCA method is frequently employed in scientific studies to comprehensively examine the environmental implications associated with wind energy (Martínez et al., 2009). This rigorous analyti-

cal approach contributes valuable insights into the broader sustainability considerations of wind power. Table 3.3 shows that the range of GHG emissions at various locations worldwide from wind farms in terms of CO_2 e/kWh. The significant variation in estimating GHG emissions from wind farms primarily stems from several factors, including the scale of the wind farm, the methodologies employed to assess GHG emissions across the life cycle of the wind farm, and the geographical locations in which the farms are installed. It is observed that the value lies in a wide range between 6-46 g/kWh. Even the highest value is about 1/12th of the global range and 1/20th of that for a coal-based plant.

Consequently, when contrasted with fossil fuel power plants, wind energy demonstrates notably compelling CO_2 emission figures that are comparable to those of nuclear energy. A comparison between a 4.5MW and a small 250W wind turbine was performed using LCA by Tremeac and Meunier, 2009. Wiedmann et al., 2011 indicated that GHG emissions only 13g CO_2 e/kWh for a 2MW offshore wind power station a pure process LCA. However, these emissions escalated to 28.7g CO2e /kWh for Integrated Hybrid LCA and 29.7g CO_2 e/kWh for IO-based Hybrid LCA. S. Verma et al., 2022 reported that GHG emissions was 11.3g CO_2 e/kWh from a 16.5MW Vestas wind turbine in India.

Table 3.3: GHG Emissions from Various Wind Energy Studies

No.	**References**	**Plant Capacity**	**Location**	**GHG Emissions [g CO_2e/kWh]**
1	Alsaleh and Sattler, 2019	2 MW	USA	18
2	Tremeac and Meunier, 2009	250 W 4.5 MW	France France	46.4 15.8
3	Wiedmann et al., 2011	2 MW	UK	13.4–29.7
4	Ardente et al., 2008	7.26 MW	Italy	8.8–18.5
5	Martínez et al., 2009	2 MW	Spain	6.6
6	Nassar et al., 2024	100 MW	Libya	46.88
7	S. Verma et al., 2022	16.5 MW	India	11.3
8	Yang et al., 2018	5 MW	China	25.5
9	Oebels and Pacca, 2013	1.5 MW	Brazil	7.1
10	Kabir et al., 2012	100 kW	Canada	17.8

Alsaleh and Sattler, 2019 conducted an LCA study for onshore wind turbines in-

stalled in the US using SimaPro8 software which followed ISO 14040 standards. Various impact categories such as human health impact, environmental impact and resource consumption were also investigated. Figure 3.5 shows the comparison of wind turbines with coal-based power plants in the US according to the environmental impact category involving water consumption, acidification potential, global warming potential. Coal based power plant of 500MW was taken into account for this comparison with and it was integrated with CO_2 removal technology known as carbon capture and sequestration (CCS) technology (Widder et al., 2011). In CCS, Mono ethanol amine (MEA) scrubbing process was used for CO2 removal. Figure 3.5 depicts that even with CCS, the coal-based power plant still significantly worsens the environment more than wind turbines for the same quantity of energy produced. The water depletion index shows that coal plants with CCS use more water than wind turbines do by almost 4600 times. Although the adoption of CCS technology reduces the greenhouse gas emissions of the coal-based plant, it remains nearly twelve times more than that emitted by the wind turbine. In case of wind turbine, only the global warming potential is present which is again negligible compared to that of coal-based plants.

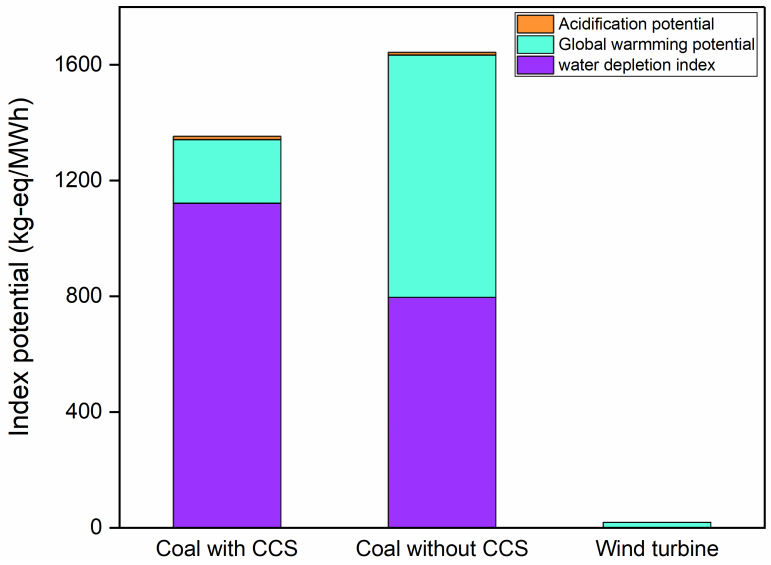

Figure 3.5: Comparison of environmental index potential between wind turbines and coal based power plants in US (Alsaleh & Sattler, 2019)

3.3 Social concerns

Despite the popularity of WECT, social concerns for wind energy system can often impede the adoption and acceptance of wind energy projects. While wind energy represents a promising solution for combating climate change, concerns persist regarding its potential negative impacts on ecosystems. It is possible for local ecosystems to be disturbed by the construction and operation of wind turbines, which could lead to the

devastation or degradation of fish, plant, and animal habitats (Tabassum-Abbasi et al., 2014). Studies that have investigated accidents involving wind turbines have discovered that fatalities are typically not particularly common. Even though the direct mortality from wind turbine collisions may not seem like much in many cases, it can still have a significant impact on wildlife populations, especially when it comes to species that are rare or endangered and have long lifespans, slow rates of reproduction, and delayed maturation. The death of even a few individuals can have cascading impacts on fragile populations, possibly altering ecosystems and weakening conservation efforts, despite the comparatively low mortality rates. A cumulative fatality that occurs across multiple installations could have a significant effect on the population (Jiguet et al., 2021). The graphical representation of socio-environmental concerns of WECT is depicted in Figure 3.6.

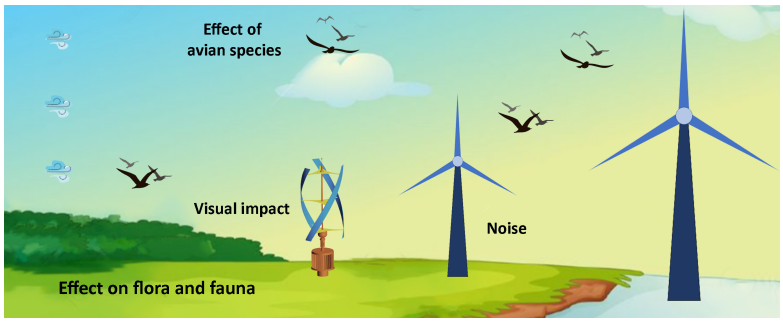

Figure 3.6: Socio-environmental concerns of WECT

3.3.1 Noise pollution and impact on human health

Noise pollution emerges as a prominent concern brought on by the wind energy industry, contributing to social issues and affecting human health. Noise pollution is harmful for people and can even affect property values in a limited area around a building site. Therefore, it is crucial to understand the many forms of noise that wind turbines emit before building one.

The high speed of rotating wind turbines has the potential to produce an audible sound and a vibration that can move through the air. Any unpleasant sound is referred to as noise and wind turbines emit specific types of noise which are caused by mechanical and aerodynamic factors. Aerodynamic noise arises from the interaction of turbine blades with the wind during operation and it gets louder with increasing rotor speed. The noise that stems from the mechanical and electrical components of the turbine is termed as mechanical noise. Both mechanical and aerodynamic factors contribute to the overall noise emissions from wind turbines. It is possible to minimize mechanical noise, leading to modern wind turbine designs that operate quietly with the integration of efficient insulation and vibration damping materials (S. Wang & Wang, 2015).

The continuous noise emitted by wind turbines is typically characterized using the L90 metric, which gauges the baseline ambient sound levels associated with the wind turbine. The noise emitted by wind turbines can be measured using prediction models. Brooks et al., 1989 developed a semi-empirical model, which is the most often used prediction models. While several semi-empirical models have been created, they often rely on complex computational fluid dynamics (CFD) solvers, incurring high computational costs and time consumption. Alternatively, measuring wind turbine noise with A-weighting method is recommended by the International Environmental Agency (IEA) (Brooks et al., 1989). However, this method is primarily designed for industrial noise measurement and are more suitable for low wind speed operations, typically ranging between 4 to 6 m/s, making it challenging to measure noise for wind turbines operating at speeds of 8m/s and beyond (Brooks et al., 1989; Kaldellis et al., 2012; Pedersen et al., 2010).

Noise can have non-auditory effects through two primary pathways: directly as well as indirectly. Directly, it induces physiological stress, which has been associated with sleep disturbances even at low noise levels. Indirectly, individuals who are awake may experience emotional stress due to discomfort caused by the noise (Babisch, 2014; Basner et al., 2014). The rapidly spinning blades have a 20 Hz audible sound frequency and vibration that can travel through the air and disrupt sleep and create headaches (Chiu et al., 2021). The noise emitted by a wind turbine operating at 5 m/s and positioned at a height of 10m measured 48.5 dB, indicating an increase of 9 dB compared to the ambient sound as reported by Kaldellis et al., 2012. This noise irritation may also trigger the release of stress hormones and can lead to persistent physiological imbalances such as chronic disorders, manifesting in a range of stress-related symptoms (McEwen, 2007). Although, according to Radun et al., 2022, only noise-related discomfort such as noise annoyance is reported by residents where sound levels are lower than 40dB LAeq and there are no significant health effects. This observation underscores that, within this specific sound threshold, adverse health effects are limited to annoyance. Whereas, an escalation in traffic noise volume has been associated with an elevated risk of various health issues, including headaches, migraines, dizziness, heart palpitations, tachycardia, pressure in the ears, and heart disease Radun et al., 2021.

Furthermore, the mortality rate of bird species may be affected by noise. Studies using thermal cameras reveal that bats tend to fly close to wind turbines for feeding. Certain bat species have been observed aligning themselves with ultrasonic sounds, indicating a potential attraction to noise generated by aerodynamics (Buchler & Childs, 1981; Horn et al., 2008; Kunz et al., 2007; Schmidt & Joermann, 1986). Many countries and international organisations have passed laws regulating noise, taking into account the detrimental effects of noise exposure on human health (Kumar et al., 2019).

3.3.2 Visual pollution

The visual impact of wind turbines extends beyond their mere presence, as its influence is shaped by various factors such as design, color, size and shape. These elements contribute to the aesthetic integration of wind turbines into their surroundings. The way the turbine blades rotate in a rhythmic manner and the way light and the interplay of light and shadow as they move can provoke mixed responses with neighbouring populations. Some people could find the sight mesmerizing, while others may experience a disturbed feeling. Additionally, the installation of wind turbines can change the natural landscape of surrounding area in ways that are not planned, and it can also have unintended consequences, potentially impacting the mental well-being of residents in the vicinity.

Enhancing the perceived aesthetics of wind farm installations often involves strategic placement, such as aligning identical-sized turbines in straight, uncomplicated rows with light-coloured columns. Evaluating these visual impressions and quantifying them turns out to be a difficult undertaking as each individual view is subjective. While there are a few tests and procedures, such the Quechee test and the Spanish approach, that can be used to analyse various visual pollution conditions (Bishop, 2002). These techniques show that running turbines have less of an effect on the environment than do stationary ones. Through the implementation of appropriate measures, the aesthetic and visual effects of wind turbines on residential areas can be mitigated, fostering to a more harmonious coexistence between renewable energy infrastructure and nearby communities.

Public perceptions in the advancements of wind energy are significantly shaped by the idea of technological acceptability. It acts as a prism through which it examines how societies perceive and adopt new energy technologies. The term ”not-in-my-backyard,” often abbreviated as ”NIMBY syndrome can be described as a strong, emotionally charged, and commonly organized resistance by local community to proposed developments or projects that they fear could result in adverse impacts to their society (Kojola, 2020; Wexler, 1996). NIMBYism captures the opposition resulting from local communities' worries about the possible effects of these technologies on their immediate surroundings. NIMBY feelings are a result of a number of factors, including perceived health hazards, environmental degradation, property values, and neighbourhood aesthetics. There are certain variants of the acronym “NIMBY” offering more subtle insights into how proximity affects the acceptability of wind energy projects. NUMBY (Not Under My Backyard), emphasizes opposition to developments that are located immediately beneath a person's land (for coal, natural gas). NIMFY (Not in my front yard), which refers to resistance to projects that are visible from one's home. Furthermore, the concept of ”inverse NIMBY” challenges conventional notions by suggesting that those closest to energy developments may actually hold more favourable opinions. This con-

cept is expanded upon by YIMBY (Yes in my backyard) and PIMBY (Place it in my backyard) (Krause et al., 2014; Wolsink, 2000; Zanocco et al., 2020). Policymakers and stakeholders need to understand and address the underlying concerns, enabling more inclusive and sustainable approaches to wind energy development, by delving deeper into these aspects and exploring the intricacies of NIMBYism.

3.3.3 Impact on wildlife

Adoption of the WECT has special impact on flora and fauna which can adversely impact biodiversity (Gibson et al., 2017; Pörtner et al., 2021). In contrast to other energy infrastructures, the impact of wind energy resonates through the surrounding aerosphere, influencing the habitats of many flying creatures (Leroux et al., 2023). Wind turbines cause severe interruptions to the airflow and increase turbulences during operation, which can be experienced for several kilometres downwind. This phenomenon is frequently referred to as the wake effect (Porté-Agel et al., 2020). The potential negative effects of wind energy on wildlife have been a subject of ecological concern.

One major negative aspect involves the direct impact on avian species, as a result of collisions with rotating turbine blades. The probability of accidents is exacerbated by factors such as lower hub heights, shorter rotor diameters and closer turbine spacing (Committee, 2010). Wind turbines have the capacity to alter the habitat preferences of birds and bats, causing them to react by either avoiding or being drawn to them. Habitat disruptions are also considered in assessments of wind energy's ecological footprint. At turbine sites, attraction increases the probability of mortality, hence jeopardizing the survival of a variety of species. However, avoidance of these practices may interfere with migration and travel routes, resulting in a wider range of landscape-scale functional losses in roosts and feeding areas (Duriez et al., 2023; Gómez-Catasús et al., 2018; Richardson et al., 2021; Roscioni et al., 2014). Avian radars and other cutting-edge monitoring systems are used to understand the complex interactions between wind energy infrastructure and wildlife.

While negative impacts of WECT is widely discussed as a matter of concern, these positive effects on biodiversity also needs scrutiny. Kingma et al., 2024 has recently discussed the way scour protection for offshore wind farm encourages benthic directly i.e. about the flora and fauna at the bottom of the seas. The wind farm foundations can be used as artificial reefs with possibilities of supporting marine life (Werner et al., 2024) as well as for pisciculture application.

Operation of wind turbines leads to loss of large amount of insects (Voigt, 2021). While for foods human beings depend on pollination by insects, reducing the menaces of insect-borne diseases can be beneficially used. Fourrier et al., 2023 has opined that honeybees colonies are not affected by presence of wind farms. Animals are found to be

drawn to base of wind turbine installation for using the area for shade or as scratching posts (Adeyeye et al., 2020). It must be understood that all kind of technologies have their impact on environment. Thus, it shall be prudent to compare energy conversion technologies for their environmental impact assessment. As on example Katovich, 2023 shows that while shale oil production has negative impact on bird counts, WECT has no such appreciable effect. This study covers all states of US for the period 2000 to 2020.

Reducing detrimental wildlife impacts, especially for vulnerable avian species needs to be a top priority Katovich, 2023. There exist viable mitigation methods aimed at minimizing the adverse impacts associated with wind energy such as modifying turbine functioning or utilizing techniques to alert discourage avian species from approaching turbines (May et al., 2015). According to De Lucas et al., 2012, deliberately halting turbine operations when griffon vultures are approaching results in an annual reduction of energy production by only 0.07%. However, this measure effectively decreases vulture mortality rates by 50%. Another way to mitigate the risk of collisions is to install wind turbines at a considerable distance from avian habitats. Employing curtailment plans provides an additional strategy to concurrently reduce habitat losses and collision risks. To optimize their spatial arrangement of WT installation, the wake effect must be taken into consideration during the planning stage. These steps will help wind turbines and bird habitats coexist more effectively, promoting sustainability and reducing adverse effects on wildlife (Magoha, 2002; Saidur et al., 2011). Comparative studies indicate that, when evaluated per unit of energy generated, wind turbines have a substantially lower impact on wildlife, particularly avian populations, compared to traditional fossil-fuelled power plants (Sovacool, 2009).

3.4 Economic Viability

The economic viability of a wind turbine system is assessed by examining its financial feasibility and profitability. It is essential to consider expenses associated with raw material production, manufacturing, shipping, and end-of-life management throughout the life cycle of a turbine. Analysing economic viability involves evaluating operational costs, potential revenue streams, required investments, and overall financial sustainability. A comprehensive assessment of economic sustainability is required before wind energy can be widely embraced. This section examines the establishment and operating costs of wind power projects compared to those of conventional energy sources aiming to assess the sustained viability in long run and economic competitiveness of the wind energy sector. Businesses and organizations must closely monitor these factors to ensure that their operations contribute to sustainable economic growth and stability.

The cost of wind energy can be delineated into four fundamental elements: fixed capital costs, variable costs, generation costs, and other cost that. Breakup of wind en-

ergy cost is shown in Figure 3.7. Fixed capital costs encompass the various components of turbines, installation and foundation expenses, transportation, grid connection, and road construction. Variable costs include operation and maintenance expenses for the turbine, as well as land rent, administrative costs, insurance, and taxes. Electricity generation costs are contingent upon wind climate and site characteristics, with the capacity factor serving as a parameter to define the percentage of electricity produced annually by a wind farm. Miscellaneous expenses, categorized as ”other costs,” comprise the discount rate and economic lifetime of the wind farm.

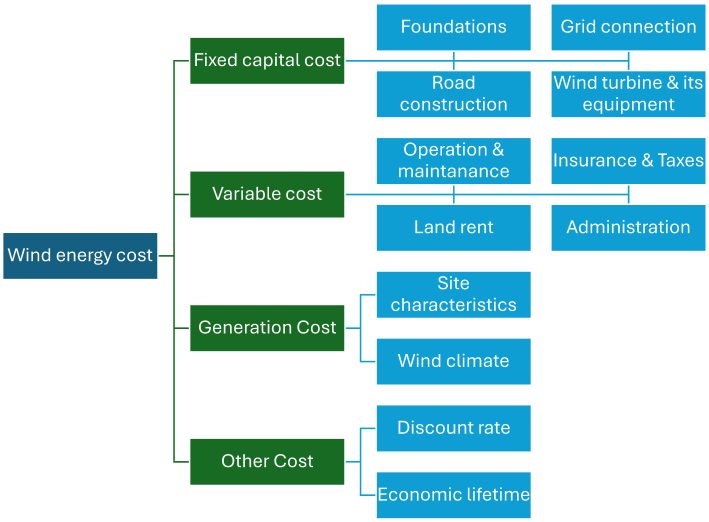

Figure 3.7: Factors affecting cost of wind energy (Blanco, 2009; Kumar et al., 2019)

WECT is a technology that demands a significant investment during the initial phase, with its capital costs representing more than 80% of the total expenditure (Blanco, 2009). The cost encompasses all components of the turbine, including the tower, rotor hub, rotor blades and bearings, gearbox, generator, yaw and pitch systems, and nacelle housing. This cost extends from material acquisition to manufacturing phases, as well as transportation of these components to the wind farm site and their subsequent installation. The hub of the rotor is made of cast iron, copper, and aluminium. The tower and gearbox both contain steel. Resin and fibreglass are used to create the rotor hub and blades. Most of the foundations for turbines are made of steel and concrete. The switch to larger turbines, which are favoured in areas with lower wind speeds, necessitated the use of significant quantities of structural materials (Elia et al., 2020). The procurement of raw materials and production of wind turbines may result in the production of carcinogens, an environmental contaminant that promotes carcinogenesis (Chiu et al., 2021; Rueda-Bayona et al., 2022).

For a WECT systems the blades are broad, the core is huge and hefty, and the framework is large and heavy. Each part of a windmill has distinct features of its own. As a result of these factors, issues with loading and unloading become a major concern.

The fact that wind turbines are continually changing products and require regular assessments and alterations to transportation arrangements adds another challenge to the process. Over the past two decades, as turbine size has increased, so too has the associated cost. In addition to the equipment costs of wind turbines, there are also expenses associated with grid connection, including transformers, electrical cables, substations, power connections, and evacuation systems. These elements account for approximately 12% of the capital cost (Blanco, 2009). Following this are the expenses related to civil works, such as foundation and road construction.

Operation and maintenance cost is the most significant variable costs for wind turbines. This encompasses the repair and replacement of spare parts, maintenance of electrical components, as well as insurance and taxes. Additionally, it includes expenses related to land rent, management, audits, and forecasting services. Technological developments in the digital sector have enabled the self-inspection and enhanced utilization of all information analytics. Modern turbines are becoming more dependable and durable, resulting in decreased Operation and maintenance expenses. Several key elements significantly impact the cost of wind power generation. These factors include the relatively low plant-capacity factor, the economic lifespan of the investment, and capital costs (encompassing expenses for turbines, foundations, and grid connection). Therefore, establishing favourable repayment terms is crucial to ensuring the project's feasibility and ultimate success. Logistics is a complex issue involve material flow of different units.

In the last decade, wind energy markets have witnessed improvements in power efficiency and capacity factors, driven by advancements in technology featuring larger rotor diameters and hub heights. Capital cost and capacity factor of wind energy in 2010 and 2022 is presented in Table 4. There has been a significant drop in capital costs for onshore and offshore wind farms, with a reduction of 41%, and 33% respectively. Moreover, the capacity factor for both types of wind farms has also been improved in the last decade.

Table 3.4: Capital cost and capacity factor of wind energy in 2010 and 2022 (IRENA, 2022)

Type of Wind Farm	**Capital Cost (2010) [$/kW]**	**Capital Cost (2022) [$/kW]**	**Capacity Factor (2010) [%]**	**Capacity Factor (2022) [%]**
Onshore wind farm	2,179	1,274	27	37
Offshore wind farm	5,217	3,461	38	42

The economic viability of a project typically involves an assessment of its levelized cost of electricity (LCOE), representing the minimum price point beyond which a re-

turn on investment could be realized (Bosch et al., 2019). LCOE has been employed to compare energy costs among various energy sources, disregarding external expenditures, and serves as an important indication that decision-makers and policymakers should pay attention to (Ram et al., 2018). A typical breakup of LCOE of wind energy is shown in Figure 3.8.

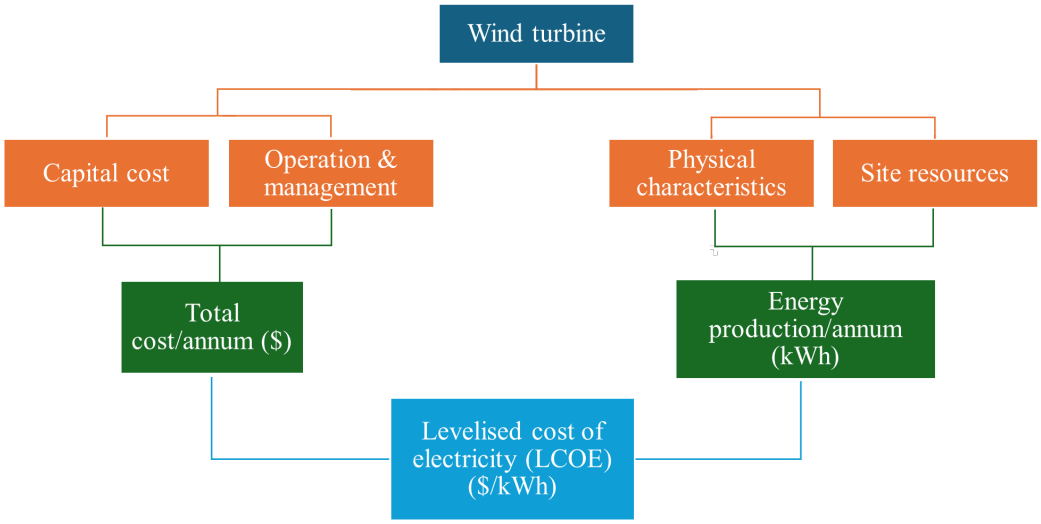

Figure 3.8: Factors affecting LCOE of wind turbine (Bosch et al., 2019; IRENA, 2022; Y. Yao et al., 2021)

In 2022, the global weighted-average LCOE for onshore wind projects was 52% lower than fossil fuel-based plants. This marks a significant shift from the scenario in 2010 when the global weighted-average LCOE of onshore wind was 95% higher (IRENA, 2022). The comparison chart of LCOE between wind energy and fossil fuel is depicted in Figure 3.9. It is worth noting that unit price of the wind power has come down to 0.033 $/kWh from 0.107 $/kWh in 2010. Success of renewable energy in general and wind energy in particular, depends heavily on price at the users end.

Over the past two decades, there has been a significant increase in the hub height of wind turbines to capture more energy. This is driven by the understanding that wind speeds generally increase with altitude as it encounters less obstruction from surface-level features such as trees, vegetation, and structures. The hub height is defined by the vertical distance between the ground and the centre of a wind turbine's rotor. During 1998-99, this height measured only 58.6 meters. However, as of 2022, this measurement has increased by 73% in the USA.

In addition to the hub height, there has been an increase in the rotor diameter. Larger rotor diameters result in a larger swept area, which in turn enhances the capacity to harness wind energy and generate more electricity. Another advantage of larger diameter wind turbines compared to shorter ones is their ability to extract energy even from regions with low wind speeds. The rotor diameter has seen a substantial increase from

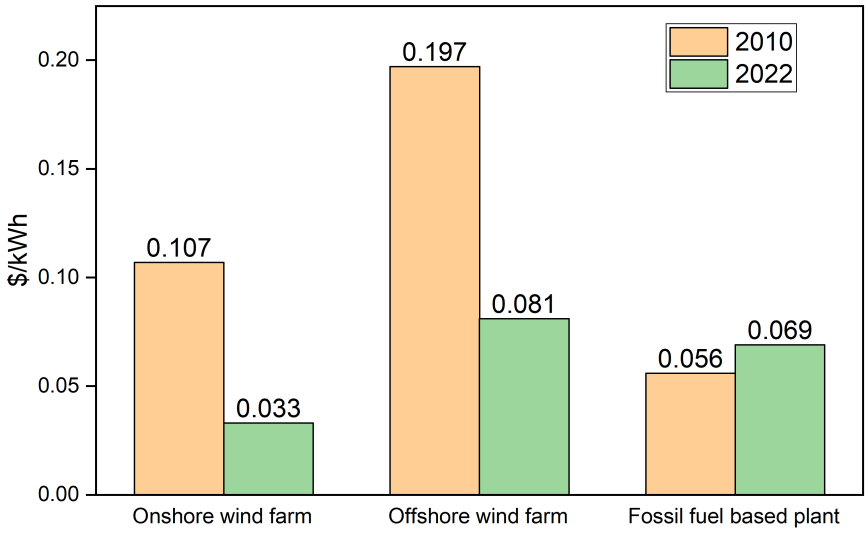

Figure 3.9: Comparison of LCOE between wind energy and fossil fuel based plants (IRENA, 2022)

48.2 meters in 1998 to 131.6 meters in 2022, representing a growth of 173%. Growth of wind turbine over the years in USA is shown in Figure 3.10.

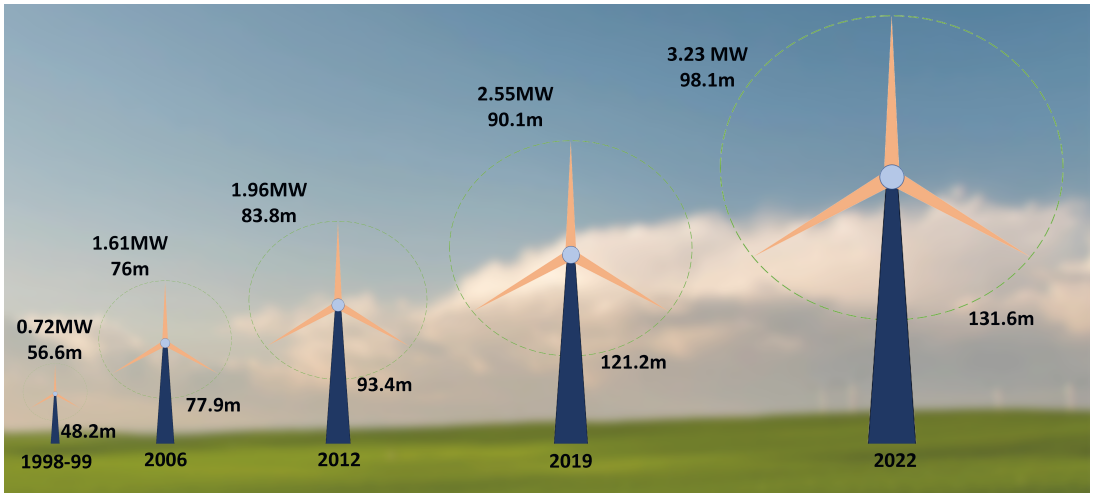

Figure 3.10: Growth of wind turbine over the years in USA (Wiser et al., 2023)

3.5 Waste disposal

Waste disposal is an important part of environmental management and thus, disposal of waste from wind power industry is a concern as already highlighted earlier. In this section, the disposal of waste materials generated during wind power generation, including turbine components at the end of their life cycle have been discussed. To ensures the sustainability of wind energy, efficient waste management strategies, recycling, and disposal procedures are also explored. Blade materials are shredded in co-processing

and these blade waste are used as raw material in the clinker production for cement industry benefits of environment in terms of material substitution (J. Chen et al., 2019; Nagle et al., 2020).

Blade disposal: The disposal of wind turbine blades presents a significant challenge due to their large size and composite material composition. Sustainable options include recycling, repurposing, or converting blades into alternative materials, such as construction materials or park benches (Majewski et al., 2022).

Steel and concrete recycling: The tower structure and foundation of wind turbines are primarily made of steel and concrete, which can be recycled or reused in various construction projects, minimizing the need for raw materials extraction (Yazdanbakhsh et al., 2018).

Lubricants and oils: To ensure the smooth operation of wind turbines, lubricants and oils are necessary. It is crucial to handle these substances with care, collecting and treating them as hazardous waste to prevent contamination of soil and water. Proper disposal or recycling at authorized facilities becomes imperative (Gonzalez-Reyes et al., 2020).

Electronic waste: Wind turbines contain electronic components that may contain hazardous materials like lead and mercury. These components should be separated and sent to specialized recycling facilities for proper handling and extraction of valuable metals (Andersen et al., 2014; Mudali et al., 2021).

In the past, landfills were frequently used to dispose of composite parts where it requires a lot of space and does not permit the recovery of the embodied energy in composites. Prior to being dumped in the ground, waste is frequently pre-treated to lessen its volume. To recover the embodied energy, incineration, a method of burning composite scrap in cement kilns, is incorporated. It also use non-combustible materials like glass fibres and mineral fillers into the production of cement (Pickering, 2006).

3.5.1 Recycling Methods

Prior to making a decision about which materials to use or how to design a product, the recycling/reusing concept must be introduced. Materials must be recovered or recycled once they reach the end of its useful life. Recycling becomes a financially viable waste management solution when the cost of the recycling process is lower than that of obtaining raw materials from reclaimed sources (Psomopoulos et al., 2019).

There are three fundamental recycling technologies: mechanical recycling, thermal and chemical treatment. Thermal recycling process includes pyrolysis and fluidized-bed processing. Mechanical recycling can be applied to both glass fibre-reinforced plastics (GFRPs) and carbon fibre-reinforced plastics (CFRPs) (Geiger et al., 2020). The method entails shredding, crushing, or milling FRPs and then, at the composite level, separating

the resulting fragments into fractions rich in fibre and rich in resin. These fractions can be used directly in the construction industry as fillers or reinforcements in new composite materials (Rathore & Panwar, 2023).

Figure 3.11 describes the waste management system in connection with WECT. A more sustainable waste management system can be achieved through continuous advancements in wind turbine design and materials. In the near future, research should focus on creating recyclable and environmentally friendly turbine parts, enhancing dismantling procedures, and identifying new alternatives for waste materials.

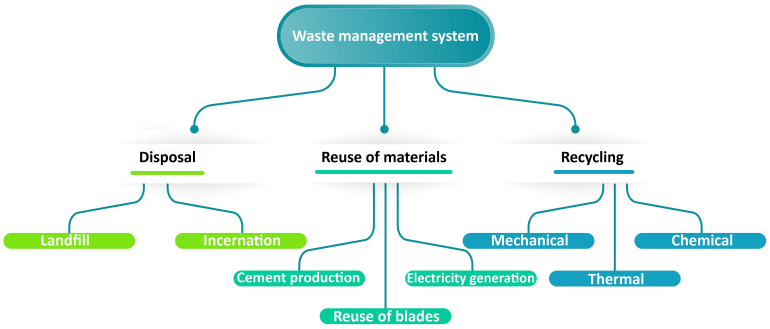

Figure 3.11: Waste management system for WECT (Rathore & Panwar, 2023)

3.6 Technology advancement

Advancements in renewable energy technologies play a pivotal role in fostering sustainable development and addressing various environmental challenges associated with energy production. The ongoing discussion highlight the innovations and research in wind turbine design, materials, and manufacturing processes which has direct bearing on sustainability. It explores the role of advanced control systems, aerodynamics, and turbine optimization techniques in enhancing the efficiency and sustainability of wind energy (Baños et al., 2011; Chehouri et al., 2015; Dhunny et al., 2019).

The performance and efficiency of a wind turbine are significantly influenced by the wind speed and the shape of airfoil used. Selecting the appropriate blade profile can substantially enhance the turbine's overall performance, contributing to greater efficiency and output (Das Karmakar & Chattopadhyay, 2022; Das Karmakar et al., 2023; Rahman et al., 2024). Consequently, the location of wind turbines is of utmost importance. To illustrate, a wind turbine situated in an area with an average wind speed of 15 mph has the potential to generate 238% more electricity compared to one located in an area with an average wind speed of 10 mph. This underscores the critical role of optimal location selection to maximize the electricity output and overall effectiveness of wind energy systems (Manwell et al., 2010)].

Furthermore, the design of wind farms holds significant importance, particularly

in the context of heterogeneous configurations. Such setups feature a combination of horizontal axis wind turbines, alternating between two and three blades In a vertically staggered wind farms, larger and smaller turbines are arranged alternatively, creating an optimized layout for efficient wind energy generation (Chatterjee & Peet, 2019; Hayat et al., 2019).

When harnessing wind for electricity generation, the size of the wind farm matters significantly. Horizontal axis wind turbines can be mounted on tall towers, some exceeding 400 feet in height, to take advantage of stronger and more stable winds found at higher altitudes. Compared to the typical blade size of 15 feet back in 1980, advancements in materials such as E-glass/polyester now allow for blade lengths of up to 150 feet (Vassilopoulos & Keller, 2011). This increase in size is noteworthy because the power output of a wind turbine is directly proportional to the square of its blade length, thus significantly enhancing its power generation capacity.

Modern turbines exhibit enhanced efficiency, particularly at lower wind speeds, a notable improvement compared to older models. Furthermore, they demonstrate the capability to operate in winds reaching up to 50 mph, a significant advancement that would have necessitated shutdowns or failures in previous turbine models. This progress signifies a notable leap forward in the reliability and performance of contemporary wind turbines.

3.6.1 Innovative designs

The latest advancements in wind turbine design, coupled with innovative airfoil technology, are driving significant strides towards sustainability in the wind energy sector. Along with this, there is a growing interest among investors on offshore wind technology, particularly in the development of floating wind turbines and bladeless wind turbines. Floating wind turbines gains more popularity for a number of reasons as they offer more consistent and greater wind speeds in deeper waters. From the utility-scale point of view, floating wind turbines have a longer farm life-roughly 25 to 30 years (Darwish & Al-Dabbagh, 2020).

Bladeless wind turbines (BWT) appear to offer greater sustainability compared to HAWT and VAWT due to their lower maintenance requirements, silent operation, and no harm to avian species (Francis et al., 2021; Tandel et al., 2021). BWT utilizes Vortex Induced Vibration (VIV) to harness energy. As the wind flows around the structure, vortices form in cyclic patterns and these patterns induce vibration in the structure and reaches resonance when the wind force touches a certain threshold (Francis et al., 2021). A new strategy is evolving to address two major challenges facing the wind industry: finding recyclable and sustainable turbine blades that can prevent blade deterioration

over time. The goal of this creative idea is to develop wind turbine blades that are as durable and environmentally friendly as possible. The innovation in airfoil design is a big step in solving the sustainability issues associated with wind energy generation.

Biomimetics, also known as biomimicry, which mimic the elegance and efficiency of biological processes, is a dynamic method that draws inspiration from natural structure patterns to address both technological and aesthetic problems. This method of designing wind turbine blades has produced novel ideas like spiroid winglets and bionic multi-tip winglets, as well as designs that are based on a variety of natural occurrences, including dolphin heads, owls, dragonflies, whales, lotuses, and biological Alula. These bio-inspired designs provide a peek of what nature-inspired solutions may do to improve the performance, sustainability, and efficiency of wind energy technologies. Biomimetic wind turbine designs, have the potential to open up new avenues for innovation in renewable energy (Krishnan et al., 2023). Mishnaevsky Jr et al., 2023 introduced a new concept of bio-inspired dual-mechanism-based interface adhesives, incorporating both mechanical interlocking of fibres and chemical adhesion. This design ensures a robust attachment during operation while allowing for adhesive joint separation, facilitating the re-use of blade parts.

3.7 Optimization, decision making and life cycle assessment

Notably, optimization algorithms emerge as valuable tools for tackling complex issues within the realm of renewable energy systems. By utilizing suitable algorithms, solutions can be efficiently derived, contributing to the enhancement of the overall efficiency, reliability, and environmental impact of renewable energy technologies. There are several optimization techniques available which are commonly employed in addressing complex problems within the realm of wind energy systems such as Lagrangian relaxation, mixed-integer and interval linear programming, quadratic programming, and the Nelder–Mead Simplex search approach. Along with that, an increasing number of studies are now turning towards heuristic optimization techniques, notably genetic algorithms and particle swarm optimization, Pareto-based multi-objective optimization, and parallel processing that hold considerable promise for further advancements in the field of wind energy (Baños et al., 2011). To improve the efficiency of a lift type VAWT under low tip speed ratios (TSR), while addressing both structural and aerodynamic goals, Rasekh and Aliabadi (Rasekh & Aliabadi, 2023) conducted a comprehensive multi-objective optimization analysis. multi-objective optimization investigation. The study utilized a proprietary non-dominated sorting genetic algorithm (NSGA-II) algorithm for the optimization process. This synergy between technological innovation and optimiza-

tion methodologies holds promise for addressing critical energy-related environmental issues and promoting a more sustainable energy landscape.

3.7.1 Multi-criteria decision making method (MCDM)

Considering the fact that the cost of wind turbines constitutes a significant portion of the total project expenditure, the selection of appropriate wind turbines is paramount. Moreover, the capacity factor of wind turbines can be influenced by their suitability for specific sites. One of the most challenging aspects of constructing a wind turbine system is figuring out the best solution that balances both technological and economic objectives effectively (Ridha et al., 2024). MCDM methods become essential in evaluating and selecting renewable energy solutions, particularly when multiple conflicting factors are considered simultaneously (A. H. Lee et al., 2012). Performance, capital cost, greenhouse gas emissions, and creating employment are the dominant factors across technical, economic, environmental, and social aspects, respectively (J.-J. Wang et al., 2009). Assessments of renewable energy projects have made use of various MCDM techniques, such as multi-objective decision making (MODM), analytic network process (ANP), analytical hierarchy process (AHP), multi-attribute utility theory (MAUT) etc. MCDM has been used in the planning of solar energy projects, geothermal projects, hydro-site selection, and in selecting the optimal location for an wind power station which is imperative for the overall success and viability of any wind energy project (Kahraman et al., 2009; San Cristóbal, 2011; J.-J. Wang et al., 2009).

Elkadeem et al., 2022 presented a novel geospatial MCDM model that maps and evaluates, the geographical, technical, and economic potential of onshore wind turbine and solar photovoltaic power facilities in Egypt. By taking sixteen different, often contradictory evaluation factors into account, they identified the regions that are favourable to wind turbine development. The Additive Ratio Assessment (ARA) MCDM method was employed by Ruiz et al., 2023 to evaluate wind power in this study. This approach utilizes a single-valued neutrosophic set to address uncertainties in the data. The findings indicate that turbine resource ranks highest, while the economic criterion performs the least favourably in the assessment.

Despite the advantages of employing MCDM techniques for site selection, there are notable drawbacks such as limited utilization of available information and potential data loss during the decision-making process, overlooking the interaction issues within the realm of the neutrosophic vicinity (Abdel-Basset et al., 2021).

3.7.2 Life cycle assessment (LCA)

A comprehensive analysis of the environmental effects of many processes, including the production of wind power, is possible through life-cycle analysis. At present,

stakeholders worldwide rely on LCA as the primary approach for evaluating the environmental impact of products (Finkbeiner et al., 2014; Sikdar, 2003b). LCA serves as a useful analytical method for assessing the possible costs and environmental effects of a product system. It involves processes which gather and examine the inputs, outputs, and possible environmental effects related to a product system over the course of its whole life cycle (Guinée, 2002).

The ISO 14040 and 14044 standards define four basic processes that are commonly followed in life cycle assessments: goal and scope definition, life cycle inventory, impact assessment, and interpretation. Important choices on the methodology, boundaries of functional units, system specifications, and the extent of environmental impact assessments are made during the goals and scope phase (Baumann & Tillman, 2004). Choices made here regarding methodologies, system boundaries, delineation points, or functional units can profoundly influence the resulting outcomes of the assessment. According to the selected system limits and techniques, the inputs and outputs for the full life cycle are estimated in the life cycle inventory (LCI). Attributional and consequential LCIs are the two main varieties (Ekvall & Weidema, 2004). An attributional LCI, concentrates on characterizing the relevant physical flows that enter and exit the life cycle system with respect to environmental effects. A consequential LCI aims to provide light on the effects of decisions made by showing how certain changes in the life cycle may affect the pertinent physical flows that affect the environment. After that, the results of the inventory are transformed into information that is useful to the environment in the following stage, the life cycle impact assessment and interpretation (LCIA).

In connection with wind energy production systems, LCA provides important insights into the whole range of greenhouse gas emissions by covering every phase, from raw material extraction to ultimate disposal or recycling. The life cycle framework encompassing material and energy flows throughout stages such as materials production, manufacturing, use and service, and end-of-life management, strengthens the relationships between activities related to production and consumption. Various tools have been created to measure the elements of environmental, economic, and social sustainability. LCA, life cycle energy analysis (LCEA), life cycle cost analysis (LCCA), and life cycle sustainability indicators are valuable analytical approaches that have been established for this purpose (Anastas & Zimmerman, 2006). This approach thoroughly investigates the whole life cycle of a wind turbine, starting from the extraction of raw materials to the disposal of materials after the product has reached the end of its useful life (I. S. Organization, 1997).

The metrics derived from LCA not only enable the assessment of environmental implications but also provide a means to monitor and enhance the ongoing development of environmental sustainability throughout the wind turbine's life cycle. Installation and maintenance, in particular, are frequently left out of turbine LCAs that only look

at greenhouse gas emissions and/or energy (Ji & Chen, 2016; Jungbluth et al., 2005; Martínez et al., 2015; Oebels & Pacca, 2013; Proops et al., 1996; Rajaei & Tinjum, 2013; Rule et al., 2009). Several previous wind turbine LCAs have included an uncertainty /scenario /sensitivity analysis for different factors. However, just one study (White, 2006) focused on medium-sized turbines (1 MW) and only measured energy and greenhouse gas emissions, looked at the effect of turbine lifetime.

An additional facet of technological advancements, particularly from a commercial economic perspective, lies in the potential for increased utilization rates within the wind energy sector. Moreover, the implementation of policies allowing for the establishment of wind farms in regions with steady and predictable wind conditions could further contribute to increasing usage rates. The trajectory of the wind energy sector towards financial stability is evidently shaped by various factors, encompassing enhanced efficiency, technological advancements, and escalating costs It's clear that the wind energy industry is heading toward financial stability and it is influenced by a number of factors, including improved efficiency, technological developments, and growing costs for other energy sources like oil and natural gas.

3.8 Concluding remarks

This study explores the issues on the sustainability of wind power, considering its social, environmental, and economic dimensions. Although using wind power instead of fossil fuels to produce electricity has the advantage of limiting carbon emissions and very low water usage, there exist certain problems as well. These include concerns related to the environmental impact of materials used, as well as issues with human health, biodiversity, and human settlements. The growth in wind energy is found to be driven by reducing cost with immense benefits in the context of global warming and ozone depletion. On the negative sides are bird mortality, noise and NIMBY type syndromes. Waste handling also becomes a challenging issue with the rapid expansion and diversification of wind-based systems. Studies show that even for existing plants, there exists ample scope for improving sustainability by proper recycling, waste disposal and site selection.

It is noted that the assessment of sustainability for wind energy is a complex field with multifaceted nuances. While environmental impact assessment is generally mandatory for building wind energy plants (in fact, for any commercial power plants), overall sustainability is not really assessed as of now. Thus, there is an urgent need for developing methodologies and tools which can be based on, e.g. MCDM techniques for the proper assessment of WECT. It has also to be borne in mind that wind power is intermittent by nature and often has to be deployed in tandem with other power sources (Das Karmakar & Chattopadhyay, 2024). In this work, the effect of hybridization of energy

sources on sustainability is not discussed as this calls for a more detailed study.

The current survey on the sustainability of WECT showed that despite being a source of green energy, there is still ample scope for improvement. The current work thus further investigates the improvement of WECT technology for higher efficiency.

CHAPTER 4

VAWT with NACA0017 Airfoil

4.1 Introduction

Demand for renewable energy has increased significantly in recent years due to the negative effects of depleted conventional fuels to the environment that led to air pollution, global warming and climate change. The rising cost of fossil fuels and the depletion of conventional energy sources have prompted researchers to seek out environmentally suitable alternatives such as wind, solar, tidal, biomass and geothermal. Among the alternative energy resources, wind energy has the potential to grow as an alternative energy source which has very less adverse effect to the environment (Rahman & Chattopadhyay, 2023). Due to its vast availability and cost effectiveness, wind energy has been used for generations to power water pumps and grain grinding equipment (Ackermann & Söder, 2000; Yannopoulos et al., 2015). Wind energy has become the primary source of electricity generation in past few decades. In the year 2020, renewable energy accounted for 11.2% of worldwide energy consumption and 29% of electric power generation. Since 2000, global cumulative installed wind capacity has expanded substantially, reaching 743 GW in 2020 (Murdock et al., 2021).

The wind energy conversion technology (WECT) is applied to extract maximum possible energy from the wind energy source. Energy resource assessment, hardware design and installation are the three basic stages of this technology. In the first stage, the wind power potential is evaluated for several parts of the world. For example, the wind power potential of East and Northeast region of India have been assessed by Rahman and Chattopadhyay by introducing a new technique to calculate the parameters involve in wind assessment (Rahman & Chattopadhyay, 2020). The second stage is comprised of installation of an efficient wind turbine system. There are basically two types of wind turbine systems. One is horizontal axis wind turbine (HAWT) and another is vertical axis wind turbine (VAWT). HAWT is widely used in the wind energy conversion technology as it has high power efficiency compared to VAWT despite it re-

quires a complex yaw mechanism (Mohammed et al., 2019). HAWTs also require high wind velocity and huge empty space to prevent aerodynamic interferences (W.-H. Chen et al., 2017). Whereas, VAWTs can be installed in urban and semi urban areas due to its omni-directional characteristics, less noise, simple construction, low installation cost and maintenance (Dossena et al., 2015). Also, VAWTs can harness energy from highly turbulent wind flows which are very common in the urban areas (W.-H. Chen et al., 2017). VAWTs can also extract wind power from low wind speed regions as well as very high wind speed regions (Bianchini et al., 2017). Recent research found that VAWT has better potentials for offshore platform compared to HAWTs in terms of scalability, and simplicity of design (Tescione et al., 2014). Based on aerodynamics principles, VAWT can be classified into two groups: lift type and drag type VAWTs (Sagharichi et al., 2018). Darrieus VAWT is an example of lift type and Savonius VAWT is an example of drag type. H-type Darrieus wind turbine provides greater efficiency than drag type (Jain & Saha, 2020b). Although VAWT offers various advantages over HAWT, the most significant downside of VAWT is its low efficiency, which scientists believe is one of the most significant challenges of VAWT. Several researchers have already carried out considerable research in the field of VAWT, utilising analytical, experimental, and numerical methods to improve its efficiency and overall performance.

Computational Fluid Dynamics (CFD) has been chosen as one of the most promising, cost-effective, and accurate approach for studying the complicated, unstable aerodynamics characteristics of VAWT, with the capacity to produce results that are comparable to those obtained from experiments. Three-dimensional solution of Navier-Stokes equation can be used to analyse VAWT as it provides better results comparable to experimental results (Jin et al., 2015). To cite some important work, Castelli et al., 2011 evaluated the aerodynamic performance of Darrieus wind turbine with three straight blades having NACA0021 blade profile. The CFD analysis of a combined Darrieus and Savonius VAWT at various conditions is performed by Debnath et al., 2009. It showed that the CFD results were as good as experimental results. Nobile et al., 2014 investigated a CFD simulation of augmented VAWT with NACA0018 blade profile. Combined experimental and CFD analysis of VAWT were presented by many authors (Bianchini et al., 2017; Franchina et al., 2019; Howell et al., 2010; Lam & Peng, 2016). Similarly, several researchers have performed CFD simulations to study aerodynamic behaviour of VAWT for enhancing its performance (Jiang et al., 2020; Lanzafame et al., 2014; Qin et al., 2011; Souza et al., 2017).

The performance parameters such as number of blades, blade shape, pitch angle, wind speed, tip speed ratio (TSR), rotor solidity need to be studied to evaluate the performance of VAWT. Blade design has been an essential research field for wind turbine technology since the airfoil profile shape has a significant impact on the aerodynamic efficiency of a wind turbine (Benim et al., 2018). The overall performance of VAWT has

been analysed by several researchers on the basis of different blade shapes and thickness. The performance of 3 bladed H-rotor Darrieus VAWT with 24 different shapes of airfoils have been analysed by Hashem and Mohamed (Hashem & Mohamed, 2018). The maximum power coefficient is provided by S1046 airfoil. NACA0015 showed maximum C_P of 0.3243 among the NACA 4 series airfoils. M. H. Mohamed et al., 2019 carried out a numerical analysis of H-type Darrieus VAWT using 25 airfoils shapes to study effects of airfoils shape and pitch angle. LS (1)-0413 and NACA63-216 airfoils gave highest power coefficient and NACA0015 airfoil provided the best efficiency followed by NACA0018 out of NACA 4-digit series airfoils. The performance of H-rotor VAWT with 20 different types of blade profiles comprising of NACA-series, 4 A-series, 4 S-series and 5 FX-series were compared by M. H. Mohamed, 2012. 2D CFD analysis showed that peak coefficient of performance was achieved by NACA0018 blade profile followed by NACA0015. Y.-T. Lee and Lim, 2015 studied the effects of parameters such as rotor diameter, chord length, pitch angle and blade shape thickness on the aerodynamic performance of Darrieus VAWT. NACA0015, NACA0018 and NACA0021 were compared and results predicted that peak efficiency obtained from the rotor with NACA0015 blade shape. 3D simulation has been performed on the performance analysis of VAWT using three different airfoils by Elkhoury et al., 2015. NACA0018, NACA0021 and NACA634-221 blade profiles were investigated. Both numerical and experimental results showed that NACA0021 has better power coefficient than the NACA0018, although NACA0018 is 3% thinner than the NACA0021. Numerical studies of VAWT having Joukowski and classical NACA airfoils were conducted by Parakkal et al., 2019. Results found that the wind turbine with Joukowski airfoils performed better than the conventional NACA series. Durrani et al., 2011 conducted 2D CFD analysis of VAWT on ten symmetric airfoils. Standard $\kappa - \epsilon$ turbulence model was implemented to evaluate the performance of VAWT. The results revealed that highest efficiency was provided by the NACA0022 airfoil. However, the performance of VAWT decreases as the airfoil thickness decreases from 22% to 12% when TSR is below 2.

The state-of-art survey as enumerated above points out to the fact that the majority of the studies aimed to improve performance of VAWT are related to traditional NACA 4-digit series with thicknesses ranging from 12% to 23%. Symmetrical aerofoils, such as NACA0015, provide the best performance, whereas NACA0018 provides the best efficiency in specific instances. Thinner airfoils, such as NACA0015, perform better when utilised with reduced solidity at high TSR as the drag forces applied to thinner blades is comparatively less whereas thicker airfoil provides better structural strength (Durrani et al., 2011). It is observed that the aerodynamic performance of NACA0017 is meagrely studied though structurally. NACA0017 airfoil demands higher attention as recent studies demonstrate that this airfoil shows best start-up and transient performance

even in comparison to that of NACA0015 and NACA0018 (Maalouly et al., 2022).

The primary goal of our current work is to evaluate the performance of three-bladed Darrieus VAWT with NACA0017 blade profile using numerical simulation. The performance of this airfoil is benchmarked against NACA0015 which has excellent performance in application of wind turbine (Hashem & Mohamed, 2018; Y.-T. Lee & Lim, 2015; M. H. Mohamed et al., 2019).

4.2 Aerodynamics and performance of VAWT

VAWT was first proposed in 1931 by an aeronautical engineer George French Jean Marie Darrieus and patented in the United States. H-type Darrieus VAWT with three blades is shown in figure 4.1. When the turbine comes into contact with free-flowing wind, it rotates with an angular speed ω around an axis of radius R.

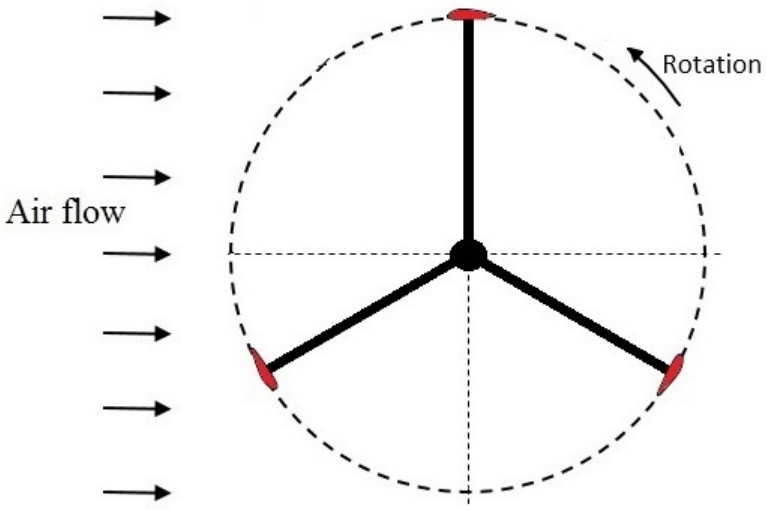

Figure 4.1: Top view of H-type Darrieus VAWT with three blades

There are several parameters which affect the performance of a VAWT, such as the number of blades, blade shape, pitch angle, wind speed, TSR, rotor solidity, torque coefficient (C_T), and power coefficient (C_P) (Nobile et al., 2014). To specify the rotor design, an important parameter known as the rotor solidity (σ) of a VAWT can be expressed as

$$\sigma = \frac{nc}{2R} \tag{4.1}$$

where n, c, and R are the number of blades, chord length of the blade, and radius of the rotor, respectively.

TSR can be defined as the ratio of the tangential speed of the tip of the blade to the free-flowing wind speed and it is expressed by equation 4.2:

$$TSR = \frac{\omega r}{v} \tag{4.2}$$

TSR determines a turbine's operating condition and plays an important role in evaluating rotor performance.

The torque coefficient (C_T) and power coefficient (C_P) are used to assess the performance of a wind turbine, which are expressed as follows:

$$C_T = \frac{2T}{\rho A R v^2} \tag{4.3}$$

$$C_P = \frac{P}{\rho v^3 H R} \tag{4.4}$$

where P is power and it is expressed as $P = \frac{T \cdot N}{60}$, N is revolutions per minute, T is torque, ρ is the density of air, v is free stream velocity, and A is the cross-sectional area of the rotor.

C_P and C_T are related through the TSR of airfoils as

$$C_P = C_T \times TSR \tag{4.5}$$

4.2.1 Computational modelling

The numerical analysis is conducted on the performance of an H-type Darrius VAWT with NACA0017 airfoil shaped straight blade with the help of CFD software ANSYS-FLUENT 16.2 version. While for capturing detailed flow structure three dimensional modelling is essential, this part of the study is limited to two-dimensional modelling as previous studies revealed that the results obtained from two dimensional CFD agreed with experimental data reasonably (Bianchini et al., 2017; Hashem & Mohamed, 2018).

4.2.1.1 Flow domain

Earlier studies show that effect of domain size on the performance of the VAWT is significant (Rezaeiha et al., 2017). The CFD analysis may give wrong results and there may be overestimation of the performance of VAWT if the computational domain is not selected properly. Rezaeiha et al., 2017 showed guidelines for selecting minimum domain size and predicted an optimum domain where results are very less affected by uncertainty in the boundary conditions. The present computational domain has inlet and outlet distances from the centre of the rotor of 22.5D and 7.5D respectively in order to allow the wake region to fully develop. A large domain width is chosen to avoid solid blockage. The domain size is shown in figure 4.2 where D is the rotor diameter. The geometry has been divided in two regions: a rotating domain of circular interface with

1.5D diameter and the rectangular stationary domain beyond the circular interface. The two regions are interconnected with each other by using sliding interface to maintain the continuity of the incoming velocity and to provide the correct values of velocities for the rotating domain.

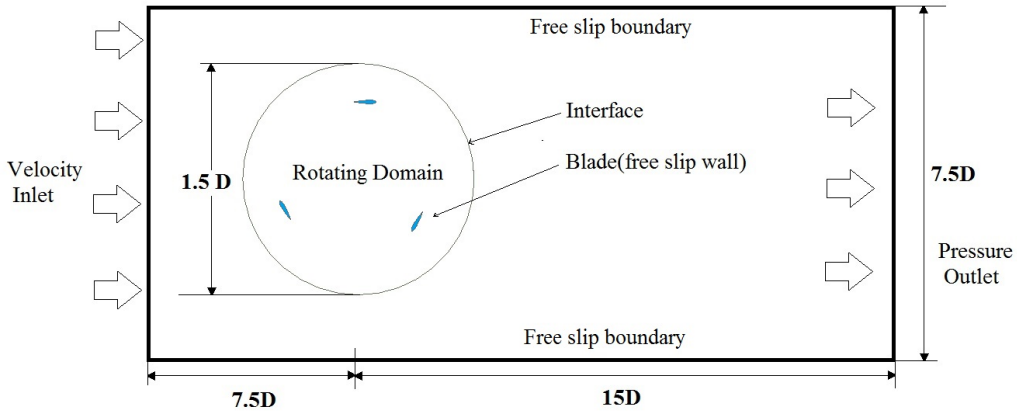

Figure 4.2: Computational domain for present study

4.2.1.2 Meshing

In the present work, quad dominant mesh waas selected for the whole computational domain. Mesh was refined near the airfoil walls with quadrilateral mesh having maximum skewness less than 0.86 for better simulation result. The mesh size was set to 0.2 mm near the blade walls to ensure a good-quality mesh. The first cell height was set to ensure that the y^+ values near blade did not exceed the SST model's upper limit i.e., y^+ 1. The non-dimensional wall distance y^+ is defined as:

$$y^+ = \frac{yu_\tau}{\nu}$$

where: y is the distance from the wall to the center of the first computational cell (in meters), $u_\tau = \sqrt{\frac{\tau_w}{\rho}}$ is the friction velocity, τ_w is the wall shear stress, ρ is the fluid density, ν is the kinematic viscosity of the fluid (in m^2/s). The growth rate parameter was fixed at 1.2.

The mesh structure of the present study is demonstrated in figure 4.3. Present simulation have been validated with the experimental and CFD results performed by Balduzzi, Bianchini, Ferrara, and Ferrari, 2016 with parameters as shown in Table 4.1. The simulation is conducted on three-bladed VAWT having NACA0018 airfoils and with the same geometrical characteristics as of Balduzzi, Bianchini, Maleci, et al., 2016.

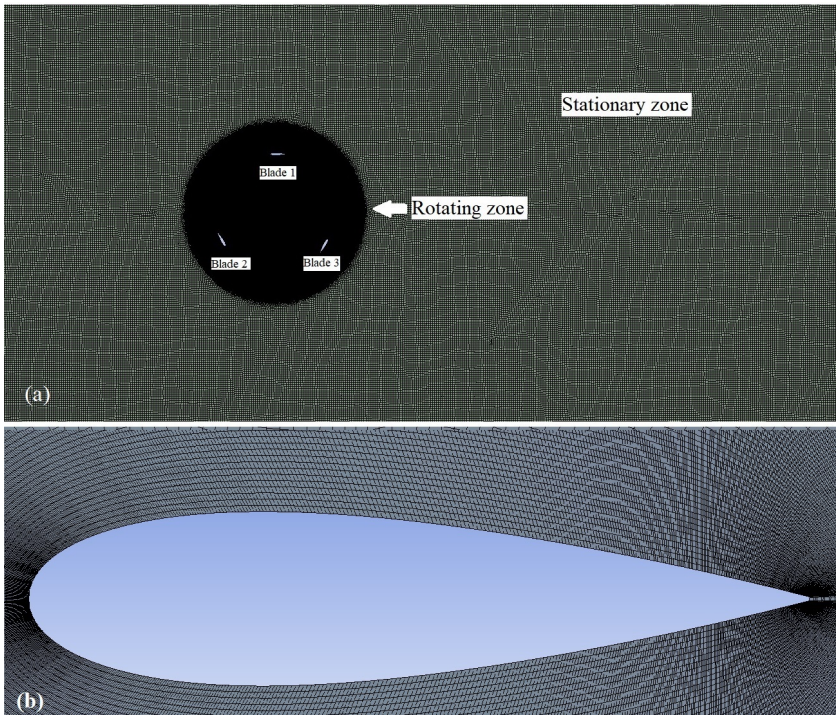

Figure 4.3: Details of meshing of the geometrical model: (a) computational domain (b) meshing around airfoil

Table 4.1: Comparison of rotor geometries

Study	Type of Aerofoil	Diameter D (m)	Chord (m)	Solidity
Present work	NACA0017	0.70	0.10	0.42
Castelli et al., 2011	NACA0021	1.03	0.0858	0.50
Balduzzi et al., 2016	NACA0018	1.70	0.246	0.44

4.2.2 Governing equations

As observed from the prior studies, CFD-based numerical investigations of VAWT have been frequently employed due to the advantages which include relatively high computational speed, with low cost, and the ability to do full scale analyses whether time dependent or independent. Unsteady Reynolds averaged Navier-Stokes (URANS) equations were implemented to calculate the velocity and pressure at each element of the computational domain as the flow field is largely turbulent. The continuity equation and the momentum equations for unsteady, incompressible flow can be expressed as:

$$\frac{\partial \bar{u}_i}{\partial t} + \frac{\partial \bar{u}_i}{\partial x_i} = 0 \tag{4.6}$$

$$\rho \frac{\partial \bar{u}_i}{\partial t} + \rho \bar{u}_i \frac{\partial \bar{u}_i}{\partial x_i} = \frac{\partial}{\partial x_j}\left[-\bar{p}\delta_{ij} + \mu\left(\frac{\partial \bar{u}_i}{\partial x_j} + \frac{\partial \bar{u}_j}{\partial x_i}\right)\right] - \tau'_{ij} \tag{4.7}$$

Where, the term $\tau'_{ij} = -\rho\overline{u'_i u'_j}$ is referred to as the Reynolds shear stress tensor. The Boussinesq assumption can be used to calculate τ'_{ij}, which is given as

$$\tau'_{ij} = \mu_t\left(\frac{\partial \bar{u}_i}{\partial x_j} + \frac{\partial \bar{u}_j}{\partial x_i}\right) - \frac{2}{3}\rho k \delta_{ij} \tag{4.8}$$

The turbulent (eddy) viscosity (μ_t) for the SST k-ω model is calculated as:

$$\mu_t = \frac{\rho\, a_1\, k}{\max\left(a_1\omega, SF_2\right)}$$

Where,

a_1 = model constant, typically 0.31, k = turbulent kinetic energy, ω = specific dissipation rate, S = invariant measure of the strain rate and F_2 = blending function (part of the SST formulation).

4.2.2.1 Boundary conditions

The approaching velocity at the inlet boundary is taken as 3 m/s, 4 m/s and 5 m/s corresponding to a Reynolds number of 20,537; 27,383; 34,229 respectively where the characteristic length for defining Reynolds number (Re) is the chord length. Turbulent intensity is set at 5% at velocity inlet. An appropriate rotational velocity is also applied to the rotating zone for mesh motion. At the outlet, atmospheric pressure condition is imposed as the domain is connected with ambient and other surfaces are considered with vanishing derivatives of flow variables i.e., free-slip.

4.2.3 Turbulence model

URANS equations are used for the turbulent flow field. SST k-ω, a two-equation turbulence model is considered for the closure of turbulent flow field (Biswas & Gupta, 2014; Jain & Saha, 2020a; Tabatabaei et al., 2019).

The transport equations for turbulent kinetic energy (k) and turbulent specific dissipation (ω) in the SST k-ω model are expressed in Equations:

$$\frac{\partial \rho k}{\partial t} + \frac{\partial \rho k u_i}{\partial x_i} = \frac{\partial}{\partial x_j}\left(\Gamma_k \frac{\partial k}{\partial x_j}\right) + G_k - Y_k + S_k \tag{4.9}$$

$$\frac{\partial \rho \omega}{\partial t} + \frac{\partial \rho \omega u_i}{\partial x_i} = \frac{\partial}{\partial x_j}\left(\Gamma_\omega \frac{\partial \omega}{\partial x_j}\right) + G_\omega - Y_\omega + S_\omega + D_\omega \tag{4.10}$$

Where G_k and G_ω are the generation of k and ω due to mean velocity gradients, respectively; Γ_k and Γ_ω are the effective diffusivities of k and ω, respectively; Y_k and Y_ω are the dissipation of k and ω due to turbulence, respectively; S_k and S_ω are source terms of k and ω, respectively; and D_ω is the cross-diffusion term (Jafaryar et al., 2016).

4.2.3.1 Grid independence test and time step setting

To get an appropriate mesh size which provide optimal result, several of numerical simulations have been conducted using seven different levels of mesh with grid numbers of 324901, 414059, 606857, 721071, 811588, 914667 and 1005719 employing SST k-ω turbulence model at TSR 3 with inlet velocities of 3 m/s, 4 m/s and 5 m/s. It is to be borne in mind that VAWTs are used at relatively low speed winds. Result shows that the power coefficient reached a stable value with last three mess sizes as shown in figure 4.4. Therefore, the mesh with element of 8,11,588 was taken into consideration for the present analysis.

To achieve a realistic unsteady simulation, a suitable temporal resolution is required (Qin et al., 2011). Time step size (TSS) and number of time steps (NOTS) are two important variables in transient analysis of wind turbine. The Courant-Friedrichs-Lewy (CFL) criterion is needed for the stability of numerical schemes and it should be less than unity (Anderson et al., 2016). Violation of CFL limit leads to large errors and divergence of solution. In previous research, the TSS was determined based on the CFL criterion, which may not be the best time step size (Bedon et al., 2016; Bianchini et al., 2017; Howell et al., 2010; Y.-T. Lee & Lim, 2015; Marinić-Kragić et al., 2018; M. H. Mohamed, 2013). Therefore, time step size sensitivity test is required to obtain the optimum TSS (Balduzzi, Bianchini, Ferrara, & Ferrari, 2016; Chowdhury et al., 2016; Elkhoury et al., 2015; Lanzafame et al., 2014; Nobile et al., 2014; Siddiqui et al., 2015). Seven different time step sizes were tested for this present analysis and the values of TSS were 0.00004, 0.00006, 0.00008, 0.0001, 0.00012, 0.00015 and 0.00018

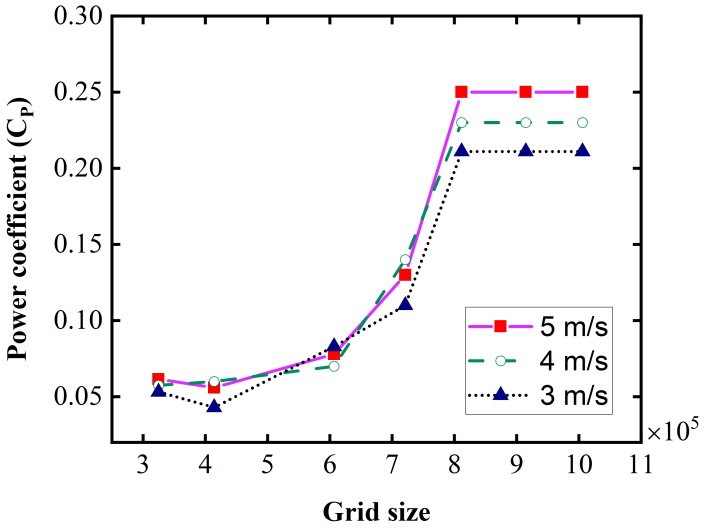

Figure 4.4: Mesh independency study at TSR=3

seconds. Time step sensitivity study performed at TSR value of 3 is shown in figure 4.5. The parameters considered for the time step size sensitivity test are CFL number, inlet velocity and mesh size. The first three values of TSS fulfilled the CFL condition and provide similar results. Therefore, the TSS of 0.00008 second is used for the present simulation. The range of CFL number is in between 0.4 to 0.7 for the present study.

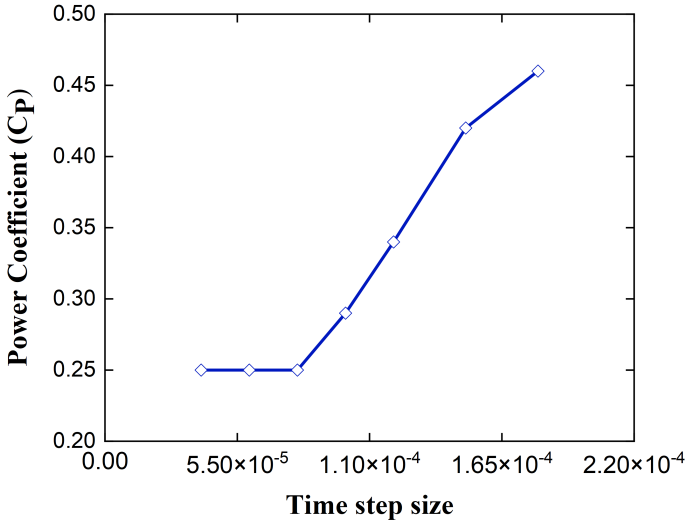

Figure 4.5: Time step sensitivity test at TSR=3

4.2.3.2 Solver setup

The solver setup is critical for achieving meaningful results in numerical analysis of complex flow fields. The flow transients must be resolved in order to examine dy-

namic stall and interactions between blade motions and wakes. Pressure based SIMPLE algorithm was selected for pressure–velocity coupling. The Green-Gauss node-based method was adopted for spatial discretization of gradients. For all spatial discretization and transient formulation, the second order upwind scheme and second order implicit scheme were used. The relative motion between rotating zone and stationary zone has been computed by using sliding mesh model. At each time step, the convergence threshold was set to 10-5. The under-relaxation parameters were set within 0.8 for continuity, momentum, and Reynolds closure equations.

4.3 Results and discussion

The computational model having three NACA0017 blade profiles has been simulated for TSR range from 1.5 to 4. Velocity of incoming wind has been taken up to 5 m/s corresponding to Re = 34,229. This range of velocity is typical for VAWT applications in urban and low wind intensity regions (Rahman & Chattopadhyay, 2020, 2023). Computations have been performed using workstation HPZ240 with 64 GB RAM. From the simulated data, at each time step, an instantaneous value of torque coefficient is obtained. This instantaneous value is now averaged over eight full cycles of rotation for obtaining average torque coefficient (C_T). The power coefficient (C_P) is then calculated by multiplying (C_T) with TSR.

The results for the present 2D numerical simulation have been validated with the experimental and numerical data from Balduzzi, Bianchini, Maleci, et al., 2016 which has similar geometrical characteristics (Table 4.1). The validation of C_P values of three-bladed VAWT having NACA0018 airfoil at a velocity of 8 m/s has been shown in figure 4.6. The results show a good agreement with the experimental data of Balduzzi, Bianchini, Maleci, et al., 2016 and the numerical results almost coincides with each other. Further, a comparison of performance curve of three-bladed VAWT having NACA0017 airfoil with the experimental data from Balduzzi, Bianchini, Maleci, et al., 2016 (NACA0018) and Castelli et al., 2011 (NACA0021) has been shown in figure 4.7 . The power coefficient increases with TSR rapidly until it reaches a maximum value, after which it gradually falls. The pattern of the curve of present study shows similarity with the other curves as the solidity values of these models are very close to each other. The comparison betweenthe simulation and experimental data is qualitative rather than the quantitative as the effects of airfoil shape, connector and rotating shaft have not been taken into consideration for numerical simulation. The present computational study shows a little lower value of power coefficient at lower TSR than the experimental results of Balduzzi, Bianchini, Ferrara, and Ferrari, 2016 but it can be accepted as a good agreement with experimental data for the wide range of operating TSR. The maximum deviation was found 29% at TSR value of 2. The present work shows

the peak power coefficient at TSR value of 3 while Balduzzi, Bianchini, Ferrara, and Ferrari, 2016 and Castelli et al., 2011 found at TSR values of 2.35 and 2.7 respectively.

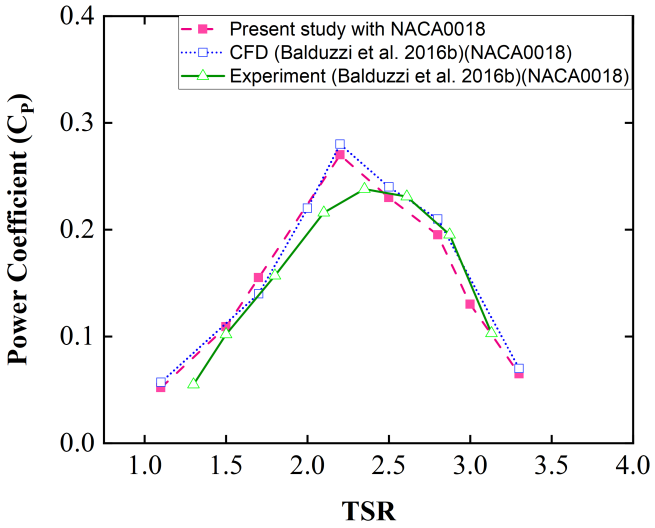

Figure 4.6: Validation of present simulation at v=8m/s

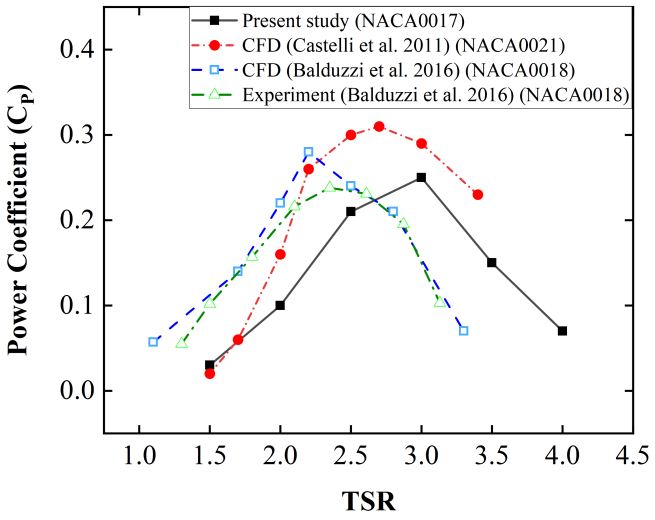

Figure 4.7: Comparison of present simulation with other works

Figure 4.8 benchmarks the performance of NACA0017 airfoil with the widely studied NACA0015 and NACA0018 in the TSR range of 1.5 to 4.0. The result reveals that the average value of power coefficient of VAWT having NACA0017 airfoil is less than the NACA0015 but slightly greater than NACA0018. Although the airfoil NACA0015 has higher peak power coefficient, NACA0017 performs slightly better at high TSR value. Maximum CP is found to be 0.31 for NACA0015, 0.25 for NACA0017 and 0.24

for NACA0018. All these values are obtained at TSR 3 with inlet velocity 5m/s corresponding to the Reynolds' number of 34,229. As the TSR goes beyond 3, the CP values decrease and almost coincide with each other.

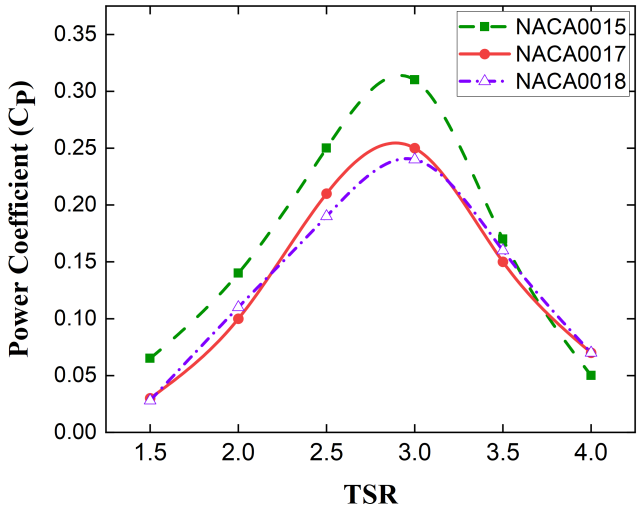

Figure 4.8: Performance comparison of VAWT having NACA0017 with NACA0015 and NACA0018 at an inlet velocity of 5 m/s

The variation of power coefficient with different inlet velocities is shown in figure 4.9. Three different inlet velocities between 3 to 5 m/s are taken into consideration for this present study. The result shows that the CP decreases with the decrease of inlet velocity which consequently diminishing the overall performance of VAWT. The value of maximum CP at velocity 3 m/s, 4 m/s and 5 m/s are 0.21, 0.23 and 0.25 respectively.

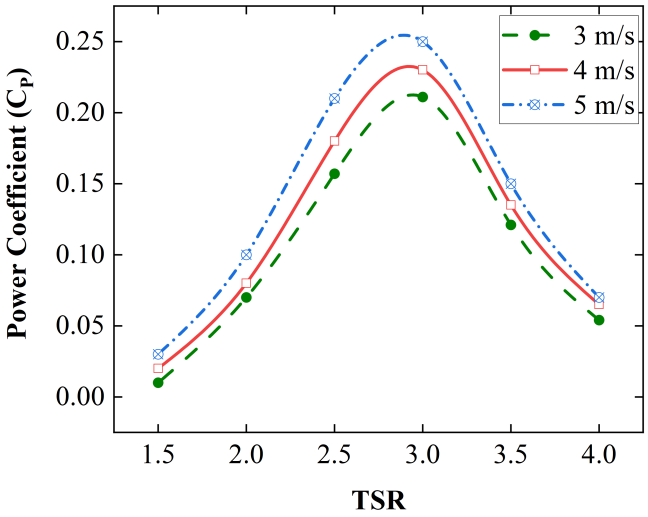

Figure 4.9: Performance of VAWT at different inlet velocities using NACA0017

The effect of different inlet velocities on instantaneous net torque coefficient at TSR ranging from 2 to 4 has been shown in figures 4.10 to 4.13. Fluctuations in instantaneous torque can be observed for lower TSR value of 2 and for higher TSR, fluctuations diminish. In the angular range of 0°-30°, 120°-150° and 240°-270°, the effect of velocity on torque coefficient is minimal. In the other range of azimuthal angles, torque coefficient is found to increase with increasing velocity. The variation in the torque curve for a certain TSR can also be explained by looking at the pressure contours of differential coefficients.

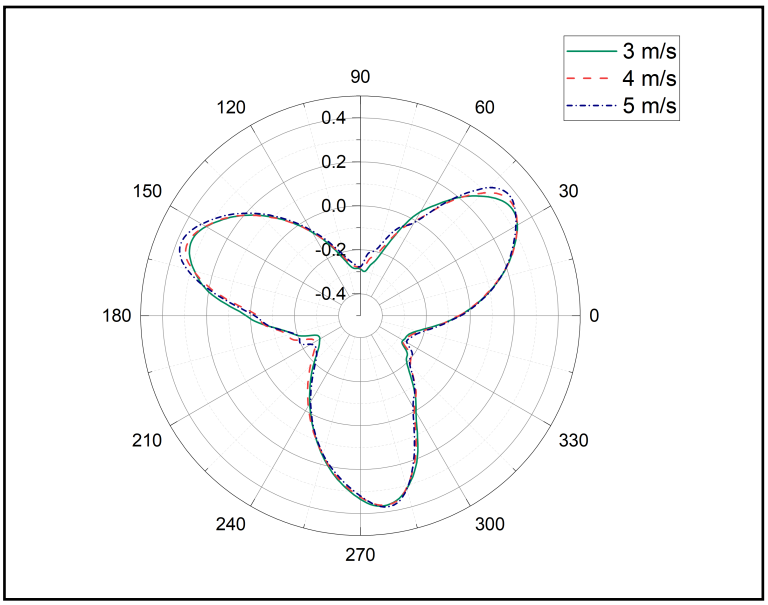

Figure 4.10: Effect of different inlet velocities on instantaneous net torque coefficient at TSR value of 2 using NACA0017

For better visualization of flow pattern, the instantaneous flow characteristics are obtained at 0°, 60°, 90°, 120°, 180°, 240°, 270°, 300° azimuthal angles at TSR values of 3 and 4 for wind velocity of 5m/s. Pressure contours of NACA0017 for different angular positions at TSR 3 and TSR 4 have been depicted in figure 4.14. Higher pressure difference is observed in the upwind region of the rotor and a vortex is formed at the inner side of the blade. For TSR value 3, pressure differences are larger than the TSR value 4, resulting in higher torque generation in rotors.

The turbulent intensity and predicted vorticity distribution around the rotor for NACA0017 profile using SST k-ω model has been shown in figure 4.15 and 4.16 respectively. Turbulent intensity indicates the strength of fluctuating part to the mean velocity component. It can be observed that a relatively high-intensity turbulence zone formed behind the returning blade due to flow separation for TSR value of 4. The returning blade is also influenced by the incoming air flow that led to increase in drag force caused by pressure on this blade. As a result, there is a reduction of power coefficient. The vortex structure is also captured for different azimuth angles. In the first half revolution, there is only

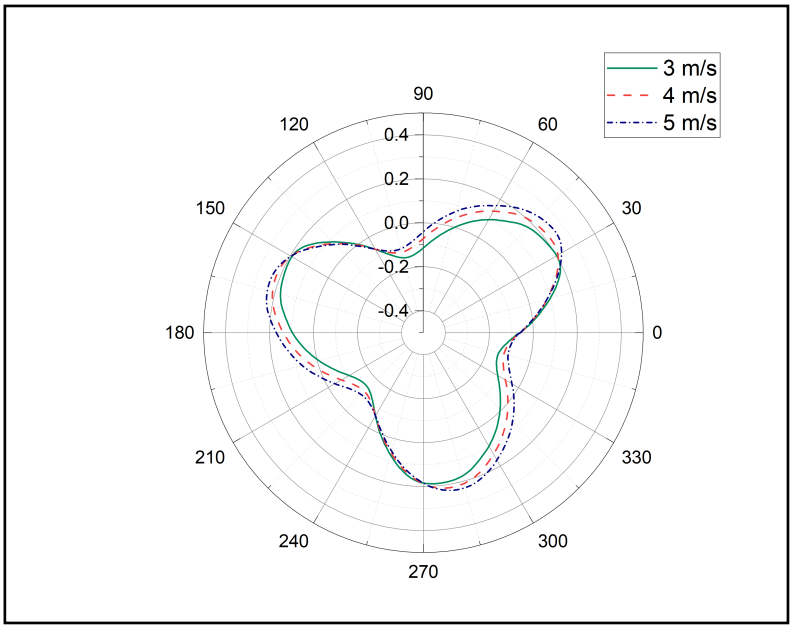

Figure 4.11: Effect of different inlet velocities on instantaneous net torque coefficient at TSR value of 3 using NACA0017

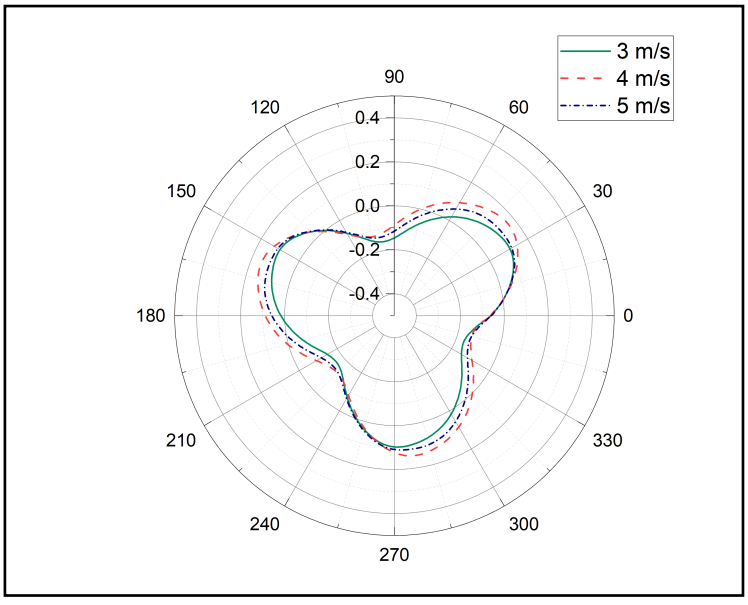

Figure 4.12: Effect of different inlet velocities on instantaneous net torque coefficient at TSR value of 3.5 using NACA0017

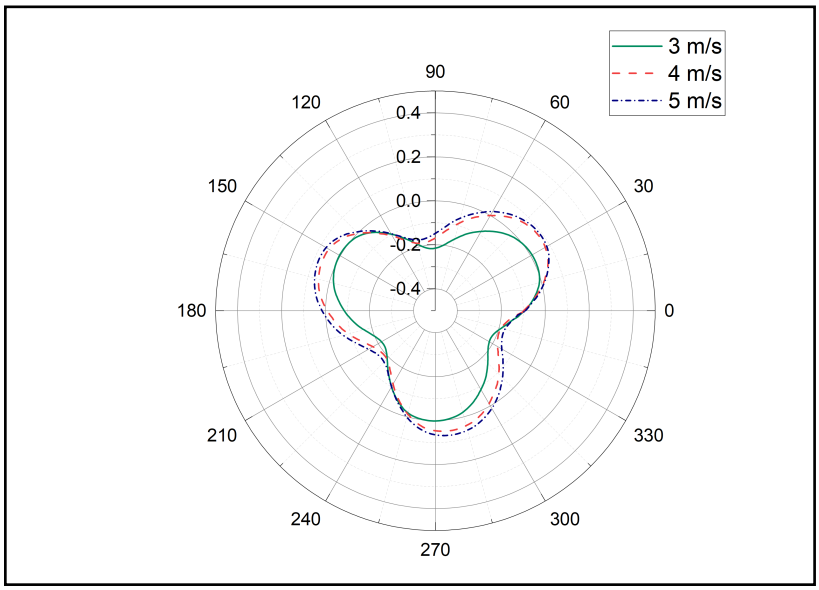

Figure 4.13: Effect of different inlet velocities on instantaneous net torque coefficient at TSR value of 4 using NACA0017

wake vortex separation on the blade surface. An irregular vortex shedding phenomenon can be observed in the next half of revolution. The shedding vortex continues to move downstream in the flow field. The results predicted that at the beginning of cycle, the turbulent vortices generated by preceding blade cause a disturbance at the leading edge of the next blade, but the intensity of tail vortices is very less due to the dissipation effect. This disturbance ultimately results in a poor performance of the turbine. It is also observed that separation of the wake region is more for TSR value of 4.

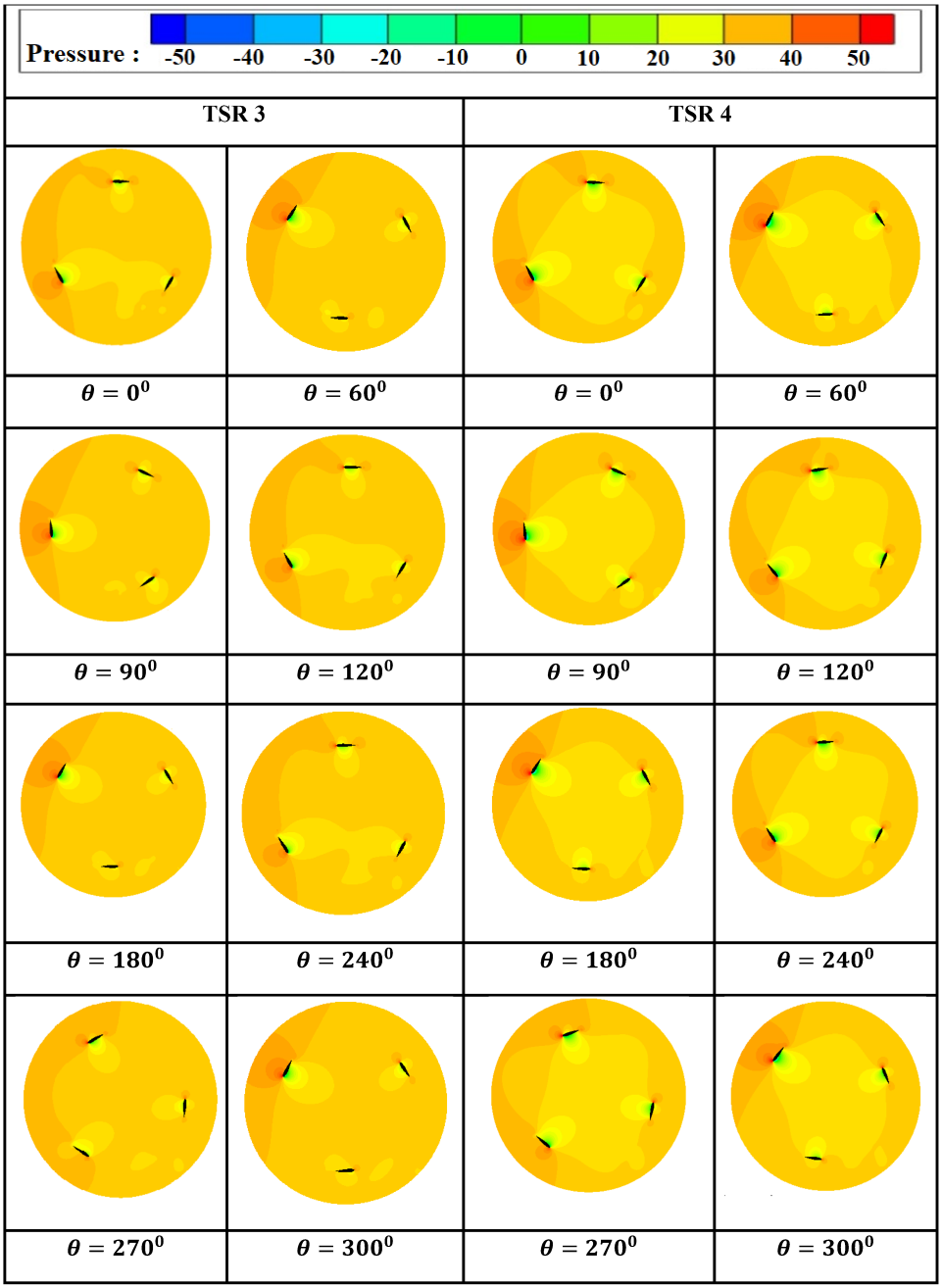

Figure 4.14: Pressure contours at different angular positions for NACA0017 at TSR value of 3 and 4 with an inlet velocity of 5m/s

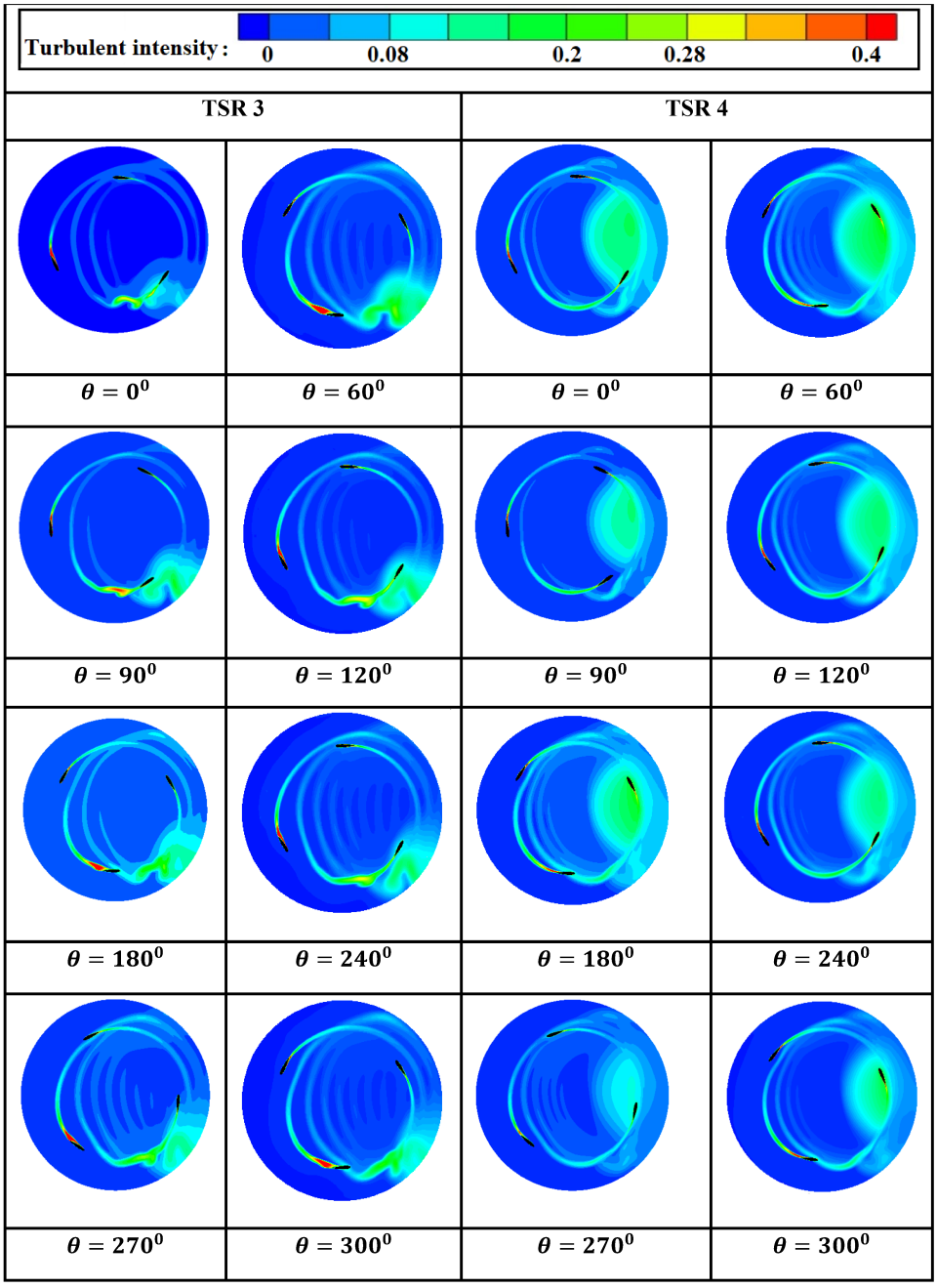

Figure 4.15: Turbulent intensity at different angular positions for NACA0017 at TSR value of 3 and 4 for inlet velocity of 5 m/s

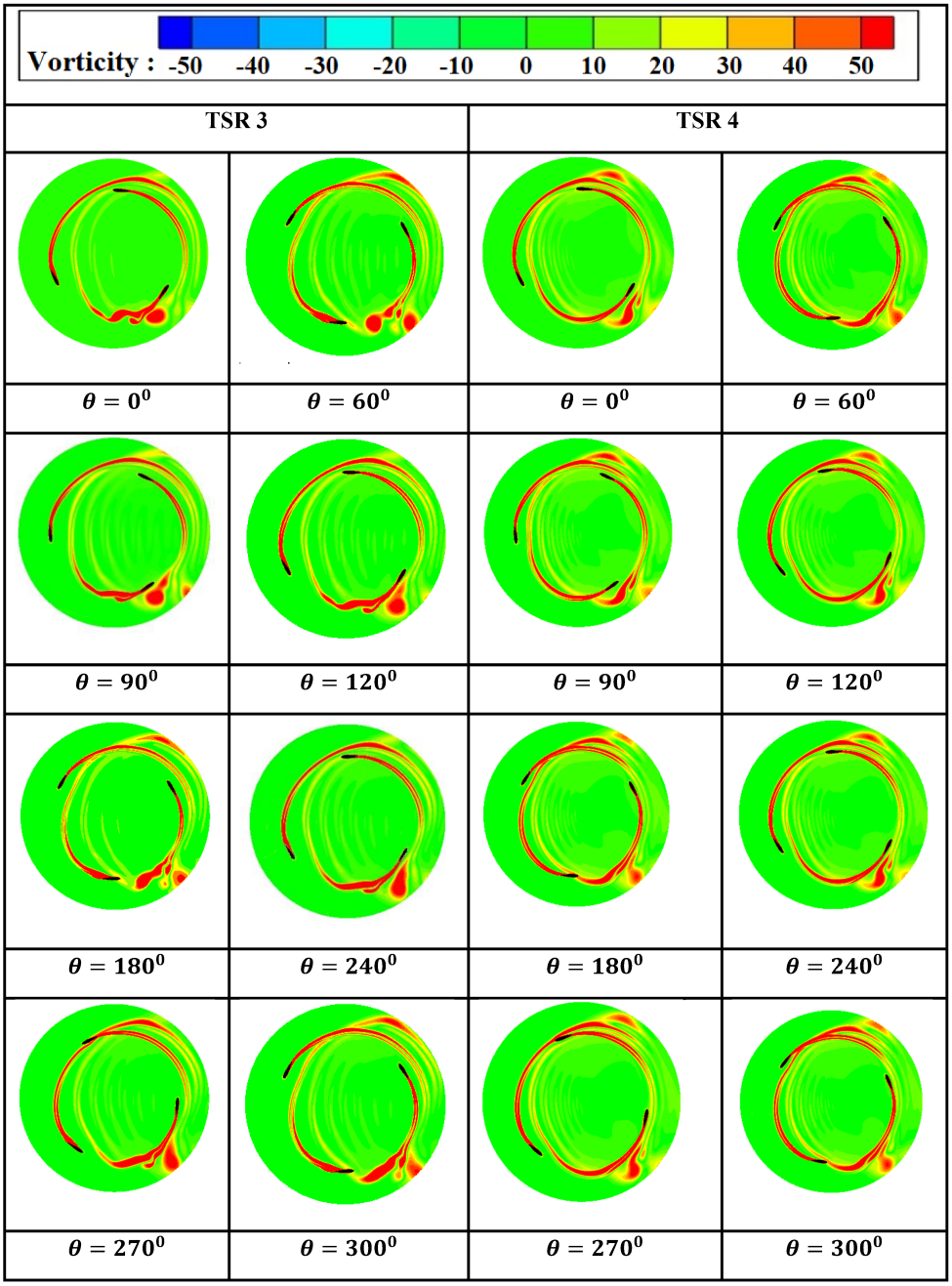

Figure 4.16: Vorticity distribution at different angular positions for NACA0017 at TSR value of 3 and 4 for inlet velocity of 5 m/s

4.4 Concluding remarks

In this paper, a two-dimensional transient simulation of Darrieus lift type turbine having NACA0017 blade profile has been carried out based on unsteady RANS formulation with SST k-ω model for turbulent closure. The study demonstrates the feasibility of NACA0017 airfoil for harnessing wind power at relatively low wind velocity. The performance of NACA0017 airfoil has been analysed for different inlet velocities and different TSR values. The salient observations are:

i. The power coefficient of VAWT having NACA0017 airfoil obtained from CFD simulation is in good agreement when compared to the results of NACA0015. Although the later has higher peak power coefficient, NACA0017 performs better at high TSR value.

ii. The effect of velocity on torque coefficient is minimal in the angular range of 0°-30°, 120°-150° and 240°-270°. Torque coefficient is found to increase with increasing velocity in the other range of azimuthal angles. Fluctuations in instantaneous torque can be observed for lower TSR value of 2 but fluctuations diminish for higher TSR. The variation in the torque curve for a certain TSR can also be explained by observing pressure contours of differential coefficients.

iii. The range of peak power coefficient is within 0.20 – 0.25 at a tip speed ratio of 3.

CHAPTER 5

VAWT Augmented with Duct

5.1 Introduction

In the coming years, a significant increase in electricity demand is anticipated due to the continuously growing global population. Concurrently, concerns about greenhouse gas emissions and the rising costs of non-renewable fuels are intensifying the focus on the renewable energy sector to meet this surging demand. Within the realm of renewable energy, wind power has witnessed the most significant technological strides in recent years. Additionally, this technology is superior from environmental perspective compared to other renewable sources (Ackermann & Söder, 2000; Fatahian et al., 2022).

Wind Energy Conversion Technology (WECT) is employed to maximize the extraction of energy from wind sources. This process comprises three stages: evaluating energy resources, designing hardware, and completing installation. The initial phase involves assessing the potential of wind power in various global locations (Rahman & Chattopadhyay, 2020, 2023). The second and third stages involve the installation of highly efficient wind turbines. The horizontal axis wind turbine (HAWT) is more prevalent in the WECT system due to its higher power coefficient compared to the vertical axis wind turbine (VAWT), despite requiring a more complex yaw mechanism (Mohammed et al., 2019). Moreover, to prevent aerodynamic interference with HAWTs, large separations and high wind speeds are necessary (W.-H. Chen et al., 2017). Conversely, VAWTs can be situated in urban and semi-urban areas due to their omni-directional nature, lower noise levels, ease of construction, cost-effective installation, and minimal maintenance requirements (Dossena et al., 2015). VAWTs generally fall into two categories: Savonius drag type and Darrieus lift type (Sagharichi et al., 2018), both of which are represented within VAWT examples. Compared to drag-type VAWTs, the H-type Darrieus wind turbine demonstrates superior performance (Jain & Saha, 2020b).

Nonetheless, the main challenges pertaining to VAWTs are their inherently low ef-

ficiency and limited capacity for self-starting. Owing to higher drag coefficients and inadequate aerodynamic performance, these turbines frequently fail to reach the same energy conversion rates as their horizontal-axis counterparts. Tayebi and Torabi, 2024 provided a summary of the various flow control strategies—passive and active—that have been used to enhance Darrieus VAWT performance. Installing a wind-capture-accelerate device and INVELOX outside the VAWT also enhanced its efficiency.

These issues can be mitigated by increasing the power coefficient through either expanding the swept area or augmenting the incoming velocity. Enlarging the swept area of the turbine allows for higher power coefficients by capturing more wind energy (Ranjbar et al., 2021). Enclosing the rotor within a duct offers a substantial improvement in wind energy capture by focusing and accelerating the airflow through the turbine, thereby increasing efficiency (Das Karmakar & Chattopadhyay, 2022). Additionally, incorporating wind-capture and acceleration devices (Kuang et al., 2022) and INVELOX (Ayaz et al., 2023), around the VAWT further enhances performance by optimizing the flow dynamics and maximizing the turbine's energy extraction potential. As the wind enters the converging section of the duct, its velocity increases due to the venturi effect. Consequently, the power output of the VAWT increases proportionally to the cube of the wind speed (M. Verma, De, et al., 2023). Ducted VAWTs offer advantages such as reduced noise, lower cut-in speed, decreased tip losses, and reduced sensitivity to yaw angle fluctuations (Avallone et al., 2020; Dilimulati et al., 2018; Manganhar et al., 2019). Numerous experimental and numerical studies have been conducted to evaluate the thrust, torque, and overall performance of ducted VAWTs (Bontempo & Manna, 2020; Bontempo & Manna, 2016; Van Bussel, 2007).

There are different designs of wind turbine ducts. It's essential to study the different components of ducts to ascertain the increase in power coefficient when ducts are utilized. Typically a duct comprises of diffusers, flanges, and nozzles. The collective impact of these elements on the VAWT's performance demands special attentions from researchers. The performance of wind turbines augmented with duct have been investigated numerically by Heikal et al., 2018. According to their results, at some wind velocities, there would be a 90% power gain. Nurur Rochman et al., 2017 examined the duct's flange form, they found that the narrower section of the duct had a 29% increase in wind velocity. Kosasih and Tondelli, 2012 measured the diffuser and flange lengths, they discovered that a longer diffuser decreased the power coefficient of ducted VAWTs whereas a longer flange increased wind velocity in the throat region. El-Zahaby et al., 2017 demonstrated that a flange angle of 15° could increase power efficiency by as much as 5%. According to Ranjbar et al., 2017, throat velocity could rise by as much as 5.4% when a nozzle is connected to the duct.

Ding et al., 2023 evaluated the performance of a ducted wind turbine across vary-

ing tip speed ratios (TSRs) using high-order large eddy simulations. Their findings revealed that the ducted turbine outperformed the bare turbine. The duct not only enhanced flow turbulence and intensified blade trailing-edge vortices but also mitigated tip and hub vortices. Safford et al., 2024 investigated the fluid flow around a ducted wind turbine using Unsteady Reynolds-Averaged Navier-Stokes (URANS) simulations at various TSRs. Their study demonstrated that the ducted turbine increased the power coefficient by 96% compared to the open rotor. Additionally, significant flow separation was observed within the interior of the duct at lower TSRs. An experimental investigation of a VAWT equipped with a duct has been conducted by Watanabe et al., 2016. They optimized the performance of the diffuser and flange by adjusting their lengths and angles. Additionally, they performed a parametric analysis, considering factors such as blade thickness, solidity, chord length, and Reynolds number. Their findings demonstrated a significant improvement in power output, achieving a two-fold increase.

Zanforlin and Letizia, 2019 focused on VAWTs augmented with diffusers for use in urban environments. They positioned the turbine rotor within a diffuser system integrated with a rooftop. Their results indicated an efficiency enhancement of approximately 40% compared to a VAWT operating without a diffuser. Hashem and Mohamed, 2018 investigated a Darrieus-type VAWT with three different duct configurations. They discovered that a duct with a cycloidal surface surrounding the turbine rotor produced the highest energy output compared to ducts with flat panels, curved surfaces, and no duct at all. Ghazalla et al., 2019 explored the optimal positioning of the rotor within a duct. Their research identified the throat, the point of minimum cross-section within the duct, as the ideal location for the rotor.

Krishnan et al., 2023 have presented innovative designs for wind turbine blades and airfoils aimed at significantly improving turbine efficiency. Their work provides comprehensive insights into optimizing the structural, aerodynamic, and aero-acoustic properties of wind turbine blades across diverse operating conditions. A key focus of their research lies in the implementation of both active and passive flow control mechanisms, as well as the integration of biomimetic adaptations, drawing inspiration from nature to enhance performance and reduce noise. Most research aimed at enhancing VAWT performance focuses on standard NACA 4-digit series airfoils, with thicknesses varying from 12-23%. Symmetrical airfoils like the NACA0015 typically offer superior performance, though in certain scenarios, the NACA0018 demonstrates the highest efficiency. According to Durrani et al., 2011, thinner airfoils such as the NACA0015 perform better at higher TSR due to reduced drag forces, while thicker airfoils like NACA0017, NACA0018 provide enhanced structural integrity. Notably, despite the structural advantages, the aerodynamic performance of the NACA0017 airfoils has been relatively underexplored. Recent studies suggest that NACA0017 excels during startup and transient operations, indicating a need for more focused research on its aerodynamic prop-

erties to fully leverage its potential benefits (Das Karmakar et al., 2023; Maalouly et al., 2022).

The main objective of our current work is to use numerical simulation to assess the performance of the ducted VAWT with NACA0017 blade profile. So far, no research has been done on the efficacy of this NACA0017 profile when used with ducted VAWT. The analysis involves a comparison of fluid mechanical performance of bare and ducted VAWT. Additionally, a comprehensive analysis of the turbulent flow field in presence of duct augmented VAWT is presented.

5.2 Numerical modelling

5.2.1 Flow domain

In the present study, two-dimensional numerical simulations were carried out to examine the performance and flow behaviour of Darrieus type ducted VAWT integrated with NACA0017 airfoils. The computational domain of Darrieus type VAWT using NACA0017 and augmented with a duct has been shown in Figure 5.1.

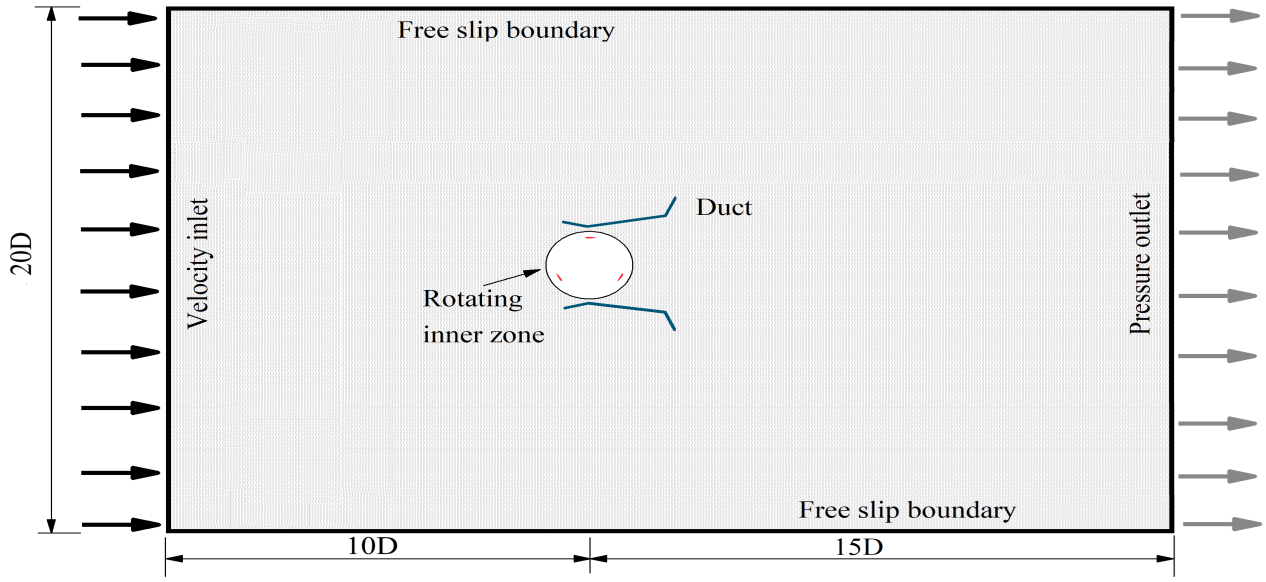

Figure 5.1: Computational domain for present study.

The computational domain features inlet, outlet and free slip boundaries with dimensions of 25D x 20D, where the rotor diameter is denoted by D. The domain dimensions are maintained sufficiently large to mitigate any effects caused by uncertainties in the exit boundary conditions. If the computational domain is not appropriately chosen, numerical analysis may yield inaccurate results and thus the size of the computational domain significantly impacts the performance analysis of VAWTs (Rezaeiha et al., 2017). The rotor has been placed 7.5D from the inlet boundary, centered equidistantly between

the upper and lower free slip boundaries of the whole domain. On the downstream side of the rotor, the domain length is extended to 15D to ensure the wake region can fully develop. The geometry has been divided in two regions: a rotating inner zone of circular interface and the rectangular stationary outer zone consisting of duct. The interconnection between the two domains has been facilitated by an sliding interface, enabling the rotating zone to rotate at a specified velocity while maintaining the mesh of the stationary zone in a fixed position. The size of rotating domain has been chosen as 1.1D (Abdullah et al., 2023). The geometrical details of present study has been shown in Table 5.1.

Table 5.1: Geometrical parameters.

Parameters	**Present study**	**Ranjbar et al., 2021**
Type of airfoils	NACA0017	NACA0015
No. of blades	3	3
Diametere of rotor, D (m)	0.7	2.5
Chord length, C (m)	0.1	0.4
Diameter of rotating domain	1.1D	1.1D

In the current analysis, an optimized duct design has been considered, that attains maximum velocity at the throat as described by Ranjbar et al., 2021 The geometrical details of the optimised duct which comprise of three components: Nozzle, diffuser, and flange is shown in Figure 5.2. The length of nozzle, diffuser and flange are 0.3D, 1.1D and 0.3D respectively. The angles form by these components with respect to horizontal axis are denoted by α, β and γ. The optimised value of these angles are $15°$, $15°$ and $70°$, respectively. A clearance between the rotor and the duct is maintained to avoid the possibility of stall by aiding in the recovery of the pressure gradient (Cresswell et al., 2015; Hansen et al., 2000; Kwong & Dowling, 1994).

5.2.2 Governing equations

As the flow field around the VAWT is mostly turbulent in nature, the incompressible URANS equations has been incorporated for evaluating pressure and velocities at each element of computational domain (Rahman et al., 2024; Zare Chavoshi & Ebrahimi, 2022). The continuity and momentum equations are given below for two dimensional unsteady incompressible flow:

$$\frac{\partial \overline{u_i}}{\partial t} + \frac{\partial \overline{u_i}}{\partial x_j} = 0 \tag{5.1}$$

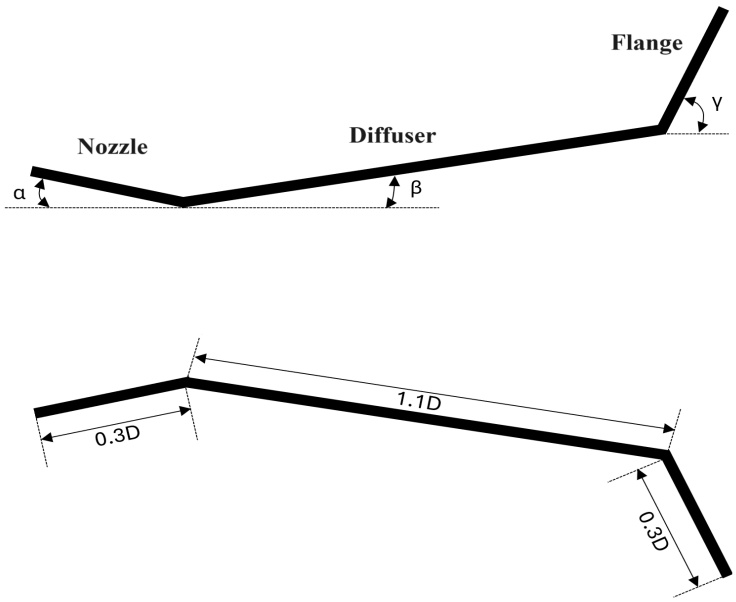

Figure 5.2: Geometrical details of optimised duct.

$$\rho\frac{\partial\overline{u}_i}{\partial t}+\rho\overline{u}_i\frac{\partial\overline{u}_i}{\partial x_i}=\frac{\partial}{\partial x_j}\left[-\overline{p}\delta_{ij}+\mu\left(\frac{\partial\overline{u}_i}{\partial x_j}+\frac{\partial\overline{u}_j}{\partial x_i}\right)\right]-\tau'_{ij} \tag{5.2}$$

where $\overline{u}_i$ indicates the air velocity, ρ is air density, μ is dynamic viscosity of air and the pressure in denoted by $\overline{p}$. The Reynolds shear stress tensor term is expressed as $\tau'_{ij}=-\rho\overline{u'_iu'_j}$ and it is calculated by using the Boussinesq assumption. τ'_{ij} is given by the following equation

$$\tau'_{ij}=\mu_t\left(\frac{\partial u_i}{\partial x_j}+\frac{\partial u_j}{\partial x_i}\right)-\frac{2}{3}\rho k\delta_{ij} \tag{5.3}$$

where turbulent viscosity and turbulent kinetic energy are denoted by μ_t and k, respectively and these quantities are obtained from the turbulence model.

A suitable turbulence model is essential for producing credible outcomes with sufficient computational stability. For the present study, SST $k-\omega$ turbulence model is selected for simulating the dynamics of Darrieus VAWTs which characteristically exhibit Complex flow phenomena, such as free shear flow and boundary layer separation and this two equation model is well suited for VAWTs as suggested by earlier studies (Balduzzi, Bianchini, Maleci, et al., 2016; Biswas & Gupta, 2014; Chowdhury et al., 2016; Jain & Saha, 2020a). The SST $k-\omega$ turbulence model is a combination of the standard $k-\varepsilon$ and $k-\omega$ models. The $k-\omega$ model captures near-wall flow characteristics accurately, while the $k-\varepsilon$ model is used for the far-field flow region away from the wall (Fatahian et al., 2022). This model was developed by Menter, 1994 and the transport equations can be expressed as

$$\frac{\partial}{\partial t}(\rho k) + \frac{\partial}{\partial x_i}(\rho u_i k) = \frac{\partial}{\partial x_j}\left(\Gamma_k \frac{\partial k}{\partial x_j}\right) + G_k - Y_k + S_k \tag{5.4}$$

$$\frac{\partial}{\partial t}(\rho \omega) + \frac{\partial}{\partial x_i}(\rho u_i \omega) = \frac{\partial}{\partial x_j}\left(\Gamma_\omega \frac{\partial \omega}{\partial x_j}\right) + G_\omega - Y_\omega + S_\omega + D_\omega \tag{5.5}$$

Where ω is turbulent specific dissipation. The generation of k and ω due to mean velocity gradients are denoted by G_k and G_ω respectively. Γ_k and Γ_ω are the effective diffusivity of k and ω. Dissipation due to turbulence are indicated by D_k and D_ω. Source terms are expressed by S_k and S_ω and D_ω is associated with the cross – diffusion term (Jafaryar et al., 2016). Computation of μ_t is already discussed in chapter 4 section 4.2.3.

5.2.3 Solution procedure

ANSYS FLUENT 2023R1 is utilized to develope geometry, meshing and simulation. Appropriate outcomes in numerical analysis of complex flow fields depend significantly on the solver setup. A pressure based solver has been incorporated as the airflow is incompressible. For spatial discretization of gradients, the Green-Gauss node-based approach has been utilised. The governing equations have been discretized using the finite volume method. A second-order upwind technique and fully implicit temporal scheme have been implemented to discretize the spatial terms and to handle the temporal terms, respectively. SIMPLE method has been selected for pressure–velocity coupling. The convergence criterion has been specified at 10^{-5}, for all variables, at each time step. The under-relaxation parameters have been set within 0.8 while solving governing equations. The sliding mesh model has been chosen for computing the relative motion between stationary and rotating zone (Rahman et al., 2024). To maintain the accuracy, the time step size has been calculated for 1 °of rotation using Eqs. 5.6.

$$\Delta t\big|_{\theta^\circ} = \frac{\theta \pi}{\omega 180} \tag{5.6}$$

The generated torque (T) is expressed as

$$T = \frac{1}{2} C_T \rho A R V^2 \tag{5.7}$$

Where C_T is toque coefficient V is free stream air velocity, ρ is air density. Swept area of rotor and the radius of the rotor are denoted by A and R, respectively.

The performance of wind turbine is measured by coefficient of power(C_P) and it is calculated by the following Eqs. 5.8

$$C_P = \frac{P}{\frac{1}{2}\rho A V^3} \tag{5.8}$$

Here P is power of wind turbine.

C_T and C_P are connected through TSR and it is expressed as

$$C_P = \lambda C_T \tag{5.9}$$

Here, TSR is denoted by λ, which is the ratio of tangential speed at the tip of airfoils to the free stream air velocity and it is denoted by Eqs. 5.10

$$\lambda = \frac{\omega R}{V} \tag{5.10}$$

5.2.4 Meshing and boundary conditions

In order to solve the governing equations, the computational domain has been to be discretized into numerous small grids to accurately capture the small scale flow patterns. This is achieved using ANSYS Meshing. Fine mesh has been generated near the solid walls as there is a common occurrence of intricate flow structures around these regions. Details of meshing of the present geometry is shown in Figure 5.3. The computational domain used a mesh primarily made of quadrilateral cells throughout. To capture the flow behavior near the airfoils and duct walls more accurately, the mesh was refined in those regions. These refined cells were also quadrilaterals and maintained a high quality (maximum skewness below 0.8). Twenty numbers of inflation layers have been applied near the airfoils walls and duct walls with a growth rate of 1.2 which gradually increase the cell size as we moved away from the airfoils and duct. The first cell height is 0.05mm that has been used in the boundary layer generation. The height of the first cell has been carefully chosen to ensure that the average value of Y^+ does not exceed 1, which is a critical criterion for the SST $k-\omega$ model.

For the present analysis, velocities $V \in [3, 10\ m/s]$ have been considered as inlet boundary conditions. Turbulent intensity has been kept at 5% of inlet velocities. The outlet boundary condition is considered as atmospheric pressure outlet since the domain is open to the environment. Upper and lower boundaries are considered as free-slip. Along with it, no slip boundary condition has been selected for airfoils and duct walls. For the rotating mesh motion, appropriate angular velocities have been applied to rotating zone, depending on TSR (λ).

5.2.5 Grid independence study and model validation

To determine the optimal mesh size for achieving the best results, mesh independence test were performed using six different mesh levels, with element sizes of 4,74,059;

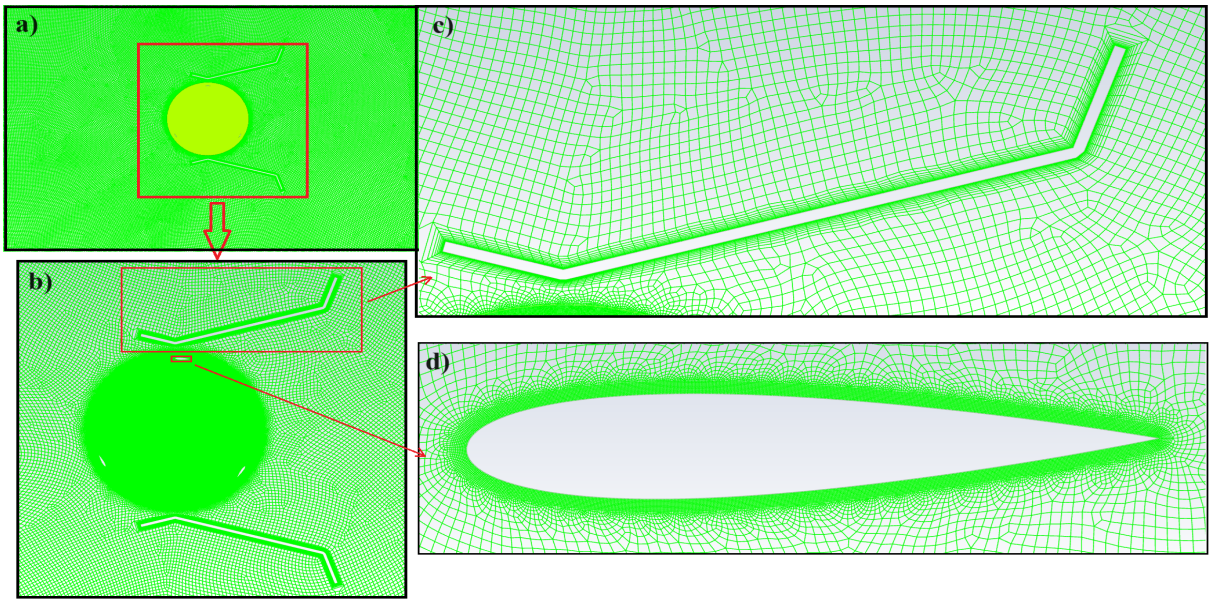

Figure 5.3: Details of meshing of the geometrical model: a) stationary outer domain b) rotating inner domain c) mesh near duct wall d) grids around airfoils.

5,59,059; 7,14,657; 8,01,071; 8,81,588 and 9,89,667. These simulations employed the SST $k-\omega$ turbulence model at a TSR of 3.5 and inlet velocities of 3 and 4 m/s and run upto 10th rotations periods for ducted VAWT with NACA0017 airfoils. The results indicated in Figure 5.4 that the coefficient of power (C_P) values stabilized with the last three mesh sizes. Consequently, the mesh with 8,01,071 elements has been selected for the current analysis.

To validate our results, numerical data of bare VAWT obtained by Ranjbar et al., 2021 has been considered and details of this comparison are presented in Figure 5.5. The details of geometrical parameters for present study and Ranjbar et al., 2021 have been shown in Table 5.2. For validation, we adopted the same geometric parameters as those used by Ranjbar et al., 2021 The results indicated a maximum error of 6% at a TSR of 2.2, which is well within the acceptable error margin of 10%.

In absence of experimental data for NACA0017, Table 5.2 presents a comparison of the C_P values for a bare VAWT equipped with a NACA0018 airfoil, operating at a wind velocity of 8 m/s. The numerical simulations show a strong correlation, with the results closely aligning with each other and demonstrating excellent agreement with the experimental findings of Balduzzi, Bianchini, Maleci, et al., 2016.

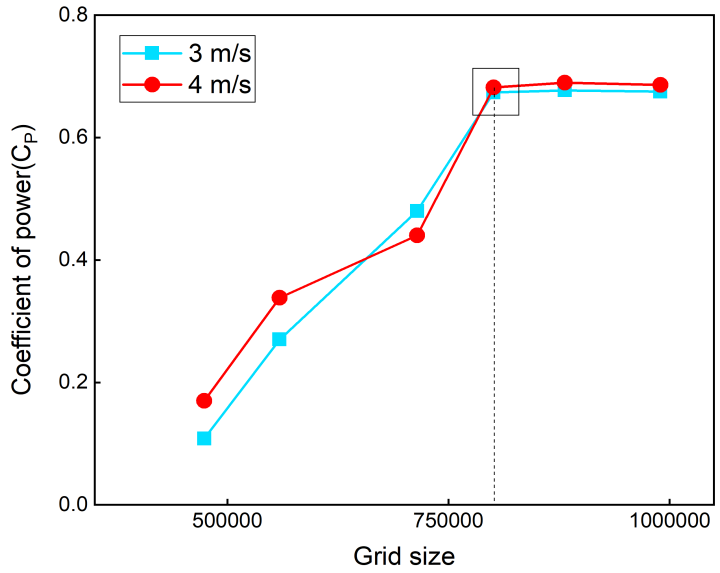

Figure 5.4: Grid independence study at TSR 3.5 for inlet velocities 3 and 4 m/s for ducted VAWT with NACA0017.

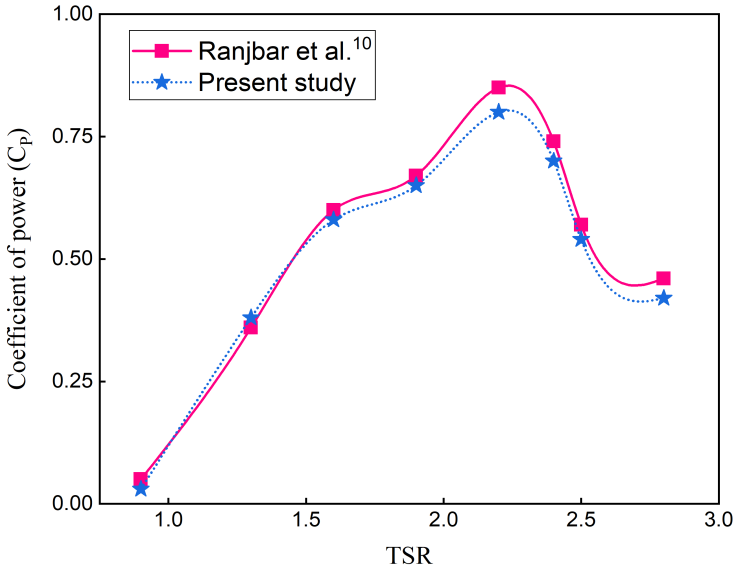

Figure 5.5: Validation of present study with Ranjbar et al., 2021 using NACA0015 for ducted VAWT.

Table 5.2: Comparison of the C_P values for a bare VAWT equipped with a NACA0018 airfoil for $TSR \in [1, 4]$ and at velocity 8 m/s.

Present study		**CFD (Balduzzi et al., 2016)**		**Experimental (Balduzzi et al., 2016)**	
TSR	C_P	**TSR**	C_P	**TSR**	C_P
1.1	0.05	1.1	0.057	1.3	0.05
1.7	0.15	1.7	0.14	1.8	0.15
2.2	0.27	2	0.22	2.1	0.21
2.5	0.23	2.2	0.28	2.35	0.24
2.8	0.19	2.5	0.24	2.61	0.23
3	0.13	2.8	0.21	2.87	0.19
3.3	0.06	3.3	0.07	3.13	0.10

5.3 Results and discussions

The computational domain featuring ducted VAWT with three NACA0017 airfoils has been investigated within the range of TSR$\in [1, 4]$. Computations have been conducted on an HPZ230 workstation equipped with 128 GB of RAM. The approaching air velocities have been selected as 3, 4 5 and 10 m/s corresponding to four levels of Reynolds number($Re = \frac{\rho c V}{\mu}$) of 19,330; 25,773; 32,216 and 64,433. Here, the characteristic length is selected as chord length of airfoils for determining the Re. It is worth noting that VAWT are suitable for low velocity regions and have potential application in low wind urban regions as noted by Rahman and Chattopadhyay, 2020. An instantaneous torque coefficient value was extracted at each time step and the average C_T is then calculated by averaging these instantaneous values over ten complete rotational cycles. Finally, the C_P is determined by multiplying the average C_T by the TSR.

Figure 5.6 depicts the variation of C_P of ducted VAWT with NACA0017 at different inlet velocities $V \in [3, 10\ m/s]$ and for TSR $\in [1, 4]$. The results indicate that the maximum C_P is found to be 0.68 at TSR 3.5 for velocity 4 m/s. At an inlet velocity of 10 m/s, the C_P values are significantly reduced across the entire range of TSR. Furthermore, the C_P values decrease at a TSR of 4 for all inlet velocities, following their peak at a TSR of 3.5. Specifically, the maximum C_P values are observed to be 0.67, 0.68, and 0.5 at inlet velocities of 3, 4 and 5 m/s, respectively. The optimal TSR minimize the negative effects such as flow separation and turbulence in the wake and enabling a more seamless and prolonged energy transfer to the VAWT. But as TSR rises above this threshold, we see diminishing C_P values because of higher drag and possible vortex formation, which brings in highly transient patterns. As the TSR increases, the blades experience a lower angle of attack, resulting in a reduced lift-to-drag ratio. This higher drag leads to a

decrease in C_P.

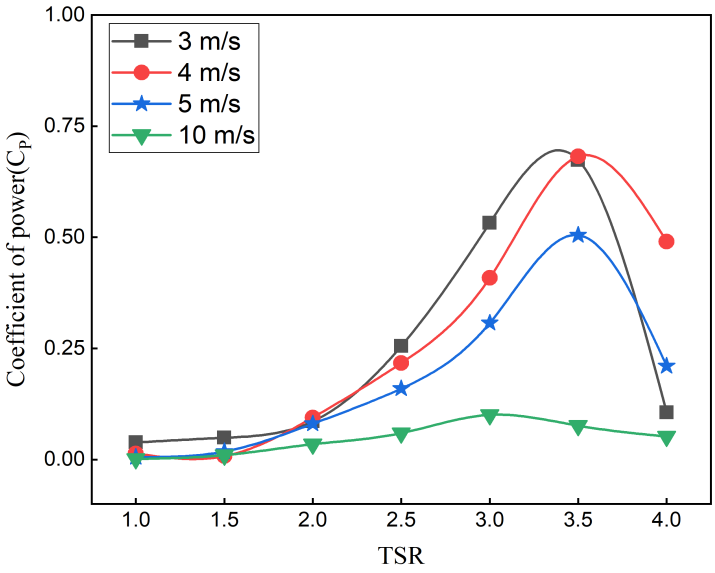

Figure 5.6: Coefficient of power (C_P) for ducted VAWT at inlet velocities $V \in [3, 10m/s]$ and TSR$\in [1, 4]$ using NACA0017.

At higher wind speeds, flow separation becomes more significant around the blades and duct walls, creating low-pressure zones that increase drag and reduce lift. With increasing wind speeds, the frequency and intensity of vortices from the blade trailing edges and duct exit may intensify, causing unsteady forces on the rotor and further decreasing C_P. Additionally, boundary layer thickening on the duct walls and blade surfaces at higher wind speeds increases friction drag.

Overall, the effectiveness of duct is optimal within a specific wind speed range, and under stronger winds, aerodynamic issues such as turbulence and higher drag surpass the benefits of airflow concentration.

The comparison of C_P for ducted and bare VAWT with NACA0017 airfoils at different inlet velocities ($V \in [3,\ 10\ m/s]$) and TSR range ($TSR \in [1,\ 4]$) is shown in Figure 5.7. The highest augmentation in C_P is observed at a TSR of 3.5. For inlet velocities, V$\in [3,\ 4\ m/s]$, C_P is enhanced by approximately fivefold compared to the bare VAWT. At an inlet velocity of 5 m/s, C_P is increased by about three times. However, at an inlet velocity of 10 m/s, the maximum C_P is approximately 10%, and the C_P values for both the bare and ducted VAWT are nearly identical. This indicates that at higher velocities, the use of a duct as an augmentation device for the VAWT yields minimal benefits.

The torque ripple factor (γ) serves as a key indicator for rotor stability and smoothness while in operation. A greater circumferential gap between airfoils leads to a more

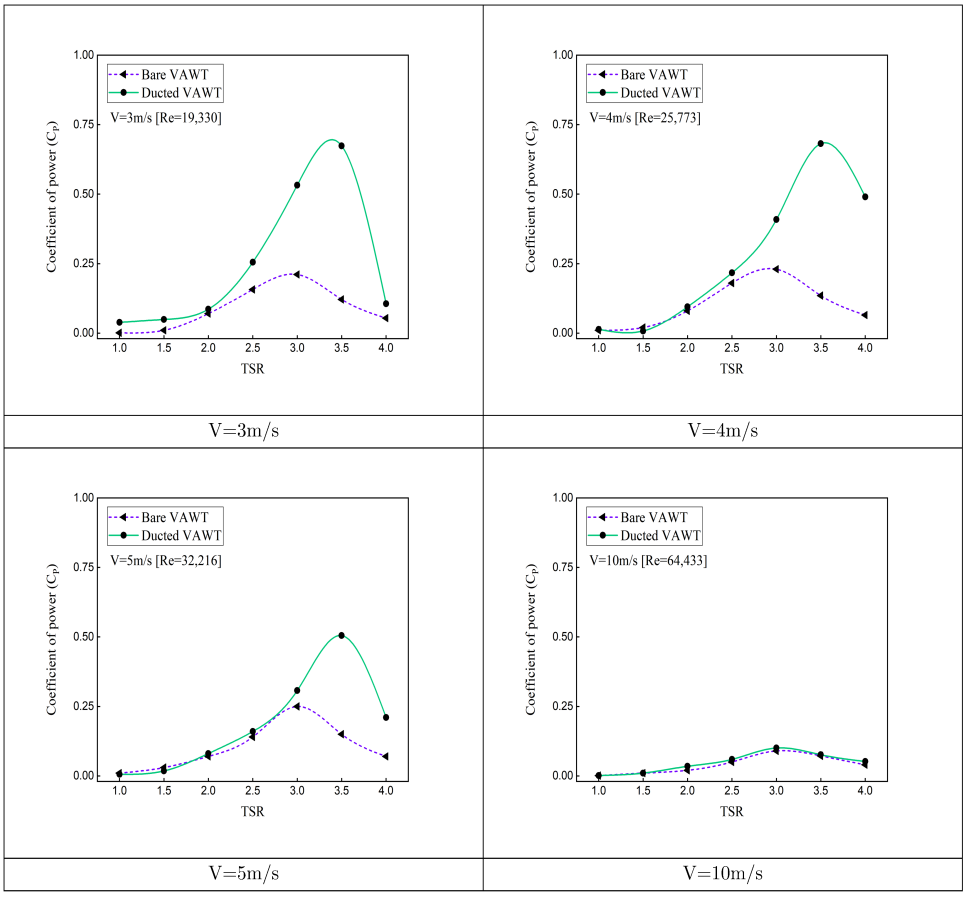

Figure 5.7: Comparison of coefficient of power (C_P) for ducted and bare VAWT at inlet velocities $V \in [3, 10m/s]$ and TSR$\in [1, 4]$ using NACA0017.

pronounced torque ripple, manifesting as amplified torque fluctuations. A lower torque ripple is prioritized in a design that aims to maximize turbine lifespan and reduce noise and vibration (Mazarbhuiya et al., 2018). In the present study, γ is calculated for different TSR and wind speed $V \in [3, 10\ m/s]$. Equation 5.11 shows this non-dimensional parameter which is derived from the maximum (T_{max}) and average torque (T_{avg}) (Reuter Jr, 1980).

$$\gamma = \frac{T_{max} - T_{avg}}{T_{avg}} \tag{5.11}$$

The variation of γ for different inlet velocities $(V \in [3, 10\ m/s])$ in relation to TSR$(\in [1, 4])$ for ducted VAWT using NACA0017 is depicted in Figure 5.8. The value of γ decreases with increasing TSR because the variation between maximum and average torque decreases. At lower TSR, this factor is on the higher side causing more instability and noise. The values of γ are minimum at TSR 3.5 where the maximum augmentation is achieved. Afterwards, γ remains almost constant.

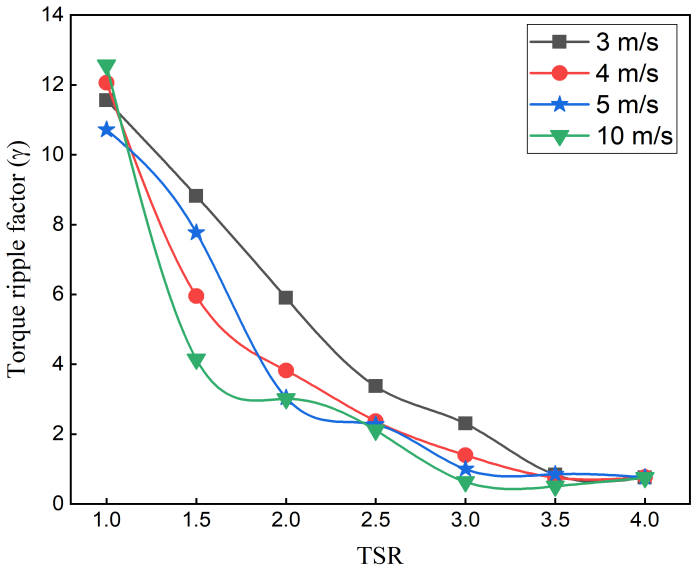

Figure 5.8: Torque ripple factor (γ) for ducted VAWT at different inlet velocities using NACA0017.

The airfoils of VAWT most likely function in a more stable flow regime at TSR 3.5, where the aerodynamic forces are more balanced, and the airflow is smoother and less turbulent. Lower torque ripple is the result of this more consistent airflow, which lessens torque output variations. The durability of VAWT is practically dependent on torque ripple. Over time, the fatigue stress cycles of VAWT are reduced and mechanical wear and tear of various components are lessened by lower, more constant torque forces.

The effect of different inlet velocities on instantaneous net torque coefficient for TSR

ranging from 1 to 4 has been shown in Figure 5.9. At lower $TSR \in [1, 2]$, significant fluctuations in instantaneous torque are evident, whereas these fluctuations diminish at higher TSR values. The maximum values of instantaneous C_T is found at $90°$, $210°$ and $330°$ within the angular interval of $120°$ for higher $TSR \in [3, 4]$. The velocity has a minimal impact on the instantaneous C_T at azimuthal angles of $30°$, $150°$ and $270°$. Notably, at a TSR of 3.5, the instantaneous C_T values at an inlet velocity of 4 m/s are higher compared to other velocities. Examining instantaneous torque coefficients aids in comprehending how a VAWT reacts to changes in wind speed and direction. Fluctuations in these coefficients offer valuable feedback for continuous design improvements.

The decrease in wind speed is measured by the wake velocity deficit, which is commonly represented as the difference between the wind speed within the wake (downstream of the turbine) and the undisturbed wind speed (upstream of the turbine) (Ryan et al., 2016) and it is given by equation

$$\Delta V = 1 - \frac{V}{V_\infty} \tag{5.12}$$

where V_∞ is free stream velocity and V is the velocity at wake location.

The wake velocity deficit significantly affects the amount of wind available to downstream turbines. As the upstream turbine consumes a large portion of the wind energy, the efficiency of turbines positioned in its wake is reduced. Understanding the wake deficit helps in designing an optimal turbine layout. The wake velocity deficit(ΔV) for $TSR \in [1, 4]$ at two positions, 5D and 10D downstream from the rotor centre, along a vertical line for ducted VAWT has been shown in Figure 5.10. For lower TSR values (TSR$\in [1, 2.5]$), the wake velocity deficit profiles are nearly identical at both the 5D and 10D downstream positions. At a TSR of 3, the wake deficit profile for the 10D location exhibits an almost linear trend for for $V \in [3, 5]$. At a TSR of 3.5 and 10D downstream, the wake velocity deficit is nearly zero across all velocities, indicating complete recovery of energy losses. This observation aligns with the fact that maximum augmentation is achieved at a TSR of 3.5.

A TSR of 3.5 likely reflects an ideal balance between the rotation rate and the aerodynamic forces acting on the turbine blades, maximizing efficiency while minimizing drag and turbulence. At this TSR, the VAWT operates in a regime where it can harvest a substantial amount of energy without unduly interfering with the downstream flow.

Turbulent intensity at different azimuthal angles(interval of $60°$) for ducted VAWT with NACA0017 airfoils have been shown in Figure 5.11, 5.12, 5.13 and 5.14 for $V \in [3, 10\ m/s]$, respectively. The ratio of the fluctuating velocity component to the mean velocity component is represented by Turbulent intensity. It can be observed that flow separation induces a relatively high-intensity turbulence zone behind the returning blade for lower TSR range ($TSR \in [1,\ 2.5]$). This turbulence is further exacerbated by the

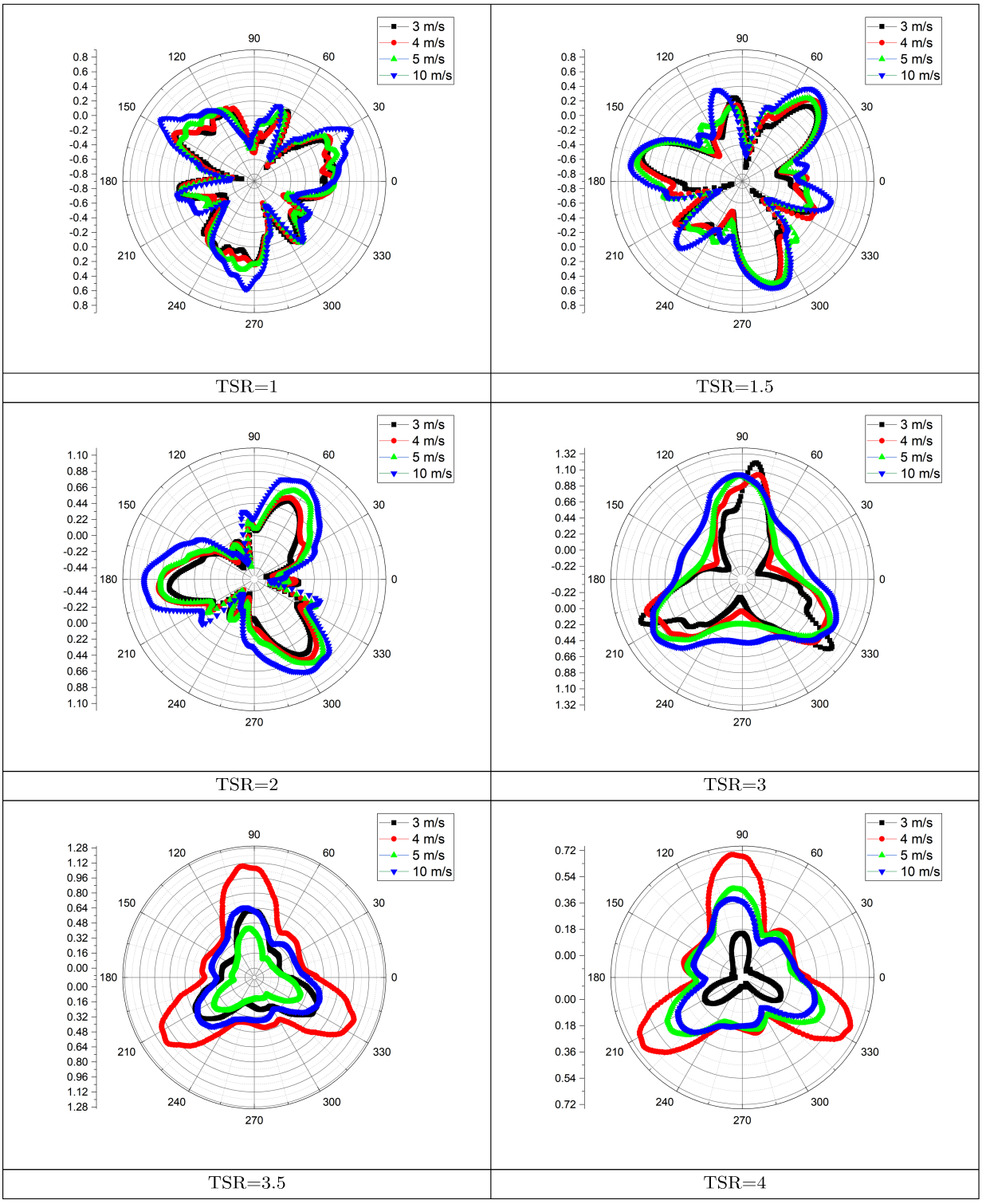

Figure 5.9: Impact of on the instantaneous net torque coefficient for $TSR \in [1, 4]$ at varying inlet velocities.

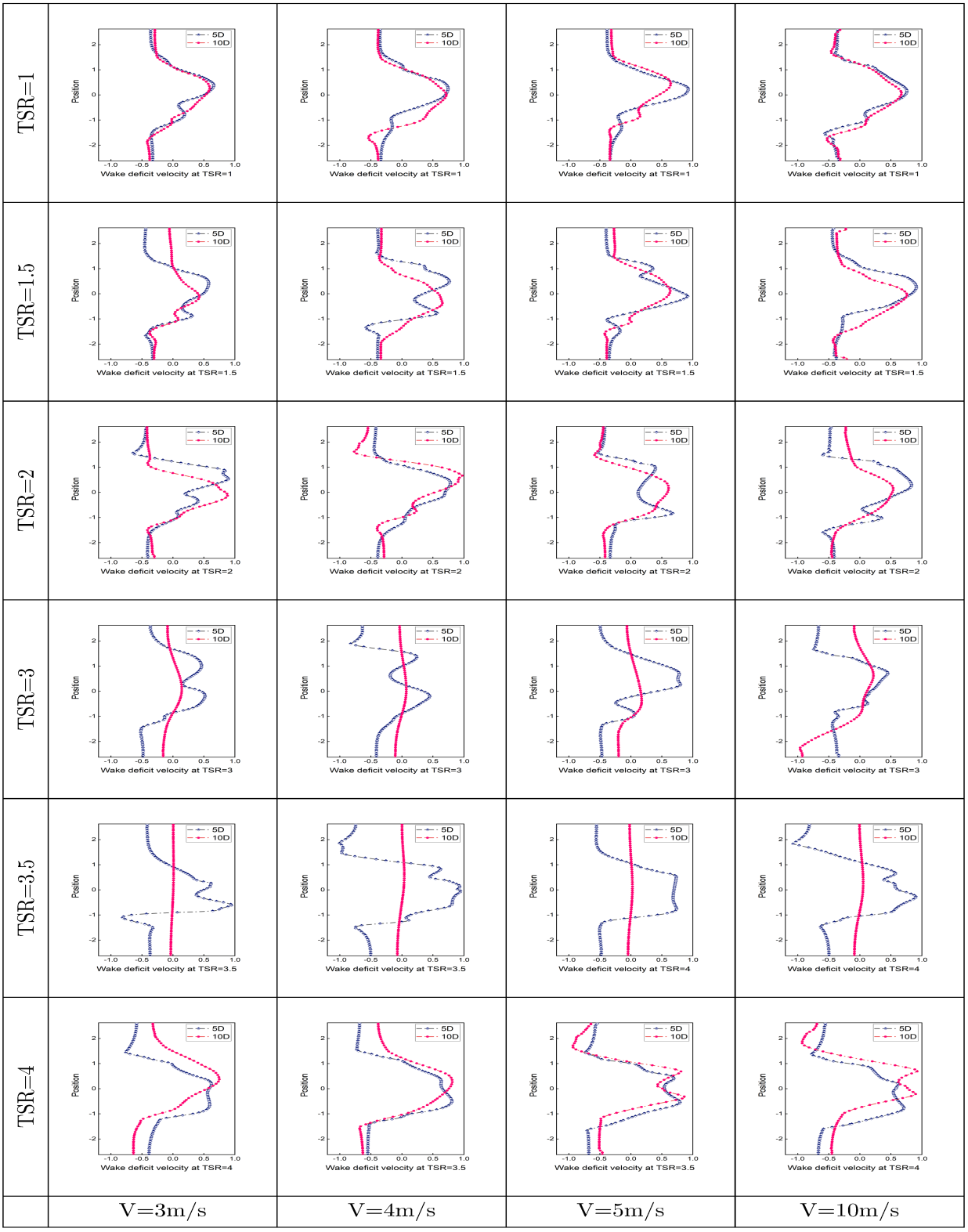

Figure 5.10: Wake velocity deficit for $TSR \in [1, 4]$ at 5D and 10D position from the rotor centre.

incoming airflow impacting the returning blade, thereby increasing the drag force. Consequently, the C_P is adversely affected and remains on the lower side. At a TSR of 3.5, the absence of significant turbulence results in a relatively higher C_P across all velocities. High turbulence intensity can cause varying loads on VAWT structures, influencing their durability. Insights into turbulence intensity help develop control strategies to stabilize turbine operation in turbulent wind conditions.

Vorticity distribution at different azimuthal angles (interval of $60°$) for ducted VAWT with NACA0017 airfoils have been shown in Figure 5.15, 5.16, 5.17 and 5.18 for four $V \in [3, 10\ m/s]$, respectively. It has been observed from the figures that at the start of the cycle, turbulent vortices generated by the preceding blade impact the leading edge of the subsequent blade. Wake vortex separation occurs on the blade surface during the early stage of revolution, while an erratic vortex shedding phenomenon is evident at higher velocities for TSR values ranging from 1 to 2.5. Ultimately, this disturbance adversely affects the turbine's performance. The shed vortices persist in the flow field and move downstream. For an inlet velocity of 10 m/s at TSR values of 3.5 and 4, vortex structures are generated behind the rotating domain. As the TSR value increases from 1 to 2.5, the intensity of these trailing vortices gradually diminishes due to the dissipation effect, leading to a higher C_P. Vorticity distribution reveals how vortices form around the blades. High vorticity may indicate areas of strong lift generation or potential flow separation, both of which affect overall turbine efficiency. This information is key to refining blade designs for better lift-to-drag ratios.

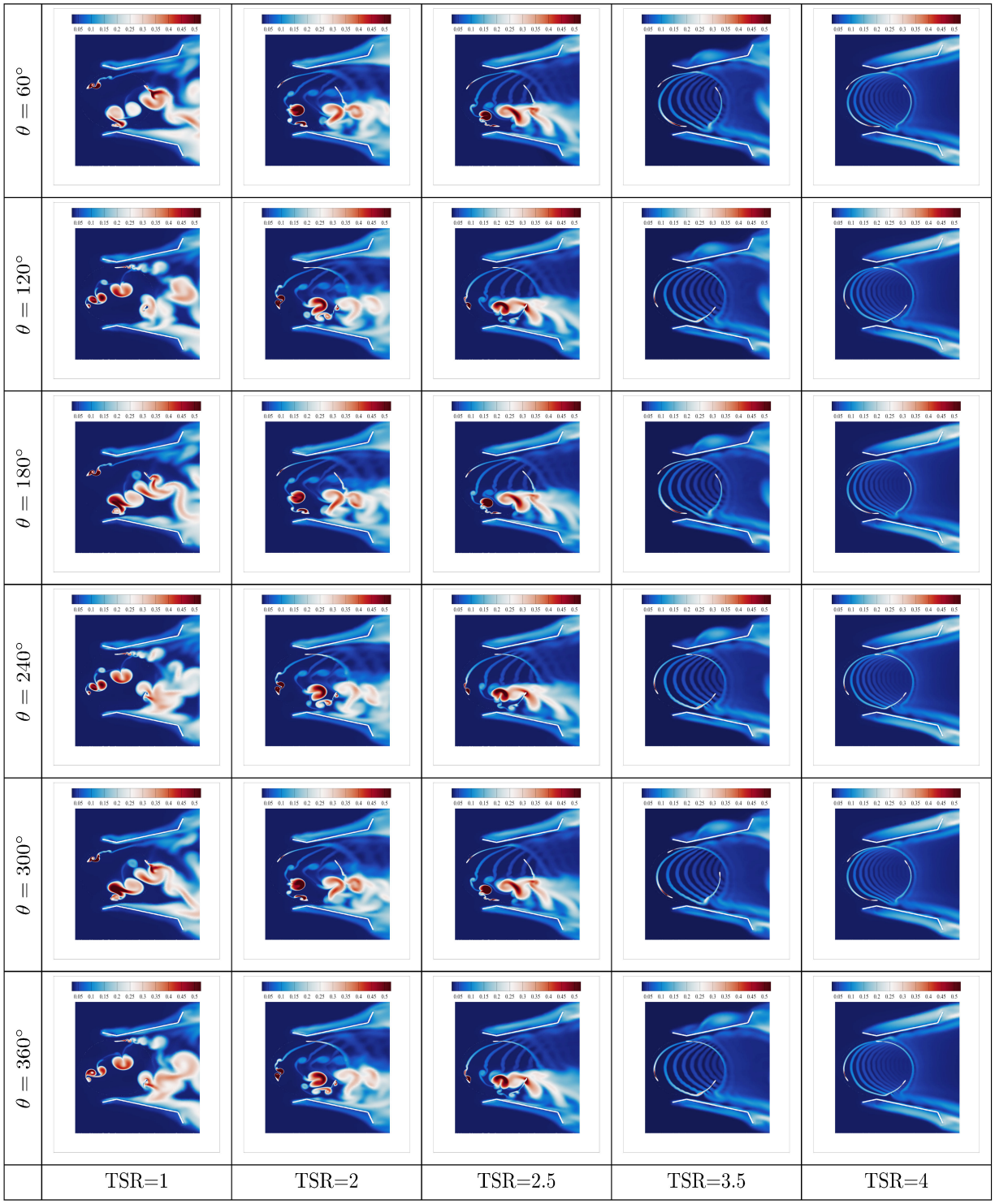

Figure 5.11: Turbulence intensity at different azimuthal positions for $TSR \in [1, 4]$ and at velocity 3 m/s.

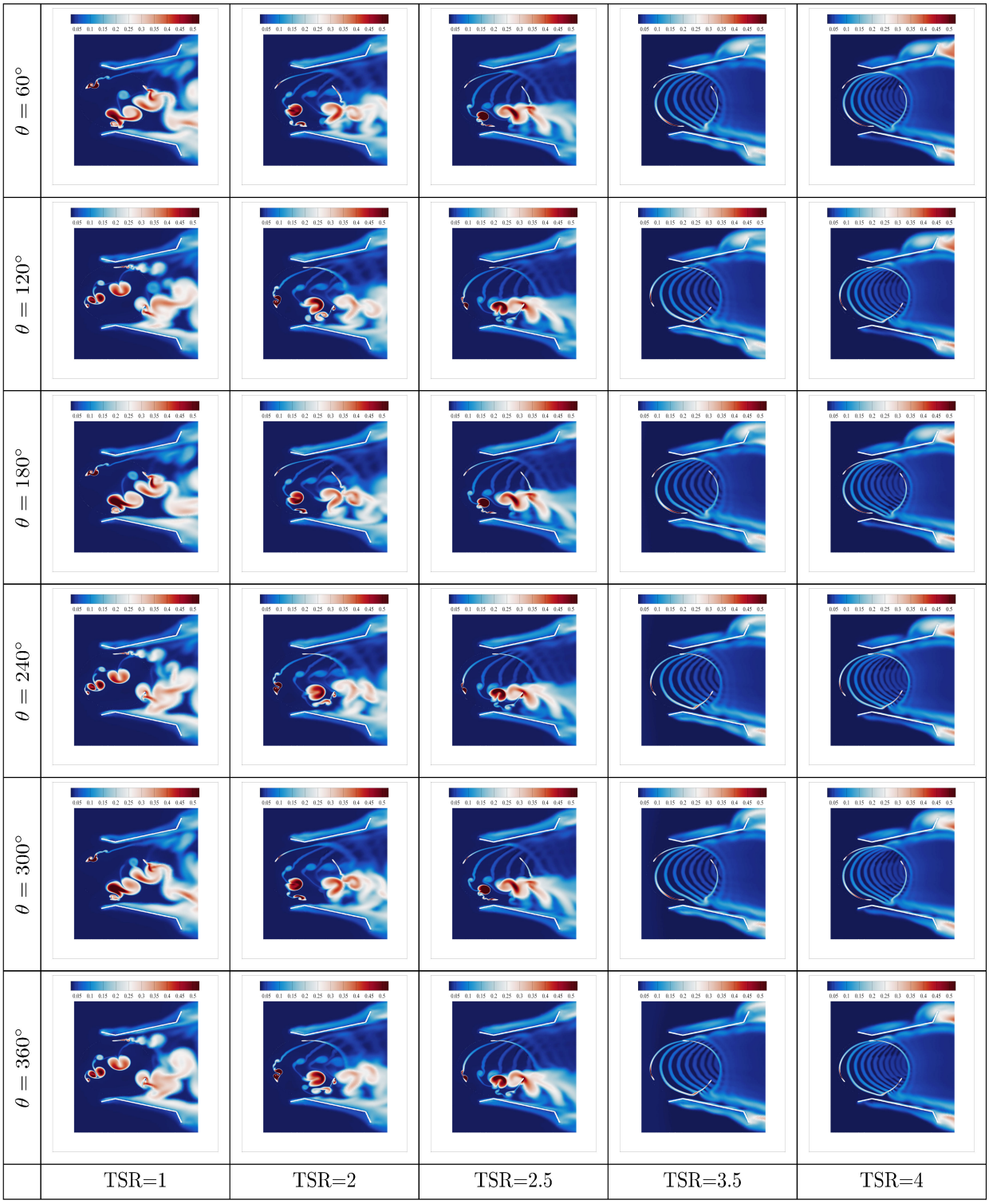

Figure 5.12: Turbulence intensity at different azimuthal positions for $TSR \in [1, 4]$ and at velocity 4 m/s.

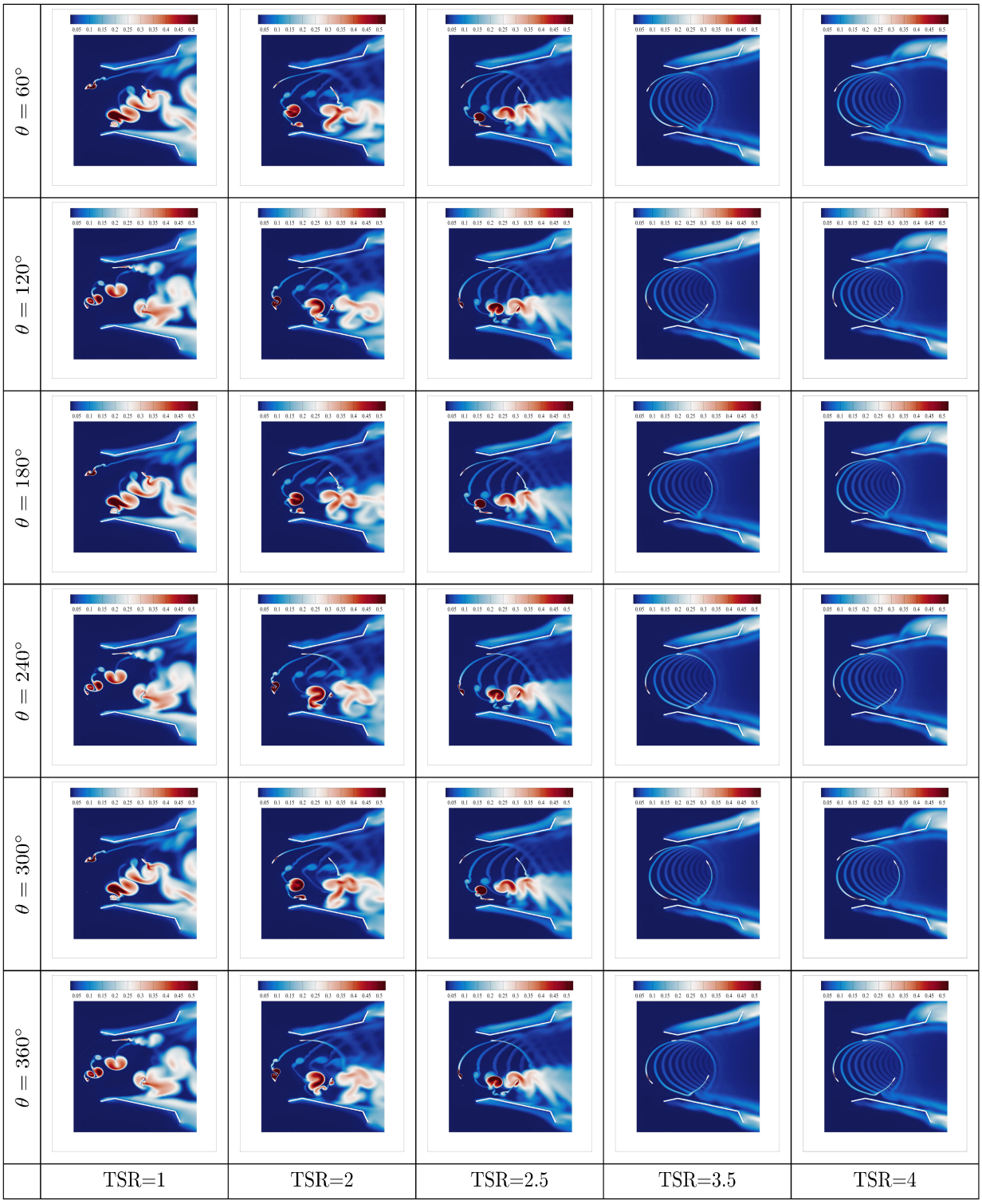

Figure 5.13: Turbulence intensity at different azimuthal positions for $TSR \in [1, 4]$ and at velocity 5 m/s.

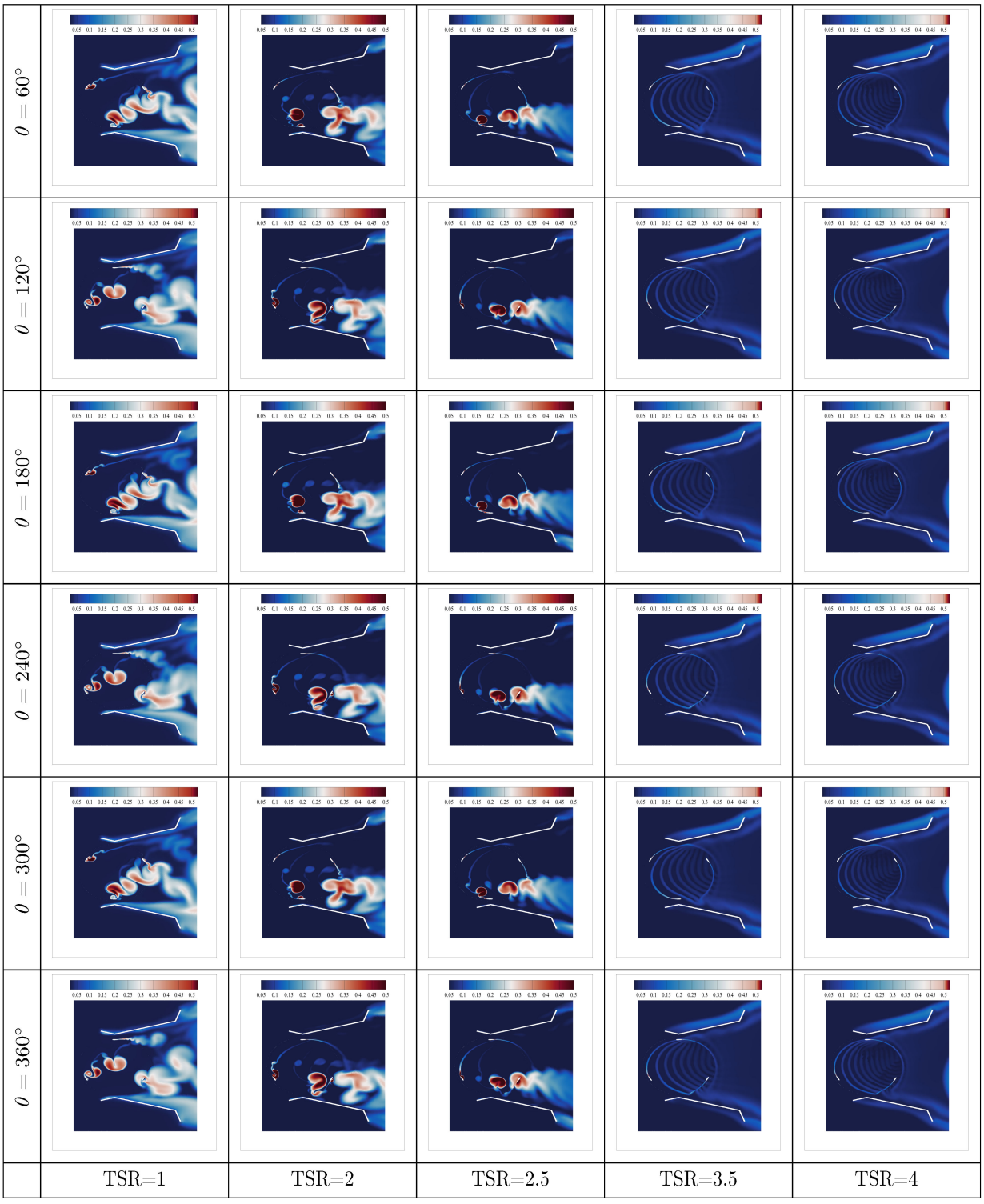

Figure 5.14: Turbulence intensity at different azimuthal positions for $TSR \in [1, 4]$ and at velocity 10 m/s.

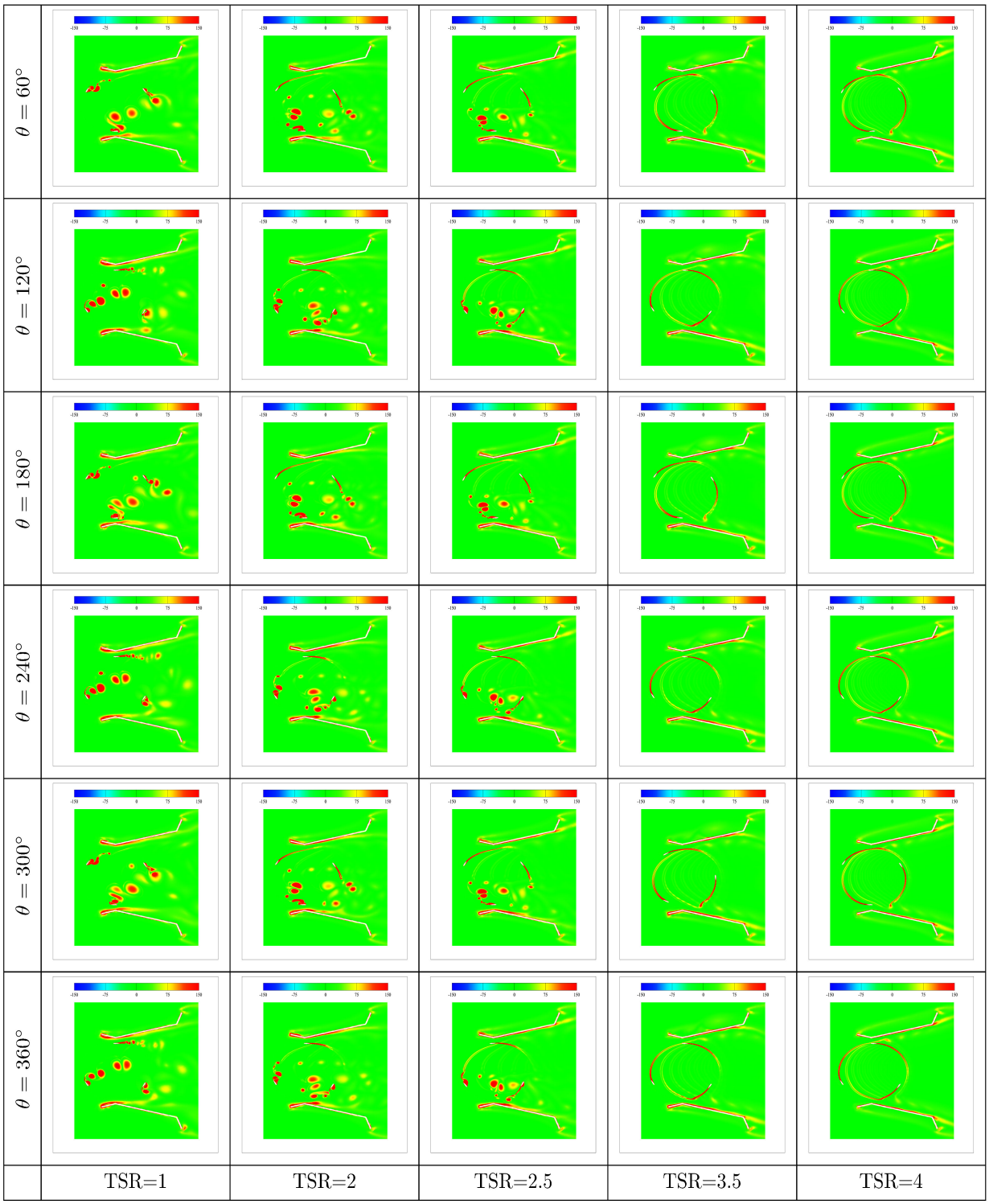

Figure 5.15: Vorticity distribution at different azimuthal positions for $TSR \in [1, 4]$ and at velocity 3 m/s.

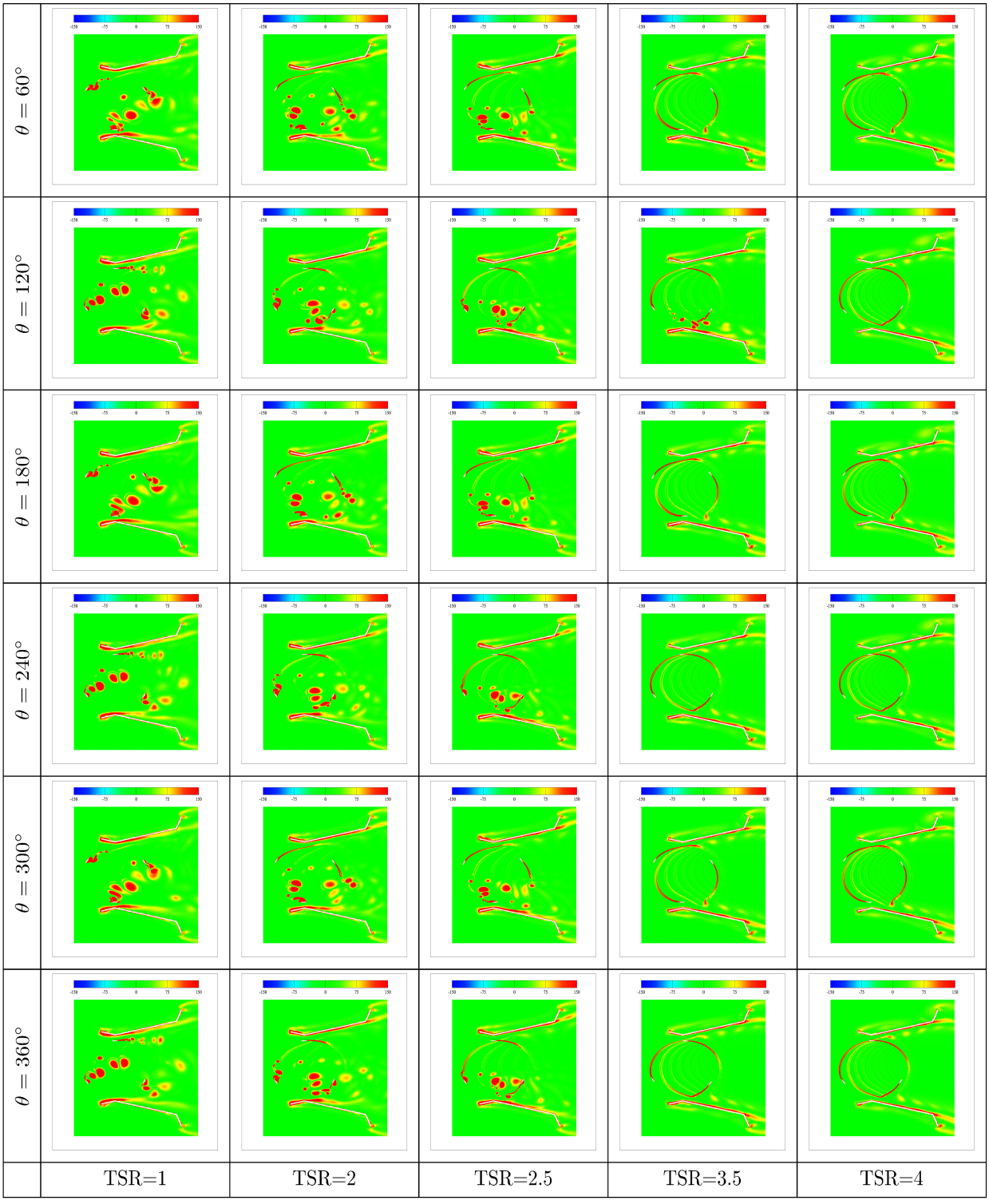

Figure 5.16: Vorticity distribution at different azimuthal positions for $TSR \in [1, 4]$ and at velocity 4 m/s.

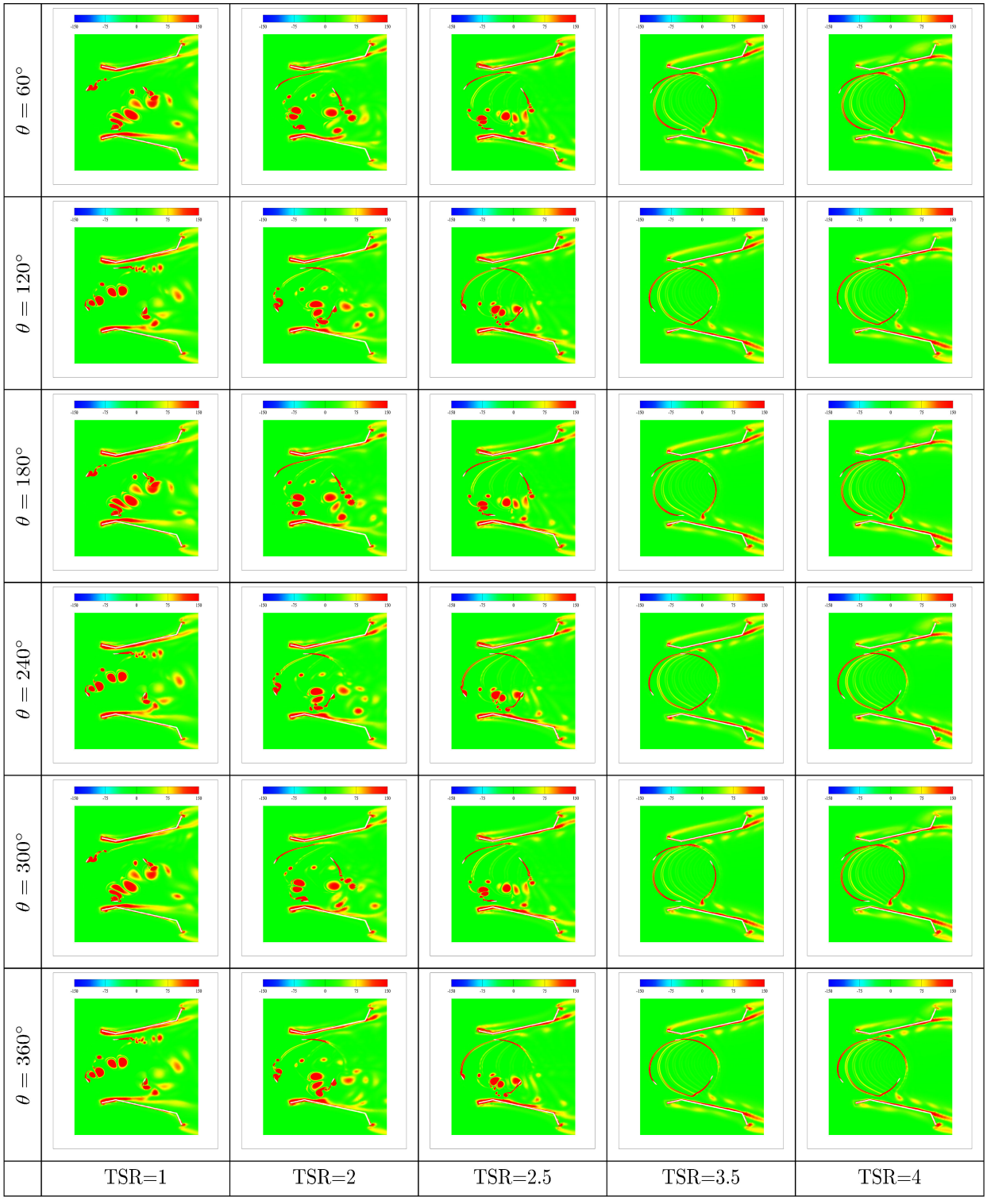

Figure 5.17: Vorticity distribution at different azimuthal positions for $TSR \in [1, 4]$ and at velocity 5 m/s.

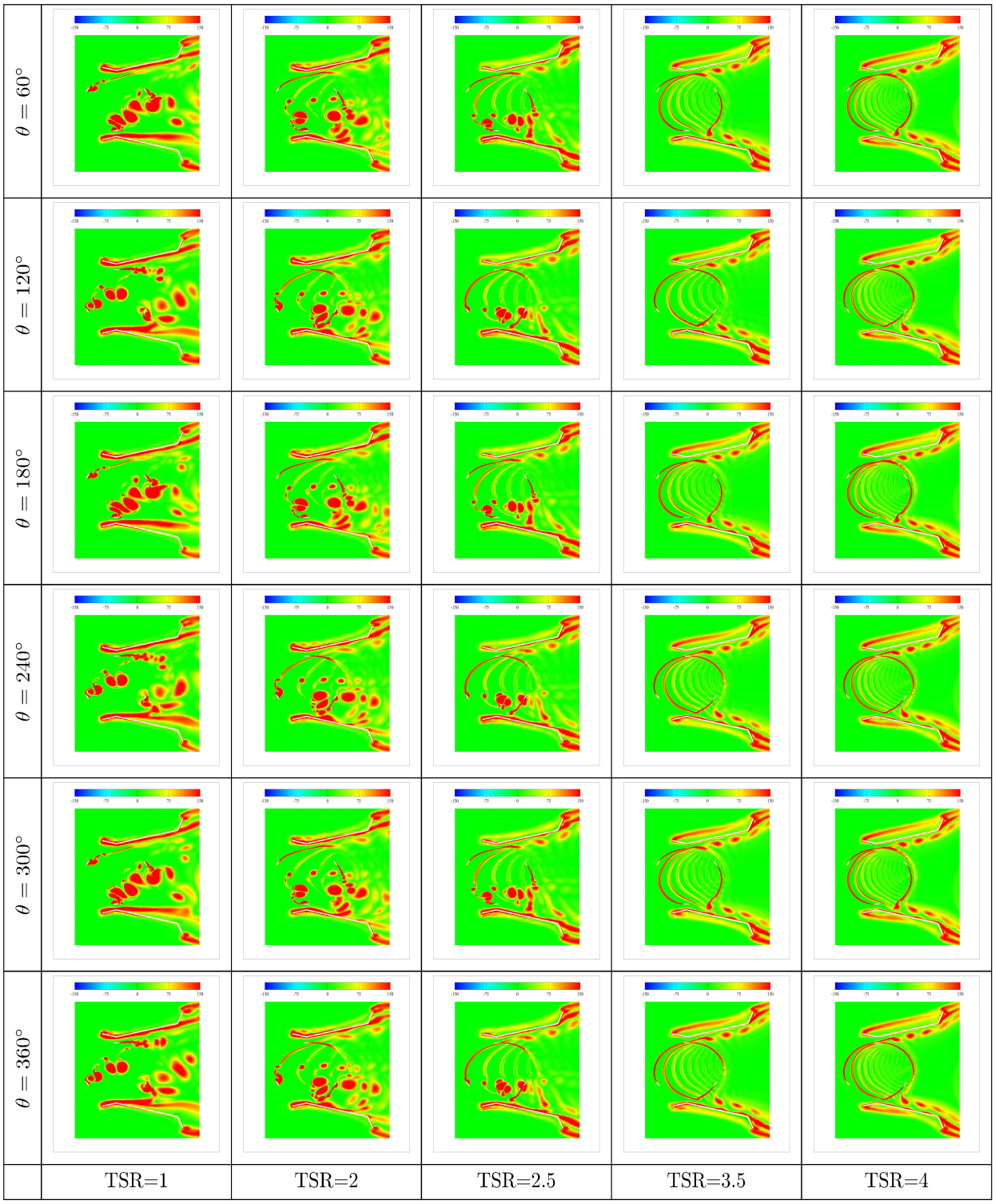

Figure 5.18: Vorticity distribution at different azimuthal positions for $TSR \in [1, 4]$ and at velocity 10 m/s.

5.4 Concluding remarks

A detailed assessment of the performance of a ducted vertical axis wind turbine using the NACA0017 blade profile has been carried out using a two-dimensional computational fluid dynamics (CFD) simulation. The geometry of duct comprises of nozzle, diffuser and flange. The flow field is calculated using URANS equations at velocity of 3, 4, 5 and 10 m/s respectively for TSR $\in [1, 4]$. To accurately account for turbulent effects, SST $k-\omega$ turbulence model is utilized for turbulent closure. The analysis involves a comparison of bare and ducted VAWT and also a thorough evaluation of torque ripple factor (γ), instantaneous net torque coefficients, wake velocity deficit, turbulent intensity and vorticity distribution. While TSR value for bare VAWT with NACA0017 airfoils offering higher C_P at 3, this value shifts to 3.5 when VAWT is augmented with duct. For ducted VAWT, the maximum C_P is 0.68 at TSR 3.5 for inlet velocity of 4 m/s. C_P is enhanced by approximately five times compared to the bare VAWT for inlet velocities V$\in [3, 4\ m/s]$. At an inlet velocity of 5 m/s, C_P is increased by about three-fold. Additionally, the torque ripple factor exhibits its lowest value at a TSR of 3.5, where the maximum augmentation is achieved. The leading-edge vortex formed more rapidly, and the separation process was delayed when the rotor was positioned inside the duct. This study establishes duct-augmented VAWTs with NACA0017 as potential systems for wind energy harvesting in low wind velocity areas with maximum velocity upto about 20 Km/h.

Admittedly, the major limitations of the work is that 2D models cannot capture the nuances of the flow physics for such problems. Although 2D simulations provide a computationally effective way to examine the basic aerodynamic behavior of ducted VAWTs, they inevitably oversimplify the intricate, three-dimensional nature of wind flow and turbine operation. To address these constraints and offer a more thorough analysis, future work should involve 3D CFD simulations of ducted VAWT. 3D visualization of the of vorticity distribution and turbulence intensity, providing a more accurate picture of how these factors affect turbine performance over time.

CHAPTER 6

VAWT Augmented with Deflector

6.1 Introduction

There has been a growing tendency toward the usage of renewable energy sources like solar, wind, hydropower, and others in the past few decades. Renewable energy sources do not produce greenhouse gas emissions and other pollutants as non-renewable sources and also it has minimal negative impact on the environment and mitigating the effects of climate change. Among the available alternative energy sources, wind energy has the potential to lead the renewable energy sector as it is a clean, renewable, and abundant energy source that can significantly reduce greenhouse gas emissions and contribute to a sustainable energy future (Das Karmakar & Chattopadhyay, 2022). To get the most energy out of the wind energy source, wind energy conversion technology (WECT) has been used in three basic stages. For different regions of the world, the wind energy potential is assessed in the first stage known as the energy resource assessment (Rahman & Chattopadhyay, 2020, 2023). Designing the hardware and installing an optimum wind turbine system make up the second and last stage.

Horizontal axis wind turbines (HAWTs) and vertical axis wind turbines (VAWTs) are the two main types of turbines that are used to convert wind energy into electrical power. VAWTs have a smaller swept area and are better suited for small-scale applications while HAWTs are mounted on large towers are the most widely utilized variety despite it requires a complex yaw mechanism (Mohammed et al., 2019). VAWTs have several advantages over HAWTs due to its Quiet operation, Wind direction independence, Durability, Cost-effectiveness (Dossena et al., 2015). According to recent study, VAWT has more potential for offshore platforms than HAWTs in terms of scalability and straightforward design (Tescione et al., 2014). Additionally, VAWTs may generate power from extremely turbulent wind flows, which are frequent in metropolitan and

urban regions (W.-H. Chen et al., 2017). VAWTs can be divided mainly into two categories based on the laws of aerodynamics: lift type and drag type (Sagharichi et al., 2018). Savonius VAWT is an illustration of the drag type, and Darrieus VAWT is an illustration of the lift type. Greater efficiency is offered by the H-type Darrieus wind turbine than the drag type (Jain & Saha, 2020a).

The performance of a VAWT can be enhanced by selecting an efficient blade profile (Castelli et al., 2011; Das Karmakar et al., 2023; M. H. Mohamed et al., 2019). In order to investigate the impacts of airfoil shape and pitch angle, M. H. Mohamed et al., 2019 performed a numerical simulation of the H-type Darrieus VAWT employing 25 different airfoil shapes. Out of the NACA-4series airfoils, NACA0015 had the highest efficiency, followed by NACA0018. Nobile et al., 2014investigated an augmented VAWT with NACA0018 blade profile using 2D CFD simulation of augmented. Similar to this, various studies have used CFD models to investigate the aerodynamic behavior of VAWT in order to improve its performance (Jiang et al., 2020; Lanzafame et al., 2014; Qin et al., 2011). The aerodynamic performance of a Darrieus wind turbine with three straight blades and NACA0021 airfoils was evaluated by Castelli et al., 2011.

Three-dimensional numerical simulations have only recently been conducted on the straight bladed darrieus VAWT by several researchers (Howell et al., 2010; Zhang et al., 2013). **jin2015** analyzed VAWT using three-dimensional solution of Navier-Stokes equation which provides comparable results with the experimental results. Combined CFD analysis and experimental of VAWT were also reported by many researchers (Bianchini et al., 2017; Franchina et al., 2019; Lam & Peng, 2016). A three-bladed straight wind turbine is examined by Zhang et al., 2013 utilising a NACA0015 airfoil. Howell et al., 2010 investigated a VAWT with three-dimensional CFD model using based on $k-\varepsilon$ turbulence model. Elkhoury et al., 2015 conducted a 3D simulation on the performance study of the VAWT with three different airfoils. They employed the blade profiles NACA0018, NACA0021, and NACA634-221. The NACA0021 has a superior power coefficient than the NACA0018, according to both numerical and experimental measurements, despite the fact that the NACA0018 is 3% thinner.

Among various power augmentation strategies, the flat plate deflector has emerged as the simplest and most effective. Mohamed et al. investigated the influence of a shielding plate positioned upstream of the returning blade of a Savonius rotor. This configuration significantly reduced the negative torque, thereby enhancing the net torque and improving the power coefficient by approximately 38.9%. Similarly, Golecha et al., 2011 demonstrated that optimal placement of a deflector upstream of a Savonius rotor could increase the power coefficient by nearly 50%, confirming the effectiveness of such augmentation.

Kim and Gharib, 2013 explored the use of straight plate deflectors for counter-rotating lift-type VAWTs. The upstream deflector, was found to accelerate the local

flow velocity around the rotor by redirecting the inflow, thereby increasing power output. However, performance deteriorated when the deflector was placed too close to the turbine due to adverse wake interactions. Their results indicated a threefold increase in peak power coefficient when the deflector width-to-rotor diameter ratio was optimized at 0.33, though the findings were limited to high-solidity, low-Reynolds-number configurations.

Jin et al., 2018 conducted experiments on counter-rotating straight-bladed VAWTs with upstream deflectors (Figure 2.3), analyzing the effects of deflector height, width, and spacing. The study found that performance improved significantly when turbines were placed outside the deflector's near-wake region. The SST turbulence model closely matched experimental results, with a deviation of just 10.3%. Under optimal conditions, the maximum power coefficient reached 0.45.

De Santoli et al., 2014 investigated a duct-augmented VAWT using a finite volume method. The converging duct accelerated incoming flow via the Venturi effect, resulting in a power increase of 125%. Despite its performance benefits, the design's scalability is hindered by the duct's size and associated costs.

Stout et al., 2017 examined the effect of a curved upstream deflector on a three-bladed Darrieus turbine. Both numerical and experimental analyses confirmed that the deflector mitigated negative torque by diverting flow away from the returning blade. The optimal power coefficients observed were 0.208 and 0.213 for deflector width angles of 45° and 36°, respectively.

Overall, most augmentation devices aim to increase the local mass flow rate through flow convergence or redirection, thereby enhancing positive torque generation. Drag-type VAWTs primarily benefit from reduced negative torque on returning blades, whereas lift-type VAWTs rely on improved flow alignment to increase lift forces. However, there is a notable research gap concerning flat plate deflectors applied to lift-type VAWTs with NACA0017 airfoils. This study aims to address that gap by investigating the effect of such a deflector under varying Reynolds numbers using 3D CFD simulations. The performance of these airfoils is benchmarked with that of NACA0021, which excels in wind turbine applications.

6.2 Computational modeling

Flow domain and boundary conditions Three-dimensional numerical analysis of an H-type Darrius VAWT with straight blade of NACA0017 airfoil is performed using ANSYS-FLUENT CFD software. Previous research demonstrates a considerable impact of domain size on the VAWT's performance (Rezaeiha et al., 2017). The present 3D computational domain has an inlet and outlet at a distance of 10D and 15D from the centre of the rotor, respectively, where the rotor diameter is denoted by D rotor height

is denoted by H. The 3D domain size is 25D x 10D x 10D, as shown in Figure 6.1. The geometry has been divided into two regions: a rotating domain with a diameter of 1.5D, containing three airfoils with a cylindrical interface, and a cuboid stationary domain beyond the circular interface. The two regions are interconnected with each other by using a sliding interface that ensures the continuity of mass and momentum exchange between cell zones. There is a small gap of 100mm between the cylindrical interface with the top and bottom edges of the rotor blade. The size of flat plate deflector is a 0.3 m × 0.9 m and the thickness is 10 mm. It is mounted vertically and placed upstream of the VAWT. It is aligned perpendicular to the flow and positioned at various horizontal distances (X = 0.3 m) and vertical offsets (Y = 0.2 m). Dimensions are provided in absolute units, but also clearly tied to rotor dimensions as length = H and width = 3D. The approaching velocity at the inlet boundary is selected upto 5 m/s, corresponding to a maximum Reynolds number of 34,229. At the outlet, atmospheric pressure is used as the domain is connected with ambient and other four surfaces are considered as symmetry walls.

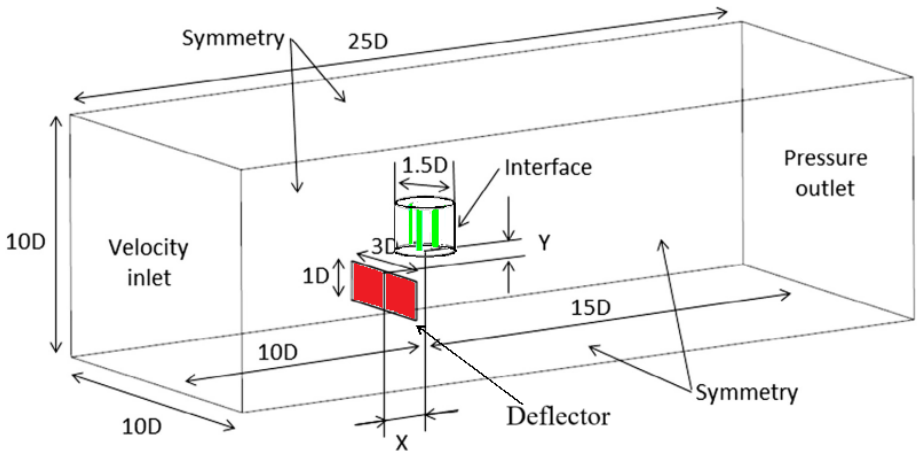

Figure 6.1: Three dimensional computational domain for present study

Wind speed (v), rotor solidity, tip speed ratio (TSR), number of blades of the turbine, shape of the airfoil, pitch angle, torque coefficient (C_T), and power coefficient (C_P) are some of the factors influencing VAWT performance.

C_T and C_P are used for performance assessment of a wind turbine and they are denoted by:

$$C_T = \frac{2T}{\rho A R v^2} \tag{6.1}$$

$$C_P = \frac{P}{\rho v^3 H R} \tag{6.2}$$

$$C_P = C_T \times \text{TSR} \tag{6.3}$$

$$\text{TSR} = \frac{\omega r}{v} \tag{6.4}$$

where P is the power, and it is expressed as

$$P = \frac{T \cdot N}{60} \tag{6.5}$$

Here, N is the number of revolutions per minute (RPM), T represents torque in Nm, ρ is the air density, A is the cross-sectional area of the rotor, and TSR is the tip speed ratio.

6.3 Meshing and model validation

Tetrahedral unstructured mesh was selected for the whole computational domain along with some prism and pyramid cells. Mesh was refined near the airfoil walls using 20 numbers of inflation layers the first layer thickness has been set at 0.5 mm and the growth rate parameter has been fixed at 1.2. Maximum skewness is found to be less than 0.86. The details of meshing of geometrical model are shown in Figure 6.2.

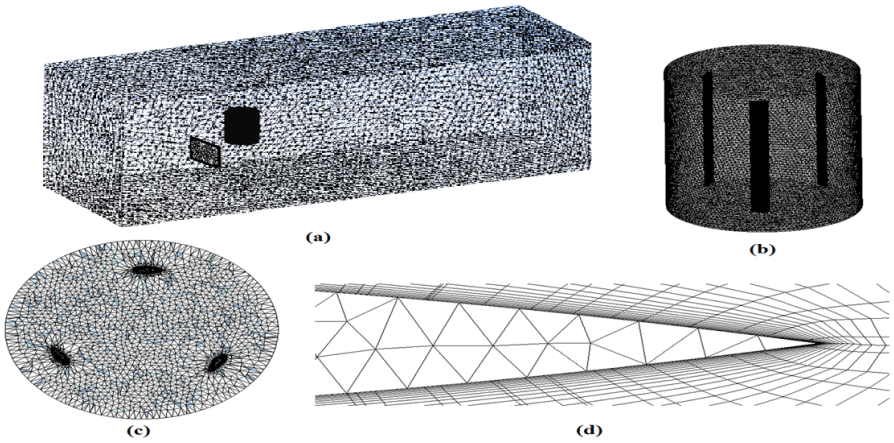

Figure 6.2: Details of meshing of the geometrical model: (a) Cuboid domain, (b) Cylindrical domain, (c) VAWT Rotor domain, (d) meshing around airfoil

Numerical simulations have been conducted using five different levels of mesh with element sizes of 1443028, 1691622, 1822789, 2047583, and 2218917 at 2.5 TSR and an input velocity upto 5 m/s in order to determine the mesh size that will produce the best results. The result shows that the torque coefficient reached a stable value with the last three mesh sizes. Therefore, the mesh with element 2047583 was taken into consideration for the present analysis. Unsteady Reynolds-average Navier-Stokes (URANS) equations are used for the turbulent flow field. SST $k-\omega$, a two-equation turbulence model, is considered for the closure of the turbulent flow field (Biswas & Gupta, 2014; Jain & Saha, 2020b; Tabatabaei et al., 2019). For simulation, the solver was configured

as a pressure-based SIMPLE algorithm. For the spatial discretization of gradients, a Green-Gauss node-based technique was used. For all transient formulations, the higher-order upwind scheme and implicit scheme were selected. At each time step, the convergence threshold has been set at 10^{-5}. For the continuity, momentum, and Reynolds' closure equations, the under-relaxation parameters were within 0.8. For Validation of our results, we considered the experimental results performed by Castelli et al., 2011. The comparison between these two cases is shown in Table 6.1.

Table 6.1: Geometrical characteristics

Study	Type of Aerofoil	No. of Blades	Diameter of Rotor, D (m)	Height of Rotor, H (m)	Chord of Blade (m)	Solidity
Present work	NACA0017	3	0.7	1.2	0.1	0.425
Castelli et al. (2011)	NACA0021	3	1.03	1.0	0.858	0.5

6.4 Results and discussions

The experimental data from Castelli et al., 2011 that has almost similar geometrical characteristics has been selected for the validation of the current results obtained from 3D numerical simulation. The validation of the current simulation using the experimental data is shown in Figure 6.3. The results of the current computational investigation have a somewhat lower value than those from the experiments. For the broad range of operating TSR, it can be taken as a good agreement with experimental evidence. At a TSR value of 2.5, the greatest deviation was found to be 26%.

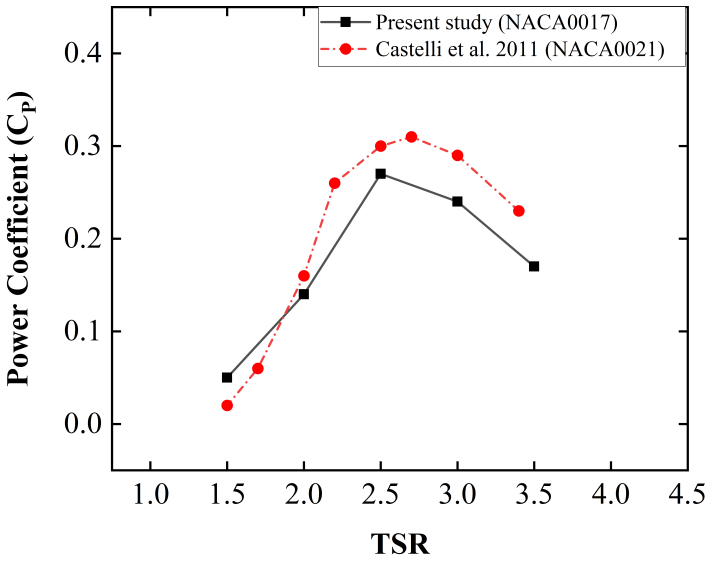

Figure 6.3: Validation of present CFD model

Figure 6.4 depicts the variations of C_P at different inlet velocities of 4 m/s and 5 m/s. Figure illustrates how the coefficient of power drops when the inlet velocity decreases,

lowering the VAWT's overall performance. Maximum power coefficient values for 4 m/s and 5 m/s are 0.23 and 0.28, respectively.

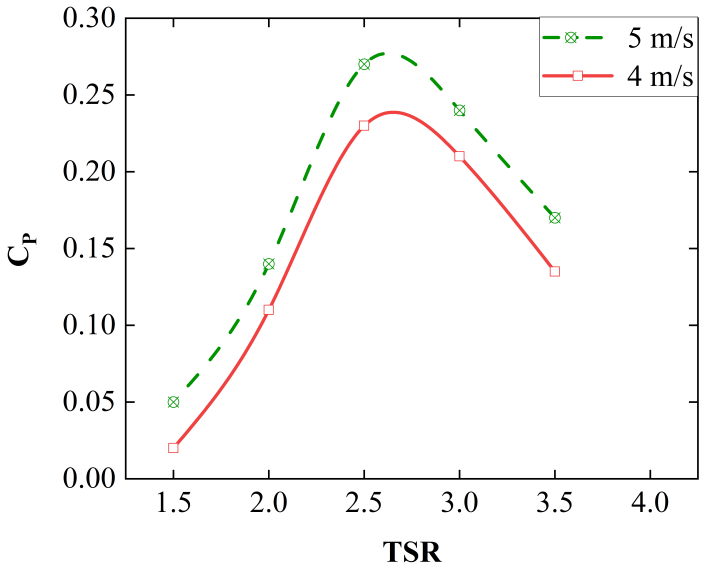

Figure 6.4: Variation of C_P at different inlet velocities for $TSR \in [1.5, 3.5]$

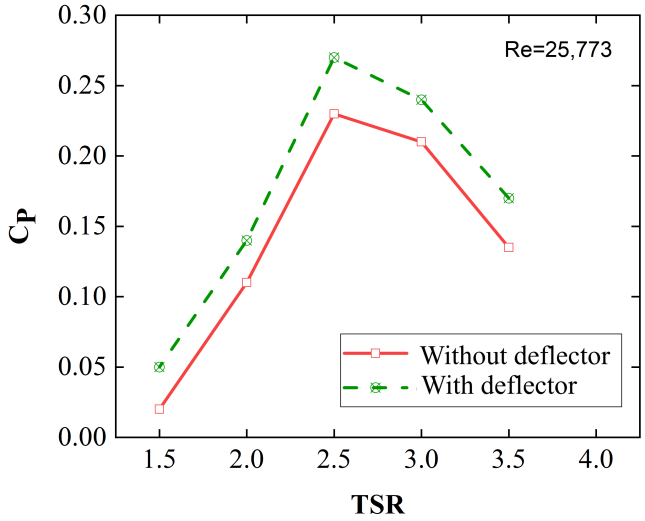

Figure 6.5: Comparison C_P for bare and deflector augmented VAWT at velocity 4 m/s for $TSR \in [1.5, 3.5]$

Figures 6.5 and 6.6 compare the C_P as a function of TSR for bare VAWT (without deflector) and deflector augmented VAWT at inlet velocities of 4 m/s (Re $=$ 25,773) and 5 m/s (Re $=$ 32,216). In both cases, the maximum C_P is observed at a TSR of 2.5, with the deflector augmented VAWT results consistently predicting higher C_P values compared to the results of without deflector due to the inclusion of three-dimensional flow effects such as spanwise motion and tip vortices. At 4 m/s, the peak C_P reaches

approximately 0.28 for deflector augmented VAWT versus 0.23 for bare VAWT, while at 5 m/s, the peak values are around 0.29 for VAWT with deflector and 0.27 for VAWT without deflector. Additionally, a slight increase in C_P is observed with increasing velocity, reflecting the influence of the Re on aerodynamic performance. Overall, the simulations provide a more accurate representation of turbine performance, highlighting their importance for capturing realistic aerodynamic phenomena and predicting the optimal operating TSR.

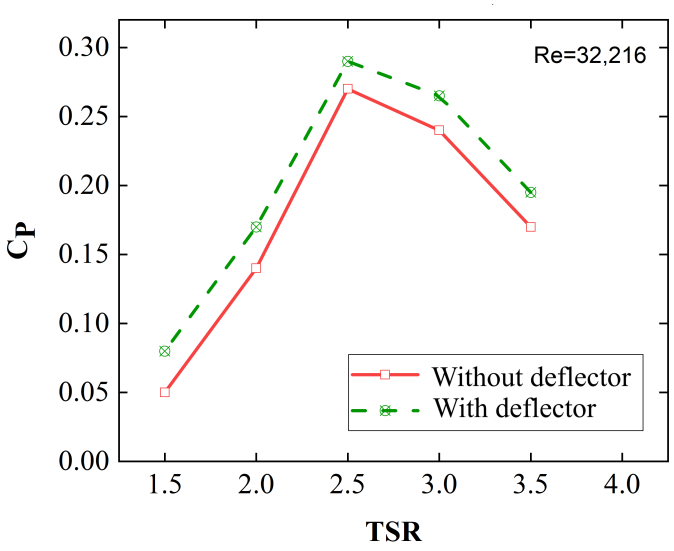

Figure 6.6: Comparison C_P for bare and deflector augmented VAWT at velocity 5 m/s for $TSR \in [1.5, 3.5]$

The wake velocity deficit, defined as the reduction in wind speed downstream of a turbine relative to the free-stream velocity (Ryan et al., 2016), is given by

$$\Delta V = 1 - \frac{V}{V_\infty} \tag{6.6}$$

where V_∞ is the undisturbed upstream velocity, and V is the local wake velocity. Figure 6.7 illustrates the wake deficit profiles for various tip speed ratios (TSRs = 1.5, 2.5, 3.5) and two inflow wind speeds ($V = 4$ m/s and $V = 5$ m/s), evaluated at 5D, 10D, and 14D downstream positions. At lower TSRs, significant wake velocity deficits are observed with minimal recovery, whereas at TSR = 3.5, the velocity profiles show near-complete wake recovery by 14D, especially for higher inflow velocities. This indicates enhanced aerodynamic performance and reduced downstream interference at the optimal TSR.

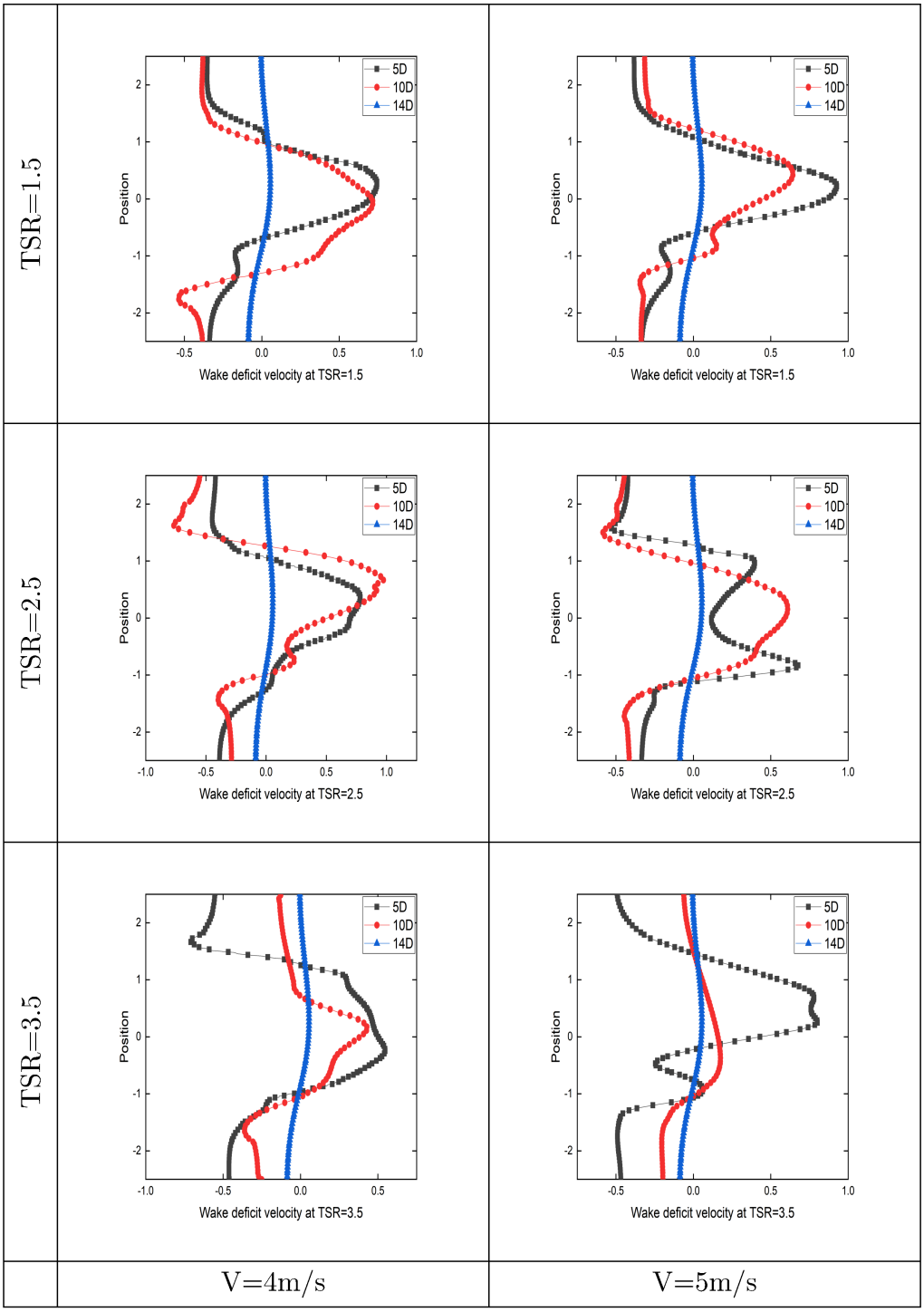

Figure 6.7: Wake velocity deficit for $TSR \in [1.5, 3.5]$ at 5D, 10D, and 14D downstream locations for wind speeds $V = 4$ m/s and $V = 5$ m/s

Q-criterion is a tool to visulize vortices in the flow domain. The value of Q is given as in equation 6.7 which shows the relative strength of vorticity over the strain rate.

Q-criterion (Kolář, 2007) is given by

$$Q = \frac{1}{2}\left(\Omega_{ij}^2 - S_{ij}^2\right) \tag{6.7}$$

where

$$\Omega_{ij} = \frac{1}{2}\left(\frac{\partial u_i}{\partial x_j} - \frac{\partial u_j}{\partial x_i}\right), \tag{6.8}$$

$$S_{ij} = \frac{1}{2}\left(\frac{\partial u_i}{\partial x_j} + \frac{\partial u_j}{\partial x_i}\right). \tag{6.9}$$

The functions Ω and S represent vorticity (a function of rotation) and shear strain (rate of shear), respectively.

Figure 6.8 shows the Q iso-surface for three airfoils colorized by vorticity at different azimuthal angles for better visualization. Different vortex's strength can be observed at different azimuthal angles and they are not axisymmetric like HAWT. The trailing edge and blade tips engage in high turbulence when the blade travels upwind and interacts with the incoming wind flow.

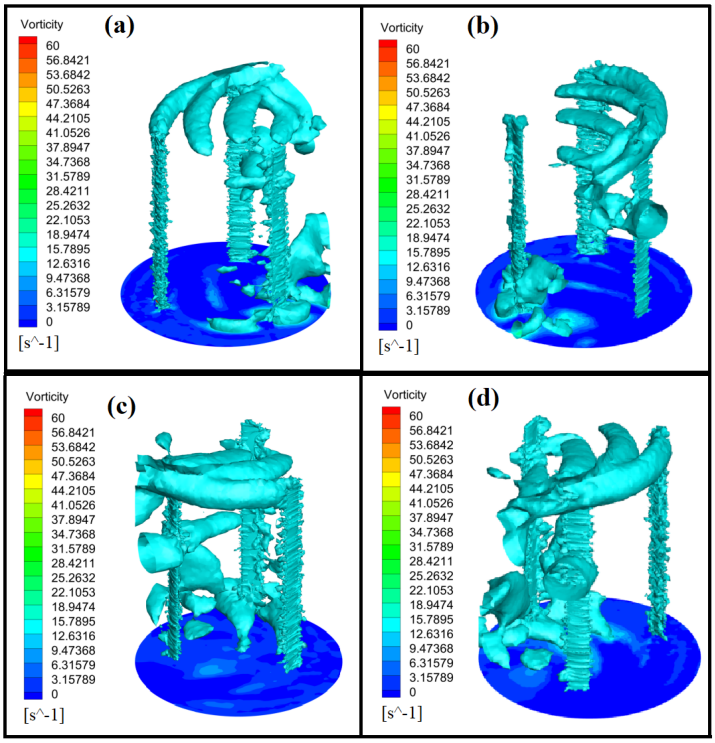

Figure 6.8: Q-criterion iso-surfaces colorized by vorticity at four azimuthal positions ($\theta = 0°$, $90°$, $180°$, and $270°$) for bare VAWT

Figure 6.9 illustrates the Q-criterion iso-surfaces (colored by velocity magnitude in m/s) at four distinct azimuthal angles ($\theta = 0°$, $90°$, $180°$, and $270°$) for a Vertical Axis Wind Turbine (VAWT) with a deflector augmentation. These iso-surfaces highlight regions dominated by rotational motion (vorticity) in the wake and around the turbine blades.

At $\theta = 0°$, strong vortical structures begin to form at the blade tips and trailing edges as the blade enters the upwind region, indicating early interaction with the oncoming flow. At $\theta = 90°$, more pronounced and asymmetric vortices are visible, showing com-

plex flow detachment and wake development due to interaction with the deflector. At $\theta = 180°$, the blades are in the downwind position, and the vortex structures exhibit increased turbulence and merging patterns in the wake. At $\theta = 270°$, the flow shows renewed vortex shedding as the blades prepare to re-enter the upwind zone. The distribution of vortices is non-axisymmetric, which is typical for VAWTs, especially with deflector influence. The presence of the deflector alters the flow field, enhances localized vorticity, and causes variations in wake behavior across azimuthal angles. It can be observed that losses of Q diminish when the deflector plate is present. In other words flow field is relatively better organized with lower loss, which causes an increase in the power coefficient.

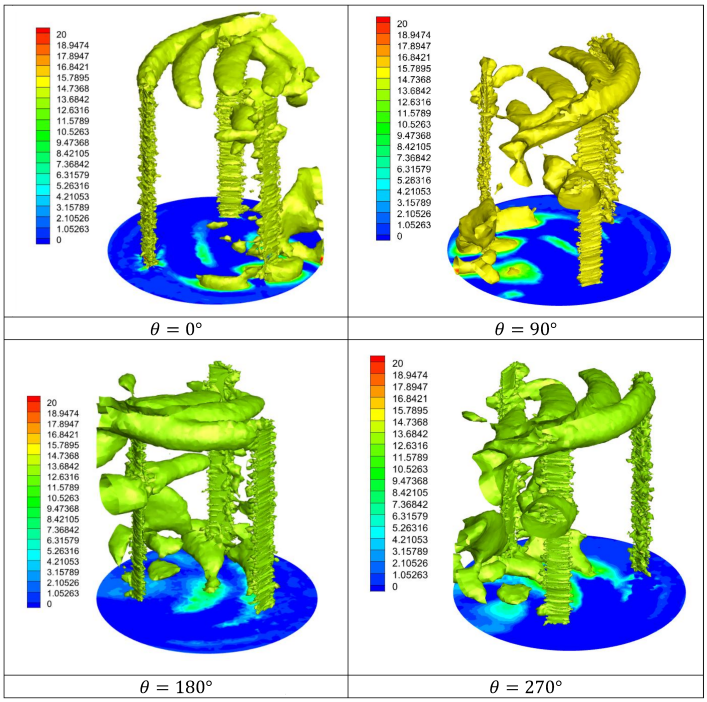

Figure 6.9: Q-criterion iso-surfaces colorized by vorticity at four azimuthal positions ($\theta = 0°$, $90°$, $180°$, and $270°$) for the deflector-augmented VAWT configuration.

6.5 Concluding remarks

This study investigates the aerodynamic performance enhancement of a lift-type VAWT aving straight bladed NACA0017 blade profile and equipped with a flat plate deflector using 3D CFD simulations. he flow field has been resolved by using an unsteady RANS based 3D simulation at inlet velocities of 4 and 5 m/s. Transition shear stress transport (SST) $K-\omega$ turbulence model has been implemented for turbulent closure.

The results confirm that deflector augmentation contributes significantly to perfor-

mance improvement by enhancing the C_P and reducing negative torque effects. Across both tested inlet velocities (4 m/s and 5 m/s), the deflector-equipped VAWT consistently outperformed the bare rotor, with a peak C_P of approximately 0.28 and 0.29, respectively, compared to 0.23 and 0.27 for the bare configuration. The improvement is more pronounced at the optimal TSR of 2.5 and is influenced by increased Reynolds number, highlighting the role of inertial forces in lift-based systems. Flow visualization using the Q-criterion revealed the development of complex, asymmetric vortical structures that vary significantly across azimuthal blade positions. The inclusion of the deflector altered the wake dynamics by organizing the flow more effectively and reducing losses, particularly at critical blade orientations. These changes led to a better-structured flow field and enhanced vortex coherence, both of which are essential for maintaining lift and minimizing performance degradation due to turbulence. The wake analysis further substantiated the aerodynamic advantage of the deflector, showing improved velocity recovery downstream at higher TSRs and inlet velocities. This indicates reduced downstream wake interference and enhanced turbine efficiency in arrays or farms.

These findings provide a strong foundation for further experimental validation and optimization of deflector geometry, positioning, and integration in future VAWT designs, especially under realistic wind conditions and urban deployment scenarios.

CHAPTER 7

Conclusions and Future Prospects

7.1 Conclusions of the present Work

Achieving high aerodynamic efficiency from small-scale vertical axis wind turbines (VAWTs) with simple and compact designs remains an ongoing challenge. This thesis has reviewed the current state-of-the-art augmentation strategies and provided computational investigations for performance improvement of VAWTs, particularly those utilizing the NACA0017 airfoil.

A systematic review revealed that augmentation devices significantly enhance the power coefficient (C_P) and self-starting ability of both lift and drag-type VAWTs. Devices such as ducts, diffusers, deflectors, guide vanes, and stators are instrumental in improving airflow distribution and generating positive torque. Single-directional augmentation systems necessitate yawing mechanisms, whereas omnidirectional setups eliminate such requirements and are particularly suitable for turbulent, rooftop environments. Among various augmentation techniques, ducted and convergent nozzle systems demonstrated over 100% performance improvement, although their structural complexity and installation costs may be limiting factors.

The numerical simulations conducted in this work further underline the potential of the NACA0017 blade profile in VAWT configurations. Two-dimensional CFD simulations showed that NACA0017, although slightly underperforming compared to NACA0015 in peak C_P, offers improved performance at higher tip speed ratios (TSR). Torque coefficient analysis revealed angular and TSR dependent behavior, providing insights into torque fluctuations and pressure differentials.

Further enhancement was observed with duct-augmented configurations, where C_P values increased up to fivefold at lower inlet velocities, with optimal performance at TSR = 3.5. Vortex formation and flow separation were more favorable inside the duct,

leading to better aerodynamic performance. However, it was noted that two-dimensional models fail to capture the full complexity of real-world wind turbine aerodynamics.

This limitation was partially addressed through three-dimensional CFD simulations, where a deflector-augmented VAWT with NACA0017 profile was evaluated. Results showed that the deflector improves power output by increasing local flow alignment and reducing negative torque effects. At both 4 m/s and 5 m/s, the deflector-equipped turbine achieved higher power coefficients, peaking at 0.28 and 0.29, respectively compared to the bare rotor. Flow visualization using the Q-criterion indicated more organized vortex structures and reduced aerodynamic losses with the deflector, especially at the optimal TSR of 2.5.

In addition to aerodynamic performance, the thesis also explored the sustainability aspects of wind power. Although wind energy provides substantial environmental benefits by reducing greenhouse gas emissions and water usage, concerns such as bird mortality, acoustic impacts, waste handling, and visual obtrusiveness were identified. The sustainability assessment also highlighted the lack of standardized methodologies to evaluate WECTs holistically, pointing to a gap in current regulatory and planning frameworks. The thorough survey on the sustainability also points out the fact that there exists ample need and scope for augmenting the performance of wind turbines.

7.2 Future prospects

The current work falls within the domain of WECT and explores the performance of VAWT with NACA0017 airfoils. Augmentations of performance were explained using the ducted passage and deflector plate. Studies were mostly limited to two-dimensional simulations due to lack of computer resources. While significant insight has been obtained from these studies, the shortcomings are also not trivial. These include a lack of experiments on the chosen airfoil and more extensive three-dimensional simulations.

Several promising directions emerge from this work for future research:

- **Three-Dimensional CFD Analysis:** Future studies should incorporate full 3D simulations to capture the spatial complexity of turbulence, vorticity, and wake effects. This would allow for a more realistic representation of the aerodynamic behaviour of ducted and deflector-augmented VAWTs.
- **Experimental Validation:** There is a pressing need for experimental studies to validate numerical predictions and evaluate the practical feasibility of augmentation devices, especially under variable wind and environmental conditions.
- **Hybrid Energy Systems:** Investigation into the integration of VAWTs with other

renewable energy sources (e.g., solar PV) may yield hybrid systems capable of overcoming intermittency issues and enhancing grid stability.

- **Optimization Techniques:** The application of optimization algorithms and Multi-Criteria Decision Making (MCDM) tools for selecting suitable augmentation configurations and assessing overall sustainability of wind power systems is a promising avenue.
- **Sustainable Material Use and Lifecycle Analysis:** Future research should also explore recyclable materials, end-of-life blade reuse strategies, and sustainable construction practices for wind turbine systems.
- **Urban Integration:** Design innovations that enable effective integration of augmented VAWTs in urban rooftops and building facades, while addressing noise, aesthetics, and safety, will be crucial for decentralized energy solutions.

In conclusion, this thesis affirms the viability of augmentation strategies in enhancing VAWT performance and presents NACA0017 as a structurally robust and aerodynamically competent blade profile for small wind applications. A shift toward more comprehensive, 3D, and sustainability-oriented analyses will be essential to realize the full potential of wind energy in future energy systems.

Bibliography

Abdel-Basset, M., Gamal, A., Chakrabortty, R. K., & Ryan, M. (2021). A new hybrid multi-criteria decision-making approach for location selection of sustainable offshore wind energy stations: A case study. *Journal of Cleaner Production*, *280*, 124462. https://doi.org/https://doi.org/10.1016/j.jclepro.2020.124462

Abdullah, M., Ishak, M., & Ismail, F. (2023). Performance improvement of the savonius turbine using a novel augmentation device with the taguchi optimization method. *Physics of Fluids*, *35*(1).

Abraham, M. A. (2006). Principles of sustainable engineering. In *Sustainability science and engineering* (pp. 3–10, Vol. 1). Elsevier.

Ackermann, T., & Söder, L. (2000). Wind energy technology and current status: A review. *Renewable and sustainable energy reviews*, *4*(4), 315–374.

Adeyeye, K., Ijumba, N., & Colton, J. (2020). Exploring the environmental and economic impacts of wind energy: A cost-benefit perspective. *International Journal of Sustainable Development World Ecology*, *27*(8), 718–731.

Aguilo, A., Taylor, D., Quinn, A., & Wiltshire, R. (2004). Computational Fluid Dynamic Modelling of wind speed enhancement through a building augmented wind concentration system. *European Wind Energy Conference*.

Akwa, J. V., Vielmo, H. A., & Petry, A. P. (2012). A review on the performance of Savonius wind turbines. *Renewable and sustainable energy reviews*, *16*(5), 3054–3064.

Alam, F., & Golde, S. (2013). An aerodynamic study of a micro scale vertical axis wind turbine. *Procedia Engineering*, *56*, 568–572.

Al-Ghriybah, M., Zulkafli, M. F., Didane, D. H., & Mohd, S. (2019). The effect of inner blade position on the performance of the Savonius rotor. *Sustainable Energy Technologies and Assessments*, *36*, 100534.

Al-Ghriybah, M., Zulkafli, M. F., Didane, D. H., & Mohd, S. (2021). The effect of spacing between inner blades on the performance of the Savonius wind turbine. *Sustainable Energy Technologies and Assessments*, *43*, 100988.

Ali, A., Golde, S., Alam, F., & Moria, H. (2012). Experimental and computational study of a micro vertical axis wind turbine. *Procedia engineering*, *49*, 254–262.

Allaei, D., & Andreopoulos, Y. (2014). INVELOX: Description of a new concept in wind power and its performance evaluation. *Energy*, *69*, 336–344.

Allaei, D., Tarnowski, D., & Andreopoulos, Y. (2015). INVELOX with multiple wind turbine generator systems. *Energy*, *93*, 1030–1040.

Alsaleh, A., & Sattler, M. (2019). Comprehensive life cycle assessment of large wind turbines in the US. *Clean Technologies and Environmental Policy*, *21*(4), 887–903.

Altan, B. D., & Atilgan, M. (2008). An experimental and numerical study on the improvement of the performance of Savonius wind rotor. *Energy Conversion and Management*, *49*(12), 3425–3432.

Altan, B. D., & Atilgan, M. (2010). The use of a curtain design to increase the performance level of a Savonius wind rotors. *Renewable Energy*, *35*(4), 821–829.

Anastas, P. T., & Zimmerman, J. B. (2006). Chapter 2 The twelve principles of green engineering as a foundation for sustainability. In M. A. B. T. .-. S. S. Abraham & Engineering (Eds.), *Defining principles* (pp. 11–32, Vol. 1). Elsevier. https://doi.org/https://doi.org/10.1016/S1871-2711(06)80009-7

Anbarsooz, M., Amiri, M., & Rashidi, I. (2019). A novel curtain design to enhance the aerodynamic performance of Invelox: A steady-RANS numerical simulation. *Energy*, *168*, 207–221.

Andersen, P. D., Bonou, A., Beauson, J., & Brøndsted, P. (2014). Recycling of wind turbines. *DTU International Energy Report*, *2014*, 92–97.

Anderson, D., Tannehill, J. C., & Pletcher, R. H. (2016). *Computational fluid mechanics and heat transfer*. Taylor Francis.

Ardente, F., Beccali, M., Cellura, M., & Lo Brano, V. (2008). Energy performances and life cycle assessment of an Italian wind farm. *Renewable and Sustainable Energy Reviews*, *12*(1), 200–217. https://doi.org/https://doi.org/10.1016/j.rser.2006.05.013

Arvesen, A., & Hertwich, E. G. (2012). Assessing the life cycle environmental impacts of wind power: A review of present knowledge and research needs. *Renewable and sustainable energy reviews*, *16*(8), 5994–6006.

Avallone, F., Ragni, D., & Casalino, D. (2020). On the effect of the tip-clearance ratio on the aeroacoustics of a diffuser-augmented wind turbine. *Renewable Energy*, *152*, 1317–1327.

Ayaz, A., Israr, A., & Khan, M. Z. (2023). Numerical and experimental investigation of geometric parameters influence on power generation of invelox wind turbine. *Energy for Sustainable Development*, *77*, 101329. https://doi.org/https://doi.org/10.1016/j.esd.2023.101329

Ayhan, D., & Sağlam, Ş. (2012). A technical review of building-mounted wind power systems and a sample simulation model. *Renewable and sustainable energy reviews*, *16*(1), 1040–1049.

Babisch, W. (2014). Updated exposure-response relationship between road traffic noise and coronary heart diseases: a meta-analysis. *Noise and Health*, *16*(68), 1–9.

Balduzzi, F., Bianchini, A., Carnevale, E. A., Ferrari, L., & Magnani, S. (2012). Feasibility analysis of a Darrieus vertical-axis wind turbine installation in the rooftop of a building. *Applied Energy*, *97*, 921–929.

Balduzzi, F., Bianchini, A., Ferrara, G., & Ferrari, L. (2016). Dimensionless numbers for the assessment of mesh and timestep requirements in CFD simulations of Darrieus wind turbines. *Energy*, *97*, 246–261. https://doi.org/https://doi.org/10.1016/j.energy.2015.12.111

Balduzzi, F., Bianchini, A., Maleci, R., Ferrara, G., & Ferrari, L. (2016). Critical issues in the cfd simulation of darrieus wind turbines. *Renewable Energy*, *85*, 419–435.

Baños, R., Manzano-Agugliaro, F., Montoya, F. G., Gil, C., Alcayde, A., & Gómez, J. (2011). Optimization methods applied to renewable and sustainable energy: A review. *Renewable and Sustainable Energy Reviews*, *15*(4), 1753–1766. https://doi.org/https://doi.org/10.1016/j.rser.2010.12.008

Basner, M., Babisch, W., Davis, A., Brink, M., Clark, C., Janssen, S., & Stansfeld, S. (2014). Auditory and non-auditory effects of noise on health. *The lancet*, *383*(9925), 1325–1332.

Baumann, H., & Tillman, A.-M. (2004). The hitch hiker's guide to LCA.

Bedon, G., De Betta, S., & Benini, E. (2016). Performance-optimized airfoil for Darrieus wind turbines. *Renewable Energy*, *94*, 328–340. https://doi.org/https://doi.org/10.1016/j.renene.2016.03.071

Benim, A. C., Diederich, M., Gül, F., Oclon, P., & Taler, J. (2018). Computational and experimental investigation of the aerodynamics and aeroacoustics of a small wind turbine with quasi-3d optimization. *Energy Conversion and Management*, *177*, 143–149. https://doi.org/https://doi.org/10.1016/j.enconman.2018.09.042

Betz, A. (1966). Introduction to the Theory of Flow Machines.(1966)(DG Randall, Trans.) Oxford.

Bhutta, M. M. A., Hayat, N., Farooq, A. U., Ali, Z., Jamil, S. R., & Hussain, Z. (2012). Vertical axis wind turbine–A review of various configurations and design techniques. *Renewable and Sustainable Energy Reviews*, *16*(4), 1926–1939.

Bhuyan, S., & Biswas, A. (2014). Investigations on self-starting and performance characteristics of simple H and hybrid H-Savonius vertical axis wind rotors. *Energy Conversion and Management*, *87*, 859–867.

Bianchini, A., Balduzzi, F., Bachant, P., Ferrara, G., & Ferrari, L. (2017). Effectiveness of two-dimensional cfd simulations for darrieus vawts: A combined numerical

and experimental assessment. *Energy Conversion and Management*, *136*, 318–328.

Bianchini, A., Balduzzi, F., Di Rosa, D., & Ferrara, G. (2019). On the use of Gurney Flaps for the aerodynamic performance augmentation of Darrieus wind turbines. *Energy conversion and management*, *184*, 402–415.

Bishop, I. D. (2002). Determination of thresholds of visual impact: the case of wind turbines. *Environment and Planning B: Planning and design*, *29*(5), 707–718.

Biswas, A., & Gupta, R. (2014). Unsteady aerodynamics of a twist bladed h-darrieus rotor in low reynolds number flow. *Journal of Renewable and Sustainable Energy*, *6*(3).

Blanco, M. I. (2009). The economics of wind energy. *Renewable and Sustainable Energy Reviews*, *13*(6-7), 1372–1382. https://doi.org/10.1016/j.rser.2008.09.004

Bontempo, R., & Manna, M. (2020). Diffuser augmented wind turbines: Review and assessment of theoretical models. *Applied Energy*, *280*, 115867.

Bontempo, R., & Manna, M. (2016). Effects of the duct thrust on the performance of ducted wind turbines. *Energy*, *99*, 274–287.

Bosch, J., Staffell, I., & Hawkes, A. D. (2019). Global levelised cost of electricity from offshore wind. *Energy*, *189*, 116357. https://doi.org/https://doi.org/10.1016/j.energy.2019.116357

BP. (2022). BP Statistical Review of World Energy 2022,(71st edition). *Bp*, 1–60.

Brooks, T. F., Pope, D. S., & Marcolini, M. A. (1989). *Airfoil self-noise and prediction* (tech. rep.).

Brundtland, G. H. (1987). Our Common Future World Commission On Environment And Developement.

Buchler, E. R., & Childs, S. B. (1981). Orientation to distant sounds by foraging big brown bats (Eptesicus fuscus). *Animal Behaviour*, *29*(2), 428–432.

Burlando, M., Ricci, A., Freda, A., & Repetto, M. P. (2015). Numerical and experimental methods to investigate the behaviour of vertical-axis wind turbines with stators. *Journal of Wind Engineering and Industrial Aerodynamics*, *144*, 125–133.

Castelli, M. R., Englaro, A., & Benini, E. (2011). The Darrieus wind turbine: Proposal for a new performance prediction model based on CFD. *Energy*, *36*(8), 4919–4934.

Chang, L. T.-C., Leys, J., Heidenreich, S., & Koen, T. (2018). Determining aerosol type using a multichannel DustTrak DRX. *Journal of Aerosol Science*, *126*, 68–84.

Chatterjee, T., & Peet, Y. (2019). Exploring the benefits of vertically staggered wind farms: Understanding the power generation mechanisms of turbines operating at different scales. *Wind Energy*, *22*(2), 283–301.

Chehouri, A., Younes, R., Ilinca, A., & Perron, J. (2015). Review of performance optimization techniques applied to wind turbines. *Applied Energy*, *142*, 361–388. https://doi.org/10.1016/J.APENERGY.2014.12.043

Chen, J., Yang, H., Yang, M., & Xu, H. (2015). The effect of the opening ratio and location on the performance of a novel vertical axis Darrieus turbine. *Energy*, *89*, 819–834.

Chen, J., Wang, J., & Ni, A. (2019). Recycling and reuse of composite materials for wind turbine blades: An overview. *Journal of Reinforced Plastics and Composites*, *38*(12), 567–577.

Chen, T.-Y., & Chen, Y.-Y. (2015). Developing a vortical stator assembly to improve the performance of Drag-type vertical-axis wind turbines. *Journal of Mechanics*, *31*(6), 693–699.

Chen, W.-H., Chen, C.-Y., Huang, C.-Y., & Hwang, C.-J. (2017). Power output analysis and optimization of two straight-bladed vertical-axis wind turbines. *Applied energy*, *185*, 223–232.

Chiu, C.-H., Lung, S.-C. C., Chen, N., Hwang, J.-S., & Tsou, M.-C. M. (2021). Effects of low-frequency noise from wind turbines on heart rate variability in healthy individuals. *Scientific reports*, *11*(1), 1–12.

Chong, W. T., Fazlizan, A., Poh, S. C., Pan, K. C., & Ping, H. W. (2012). Early development of an innovative building integrated wind, solar and rain water harvester for urban high rise application. *Energy and Buildings*, *47*, 201–207.

Chong, W. T., Pan, K. C., Poh, S. C., Fazlizan, A., Oon, C. S., Badarudin, A., & Nik-Ghazali, N. (2013). Performance investigation of a power augmented vertical axis wind turbine for urban high-rise application. *Renewable Energy*, *51*, 388–397.

Chong, W. T., Wang, X. H., Wong, K. H., Mojumder, J. C., Poh, S. C., Saw, L. H., & Lai, S. H. (2016). Performance assessment of a hybrid solar-wind-rain eco-roof system for buildings. *Energy and Buildings*, *127*, 1028–1042.

Chong, W.-T., Muzammil, W. K., Wong, K.-H., Wang, C.-T., Gwani, M., Chu, Y.-J., & Poh, S.-C. (2017). Cross axis wind turbine: Pushing the limit of wind turbine technology with complementary design. *Applied Energy*, *207*, 78–95.

Chong, W.-T., Wong, K.-H., Wang, C.-T., Gwani, M., Chu, Y.-J., Chia, W.-C., & Poh, S.-C. (2017). Cross-axis-wind-turbine: a complementary design to push the limit of wind turbine technology. *Energy Procedia*, *105*, 973–979.

Chong, W., Fazlizan, A., Poh, S., Pan, K., Hew, W., & Hsiao, F. (2013). The design, simulation and testing of an urban vertical axis wind turbine with the omni-direction-guide-vane. *Applied Energy*, *112*, 601–609.

Chowdhury, A. M., Akimoto, H., & Hara, Y. (2016). Comparative cfd analysis of vertical axis wind turbine in upright and tilted configuration. *Renewable energy*, *85*, 327–337.

Committee, N. W. C. (2010). Wind turbine interactions with birds, bats, and their habitats: a summary of research results and priority questions.

Council, G. W. E. (2023). Global wind report 2023. *GWEC: Brussels, Belgium*.

Cresswell, N., Ingram, G., & Dominy, R. (2015). The impact of diffuser augmentation on a tidal stream turbine. *Ocean Engineering*, *108*, 155–163.

Dannecker, R. K. W., & Grant, A. D. (2002). Investigations of a building□integrated ducted wind turbine module. *Wind Energy: An International Journal for Progress and Applications in Wind Power Conversion Technology*, *5*(1), 53–71.

Darwish, A. S., & Al-Dabbagh, R. (2020). Wind energy state of the art: Present and future technology advancements. *Renewable Energy and Environmental Sustainability*, *5*, 7.

Das Karmakar, S., & Chattopadhyay, H. (2022). A review of augmentation methods to enhance the performance of vertical axis wind turbine. *Sustainable Energy Technologies and Assessments*, *53*, 102469.

Das Karmakar, S., & Chattopadhyay, H. (2024). Role of pumped hydro storage to mitigate intermittency in renewable energy systems. In *Challenges and opportunities of distributed renewable power* (pp. 305–321). Springer.

Das Karmakar, S., Rahman, S. M., & Chattopadhyay, H. (2023). Numerical investigations on the performance of darrieus vertical axis wind turbine with naca0017 blade profile. *Progress in Computational Fluid Dynamics, an International Journal*, *23*(5), 292–302. https://doi.org/10.1504/PCFD.2023.134191

Davidsson, S., Höök, M., & Wall, G. (2012). A review of life cycle assessments on wind energy systems. *The International Journal of Life Cycle Assessment*, *17*(6), 729–742.

Dayan, E. (2006). Wind energy in buildings: Power generation from wind in the urban environment-where it is needed most. *Refocus*, *7*(2), 33–38.

De Lucas, M., Ferrer, M., Bechard, M. J., & Muñoz, A. R. (2012). Griffon vulture mortality at wind farms in southern Spain: Distribution of fatalities and active mitigation measures. *Biological Conservation*, *147*(1), 184–189.

De Santoli, L., Albo, A., Garcia, D. A., Bruschi, D., & Cumo, F. (2014). A preliminary energy and environmental assessment of a micro wind turbine prototype in natural protected areas. *Sustainable Energy Technologies and Assessments*, *8*, 42–56.

Debnath, B. K., Biswas, A., & Gupta, R. (2009). Computational fluid dynamics analysis of a combined three-bucket Savonius and three-bladed Darrieus rotor at various overlap conditions. *Journal of Renewable and Sustainable energy*, *1*(3), 33110.

Dewan, A., Gautam, A., & Goyal, R. (2021). Savonius wind turbines: A review of recent advances in design and performance enhancements. *Materials Today: Proceedings*.

Dhunny, A. Z., Allam, Z., Lobine, D., & Lollchund, M. R. (2019). Sustainable renewable energy planning and wind farming optimization from a biodiversity perspective. *Energy*, *185*, 1282–1297. https://doi.org/https://doi.org/10.1016/j.energy.2019.07.147

Dilimulati, A., Stathopoulos, T., & Paraschivoiu, M. (2018). Wind turbine designs for urban applications: A case study of shrouded diffuser casing for turbines. *Journal of Wind Engineering and Industrial Aerodynamics*, *175*, 179–192.

Ding, C., Zhang, B., Liang, C., Visser, K., & Yao, G. (2023). High-order large eddy simulations of a wind turbine in ducted and open-rotor configurations. *J. Fluids Eng.*, *145*(2), 021201.

Dossena, V., Persico, G., Paradiso, B., Battisti, L., Dell'Anna, S., Brighenti, A., & Benini, E. (2015). An experimental study of the aerodynamics and performance of a vertical axis wind turbine in a confined and unconfined environment. *Journal of Energy Resources Technology*, *137*(5), 051207.

Duriez, O., Pilard, P., Saulnier, N., Boudarel, P., & Besnard, A. (2023). Windfarm collisions in medium-sized raptors: even increasing populations can suffer strong demographic impacts. *Animal Conservation*, *26*(2), 264–275.

Durrani, N., Hameed, H., Rahman, H., & Chaudhry, S. (2011, January). A Detailed Aerodynamic Design and Analysis of a 2-D Vertical Axis Wind Turbine Using Sliding Mesh in CFD. In *49th aiaa aerospace sciences meeting including the new horizons forum and aerospace exposition*. American Institute of Aeronautics; Astronautics. https://doi.org/doi:10.2514/6.2011-541 doi:10.2514/6.2011-541.

Ekvall, T., & Weidema, B. P. (2004). System boundaries and input data in consequential life cycle inventory analysis. *The international journal of life cycle assessment*, *9*(3), 161–171.

El-Askary, W. A., Nasef, M. H., Abdel-Hamid, A. A., & Gad, H. E. (2015). Harvesting wind energy for improving performance of Savonius rotor. *Journal of Wind Engineering and Industrial Aerodynamics*, *139*, 8–15.

Elia, A., Taylor, M., Gallachóir, B. Ó., & Rogan, F. (2020). Wind turbine cost reduction: A detailed bottom-up analysis of innovation drivers. *Energy Policy*, *147*, 111912.

Elkadeem, M. R., Younes, A., Mazzeo, D., Jurasz, J., Campana, P. E., Sharshir, S. W., & Alaam, M. A. (2022). Geospatial-assisted multi-criterion analysis of solar and wind power geographical-technical-economic potential assessment. *Applied Energy*, *322*, 119532.

Elkhoury, M., Kiwata, T., & Aoun, E. (2015). Experimental and numerical investigation of a three-dimensional vertical-axis wind turbine with variable-pitch. *Journal of wind engineering and Industrial aerodynamics*, *139*, 111–123.

El-Zahaby, A. M., Kabeel, A., Elsayed, S., & Obiaa, M. (2017). Cfd analysis of flow fields for shrouded wind turbine's diffuser model with different flange angles. *Alexandria Engineering Journal*, *56*(1), 171–179.

Eriksson, S., Bernhoff, H., & Leijon, M. (2008). Evaluation of different turbine concepts for wind power. *renewable and sustainable energy reviews*, *12*(5), 1419–1434.

Fatahian, E., Ismail, F., Ishak, M. H. H., & Chang, W. S. (2022). The role of wake splitter deflector on performance enhancement of Savonius wind turbine. *Physics of Fluids*, *34*(9), 095111. https://doi.org/10.1063/5.0111568

Finkbeiner, M., Ackermann, R., Bach, V., Berger, M., Brankatschk, G., Chang, Y.-J., Grinberg, M., Lehmann, A., Martínez-Blanco, J., & Minkov, N. (2014). Challenges in life cycle assessment: an overview of current gaps and research needs. *Background and future prospects in life cycle assessment*, 207–258.

Fourrier, J., Fontaine, O., Peter, M., Vallon, J., Allier, F., Basso, B., & Decourtye, A. (2023). Is it safe for honey bee colonies to locate apiaries near wind turbines? *Entomologia Generalis*, *43*(4).

Franchina, N., Persico, G., & Savini, M. (2019). 2D-3D computations of a vertical axis wind turbine flow field: Modeling issues and physical interpretations. *Renewable Energy*, *136*, 1170–1189.

Francis, S., Umesh, V., & Shivakumar, S. (2021). Design and analysis of vortex bladeless wind turbine. *Materials Today: Proceedings*, *47*, 5584–5588.

Fujisawa, N., & Gotoh, F. (1992). Visualization study of the flow in and around a Savonius rotor. *Experiments in Fluids*, *12*(6), 407–412.

Geiger, R., Hannan, Y., Travia, W., Naboni, R., & Schlette, C. (2020). Composite wind turbine blade recycling-value creation through Industry 4.0 to enable circularity in repurposing of composites. *IOP Conference Series: Materials Science and Engineering*, *942*(1), 12016.

Ghazalla, R., Mohamed, M., & Hafiz, A. (2019). Synergistic analysis of a darrieus wind turbine using computational fluid dynamics. *Energy*, *189*, 116214.

Gibson, L., Wilman, E. N., & Laurance, W. F. (2017). How green is 'green'energy? *Trends in ecology evolution*, *32*(12), 922–935.

Golecha, K., Eldho, T., & Prabhu, S. V. (2011). Influence of the deflector plate on the performance of modified savonius water turbine. *Applied Energy*, *88*(9), 3207–3217.

Gómez-Catasús, J., Garza, V., & Traba, J. (2018). Wind farms affect the occurrence, abundance and population trends of small passerine birds: The case of the Dupont's lark. *Journal of applied ecology*, *55*(4), 2033–2042.

Gonzalez-Reyes, G. A., Bayo-Besteiro, S., Vich Llobet, J., & Anel, J. A. (2020). Environmental and economic constraints on the use of lubricant oils for wind and hydropower generation: the case of NATURGY. *Sustainability*, *12*(10), 4242.

Grant, A., Johnstone, C., & Kelly, N. (2008). Urban wind energy conversion: The potential of ducted turbines. *Renewable Energy*, *33*(6), 1157–1163.

Guinée, J. B. (2002). *Handbook on life cycle assessment: operational guide to the ISO standards* (Vol. 7). Springer Science Business Media.

Hansen, M. O. L., Sørensen, N. N., & Flay, R. (2000). Effect of placing a diffuser around a wind turbine. *Wind Energy: An International Journal for Progress and Applications in Wind Power Conversion Technology*, *3*(4), 207–213.

Hara, Y., Kawamura, T., Akimoto, H., Tanaka, K., Nakamura, T., & Mizumukai, K. (2014). Predicting double-blade vertical axis wind turbine performance by a quadruple-multiple streamtube model. *International Journal of Fluid Machinery and Systems*, *7*(1), 16–27.

Hashem, I., & Mohamed, M. H. (2018). Aerodynamic performance enhancements of H-rotor Darrieus wind turbine. *Energy*, *142*, 531–545.

Hayashi, T., Li, Y., & Hara, Y. (2005). Wind tunnel tests on a different phase three-stage Savonius rotor. *JSME International Journal Series B Fluids and Thermal Engineering*, *48*(1), 9–16.

Hayat, I., Chatterjee, T., Liu, H., Peet, Y. T., & Chamorro, L. P. (2019). Exploring wind farms with alternating two-and three-bladed wind turbines. *Renewable energy*, *138*, 764–774.

Heikal, H. A., Abu-Elyazeed, O. S., Nawar, M. A., Attai, Y. A., & Mohamed, M. M. (2018). On the actual power coefficient by theoretical developing of the diffuser flange of wind-lens turbine. *Renewable energy*, *125*, 295–305.

Heymann, M. (1998). Signs of hubris: the shaping of wind technology styles in Germany, Denmark, and the United States, 1940-1990. *Technology and culture*, *39*(4), 641–670.

Horn, J. W., Arnett, E. B., & Kunz, T. H. (2008). Behavioral responses of bats to operating wind turbines. *The Journal of Wildlife Management*, *72*(1), 123–132.

Hosseini, A., & Goudarzi, N. (2019). Design and CFD study of a hybrid vertical-axis wind turbine by employing a combined Bach-type and H-Darrieus rotor systems. *Energy conversion and management*, *189*, 49–59.

Hosseini, S. R., & Ganji, D. D. (2020). A novel design of nozzle-diffuser to enhance performance of INVELOX wind turbine. *Energy*, *198*, 117082.

Howell, R., Qin, N., Edwards, J., & Durrani, N. (2010). Wind tunnel and numerical study of a small vertical axis wind turbine. *Renewable energy*, *35*(2), 412–422.

Irabu, K., & Roy, J. N. (2007). Characteristics of wind power on Savonius rotor using a guide-box tunnel. *Experimental thermal and fluid science*, *32*(2), 580–586.

IRENA, I. R. E. A. (2022). *Renewable power generation costs in 2022*. eBook Partnership.

Ismail, M. F., & Vijayaraghavan, K. (2015). The effects of aerofoil profile modification on a vertical axis wind turbine performance. *Energy*, *80*, 20–31.

Jafaryar, M., Kamrani, R., Gorji-Bandpy, M., Hatami, M., & Ganji, D. (2016). Numerical optimization of the asymmetric blades mounted on a vertical axis cross-flow wind turbine. *International Communications in Heat and Mass Transfer*, *70*, 93–104.

Jain, S., & Saha, U. K. (2020a). Capturing the dynamic stall in h-type darrieus wind turbines using different urans turbulence models. *J Energy Res Technol*, *142*(9), 091302.

Jain, S., & Saha, U. K. (2020b). The state-of-the-art technology of h-type darrieus wind turbine rotors. *Journal of Energy Resources Technology*, *142*(3), 030801.

Jamieson, P. (2011). Upscaling of wind turbine system. *Innovation in Wind Turbine Design*, 90–94.

Ji, S., & Chen, B. (2016). LCA-based carbon footprint of a typical wind farm in China. *Energy Procedia*, *88*, 250–256.

Jiang, Y., Zhao, P., Zou, L., Zong, Z., & Wang, K. (2020). Two-Dimensional Computational Fluid Dynamics Study on the Performance of Twin Vertical Axis Wind Turbine With Deflector. *Journal of Energy Resources Technology*, *142*(8), 81303.

Jiguet, F., Schwemmer, P., Rousseau, P., & Bocher, P. (2021). GPS tracking data can document wind turbine interactions: evidence from a GPS-tagged Eurasian curlew. *Forensic Science International: Animals and Environments*, *1*, 100036.

Jin, X., Wang, Y., Ju, W., He, J., & Xie, S. (2018). Investigation into parameter influence of upstream deflector on vertical axis wind turbines output power via three-dimensional cfd simulation. *Renewable Energy*, *115*, 41–53.

Jin, X., Zhao, G., Gao, K., & Ju, W. (2015). Darrieus vertical axis wind turbine: Basic research methods. *Renewable and Sustainable Energy Reviews*, *42*, 212–225.

Jungbluth, N., Bauer, C., Dones, R., & Frischknecht, R. (2005). Life cycle assessment for emerging technologies: case studies for photovoltaic and wind power (11 pp). *The International Journal of Life Cycle Assessment*, *10*(1), 24–34.

Kabir, M. R., Rooke, B., Dassanayake, G. D. M., & Fleck, B. A. (2012). Comparative life cycle energy, emission, and economic analysis of 100 kW nameplate wind power generation. *Renewable Energy*, *37*(1), 133–141.

Kahraman, C., Kaya, İ., & Cebi, S. (2009). A comparative analysis for multiattribute selection among renewable energy alternatives using fuzzy axiomatic design and fuzzy analytic hierarchy process. *Energy*, *34*(10), 1603–1616.

Kaldellis, J. K., Garakis, K., & Kapsali, M. (2012). Noise impact assessment on the basis of onsite acoustic noise immission measurements for a representative wind farm. *Renewable Energy*, *41*, 306–314.

Kalluvila, J. B. S., & Sreejith, B. (2018). Numerical and experimental study on a modified Savonius rotor with guide blades. *International journal of green energy*, *15*(12), 744–757.

Katovich, E. (2023). Quantifying the Effects of Energy Infrastructure on Bird Populations and Biodiversity. *Environmental Science Technology*, *58*(1), 323–332.

Kim, D., & Gharib, M. (2013). Efficiency improvement of straight-bladed vertical-axis wind turbines with an upstream deflector. *Journal of Wind Engineering and Industrial Aerodynamics*, *115*, 48–52.

Kim, D., & Gharib, M. (2014). Unsteady loading of a vertical-axis turbine in the interaction with an upstream deflector. *Experiments in fluids*, *55*(1), 1–11.

Kingma, E. M., ter Hofstede, R., Kardinaal, E., Bakker, R., Bittner, O., van der Weide, B., & Coolen, J. W. P. (2024). Guardians of the seabed: Nature-inclusive design of scour protection in offshore wind farms enhances benthic diversity. *Journal of Sea Research*, *199*, 102502.

Kojola, E. (2020). Who Speaks for the Place? Cultural Dynamics of Conflicts Over Hazardous Industrial Development. *Sociological Forum*, *35*(3), 673–695. https://doi.org/10.1111/socf.12620

Kolář, V. (2007). Vortex identification: New requirements and limitations. *International journal of heat and fluid flow*, *28*(4), 638–652.

Kosasih, B., & Tondelli, A. (2012). Experimental study of shrouded micro-wind turbine. *Procedia Engineering*, *49*, 92–98.

Krause, R. M., Carley, S. R., Warren, D. C., Rupp, J. A., & Graham, J. D. (2014). "Not in (or Under) My Backyard": Geographic Proximity and Public Acceptance of Carbon Capture and Storage Facilities. *Risk Analysis*, *34*(3), 529–540. https://doi.org/https://doi.org/10.1111/risa.12119

Krishnan, A., & Paraschivoiu, M. (2016). 3D analysis of building mounted VAWT with diffuser shaped shroud. *Sustainable Cities and Society*, *27*, 160–166.

Krishnan, A., Al-Obaidi, A. S. M., & Hao, L. C. (2023). A comprehensive review of innovative wind turbine airfoil and blade designs: Toward enhanced efficiency and sustainability. *Sustainable Energy Technologies and Assessments*, *60*, 103511. https://doi.org/https://doi.org/10.1016/j.seta.2023.103511

Kuang, L., Su, J., Chen, Y., Han, Z., Zhou, D., Zhang, K., Zhao, Y., & Bao, Y. (2022). Wind-capture-accelerate device for performance improvement of vertical-axis wind turbines: External diffuser system. *Energy*, *239*, 122196. https://doi.org/https://doi.org/10.1016/j.energy.2021.122196

Kumar, J. C. R., Kumar, D. V., & Majid, M. A. (2019). Wind energy programme in India. *Energy & Environment*, *30*(7), 1135–1189.

Kunz, T. H., Arnett, E. B., Erickson, W. P., Hoar, A. R., Johnson, G. D., Larkin, R. P., Strickland, M. D., Thresher, R. W., & Tuttle, M. D. (2007). Ecological impacts of wind energy development on bats: questions, research needs, and hypotheses. *Frontiers in Ecology and the Environment*, *5*(6), 315–324.

Kwong, A. H., & Dowling, A. P. (1994). Active boundary-layer control in diffusers. *AIAA journal*, *32*(12), 2409–2414.

Lam, H. F., & Peng, H. Y. (2016). Study of wake characteristics of a vertical axis wind turbine by two-and three-dimensional computational fluid dynamics simulations. *Renewable Energy*, *90*, 386–398.

Lanzafame, R., Mauro, S., & Messina, M. (2014). 2D CFD modeling of H-Darrieus wind turbines using a transition turbulence model. *Energy Procedia*, *45*, 131–140.

Lee, A. H., Hung, M.-C., Kang, H.-Y., & Pearn, W. (2012). A wind turbine evaluation model under a multi-criteria decision making environment. *Energy Conversion and Management*, *64*, 289–300.

Lee, Y.-T., & Lim, H.-C. (2015). Numerical study of the aerodynamic performance of a 500 W Darrieus-type vertical-axis wind turbine. *Renewable energy*, *83*, 407–415.

Leroux, C., Le Viol, I., Valet, N., Kerbiriou, C., & Barré, K. (2023). Disentangling mechanisms responsible for wind energy effects on European bats. *Journal of Environmental Management*, *346*(September). https://doi.org/10.1016/j.jenvman.2023.118987

Leung, D. Y. C., & Yang, Y. (2012). Wind energy development and its environmental impact: A review. *Renewable and sustainable energy reviews*, *16*(1), 1031–1039.

Li, D., Li, C., Zhang, W., & Zhu, H. (2021). Effect of building diffusers on aerodynamic performance for building augmented vertical axis wind turbine. *Journal of Renewable and Sustainable Energy*, *13*(2), 023306. https://doi.org/10.1063/5.0025742

Li, Y., Zhao, S., Qu, C., Tong, G., Feng, F., Zhao, B., & Kotaro, T. (2020). Aerodynamic characteristics of Straight-bladed Vertical Axis Wind Turbine with a curved-outline wind gathering device. *Energy Conversion and Management*, *203*, 112249.

Li, Y., Zhao, S., Tagawa, K., & Feng, F. (2018). Starting performance effect of a truncated-cone-shaped wind gathering device on small-scale straight-bladed vertical axis wind turbine. *Energy conversion and management*, *167*, 70–80.

Loganathan, B., Chowdhury, H., Mustary, I., & Alam, F. (2015). An experimental study of a cyclonic vertical axis wind turbine for domestic scale power generation. *Procedia Engineering*, *105*, 686–691.

Maalouly, M., Souaiby, M., ElCheikh, A., Issa, J., & Elkhoury, M. (2022). Transient analysis of h-type vertical axis wind turbines using cfd. *Energy Reports*, *8*, 4570–4588.

Magoha, P. (2002). Footprints in the wind? Environmental impacts of wind power development. *Renewable Energy Focus*.

Majewski, P., Florin, N., Jit, J., & Stewart, R. A. (2022). End-of-life policy considerations for wind turbine blades. *Renewable and Sustainable Energy Reviews*, *164*, 112538.

Manganhar, A. L., Rajpar, A. H., Luhur, M. R., Samo, S. R., & Manganhar, M. (2019). Performance analysis of a savonius vertical axis wind turbine integrated with wind accelerating and guiding rotor house. *Renewable Energy*, *136*, 512–520.

Manganhar, A. L., Samo, S. R., Luhur, M. R., & Rajpar, A. H. (2016). DESIGN AND ANALYSIS OF WIND ACCELERATING AND GUIDING ROTOR HOUSE FOR A VERTICAL AXIS WIND TURBINE. *Quaid-e-Awam University Research Journal of Engineering*, *15*(1).

Manwell, J. F., McGowan, J. G., & Rogers, A. L. (2010). *Wind energy explained: Theory, design and application*. John Wiley & Sons.

Marinić-Kragić, I., Vučina, D., & Milas, Z. (2018). Numerical workflow for 3D shape optimization and synthesis of vertical-axis wind turbines for specified operating regimes. *Renewable Energy*, *115*, 113–127. https://doi.org/https://doi.org/10.1016/j.renene.2017.08.030

Martínez, E., Blanco, J., Jiménez, E., Saenz-Díez, J. C., & Sanz, F. (2015). Comparative evaluation of life cycle impact assessment software tools through a wind turbine case study. *Renewable Energy*, *74*, 237–246.

Martínez, E., Sanz, F., Pellegrini, S., Jiménez, E., & Blanco, J. (2009). Life cycle assessment of a multi-megawatt wind turbine. *Renewable energy*, *34*(3), 667–673.

May, R., Reitan, O., Bevanger, K., Lorentsen, S.-H., & Nygård, T. (2015). Mitigating wind-turbine induced avian mortality: Sensory, aerodynamic and cognitive constraints and options. *Renewable and Sustainable Energy Reviews*, *42*, 170–181.

Mazarbhuiya, H. M. S. M., Biswas, A., & Sharma, K. K. (2018). Performance investigations of modified asymmetric blade h-darrieus vawt rotors. *Journal of Renewable and Sustainable Energy*, *10*(3).

McEwen, B. S. (2007). Physiology and neurobiology of stress and adaptation: central role of the brain. *Physiological reviews*, *87*(3), 873–904.

Menter, F. R. (1994). Two-equation eddy-viscosity turbulence models for engineering applications. *AIAA journal*, *32*(8), 1598–1605.

Mishnaevsky Jr, L., Jafarpour, M., Krüger, J., & Gorb, S. N. (2023). A new concept of sustainable wind turbine blades: Bio-inspired design with engineered adhesives. *Biomimetics*, *8*(6), 448.

Mohamed, M. H. (2012). Performance investigation of H-rotor Darrieus turbine with new airfoil shapes. *Energy*, *47*(1), 522–530.

Mohamed, M. H. (2013). Impacts of solidity and hybrid system in small wind turbines performance. *Energy*, *57*, 495–504. https://doi.org/https://doi.org/10.1016/j.energy.2013.06.004

Mohamed, M. H., Dessoky, A., & Alqurashi, F. (2019). Blade shape effect on the behavior of the H-rotor Darrieus wind turbine: Performance investigation and force analysis. *Energy*, *179*, 1217–1234.

Mohamed, M. H., Janiga, G., Pap, E., & Thévenin, D. (2010). Optimization of Savonius turbines using an obstacle shielding the returning blade. *Renewable Energy*, *35*(11), 2618–2626.

Mohamed, M. H., Janiga, G., Pap, E., & Thévenin, D. (2011). Optimal blade shape of a modified Savonius turbine using an obstacle shielding the returning blade. *Energy Conversion and Management*, *52*(1), 236–242.

Mohamed, O. S., Ibrahim, A. A., Etman, A. K., Abdelfatah, A. A., & Elbaz, A. M. R. (2020). Numerical investigation of Darrieus wind turbine with slotted airfoil blades. *Energy Conversion and Management: X*, *5*, 100026.

Mohammadi, M., Mohammadi, R., Ramadan, A., & Mohamed, M. H. (2018). Numerical investigation of performance refinement of a drag wind rotor using flow augmentation and momentum exchange optimization. *Energy*, *158*, 592–606.

Mohammed, A. A., Ouakad, H. M., Sahin, A. Z., & Bahaidarah, H. M. (2019). Vertical axis wind turbine aerodynamics: Summary and review of momentum models. *Journal of Energy Resources Technology*, *141*(5), 050801.

Moreno-Camacho, C. A., Montoya-Torres, J. R., Jaegler, A., & Gondran, N. (2019). Sustainability metrics for real case applications of the supply chain network design problem: A systematic literature review. *Journal of Cleaner Production*, *231*, 600–618.

Mudali, U. K., Patil, M., Saravanabhavan, R., & Saraswat, V. K. (2021). Review on E-waste recycling: Part I—a prospective urban mining opportunity and challenges. *Transactions of the Indian National Academy of Engineering*, *6*, 547–568.

Murdock, H., Duncan, G., & Thomas, A. (2021). Renewables global status report. *International Nuclear Information System: Vienna, Austria*.

Nagle, A. J., Delaney, E. L., Bank, L. C., & Leahy, P. G. (2020). A Comparative Life Cycle Assessment between landfilling and Co-Processing of waste from decommissioned Irish wind turbine blades. *Journal of Cleaner Production*, *277*, 123321.

Nardecchia, F., Groppi, D., Garcia, D. A., Bisegna, F., & de Santoli, L. (2021). A new concept for a mini ducted wind turbine system. *Renewable Energy*, *175*, 610–624.

Nassar, Y. F., El-Khozondar, H. J., El-Osta, W., Mohammed, S., Elnaggar, M., Khaleel, M., Ahmed, A., & Alsharif, A. (2024). Carbon footprint and energy life cycle assessment of wind energy industry in Libya. *Energy conversion and management*, *300*, 117846.

Nimvari, M. E., Fatahian, H., & Fatahian, E. (2020). Performance improvement of a Savonius vertical axis wind turbine using a porous deflector. *Energy Conversion and Management*, *220*, 113062.

Nobile, R., Vahdati, M., Barlow, J. F., & Mewburn-Crook, A. (2014). Unsteady flow simulation of a vertical axis augmented wind turbine: A two-dimensional study. *Journal of Wind Engineering and Industrial Aerodynamics*, *125*, 168–179.

Nurur Rochman, M., Nasution, A., & Nugroho, G. (2017). Cfd studies on the flanged diffuser augmented wind turbine with optimized curvature wall. *ICoSI 2014: Proceedings of the 2nd International Conference on Sustainable Innovation*, 347–355.

Oebels, K. B., & Pacca, S. (2013). Life cycle assessment of an onshore wind farm located at the northeastern coast of Brazil. *Renewable Energy*, *53*, 60–70.

Oler, J. W., Strickland, J. H., Im, B. J., & Graham, G. H. (1983). *Dynamic-stall regulation of the Darrieus turbine* (tech. rep.). Texas Tech Univ., Lubbock (USA). Dept. of Mechanical Engineering.

Organization, I. S. (1997). *ISO 14040: Environmental Management-Life Cycle Assessment-Principles and Framework*.

Organization, W. H. (2023). World health statistics 2023.

Parakkal, J. U., Kadi, K. E., El-Sinawi, A., Elagroudy, S., & Janajreh, I. (2019). Numerical analysis of VAWT wind turbines: Joukowski vs classical NACA rotor's blades. *Energy Procedia*, *158*, 1194–1201. https://doi.org/https://doi.org/10.1016/j.egypro.2019.01.306

Park, J., Jung, H.-J., Lee, S.-W., & Park, J. (2015). A new building-integrated wind turbine system utilizing the building. *Energies*, *8*(10), 11846–11870.

Patel, S. N. (2018). Numerical simulation of flow through invelox wind turbine system. *International Journal of Renewable Energy Research (IJRER)*, *8*(1), 291–301.

Pedersen, E., Van den Berg, F., Bakker, R., & Bouma, J. (2010). Can road traffic mask sound from wind turbines? Response to wind turbine sound at different levels of road traffic sound. *Energy policy*, *38*(5), 2520–2527.

Pickering, S. J. (2006). Recycling technologies for thermoset composite materials—current status. *Composites Part A: applied science and manufacturing*, *37*(8), 1206–1215.

Pope, K., Dincer, I., & Naterer, G. (2010). Energy and exergy efficiency comparison of horizontal and vertical axis wind turbines. *Renewable energy*, *35*(9), 2102–2113.

Pope, K., Rodrigues, V., Doyle, R., Tsopelas, A., Gravelsins, R., Naterer, G., & Tsang, E. (2010). Effects of stator vanes on power coefficients of a zephyr vertical axis wind turbine. *Renewable Energy*, *35*(5), 1043–1051.

Porté-Agel, F., Bastankhah, M., & Shamsoddin, S. (2020). Wind-turbine and wind-farm flows: A review. *Boundary-layer meteorology*, *174*(1), 1–59.

Pörtner, H.-O., Scholes, R. J., Agard, J., Archer, E., Arneth, A., Bai, X., Barnes, D., Burrows, M., Chan, L., & Cheung, W. L. W. (2021). Scientific outcome of the IPBES-IPCC co-sponsored workshop on biodiversity and climate change.

Proops, J. L. R., Gay, P. W., Speck, S., & Schröder, T. (1996). The lifetime pollution implications of various types of electricity generation. An input-output analysis. *Energy policy*, *24*(3), 229–237.

Psomopoulos, C. S., Kalkanis, K., Kaminaris, S., Ioannidis, G. C., & Pachos, P. (2019). A review of the potential for the recovery of wind turbine blade waste materials. *Recycling*, *4*(1), 7.

Qin, N., Howell, R., Durrani, N., Hamada, K., & Smith, T. (2011). Unsteady flow simulation and dynamic stall behaviour of vertical axis wind turbine blades. *Wind Engineering*, *35*(4), 511–527.

Radun, J., Maula, H., Rajala, V., Scheinin, M., & Hongisto, V. (2021). Speech is special: The stress effects of speech, noise, and silence during tasks requiring concentration. *Indoor air*, *31*(1), 264–274.

Radun, J., Maula, H., Saarinen, P., Keränen, J., Alakoivu, R., & Hongisto, V. (2022). Health effects of wind turbine noise and road traffic noise on people living near wind turbines. *Renewable and Sustainable Energy Reviews*, *157*, 112040.

Rahman, S. M., & Chattopadhyay, H. (2020). A new approach to estimate the weibull parameters for wind energy assessment: Case studies with four cities from the northeast and east india. *International Transactions on Electrical Energy Systems*, *30*(11), e12574.

Rahman, S. M., & Chattopadhyay, H. (2023). Statistical assessment of wind energy potential for power generation at imphal, manipur (india). *Energy Sources, Part A: Recovery, Utilization, and Environmental Effects*, *45*(3), 7376–7388.

Rahman, S. M., Chattopadhyay, H., & Dutta, P. (2024). Computational fluid dynamics analysis on performance assessment of darrieus-type vertical axis wind turbine using naca0016, naca0019 and naca0020 airfoil sections. *International Journal of Ambient Energy*, *45*(1), 2315489.

Rajaei, M., & Tinjum, J. M. (2013). Life cycle assessment of energy balance and emissions of a wind energy plant. *Geotechnical and Geological Engineering*, *31*(6), 1663–1670.

Ram, M., Child, M., Aghahosseini, A., Bogdanov, D., Lohrmann, A., & Breyer, C. (2018). A comparative analysis of electricity generation costs from renewable, fossil fuel and nuclear sources in G20 countries for the period 2015-2030. *Journal of Cleaner Production*, *199*, 687–704. https://doi.org/https://doi.org/10.1016/j.jclepro.2018.07.159

Ranjbar, M. H., Nasrazadani, S. A., & Gharali, K. (2017). Optimization of a flanged dawt using a cfd actuator disc method. *International Conference on Applied Mathematics, Modeling and Computational Science*, 219–228.

Ranjbar, M. H., Rafiei, B., Nasrazadani, S. A., Gharali, K., Soltani, M., Al-Haq, A., & Nathwani, J. (2021). Power enhancement of a vertical axis wind turbine equipped with an improved duct. *Energies*, *14*(18), 5780.

Rasekh, S., & Aliabadi, S. K. (2023). Toward improving the performance of a variable pitch vertical axis wind turbine (vp-vawt), part 2: Multi-objective optimization using nsga-ii with cfd in the loop. *Ocean Engineering*, *278*, 114308.

Rathore, N., & Panwar, N. L. (2023). Environmental impact and waste recycling technologies for modern wind turbines: An overview. *Waste Management Research*, *41*(4), 744–759.

Reupke, P., & Probert, S. D. (1991). Slatted-blade Savonius wind-rotors. *Applied Energy*, *40*(1), 65–75.

Reuter Jr, R. C. (1980). *Torque ripple in a darrieus, vertical axis wind turbine* (tech. rep.). Sandia National Lab.(SNL-NM), Albuquerque, NM (United States).

Rezaeiha, A., Kalkman, I., & Blocken, B. (2017). Cfd simulation of a vertical axis wind turbine operating at a moderate tip speed ratio: Guidelines for minimum domain size and azimuthal increment. *Renewable energy*, *107*, 373–385.

Richardson, S. M., Lintott, P. R., Hosken, D. J., Economou, T., & Mathews, F. (2021). Peaks in bat activity at turbines and the implications for mitigating the impact of wind energy developments on bats. *Scientific Reports*, *11*(1), 3636.

Ridha, H. M., Hizam, H., Basil, N., Mirjalili, S., Othman, M. L., Ya'acob, M. E., & Ahmadipour, M. (2024). Multi-objective and multi-criteria decision making for technoeconomic optimum design of hybrid standalone renewable energy system. *Renewable Energy*, *223*, 120041.

Riegler, H. (2003). HAWT versus VAWT: Small VAWTs find a clear niche. *Refocus*, *4*(4), 44–46.

Roscioni, F., Rebelo, H., Russo, D., Carranza, M. L., Di Febbraro, M., & Loy, A. (2014). A modelling approach to infer the effects of wind farms on landscape connectivity for bats. *Landscape ecology*, *29*, 891–903.

Roshan, M. Y., Khaleghinia, J., Nimvari, M. E., & Salarian, H. (2021). Performance improvement of Darrieus wind turbine using different cavity layouts. *Energy Conversion and Management*, *246*, 114693.

Roy, S., & Saha, U. K. (2013). Review of experimental investigations into the design, performance and optimization of the Savonius rotor. *Proceedings of the Institution of Mechanical Engineers, Part A: Journal of Power and Energy*, *227*(4), 528–542.

Rueda-Bayona, J. G., Eras, J. J. C., & Chaparro, T. R. (2022). Impacts generated by the materials used in offshore wind technology on human health, Natural Environment and Resources. *Energy*, 125223.

Ruiz, D. P., Flores, M. L., Silva, G. P., & Ibrahim, M. (2023). Single valued neutrosophic sets approach for assessment wind power plant. *International Journal of Neutrosophic Science*, *23*(1), 205–216.

Rule, B. M., Worth, Z. J., & Boyle, C. A. (2009). Comparison of life cycle carbon dioxide emissions and embodied energy in four renewable electricity generation technologies in New Zealand. *Environmental science technology*, *43*(16), 6406–6413.

Ryan, K. J., Coletti, F., Elkins, C. J., Dabiri, J. O., & Eaton, J. K. (2016). Three-dimensional flow field around and downstream of a subscale model rotating vertical axis wind turbine. *Experiments in Fluids*, *57*, 1–15.

Saad, A. S., Elwardany, A., El-Sharkawy, I. I., Ookawara, S., & Ahmed, M. (2021). Performance evaluation of a novel vertical axis wind turbine using twisted blades in multi-stage Savonius rotors. *Energy Conversion and Management*, *235*, 114013.

Sadorsky, P. (2021). Wind energy for sustainable development: Driving factors and future outlook. *Journal of Cleaner Production*, *289*, 125779.

Safford, D. A., Wang, J., Liang, C., & Visser, K. (2024). Unsteady reynolds-averaged navier–stokes simulations of a ducted wind turbine. *J. Fluids Eng.*, *146*(3), 031202.

Sagharichi, A., Zamani, M., & Ghasemi, A. (2018). Effect of solidity on the performance of variable-pitch vertical axis wind turbine. *Energy*, *161*, 753–775.

Saidur, R., Rahim, N. A., Islam, M. R., & Solangi, K. H. (2011). Environmental impact of wind energy. *Renewable and sustainable energy reviews*, *15*(5), 2423–2430.

San Cristóbal, J. R. (2011). Multi-criteria decision-making in the selection of a renewable energy project in spain: The vikor method. *Renewable energy*, *36*(2), 498–502.

Schmidt, U., & Joermann, G. (1986). The influence of acoustical interferences on echolocation in bats.

Sharpe, T., & Proven, G. (2010). Crossflex: Concept and early development of a true building integrated wind turbine. *Energy and Buildings*, *42*(12), 2365–2375.

Shaughnessy, B. M., & Probert, S. D. (1992). Partially-blocked Savonius rotor. *Applied Energy*, *43*(4), 239–249.

Sheldahl, R. E., Blackwell, B. F., & Feltz, L. V. (1978). Wind tunnel performance data for two-and three-bucket Savonius rotors. *Journal of Energy*, *2*(3), 160–164.

Shikha, Bhatti, T. S., & Kothari, D. P. (2003). Vertical axis wind rotor with concentration by convergent nozzles. *Wind Engineering*, *27*(6), 555–959.

Siddiqui, M. S., Durrani, N., & Akhtar, I. (2015). Quantification of the effects of geometric approximations on the performance of a vertical axis wind turbine. *Renewable Energy*, *74*, 661–670. https://doi.org/https://doi.org/10.1016/j.renene.2014.08.068

Sikdar, S. K. (2003a). Journey towards sustainable development: A role for chemical engineers. *Environmental Progress*, *22*(4), 227–232.

Sikdar, S. K. (2003b). Sustainable development and sustainability metrics. *AIChE journal*, *49*(8), 1928–1932.

Sikdar, S. K. (2004). Science of sustainability. *Clean Technologies and Environmental Policy*, *7*(1), 1–2.

Sikdar, S. K. (2009). On aggregating multiple indicators into a single metric for sustainability. *Clean Technologies and Environmental Policy*, *11*, 157–161.

Sotoudeh, F., Kamali, R., & Mousavi, S. M. (2019). Field tests and numerical modeling of INVELOX wind turbine application in low wind speed region. *Energy*, *181*, 745–759.

Souza, L. M. D., Janiga, G., & Thévenin, D. (2017). Multi-objective optimisation of the model parameters for the realisable k-ε turbulence model. *Progress in Computational Fluid Dynamics, an International Journal*, *17*(2), 90–101.

Sovacool, B. K. (2009). Contextualizing avian mortality: A preliminary appraisal of bird and bat fatalities from wind, fossil-fuel, and nuclear electricity. *Energy Policy*, *37*(6), 2241–2248.

Stanek, W., Mendecka, B., Lombardi, L., & Simla, T. (2018). Environmental assessment of wind turbine systems based on thermo-ecological cost. *Energy*, *160*, 341–348.

Stout, C., Islam, S., White, A., Arnott, S., Kollovozi, E., Shaw, M., Droubi, G., Sinha, Y., & Bird, B. (2017). Efficiency improvement of vertical axis wind turbines with an upstream deflector. *Energy procedia*, *118*, 141–148.

Tabassum-Abbasi, Premalatha, M., Abbasi, T., & Abbasi, S. A. (2014). Wind energy: Increasing deployment, rising environmental concerns. *Renewable and Sustainable Energy Reviews*, *31*, 270–288. https://doi.org/https://doi.org/10.1016/j.rser.2013.11.019

Tabatabaei, N., Gantasala, S., & Cervantes, M. J. (2019). Wind Turbine Aerodynamic Modeling in Icing Condition: Three-Dimensional RANS-CFD Versus Blade Element Momentum Method. *Journal of energy resources technology*, *141*(7).

Takao, M., Kuma, H., Maeda, T., Kamada, Y., Oki, M., & Minoda, A. (2009). A straight-bladed vertical axis wind turbine with a directed guide vane row—Effect of guide vane geometry on the performance—. *Journal of thermal Science*, *18*(1), 54–57.

Tandel, R., Shah, S., & Tripathi, S. (2021). A state-of-art review on bladeless wind turbine. *Journal of Physics: Conference Series*, *1950*(1), 012058.

Tayebi, A., & Torabi, F. (2024). Flow control techniques to improve the aerodynamic performance of darrieus vertical axis wind turbines: A critical review. *Journal of Wind Engineering and Industrial Aerodynamics*, *252*, 105820. https://doi.org/https://doi.org/10.1016/j.jweia.2024.105820

Tescione, G., Ragni, D., He, C., Ferreira, C. J. S., & Van Bussel, G. J. W. (2014). Near wake flow analysis of a vertical axis wind turbine by stereoscopic particle image velocimetry. *Renewable Energy*, *70*, 47–61.

Tian, W., Mao, Z., & Ding, H. (2019). Numerical study of a passive-pitch shield for the efficiency improvement of vertical axis wind turbines. *Energy conversion and management*, *183*, 732–745.

Toja-Silva, F., Colmenar-Santos, A., & Castro-Gil, M. (2013). Urban wind energy exploitation systems: Behaviour under multidirectional flow conditions—Opportunities and challenges. *Renewable and Sustainable Energy Reviews*, *24*, 364–378.

Tong, W. (2010). *Wind power generation and wind turbine design*. WIT press.

Tremeac, B., & Meunier, F. (2009). Life cycle analysis of 4.5 MW and 250 W wind turbines. *Renewable and sustainable energy reviews*, *13*(8), 2104–2110.

Turconi, R., O'Dwyer, C., Flynn, D., & Astrup, T. (2014). Emissions from cycling of thermal power plants in electricity systems with high penetration of wind power: Life cycle assessment for Ireland. *Applied energy*, *131*, 1–8.

United Nations, 2015. Sustainable Development Goals (SDGs). (2015).

Van Bussel, G. J. (2007). The science of making more torque from wind: Diffuser experiments and theory revisited. *Journal of Physics: Conference Series*, *75*(1), 012010.

Vassilopoulos, A. P., & Keller, T. (2011). *Fatigue of fiber-reinforced composites*. Springer Science Business Media.

Verma, M., De, A., et al. (2023). Performance analysis of vertical-axis wind turbine clusters: Effect of inter-turbine spacing and turbine rotation. *Physics of Fluids*, *35*(10).

Verma, S., Paul, A. R., & Haque, N. (2022). Selected Environmental Impact Indicators Assessment of Wind Energy in India Using a Life Cycle Assessment. *Energies*, *15*(11). https://doi.org/10.3390/en15113944

Voigt, C. C. (2021). Insect fatalities at wind turbines as biodiversity sinks. *Conservation Science and Practice*, *3*(5), e366.

Wang, J.-J., Jing, Y.-Y., Zhang, C.-F., & Zhao, J.-H. (2009). Review on multi-criteria decision analysis aid in sustainable energy decision-making. *Renewable and sustainable energy reviews*, *13*(9), 2263–2278.

Wang, S., & Wang, S. (2015). Impacts of wind energy on environment: A review. *Renewable and Sustainable Energy Reviews*, *49*, 437–443.

Wang, X. H., Chong, W. T., Wong, K. H., Saw, L. H., Lai, S. H., Wang, C.-T., & Poh, S. C. (2017). The design, simulation and testing of V-shape roof guide vane integrated with an eco-roof system. *Energy Procedia*, *105*, 750–763.

Watanabe, K., Takahashi, S., & Ohya, Y. (2016). Application of a diffuser structure to vertical-axis wind turbines. *Energies*, *9*(6), 406.

Welch, J. B., & Venkateswaran, A. (2009). The dual sustainability of wind energy. *Renewable and Sustainable Energy Reviews*, *13*(5), 1121–1126. https://doi.org/10.1016/j.rser.2008.05.001

Werner, K. M., Haslob, H., Reichel, A. F., Gimpel, A., & Stelzenmüller, V. (2024). Offshore wind farm foundations as artificial reefs: The devil is in the detail. *Fisheries Research*, *272*, 106937.

Wexler, M. N. (1996). A sociological framing of the nimby (not-in-my-backyard) syndrome. *International Review of Modern Sociology*, 91–110.

White, S. W. (2006). Net energy payback and co2 emissions from three midwestern wind farms: an update. *Natural Resources Research*, *15*(4), 271–281.

Widder, S. H., Butner, R. S., Elliott, M. L., & Freeman, C. J. (2011). *Sustainability assessment of coal-fired power plants with carbon capture and storage* (tech. rep.). Pacific Northwest National Lab.(PNNL), Richland, WA (United States).

Wiedmann, T. O., Suh, S., Feng, K., Lenzen, M., Acquaye, A., Scott, K., & Barrett, J. R. (2011). Application of hybrid life cycle approaches to emerging energy technologies–the case of wind power in the UK. *Environmental science & technology*, *45*(13), 5900–5907.

Wiser, R., Bolinger, M., Hoen, B., Millstein, D., Rand, J., Barbose, G., Darghouth, N., Gorman, W., Jeong, S., O'Shaughnessy, E., et al. (2023). Land-based wind market report: 2023 edition.

Wolsink, M. (2000). Wind power and the NIMBY-myth: institutional capacity and the limited significance of public support. *Renewable Energy*, *21*(1), 49–64. https://doi.org/https://doi.org/10.1016/S0960-1481(99)00130-5

Wong, K. H., Chong, W. T., Yap, H. T., Fazlizan, A., Omar, W. Z. W., Poh, S. C., & Hsiao, F. B. (2014). The design and flow simulation of a power-augmented shroud for urban wind turbine system. *Energy procedia*, *61*, 1275–1278.

Wong, K. H., Chong, W. T., Poh, S. C., Shiah, Y.-C., Sukiman, N. L., & Wang, C.-T. (2018). 3D CFD simulation and parametric study of a flat plate deflector for vertical axis wind turbine. *Renewable energy*, *129*, 32–55.

Wong, K. H., Chong, W. T., Sukiman, N. L., Poh, S. C., Shiah, Y.-C., & Wang, C.-T. (2017). Performance enhancements on vertical axis wind turbines using flow augmentation systems: A review. *Renewable and Sustainable Energy Reviews*, *73*, 904–921.

Wong, K. H., Chong, W. T., Sukiman, N. L., Shiah, Y.-C., Poh, S. C., Sopian, K., & Wang, W.-C. (2018). Experimental and simulation investigation into the effects of a flat plate deflector on vertical axis wind turbine. *Energy conversion and management*, *160*, 109–125.

Yang, J., Chang, Y., Zhang, L., Hao, Y., Yan, Q., & Wang, C. (2018). The life-cycle energy and environmental emissions of a typical offshore wind farm in china. *Journal of Cleaner Production*, *180*, 316–324.

Yannopoulos, S. I., Lyberatos, G., Theodossiou, N., Li, W., Valipour, M., Tamburrino, A., & Angelakis, A. N. (2015). Evolution of water lifting devices (pumps) over the centuries worldwide. *Water*, *7*(9), 5031–5060.

Yao, Y. X., Tang, Z. P., & Wang, X. W. (2013). Design based on a parametric analysis of a drag driven VAWT with a tower cowling. *Journal of wind engineering and industrial aerodynamics*, *116*, 32–39.

Yao, Y., Xu, J.-H., & Sun, D.-Q. (2021). Untangling global levelised cost of electricity based on multi-factor learning curve for renewable energy: Wind, solar, geothermal, hydropower and bioenergy. *Journal of Cleaner Production*, *285*, 124827. https://doi.org/https://doi.org/10.1016/j.jclepro.2020.124827

Yazdanbakhsh, A., Bank, L. C., Rieder, K.-A., Tian, Y., & Chen, C. (2018). Concrete with discrete slender elements from mechanically recycled wind turbine blades. *Resources, Conservation and Recycling*, *128*, 11–21.

Ying, P., Chen, Y. K., Xu, Y. G., & Tian, Y. (2015). Computational and experimental investigations of an omni-flow wind turbine. *Applied Energy*, *146*, 74–83.

Zanforlin, S., & Letizia, S. (2019). Effects of upstream buildings on the performance of a synergistic roof-and-diffuser augmentation system for cross flow wind turbines. *Journal of Wind Engineering and Industrial Aerodynamics*, *184*, 329–341.

Zanocco, C., Boudet, H., Clarke, C. E., Stedman, R., & Evensen, D. (2020). NIMBY, YIMBY, or something else? Geographies of public perceptions of shale gas development in the Marcellus Shale. *Environmental Research Letters*, *15*(7), 74039.

Zare Chavoshi, M., & Ebrahimi, A. (2022). Plasma actuator effects on the flow physics of dynamic stall for a vertical axis wind turbine. *Physics of Fluids*, *34*(7).

Zeiner-Gundersen, D. H. (2014). A vertical axis hydrodynamic turbine with flexible foils, passive pitching, and low tip speed ratio achieves near constant RPM. *Energy*, *77*, 297–304.

Zhang, X., Chen, Y. K., & Calay, R. K. (2013). Modelling and analysis of a novel wind turbine structure. *International Journal of Modelling, Identification and Control*, *19*(2), 142–149.

Zhao, P., Jiang, Y., Liu, S., Stoesser, T., Zou, L., & Wang, K. (2021). Investigation of fundamental mechanism leading to the performance improvement of vertical axis wind turbines by deflector. *Energy Conversion and Management*, *247*, 114680.

Signature of the Candidate : Satyajit Das Karmakar

(Author's Name)

Date : 24/07/2025